D80086

TITLE STUDIES OF ORGANOPHOSPHORUS COMPOUNDS BY NUCLEAR MAGNETIC RESONANCE SPECTROSCOPY WITH TWO FREQUENCY DIMENSIONS.

AUTHOR DON-ROGER PARKINSON.

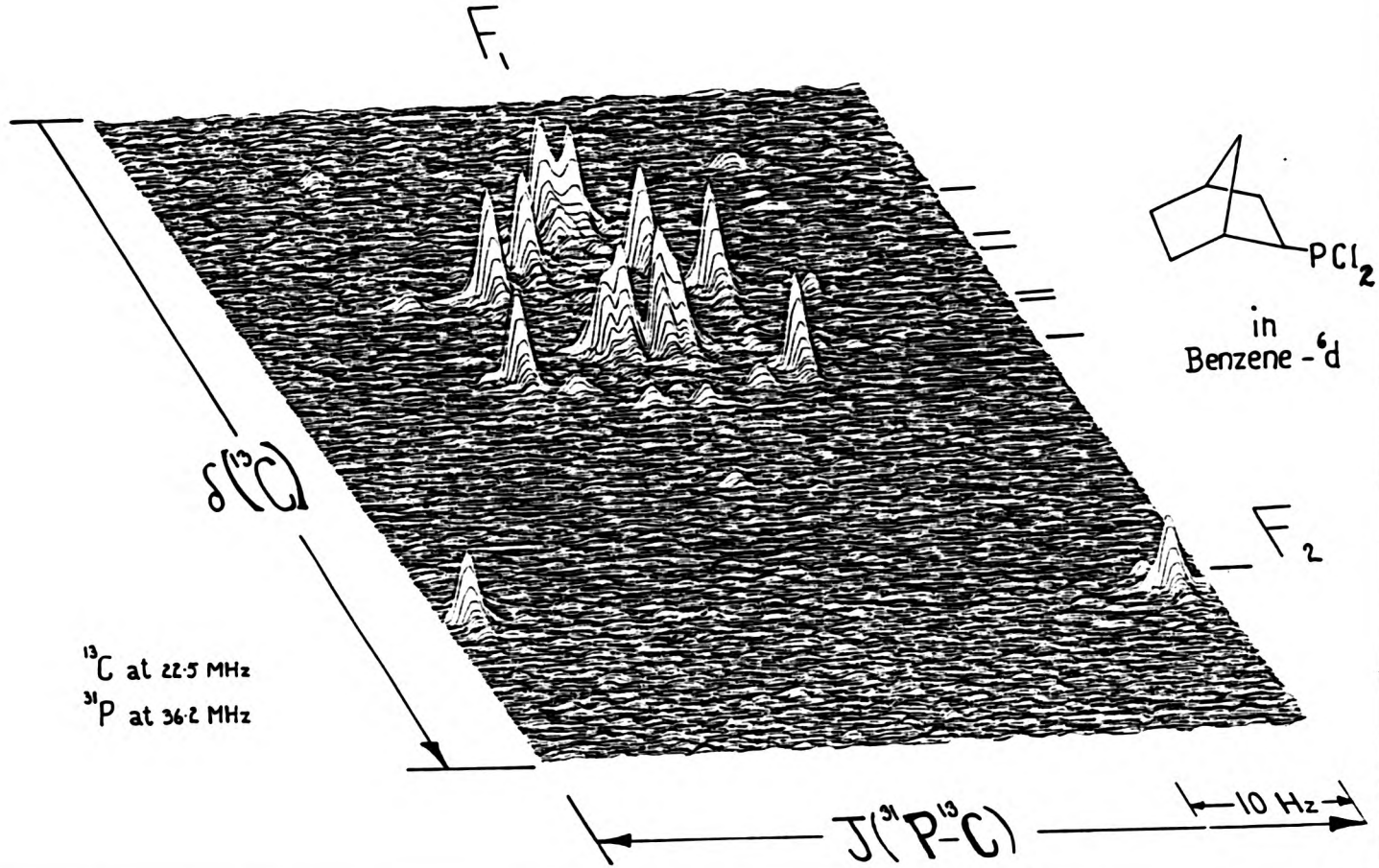
F1
PCl2
in
Benzene - d6
δ(13C)
F2
13C at 22.5 MHz
31P at 36.2 MHz
J(31P-13C)
10 Hz

STUDIES OF ORGANOPHOSPHORUS COMPOUNDS BY NUCLEAR MAGNETIC RESONANCE SPECTROSCOPY WITH TWO FREQUENCY DIMENSIONS

A Thesis submitted to the Council for National Academic Awards in Partial Fulfilment of the Requirements for the Degree of Doctor of Philosophy.

by

Don-Roger Parkinson, B.Sc.

Department of Chemistry
Sir John Cass Faculty of Science and Technology
City of London Polytechnic
31 Jewry Street
London EC3N 2EY

July 1987

ABSTRACT

Studies of Organophosphorus Compounds by Nuclear Magnetic Resonance Spectroscopy with Two Frequency Dimensions.

D-R. Parkinson

A range of organophosphorus compounds with bicyclic and tricyclic cage structures has been prepared and studied by n.m.r. spectroscopy. One and two-dimensional experiments have been used to determine chemical shifts and spin-spin coupling constants for ^{31}P, ^{13}C and ^{1}H nuclei in these systems. The data are a novel and substantial collection of results which relate interactions between P(III) and the C and H atoms in the norbornyl and adamantyl cages according to their relative positions.

The use of 2D n.m.r., in particular the $^{13}C/^{1}H$ shift correlation experiment and a newly designed 2D C[P,H]/J(P,C) pulse sequence, has allowed the measurement of otherwise inaccessible short- and long-range couplings and the proton chemical shifts in both pure compounds and in complex isomeric mixtures. In particular it was possible to separate proton and ^{13}C signals into different frequency dimensions and hence determine (effective) chemical shifts even in these complex spin systems. This feature then made it possible to measure values of $^{n}J(^{31}P,H)$ and determine their signs relative to the corresponding $^{(n-1)}J(^{31}P,C)$. Similar techniques were also applied to the study of $^{n}J(^{19}F,H)$ in fluoronaphthalenes.

The values of the spin-spin couplings J(P(III) - ^{n}C) and J(P(III) - ^{n}C - H) range from 0.2 - 60 and 0.2 - 20 Hz respectively and are found to be related to the elctronegativity of the phosphorus substituents. In exo, endo or syn, anti isomeric pairs different values of coupling are found indicating that orientational and conformational effects are important. This provided a method for the determination of the configurations of particular structures. Correlations of dihedral angles with three-bond coupling constants showed the expected form of dependence in these rigid ring systems.

Acknowledgements

Here I would like to thank Professor William McFarlane who suggested the initial line of work, for his unfailing good humour, inspiration and supervisory help in ascending the various obstacles one encounters over the course of a research study.

Special thanks are also given to Dr Ian Colquhoun and to Dr B. Wood for their initial discussions and assistance with software and preparative problems and to Mr S. Richards for his help with some of the drawings.

In addition I would like to thank all in both Departments of Chemistry - at Sir John Cass Faculty of Science and Technology and at Royal Holloway and Bedford New College - for their encouragement and in particular, patience in allowing me time to complete this work.

Frontispiece: A 2D $^{13}C\{^{31}P,^{1}H\}/J(C,P)\{^{1}H\}$ J-Resolved Stack Plot of exo 2-norbornyl dichloro phosphine

---

Statement of Advanced Studies

The author has attended and presented material at national and international meetings of the Royal Society of Chemistry on n.m.r. spectroscopy in London, Cambridge and Edinburgh and has attended seminars and specialised lectures including topics on stereo and Group IV organometallic chemistry in London and in Coventry. He has read the relevant literature - both review articles and primary journals - and has used and cited these publications throughout the term of study and thesis to keep in the forefront of the subject and in chemistry in general. The journals include: Organic Magnetic Resonance, Journal of Mangetic Resonance, Phosphorus and Sulphur, The Canadian Journal of Chemistry, The Journal of the American Chemical Society and the Journal of the Chemistry Society.

CONTENTS

CHAPTER 1

INTRODUCTION

1.1 Historical Background to 2D-NMR

Until 1966, high resolution NMR spectra were obtained either by sweeping the magnetic field or by sweeping the radio frequency on continuous wave machines. In that year, developments by Ernst and Anderson[1] led to the advent of the first one-dimensional Fourier transform (1D FT) NMR spectrometer. This was the beginning of a significant improvement in NMR sensitivity and of the possibility of running spectra from insensitive nuclei (e.g. ^{13}C and ^{15}N) on a routine basis. Soon after, computer systems were directly integrated into the NMR spectrometer. This allowed a much more efficient way of transforming spectra and also had the advantage of allowing sampling by pulse excitation which gave the opportunity to perform different pulse sequences such as longitudinal[2] and transverse[3] relaxation measurements, Driven Equilibrium Fourier Transform (DEFT)[4], Insensitive Nuclei Enhanced by Polarisation Transfer (INEPT)[5], and rapid scanning[6] trains. With the advancement of sophisticated computer software in direct and in indirect control over many of the spectrometer variables it then became possible to use NMR to study many of the elements in the periodic table including nuclei with $I > 1/2$.

The normal 1D FT operation converts the time-domain Free Induction Decay (FID) signal which consists of data points separated by a dwell time into a frequency-domain spectrum containing peaks of varying intensities that are separated in frequency due to chemical shift differences and spin-spin couplings. The signal intensity

f(w) is a measure of the probability of the occurrence of the frequency (w) value[7].

In 1971 Jeener[8] first introduced the idea of two-dimensional (2D-NMR) whereby the transformation of the NMR signal is performed with respect to two time variables. This yields a spectrum which is a function of two frequency variables. Since the presentation of the first experimental results in 1974[9] a considerable number of promising techniques have been developed to generate 2D spectra of liquids and solids. These include J-[10] and shift-correlated[11] spectroscopy, and multiple quantum coherence[12] and chemical exchange[13] spectroscopy. 2D spectroscopy allows a more detailed study of systems by simplification of spectra through two dimensional spreading, and by a more complete characterisation of non-linear systems. It proved invaluable in the present work in view of the complexity of many of the molecules studied.

1.2 The Role of Phosphorus as an Aid in 2D-NMR

It is well known that the NMR technique can be very useful in: (1) providing chemical backbone framework connectivities and (2) yielding stereochemical information for complex structures. Phosphorus in particular has been very useful as an NMR probe in many systems since ^{31}P has 100% natural abundance with spin = $\frac{1}{2}$, and is very sensitive to its environmental surroundings.

The aim of this thesis is to use some special NMR techniques to study the effects of environment on coupling constants and chemical shifts in organo-phosphorus compounds whose spectra have previously been too complex for detailed examination. In particular, rigid systems of known or calculable geometry have been synthesised and studied.

In the case of primitive diamondoid molecules such as bicyclic-(norbornanes) and tricyclic-(adamantanes) structures, problems in the synthesis of pure compounds frequently occur as a result of the formation of mixtures of isomers (exo or endo, and/or syn or anti - depending on where the substituents lie). The isomers, in the cases where they are well defined (situations are few in which chemical separations can be achieved), may have virtually identical, or random boiling points or melting points in a particular series of compounds. Also, identification of the isomers is a non-trivial chemical problem. Hence, having a phosphorus substituent on a particular site of interest would seem a likely approach to aid in this characterisation and confirmation of structure. However, to be able to identify the particular isomer can still be difficult as signals arising from the cyclic structure lie within a very close range (35 ppm in the ^{13}C NMR spectrum) and the additional coupling to phosphorus in this case adds to the difficulties. Hence a 2D-NMR spectrum would be very useful for the alleviation of this overcrowding problem by giving dispersion in a second frequency dimension. Previous work in this area has only used 1D-NMR, and even then data have been limited and sketchy, thus a brief review shall be undertaken.

1.3 Background to Norbornane- and Adamantane-Phosphorus Derivatives

In bicyclic-systems such as norbornane shown in Structure 1-[a], the bonds of the systems are limited to a form of pseudorotation[14] where torsion angles do not exceed 14°[15]. Such systems can therefore be regarded as rigid in the present context. Systems of this sort have therefore been studied in anticipation of clarifying the various steric influences on chemical shifts. Quin et al.[16] have observed,

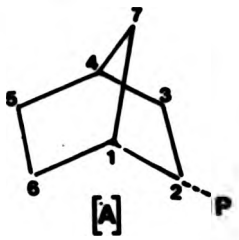

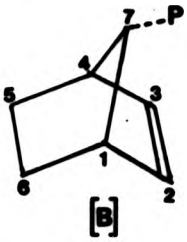

Structure 1

and it now has been verified, that ^{31}P, ^{13}C and ^{15}N nuclei undergo steric compression effects from functional groups in a chain. These have been noted for bicyclic systems[17,18], and the observation of γ-steric effects on ^{13}C chemical shifts plays an important role in assigning ^{13}C chemical shifts in the NMR spectra of exo- and endo-2-norbornyl phosphorus compounds[15] and in syn- and anti-7-norbornenyl phosphorus dichlorides[16]. Quin et al.[17] have measured ^{31}P chemical shifts in a number of norbornyl and norbornenyl derivatives having a phosphorus atom in the 2 or 7 position denoted in Structure 1 , and some of their results are given in Table 1.3-1.

TABLE 1.3-1 ^{31}P NMR Chemical Shifts of syn- and anti-7-norbornenyl Phosphorus Derivatives*

		
Derivative P	δ/ppm	δ/ppm
Me_2P	-60.2	-61.3
Cl_2P	190.9	199.7
$Me_2(S)P$	30.2	36.5
$Me_3P^+I^-$	19.8	24.2

* Taken from ref. 17

The ^{31}P chemical shift differences between the pairs of *syn* and *anti* isomers shown in Table 1.3-1 have been accounted for in terms of reduced steric crowding in moving from the *anti* to the *syn* configuration[17]. Also in the case of the *syn* isomer, it has been proposed that the magnetic anisotropy effect arising from the π-orbital interaction of the 2-3 double bond would cause a shielding effect on the phosphorus. Quin's[16,17] interpretation differs from Gorenstein's[18] explanation which relates bond angle distortions (arising from a coupling of bond angles to torsion angles) to steric compression effects on ^{31}P and ^{13}C chemical shifts.

However, as shown in Table 1.3-1, this is not as straightforward as it seems, as for the $-PMe_2$ derivative the values for the *syn* and *anti* forms differ with respect to the other three *syn* and *anti* isomer derivatives. At present, lack of data is a major problem in generalising explanations of this kind. In terms of spin-spin coupling constants for bicyclic-phosphorus systems, there have been some investigations[16,19-24] of $^{1}J(P,C)$. However, there does not appear to be a consistent relationship between $^{1}J(P,C)$ and steric crowding. For example, Quin and Littlefield[16] have found steric crowding produces a small increase in $^{1}J(P,C)$ for *syn* vs *anti* in P(III) derivatives, whereas the opposite has been reported[26,27] in alkyl phosphonates. A number of geminal $^{2}J(PC,)$[16,23-25] and $^{2}J(P,H)$[28-30] couplings in singly and multisubstituted norbornyl systems have been reported. These seem to accord with the hypothesis of Laszlo and Schleyer[31] that $^{2}J(P,X)$ depends on the bond angle relating the two atoms P and X if one disregards substituent electronegativity effects, though more data are needed to make definitive statements. For $^{3}J(P,X)$ couplings a dihedral angle dependence seems associated with the state of hybridisation of the phosphorus atom. Please see

Chapter 3 for more information on this. In the case of adamantane-phosphorus derivatives, very little work has been published. However, Crealy et al.[32] have synthesized the system R-OPX_2, where R = adamantyl. Their interest was mainly in the effect of phosphorylation on adamantanes and no NMR data were given. However, considerations of possible reaction mechanisms of phosphorus addition suggest that an adamantene dimer intermediate may be formed in organo-metallic and Friedel-Crafts reactions as shown in Fig.1.3-1. This agrees with suggestions of W. Barns et al.[33], though conflicting mechanisms have been proposed and thus this is not a well understood area.

FIGURE 1.3-1 A Suggested Mechanism for Adamantene Dimer Intermediate Formation

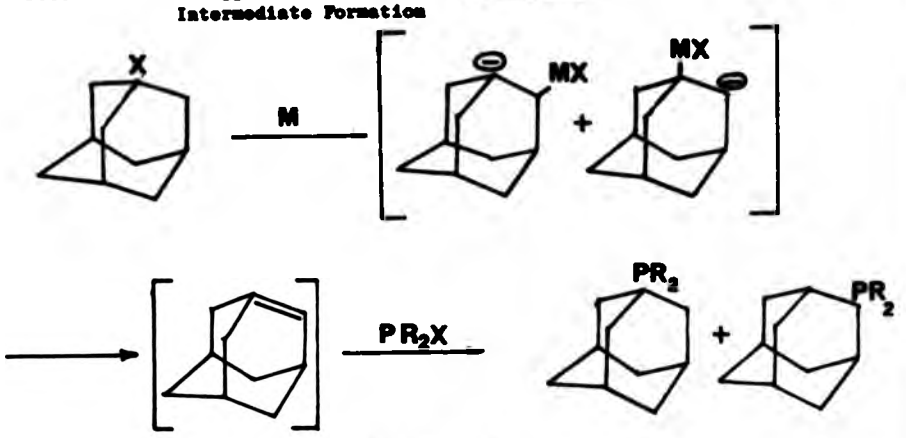

where M = metal and x = halogen(s)

1.4 NMR Parameters

In this thesis the nuclei studied by liquid state NMR are of spin ½ and their nuclear properties are shown in Table 1.4-1.

TABLE 1.4-1 Properties of the Magnetic Nuclei in a Field Strength of 2.1 Tesla

Isotope	Larmor Frequency in MHz	Natural Abundance %	Magnetogyric Ratio (10^7 rad^{-1} T^{-1} s)	Magnetic Moment μ
^{1}H	89.56	99.98	26.75	4.83
^{19}F	84.26	100.00	25.16	4.55
^{31}P	36.20	100.00	10.82	1.95
^{13}C	22.50	1.10	6.72	1.21
^{195}Pt	19.82	33.80	5.75	1.03

For a particular nucleus there are five parameters which can be measured by the NMR experiment. They are: Chemical Shifts, δ (1.4.1); Coupling Constants, J (1.4.2); Line Intensities (1.4.3); Spin Lattice relaxation times, T_1 (1.4.4); and Spin-Spin relaxation times, T_2 (1.4.5). Parameters 1,2,3 normally yield structural information while 4 and 5 highlight aspects of molecular motion.

1.4.1 Chemical Shifts (δ)

When a nucleus is placed in a magnetic field, the motion of the surrounding electrons induces a secondary magnetic field at the nucleus; the direction of the secondary magnetic field is usually such that it opposes the applied field and thus it partially screens or shields the nucleus from the applied field. The magnitude of shielding of a particular nucleus depends on the local electron density and on the

electron shielding from the other parts of the molecule. Each different kind of nucleus in the sample will experience a magnetic field that differs from the applied field by a small amount:

$$B_{nuc.} = B_o (1 - \sigma) \qquad [1.1]$$

where B_o is the applied magnetic field and σ is the screening/shielding constant.

Substituting equation [1.1] into the Larmor equation:

$$\nu_o = \gamma/2\pi B_o \qquad [1.2]$$

for the precessional frequency ν_o, we obtain the resonance condition[34] as:

$$\nu = \gamma/2\pi B_o (1 - \sigma) \qquad [1.3]$$

Different chemical shifts arise then from the fact that the magnetic field experienced by the nucleus depends upon its environment. In practice, information is rarely available to determine σ, as this would require measuring the absorption of a bare nucleus stripped of its electrons[35]. However a reference compound may be employed and all chemical shifts are then determined as a chemical shift difference with respect to the absorption of the reference compound. For precision, chemical shifts may be quoted as the resonance frequency, $\Xi(x)$, at a field strength such that the proton resonance in tetramethylsilane (Me_4Si, TMS) is at exactly 100 MHz. However, in general chemical work they are usually quoted in units of ppm. The extent to which nuclear shielding is sensitive to chemical environment varies greatly from nucleus to nucleus, but in comparable molecules, it usually increases with atomic number as one descends any particular group in the periodic table[36]. The Chemical Shift ranges of the particular nuclei studied here are shown in Table 1.4-2.

TABLE 1.4-2 Chemical Shift Ranges of Nuclei Studied

Element	Z	Range/ppm
H	1	15*
C	6	600
F	9	1400
P	15	1000
Pt	78	15000

* ^{1}H chemical shift range may be extended to 60 ppm if transition metal compounds are included[37].

1.4.1.1 Isotope Effects on Shielding

Primary isotope effects (e.g. $^{14/15}N$, $^{117/119}Sn$) have not been shown to have a marked effect upon shielding constants[38]. The exception may be for ^{1}H, D, T, where the mass change is greatest[39]. For most purposes, such effects can be ignored. Secondary Isotope effects, i.e. those whereby the isotopic mass of a neighbouring atom is changed, may however be significant. These changes may affect the zero-point energy of the bonds, and in the case of $^{12}C/^{13}C$ — Transition metal bonding, the transition metal shielding can differ by several ppm[40]. However this kind of effect was ignored in the present work.

1.4.1.2 Theory

An extensive and detailed study of heavy atom (^{31}P) chemical shifts has been presented in a monograph[41] and in a more up to date survey[42]. Here only a brief summary of the various factors influencing phosphorus chemical shifts is given.

A heavy atom chemical shift results from the summation of shielding contributions given by Ramsey[43] in the equation[44]:

$$\sigma_{Total} = \sigma d + \sigma p + \sigma (neigh) \qquad [1.4]$$

The diamagnetic term (σd) arises from the rotation of electrons about the nucleus and the paramagnetic term (σp) arises from the hindrance of the rotation of electrons about the nucleus, in an applied magnetic field. As they are both of similar magnitude, small changes in either can affect the total shielding contribution. Also since the total shielding contribution is dependent upon the effect of all terms, one cannot treat each term alone, as they are not mutually exclusive. It is assumed, however that the σd term will usually remain unaffected, since it is associated with the inner electrons of the atom, which are little affected by changes in bonding[41]. Thus for the most part, variations in the shielding contribution can generally be seen for the phosphorus atom as being dominated by σp. (An exception possibly occurs for tetrahedrally surrounded cases[45].) This σp effect will produce a shift to higher frequency. In lighter atoms, such as hydrogen, the diamagnetic term plays the more important role. The third term (σ (neigh)), shielding from other neighbouring atoms, in equation [1.4] is included because the diamagnetic and the paramagnetic terms differ for different nuclei in the same molecule[43] due to an uneven distribution of electron density. This may affect the overall shielding contribution. The overall chemical shift is affected by changes in orbital overlap and by hybridisation changes, as well as by changes in the average electronic excitation energy, all of which are contained in the paramagnetic term[42]. This is given by equation[42] [1.5]:

$$\sigma p = - \frac{e^2 \hbar^2}{2m^2 c^2} \langle r^{-3} \rangle_{np} (\Delta E^{-1}_{av.}) \sum_{B}^{i} QAB \qquad [1.5]$$

where $\langle r^{-3} \rangle_{np}$ is the mean inverse cube radius for an atom of np orbitals; $\Delta E_{av.}$ is the average electronic excitation energy; and QAB

Table 14-3 A Range of ^{31}P Chemical Shifts for P(III) and P(V) Substituted Compounds

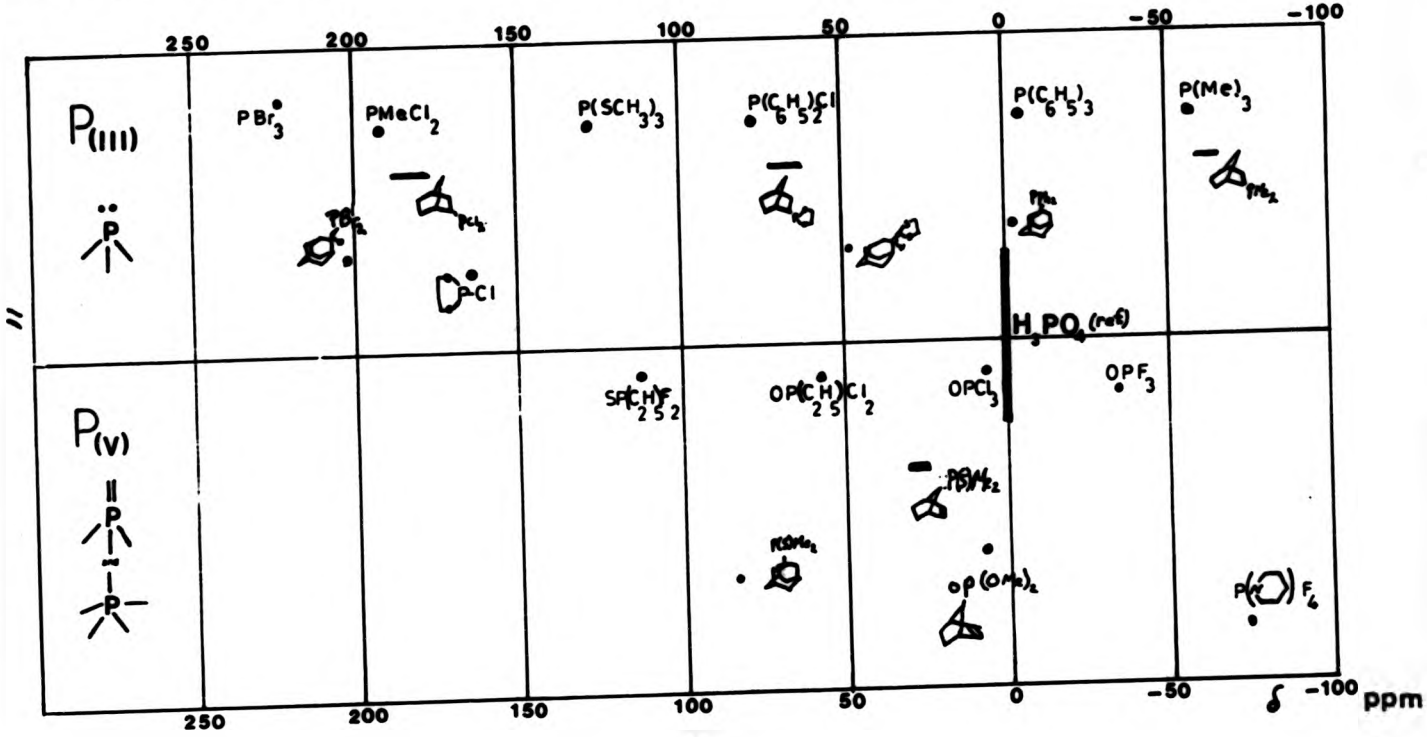

is a function of the charge bond order between the two atoms A and B and is known as the orbital unbalancing term. This theory generally accounts for major trends in a particular class of phosphorus co-ordination in a chemical shift range. Table 1.4-3 illustrates this.

For a given co-ordination number certain patterns do emerge. Thus for di- and tri-valent phosphorus compounds consideration of only s and p orbitals seems necessary. For P(III) compounds the lone pair electrons play an important role (especially for tetrahedrally surrounded atoms)[46]. For P(IV), P(V) and P(VI) atoms, d electrons play an important role as they strongly decrease the paramagnetic shift contribution and hence a net lower frequency shift arises[45]. Small variations within a class present a more complicated problem[42], but qualitative relationships are possible. Grim et al.[47,48] have established a relation for empirical correlation for P(III) and P(IV)+ compounds given by the general equation:

$$\delta = K - \sum_{1}^{n} \sigma^{P} \qquad [1.6]$$

where K is a particular constant for the phosphine class and σ^{P} is an additive constant which can be calculated for a particular R group. Table 1.4-4 illustrates this relationship.

TABLE 1.4-4 Empirical Correlations for Various R groups*

R group	σ^{P}
CH_3	0
C_2H_5	+14
iso C_3H_7	+27
C_6H_5	+18
$C_6H_5CH_2$	+17

* Taken from ref. 47,48

Also Quin et al.[49] have suggested that steric compression effects are operative on phosphorus as they are on ^{13}C and ^{15}N nuclei regardless of tri- or tetra-covalency. The ^{31}P chemical shift may be calculated by Equation [1.7]

$$\delta^{31}P = \delta(\text{parent}) + m\beta + n\gamma \qquad [1.7]$$

where m is the number of β carbons and n is the number of γ carbons. As in ^{13}C spectroscopy, when a proton is replaced by a second carbon a deshielding (α) effect is found; extension of the chain by addition of another carbon gives a further deshielding (β) effect; and addition of a further carbon gives instead a shielding (γ) effect. The β-effect is not well understood, but the γ-effect is associated with the effect of the bonding α carbon. This γ-effect is said to be associated with steric compression effects[50]. An example of this phenomenon can be seen by comparing the position of the electron pair in P(III) derivatives where the unbound electron pair is in an eclipsed or staggered position. However, because of the variations of hybridization associated with phosphorus bonding, which may involve mixed s, p, and d orbital participations, no overall simple patterns for all ^{31}P chemical shift changes with substituent electronegativity or structural charge have been found as yet. Unified theoretical treatments for all classes has been attempted[51-54]. A reasonable approach using quantum-mechanical calculations has been demonstrated by Letcher and Van Wazer[51]. In this they describe the change in chemical shift differences ($\Delta\delta$) as the sum of: the difference in the electronegativity in the P-X bond (ΔX_x), the change in the π-electron overlap (Δn_π), and the change in the σ-bond angle, ($\Delta\theta$). This is shown in Equation [1.8]

$$\Delta\delta = -C\Delta X_x + K\Delta n_\pi + A\Delta\theta \qquad [1.8]$$

where C, K and A are constants.

1.4.2 Spin-Spin Coupling Constants

Information gained from NMR spin-spin coupling constants often complements and extends that which can be gathered from studies of NMR chemical shifts.

Since all samples are run as solutions the rapid tumbling of the molecules averages their nuclear dipolar interactions and hence the magnetic dipole-dipole couplings to zero. Thus the couplings of concern here are the so-called J-couplings which occur when the nuclear spin interaction is mediated by the electrons of the bond. This is an indirect interaction between spins of neighbouring nuclei; the interaction is independent of the magnetic field strength and is measured in Hertz (or cycles/sec). Our primary interest is in the couplings $^{n}J(H,H)$; $^{n}J(H,P)$; $^{n}J(C,P)$ and $^{n}J(H,F)$, where n is the number of intervening bonds.

1.4.2.1 Theoretical Background to a Coupling Interaction 'J'

As this topic has been exhaustively discussed in various reviews [43,45,46,56] including those of Gorenstein[42] and Kowaleski[55], only an overview will be undertaken here.

Spin-spin coupling can be conceptualised by the Dirac Vector Model for the H-D molecule which may be extended superficially for most nuclei where the two nuclei A and B are linked by a direct bond. If the nuclear spin of A is orientated parallel to a particular direction, the electron near A will tend to align its spin antiparallel to it due to the pairing of magnetic moments. As the Pauli exclusion principle states that in any orbital there cannot be two electrons with the same quantum numbers, then the other electron of the bond must have the opposite spin orientation. Similarly, nucleus B will tend to have its spin aligned antiparallel to this second electron, and the overall

result is that nuclei A and B tend to have their spins aligned anti-parallel. This is known as the Fermi contact mechanism. The coupling constant is the difference between the two energy states $\alpha\alpha$ and $\alpha\beta$; or $\beta\beta$ and $\beta\alpha$ in the absence of the magnetic field. (Please see section 1.4.2.2 Signs of Coupling Constants.) The configuration with the lowest energy will be when the spins are anti-parallel provided that the coupling constant is positive. The energy of a given interaction between nuclei A and B ($E_{A,B}$) is:

$$E_{A,B} = h J_{(A,B)} I_A I_B \qquad [1.9]$$

where J(A,B) is the coupling constant between the two nuclei A and B, and I is the nuclear spin of A and of B.

This model predicts that all coupling constants will be positive if the magnetogyric ratios are positive, though experimentally some negative values have been found. For ^{1}H, ^{19}F, ^{13}C, ^{31}P nuclei the magnetic moments and the angular momentum are in the same direction and the magnetogyric ratio, γ is positive. Some other nuclei such as ^{15}N have a negative γ. Since theoretical expressions for describing J(A,B) include the magnetogyric ratios of the two nuclei and the electronic environment of the coupled nuclei, a reduced coupling constant $K_{A,B}$, which may be positive or negative is preferred so as to remove the dependence upon individual nuclear properties especially when examining coupling constants where mixed (positive and negative) γ are involved. It is given by[57]:

$$K_{A,B} = \frac{4\pi^2 J(A,B)}{h \gamma_A \gamma_B} \qquad [1.10]$$

We are interested in non-reduced coupling constants as all nuclei concerned here have positive γ. Spin-spin coupling is a second-order electronic property of the molecule and hence subtle changes in environment may change the overall coupling constant. Perturbation

approximations and a quantum mechanical handling are needed to accurately express the overall coupling effect. This was first provided by Ramsey[58] with a theoretical treatment of the H-D molecule and expanded by McConnell[59] to include other interactions by using Molecular Orbital theory. Further treatments are by Karplus and Anderson[60,61] (Valence Bond theory), and Pople et al.[57] using the Finite Perturbation Theory - Intermediate Neglect of Differential Overlap technique (FPT-INDO). All these treatments are usually based on the initial approximation by Ramsey who proposed that the total coupling may be expressed as a sum of the orbital, the spin-dipolar, and the Fermi contact interaction terms. The orbital term is defined as the interaction between the nuclear magnetic moment and the magnetic field produced from the orbital motion of the electrons. The spin-diplolar term is associated with the interaction between the nuclear magnetic moment and the spin magnetic moment of an extra-nuclear electron. The Fermi contact term is the interaction between the electron density within the region of the nucleus and the nuclear magnetic moment. Most calculations[62] reveal that the Fermi contact term accounts for more than 90% of spin-spin interactions[63,64] including those for phosphorus P-X bonds[65], and therefore discussion is usually confined to this. Pople et al.[57] have expressed these contributions in terms of the reduced coupling constant. As an example, if we consider a less electronegative element, phosphorus, the energy of say the 3s orbital is such that sign changes in the coupling constant $J_k(P,X)$ may occur through effects on bond overlapping between s orbitals produced by substituent changes. As the Fermi contact term depends upon there being a finite electron density at the nucleus, s electrons contribute to it, whereas p and d electrons, whose orbitals have a node at the nucleus, do not. This then is referred to as the s-character of the

orbital used to form a particular bond. It follows from this that an increase in the s-character is generally associated with an increase in the coupling constant[65]. It should be stated that an increase in s-character associated with one particular bond to an atom reduces the s-character in the other bonds. Hence s-character is not created but is merely transformed and localised depending upon the particular electronic configurations in a molecule. The s-character of the orbitals used to form the bond is determined by the hybridization of atoms P and X and the electronegativity and bulk of the substituents. In tri-valent phosphorus compounds the electron pair is believed[45] to occupy an orbital with high s-character so that the s-character is drawn away from the rest of the substituents resulting in small inter-bond angles which reflect the use of mainly p orbitals. As the bulkiness of substituents increases, the percent s-character of that P-X bond increases and hence the inter-bond angle will increase, with a concomitant increase in $^{1}J(P,X)$. Obviously not all situations can be accounted for by this idealised conception as other factors will intervene for specific examples.

1.4.2.2 Signs of Coupling Constants

Whereas a nuclear spin-spin coupling constant J(A,B) is a measure of interaction between a pair of atoms, it however may or may not be directly related to the strength of the chemical bond or bonds involved. As examples, $^{1}J(P,C)$ = 50-60 Hz for the methyl carbon shown in Structure 2 and the $^{1}J(P,C)$ is at 10 Hz[42] in the more stable triphenyl phosphine.

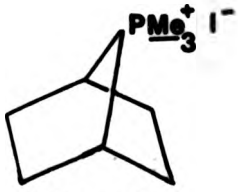

Structure 2

For the structure $Me_2PC_6H_5$ J(P,C) = 14 Hz and for $Me_2P^+ C_6H_5Br^-$ J(P,C) = 56 Hz[68]. These seeming discrepancies arise because the coupling constant is made up of several large terms of opposite signs which may give a small sum. Thus a small change in a term can give a comparatively large effect on J and may lead to a change in its sign. By convention a positive coupling constant is defined to occur when the more stable state is that with the spins of the coupled nuclei aligned anti-parallel. That is when the $\alpha\beta$ and $\beta\alpha$ are of lower energy than the $\alpha\alpha$ and $\beta\beta$ states in the absence of a magnetic field. The determination of the absolute signs of coupling constants is difficult and requires the use of molecular beam experiments or orientated molecules. A reversal of the signs of all of the coupling constants in a system has no effect at all upon the appearance of its NMR spectrum. However, if the spectrum has second order features, reversal of some of the signs of the couplings may change the appearance of the spectrum. Relative signs can usually be determined via double resonance techniques by relating and comparing them to a coupling which has an absolute sign. A number of absolute signs of coupling constants are well established and those which pertain to this thesis are listed in Table 1.4-5.

TABLE 1.4-5 A Selection of Established Signs of Coupling Constants

Coupling Constant	Absolute Sign
$^1J(^{13}C, ^1H)$	+
$^1J(^{31}P, ^1H)$	+
$^3J(^1H, ^1H)$	+
$^1J(^{195}Pt, ^{31}P)$	+
$^1J(^{13}C, ^{19}F)$	-
$^1J(^{31}P, ^{19}F)$	-

The determination of signs of coupling constants can be of diagnostic value in drawing conclusions about electronic configuration and position. For example $^{2}J(^{31}P,^{13}C)$ and $^{3}J(^{31}P,^{13}C)$ often have opposite signs whereas their magnitudes may be similar[69].

1.4.2.3 Solvent Effects on Coupling Constants

The sensitivity of proton couplings, especially between P and H nuclei, to the change of solvent has been known for some time. The nature of the solvent is generally more important than the concentration[70]. The variation of couplings seems to depend on (1) co-ordination (for example phosphonium compounds are more susceptible than phosphorylated compounds[70]) and (2) on solvent polarity (pyridine causes greater sensitivity than chloroform or acetone[46]). Chlorinated species seem to produce a greater sensitivity (perhaps due to the polarisability of the chlorine) than non-chlorinated species. For example CH_3SPOCl_2 has J(P,H) of 25 Hz as a neat liquid whereas in a 50/50 cyclohexane solution J(P,H) is 19 Hz. Also when dealing with Lewis acids and bases, complexing contributions must be taken into account. Complexing behaviour is expected to produce the same effect as increasing substituent electronegativity. To a lesser extent $^{n}J(P,C)$ couplings exhibit solvent effects though it is difficult to assess all of the factors contributing to such minute effects.

1.4.2.4 $^{1}J(A,B)$ One-bond spin-spin coupling

Whereas $^{1}J(P,H)$ seems always to be positive and varies from about 100 to 1200 Hz, other P-X coupling constants vary over a similar range but can be positive or negative. This behaviour has been rationalised in terms of the Fermi contact interaction. For tetra-co-ordinate phosphorus species the phosphorus hybridisation is usually reasonably close to sp^3 and the behaviour is not unlike that of carbon in a

similar environment. In particular, the expected variations in response to changes in substituent electronegativity and small changes in the s-character of the orbitals are found. However, for tri-co-ordinate phosphorus much of the s-character is associated with the electron lone pair and very wide ranges in couplings can arise from comparatively small molecular changes.

1.4.2.5 $^{2}J(A,B)$ Geminal and $^{3}J(A,B)$ Vicinal Coupling Constants

Where spin-spin interactions occur over more than one bond, it is necessary also to include the properties of the intermediate atoms. If we use the simple example of CH_2 and consider the $^{2}J(H,H)$ coupling constant via the carbon, Hunds' Law of Maximum Multiplicity states that the two electrons nearest the carbon atom will tend to have parallel spins while the spins of the electrons associated with the two hydrogen atoms will be determined by the Pauli Principle and the Fermi contact interaction. This then will mean that the state with the lowest energy will be where the two protons have parallel spins, thus giving a negative value for $^{2}J(H,H)$. Experimentally this is true for a tetrahedral carbon atom but $^{2}J(H,H)$ can become less negative as the carbon-X bond increases in s-character with electronegative substituents through hybridisation effects, and may even be positive. For geminal coupling involving heavier atoms such as phosphorus, the atom tends to concentrate or polarise s-character in bonds with more electropositive groups (Walsh's Rule). This is well demonstrated by penta-co-ordinated compounds with different hybridisation. For example in Structure 3:

	sp^3d^2	p^3	sp^3
^2J(PCH) signs of couplings:	-	+	-

Structure 3

It is necessary to realise that there are more orbitals to be taken into account on the phosphorus and on the carbon atoms, and the effect of their substituents must be taken into consideration when estimating the sign and magnitude of the coupling constant. The stereospecificity of two bond coupling constants is also a factor[71] where cis and trans isomers are possible. The trans isomers generally have larger couplings. This can be extended to exo and endo and to syn and anti isomers. In phosphorus (III) compounds, the smaller coupling constants found for endo isomers are attributed to greater restriction of rotation around the P-C bonds when the lone pair is in an exo position. In tightly bound aliphatic systems, norbornanes for example, where geminal and vicinal couplings occur, evidence is accumulating that couplings between hydrogen and an element of the first or second row (e.g. ^3J(H,C), ^3J(H,F) depend on the appropriate dihedral angle in a similar way to the well studied ^3J(H,H) coupling in ethanes[72]. This relationship has been extended to other elements, for example ^{31}P [73], ^{119}Sn [74], ^{199}Hg [75]. An example is the dependence on dihedral angles ϕ for ^3J(P,H) as given by the Karplus-like equation[73] [1.11]:

$$^3J = A + B\cos\phi + C\cos 2\phi \qquad [1.11]$$

where A, B, and C are constants determined for particular systems. These relationships seem dependent upon the particular class of compound

and as yet no general relationship has evolved other than that for the vicinal coupling constants where a minimum is found to be near ϕ = 90°[42]. It also appears that there is a correlation between $^{2}J(P,C)$ and $^{3}J(P,H)$. Please see Section 3.3 for further examination of this relationship.

The introduction of electronegative substituents affects the coupling constants and a simple equation for calculating the couplings associated with a gauche orientation is given by equation [1.12]:

$$J_{H,H} = 4.0 + \Sigma(X_g + X_t) \qquad [1.12]$$

where X_g and X_t are shown by the Newman projection in Fig.1.4-1.

Fig. 1.4-1

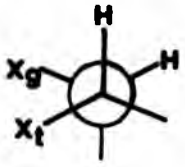

Table 1.4-6 gives representative values of effects for electronegative groups X_g and X_t for different groups. The trans-orientated coupling is usually obtained by comparison with a compound of fixed conformation.

TABLE 1.4-6 Effects of Electronegativity on Coupling Constants

X	H	C	Br	N	Cl	O	F
X_g	0.0	0.2	0.5	0.5	0.7	0.9	1.1
X_t	0.0	-0.6	-1.1	-1.4	-1.6	-1.8	-2.6

1.4.3.6 Long range Coupling Constants

The so-called 'Long range' interproton coupling is defined[76] as coupling between protons separated by more than three bonds. Typical magnitudes are up to 3 Hz and are thus normally smaller than for geminal or vicinal coupling constants. Long range couplings across metals in organometallic derivatives have also been reported[77]. Methods of calculation do not differ in kind from those for short range coupling constants, however a number of separate interactions involving the various electrons from intervening atoms must be considered. These have a characteristic dependence on steric and electronic factors. For example, long range coupling constants are more likely to be significant if the bond interaction pathway is planar[76] as is shown in Structure 4. The two most common types of

for H-C-C-C-C-H

Structure 4

long range interaction involve (1) coupling via the π-electron framework in unsaturated systems (σ-π configuration interaction) and (2) coupling across four single bonds. These treatments predict stereospecific pathways for effective coupling. However, any pair of protons or groups of protons in a real molecule may interact simultaneously via more than one path, with the result that actually observed coupling constants may be the algebraic sum of the interactions expected for each separate pathway.

1.4.3 Line Intensities

Factors which affect line intensities include NOE effects, line widths, line shape, pulsing rates, etc. and must be considered when comparing lines obtained in different spectra under similar conditions.

1.4.4 and 1.4.5 Relaxation

Nuclear relaxation provides the mechanism for the magnetic nuclei to lose the energy acquired in the NMR experiment. There are two major mechanisms of relaxation. One is when there is an establishment of thermal equilibrium between an assemblage of nuclear magnets with different quantum numbers (nuclear magnetization) along the magnetic field axis. This is termed Longitudinal Relaxation and denoted by T_1. The second occurs when there is an exchange of energy between two spin systems, for example between the spin energised in their NMR absorption process and the neighbouring nuclei possessing a magnetic moment. The associated relaxation time is known as the Spin-Spin Relaxation Time denoted by T_2.

1.5 The NMR Phenomenon in Detail

High resolution nuclear magnetic resonance spectroscopy is now usually accomplished by operating in the pulsed Fourier transform mode (FT-NMR). This is achieved by using a high-power radio frequency pulse of short duration which is applied to the sample. This causes a transient response and gives rise to the free induction decay (FID) in the time domain. The FID is sampled and is stored in the computerised data acquisition system. This FID in turn is Fourier transformed once with respect to one variable and yields the now familiar frequency domain one dimensional (1D) spectrum. Alternatively it can be double Fourier transformed with respect to two variables to yield a two dimensional (2D) spectrum. The experiment may be repeated many times to allow signal averaging and to improve upon the signal-to-noise ratio of the absorptions in the FID.

In present NMR spectrometers, where co-ordination of all timing and phase changes is under software control, the application of multiple R F pulses can be implemented and used to enhance resolution and elucidate particular phenomena. Many authoritative reviews have been previously provided, and especially applicable are those by Shaw[35], Gunther[78], Turner[79], Bax[80], and Ernst et al[81,82]. Hence only a brief summary of one-dimensional and two-dimensional theory will be undertaken here, and the description of pulse sequences, for the most part, will be of those which are applicable to this thesis and which are useful to organophosphorus chemistry.

1.5.1 One-Dimensional (1D) NMR

In a NMR experiment the effect of the pulse sequence, which may encompass a single pulse or a series of pulses depending upon the experiment, is acquired over a period of time to give rise to the

desired FID and hence the NMR spectrum. This time period or time axis may be broken into three major intervals which may help in the understanding of its components. This is shown in Fig. 1.8-1.

FIG. 1.8-1 General Subdivision of the Time Axis in a Multiple Pulse Experiment

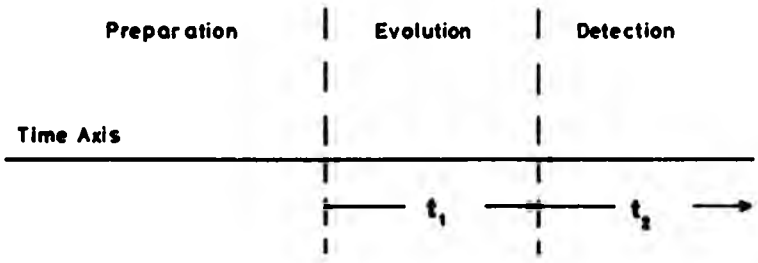

(a) The preparation period: initially the preparation period commences with a time interval that is long compared to the longitudinal relaxation time T_1. This allows the spins to come to thermal equilibrium. Then, at or near the end of the period at time $t=0$, a non-equilibrium state is created by, for example, a single $\frac{\pi}{2}$ R F pulse.

(b) The evolution period: as the time passes through the initial interval $t < t_1$ the non-equilibrium system evolves under the influence of the high field Hamiltonian $\mathcal{H}$ and the relaxation parameters and is dependent on the elapsed time ($t_{\mathcal{H}}$) in the experiment.

(c) The detection period: data collection starts at the end of the evolution period with the detection time.

Bloch Vector Model Diagrams[83] may be used to show schematically the effect of the pulse sequence on the Hamiltonian spin function(s). There now follows a description of some of the more important pulse sequences.

1.5.1.1 One-Pulse Sequence

This experimental pulse sequence is shown in Fig. 1.5-2.

FIG. 1.5-2 The One-Pulse Sequence

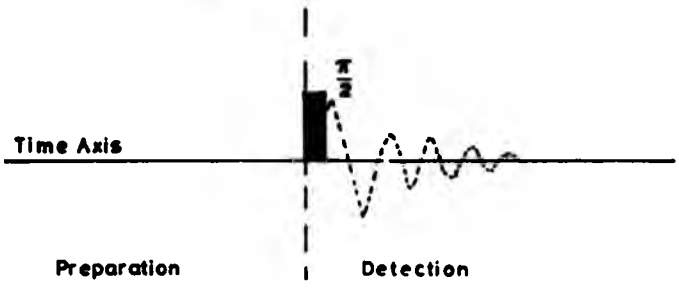

As can be seen, in this single pulse sequence no evolution time period exists as the FID is directly acquired after the application of the $\frac{\pi}{2}$ pulse.

Theory

When a spin-1/2 nucleus is placed in a magnetic field, the spinning nucleus will generate a magnetic field and may be therefore thought of as a magnetic dipole with a magnet moment $\underline{\mu}$. It can be shown by classical mechanics that a torque is exerted on the dipole with the result that $\underline{\mu}$ varies with time. The equation of motion is:

$$\dot{\mu} = \gamma_N \hbar [I(I+k)]^{1/2} = \gamma_N \hbar \underline{I} \qquad [1.13]$$

where γ_N is a constant known as the magnetogyric ratio which characterises the particular nucleus. Equation [1.13] can be solved to show that the dipole precesses around the field direction $\underline{B}_o$ with angular velocity given by:

$$\bar{\omega} = -\gamma_N \underline{B}_o \qquad [1.14]$$

This type of precession is called Larmor precession where $/\bar{\omega}/$ is the Larmor frequency and is given by:

$$\nu_o = \frac{\gamma_N}{2\pi} B_o \qquad [1.15]$$

For example, for an induction of 2.1 Tesla, the proton Larmor frequency is 89.56 MHz, and resonance is said to occur when equation [1.15] is exactly fulfilled.

In the Rotating Frame

Here we are concerned with the way the magnetic moments $\underline{\mu}_i$ of the nuclei move with time in the external magnetic field $\underline{B}_o$ under the influence of an applied radiofrequency. We may define a stationary co-ordinate system (x',y',z') and a second system (x,y,z) which rotates about $\underline{B}_o$ in the same direction as $\underline{\mu}_i$ and at the same angular velocity $\bar{\omega}$. We can observe $\underline{\mu}_i$ in this rotating frame (x,y,z,). It can then be shown that the time dependence of the magnetic moment has the form:

$$\mu_{rot.} = \gamma_N \bar{\mu}(B_o + \bar{\omega}/\gamma_N) \qquad [1.16]$$

$\bar{\omega}/\gamma_N$ can be considered as a "fictitious field" arising from the effect of rotation as observed in the rotating frame. If we let $B_o + \bar{\omega}/\gamma_N = B_o$ eff. where B_o eff. is the effective field then the magnetic moment is given by:

$$\mu_{rot} = \gamma_N \bar{\mu} B_o \text{eff.} \qquad [1.17]$$

Hence the magnetic moment precesses about B_o eff. and rotates about B_o.

In the NMR experiment however, we are interested in the bulk magnetic moment of a large number of nuclei where $\underline{M}$ is the vector sum of the $\bar{\mu}$ for each nucleus. It can be shown that the equations just described for a single magnetic moment are equally applicable to $\underline{M}$.

$$M = \gamma_N . M . B_o \qquad [1.18]$$

$$M_{rot} = \gamma_N \quad M . B_o \text{eff.} \qquad [1.19]$$

Thus in the rotating frame M will precess about B_o eff.

Previously we have shown that a nucleus of moment μ will precess about an applied field B_o. Other identical nuclei will also behave

similarly and we can represent their μ_1 by vectors all with the same origin, spread on the surface of a cone as shown in Fig. 1.5-3. The z components of μ can be considered to be with or against the field. Since slightly less nuclei will be in the higher energy level, there is a resultant component of magnetization along the z-axis and therefore in the same direction as B_o.

FIG. 1.5-3 Overall Bulk Magnetization with Magnitude M_o in Direction of B_o

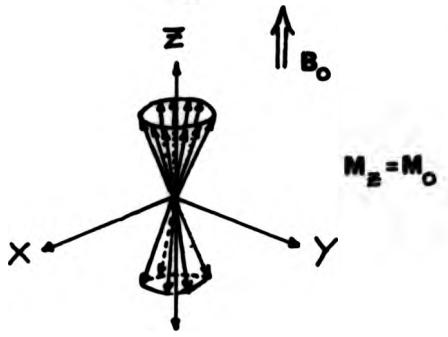

Since the individual μ's are randomly spread out over the surface of the cone their x- and y- components cancel. Thus the bulk residual magnetization of vector M will have a total magnitude of M_o and will lie in the same z direction as B_o. If we now consider the application of a one-pulse sequence in terms of this concept, this can be demonstrated by the Bloch Vector model in Fig. 1.5-4[A].

FIG. 1.5-4 A Bloch Vector Model of the One-Pulse Sequence

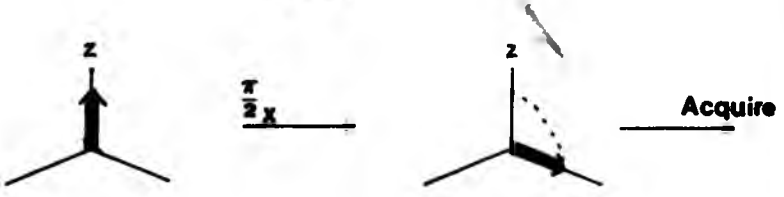

At equilibrium, prior to the $\frac{\pi}{2}$ pulse , the transverse magnetisation is zero. However when a $\frac{\pi}{2}$ pulse is applied along the x-axis, M_o is rotated through 90° and becomes colinear with the y-axis giving rise to magnetisation which is detected by the spectrometer to give the NMR signal. This system is now in a nonequilibrium condition because the axes are rotating at resonance frequency and thus the system returns to equilibrium by the two relaxation processes T_1 and T_2. The magnetisation returns to equilibrium along the z-axis by the spin-lattice relaxation mechanism governed by:

$$M_z = M_o \left(1 - e^{-t/T_1}\right) \qquad [1.20]$$

where t is the time taken after the $\frac{\pi}{2}$ pulse and is associated with a loss in magnitude of the signal. Also at the same time magnetisation in the x-y plane relaxes according to the spin-spin relaxation mechanism governed by:

$$M_{xy} = M_o e^{-t/T_2} \qquad [1.21]$$

The other major contributions to relaxation in the x-y plane arises from spin-spin coupling to neighbouring nuclei and the inhomogeneity of the external magnetic field B_o. The latter point is generally the major contribution to relaxation, and to take into account of the effects of field inhomogeneity and the small amount of true T_2 relaxation, this relaxation is expressed as an effective transverse relaxation time T_2^* and is defined as:

$$\frac{1}{T_2^*} = \frac{1}{T_2} + \gamma \Delta B_o \qquad [1.22]$$

such that ΔB_o is the magnetic field inhomogeneity across the sample.

In addition to the effect of the relaxation mechanisms T_1 and T_2, the magnetisation along the y-axis is modulated as a result of the

difference between the Larmor frequency itself and the frequency of the rotating frame (the spectrometer carrier frequency). These individual frequency modulations arising from single frequency resonances from the rotating magnetic vectors (v) in the x-y plane produce an induced voltage in the receiver coil from their intensities, and this is detected as the NMR signal. This may be plotted on a graph of induced voltage vs. time and will be shown as a damped oscillation which is called a Free Induction Decay (FID). This is shown in Fig. 1.5-5.

FIG 1.5-5 A ^{31}P NMR Resonance FID of Triethyl Phosphine

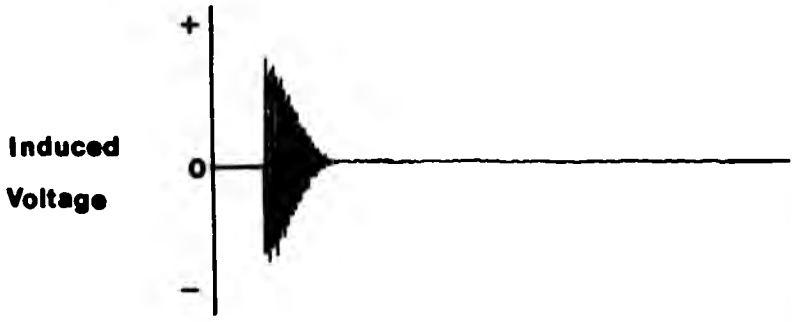

This however is an over simplification and though modern-day magnets have vastly improved since the pioneering days of Hahn, slight magnetic field inhomogeneities still exist throughout this macroscopic ensemble of nuclei. This will mean that the individual vectors v will have slightly different associated Larmor frequencies and a small fanning will occur arising from those vectors which rotate faster (I) and those that rotate slower (II) than the local average condition. The overall effect of this fanning is to further reduce the effective magnitude M_o in the x-y plane. This can be shown in vector notation in Fig. 1.5-6.

FIG. 1.5-6 The Precession of Spins in a Rotating Frame

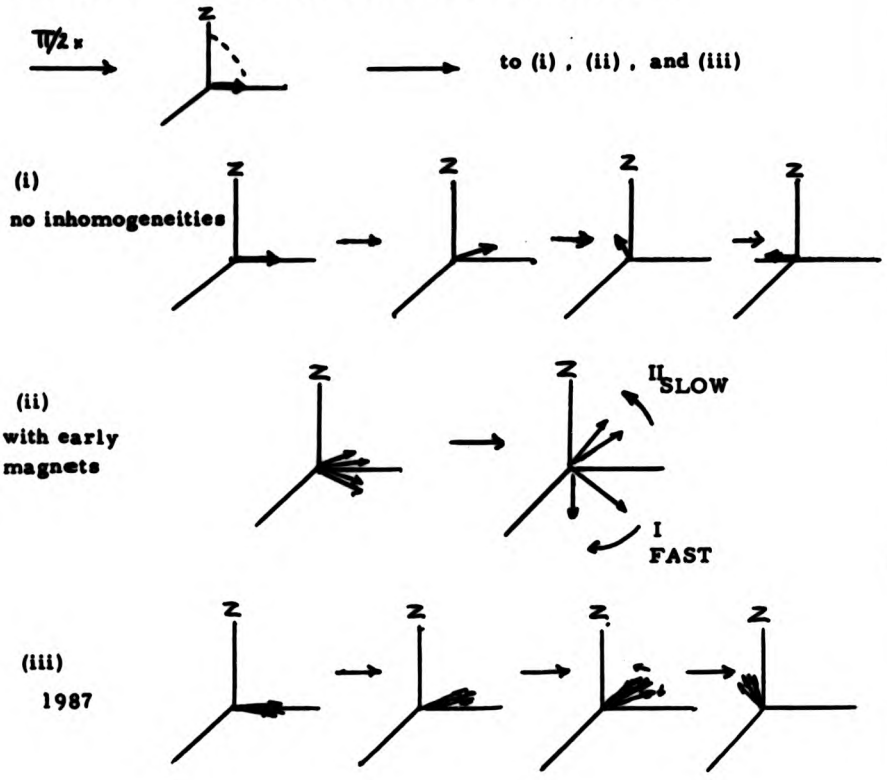

This generates an inhomogeneity in frequency which contributes substantially to the total transverse relaxation and may be detected as line broadening.

1.5.1.2 1D Spin-Echo Sequence

The spin-echo experiment developed by Hahn[84] to eliminate the effect of the inhomogeneity B_o on the measurement of T_2, is shown in Fig. 1.5-7.

FIG. 1.5-7 The Pulse Sequence of a Spin-echo Experiment

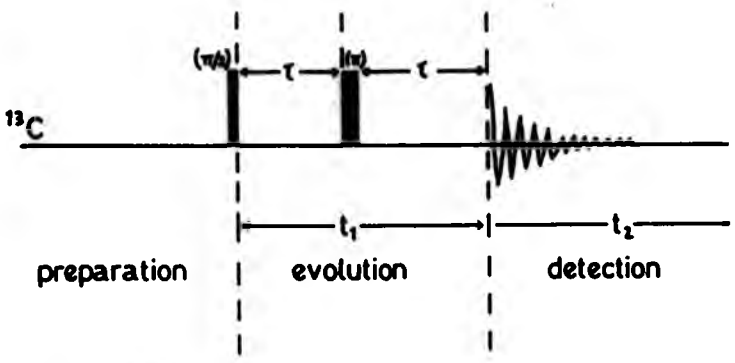

When a $\frac{\pi}{2}\underline{x}$ pulse is applied, this will rotate the net magnetization vector into the x-y plane where it will then precess and decay by a T_2 mechanism.

Precession is allowed for a precise time $\underline{\tau}$ at which point a $\underline{\pi y}$ pulse is applied. This flips all magnetization vectors $\underline{v}$ about the $\underline{x}$-axis but it does not affect their rotational direction. See Fig. 1.5-8[B].

FIG. 1.5-8 Manifestation of a Spin Echo

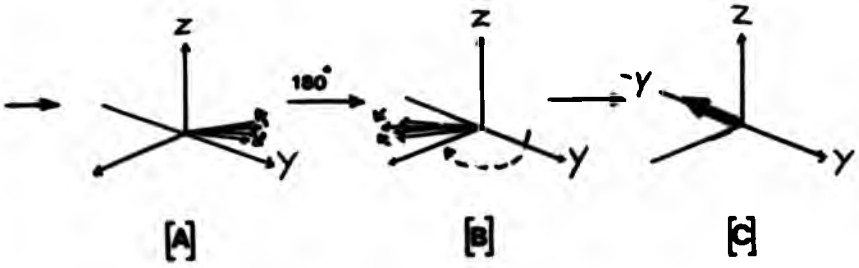

After a further $\underline{\tau}$ period this will refocus all vectors to their original positions along the $\underline{y}$-axis. This is called the Spin-echo, Fig. 1.5-8[C]. The magnitude of the echo will be less than of the original magnitude value $\underline{M_o}$ of $\underline{M}$. The decay in the signal as the

system returns to equilibrium to produce the FID will thus be a measure of the real T_2, the random processes of transverse relaxation[85]. If a particular sample contains nuclei with different T_2 relaxation times, the decrease in spin-echo maximum amplitude will be different for their different resonances. Thus the experiment may be repeated by changing the τ interval, storing that information in the computer and incrementing systematically the τ to produce a set of data (a stack) to determine those different T_2 relaxation times.

Though the spin-echo experiment as such was not used in this thesis, it is a basis from which many other applications which are useful to the organo-phosphorus chemist occur. Of these we will describe an assign or GASPE pulse sequence[86].

1.8.1.3 The GAted SPin Echo (GASPE) Pulse Sequence

The basic pulse sequence is given in Fig. 1.8-9.

FIG. 1.8-9 The GASPE Pulse Sequence for Heteronuclear Multiplicity Selection

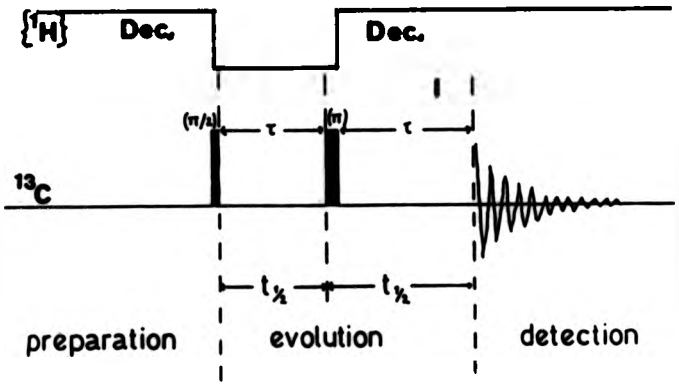

In this thesis the GASPE pulse sequence is used to separate resonance of CH and CH_3 groups from CH_2 and quaternary groups by multiplicity selection.

Multiplicity Selection

Consider a spin-echo experiment performed in the rotating frame upon an isolated AX spin system, such as chloroform, where carbon is the detected nucleus. If we ignore magnetic field inhomogeneities then there are two carbon vectors associated with the opposite spin states of hydrogen. They are CH_α and CH_β. These will precess at a rate relative to the mean chemical shift. After a time $t = \frac{1}{J}$ the vectors H_α and H_β will have diverged ahead and behind of the mean position. Application of the π refocussing pulse on carbon will flip these vectors so as to interchange their positions. They will however continue to precess at the same relative rates and at a further time $t = \frac{1}{J}$ they will be re-aligned along the y-axis and a normal spectrum will occur. On the other hand, if proton decoupling was turned on just after the refocussing pulse, then the two carbon vectors will precess at the same rate as the mean chemical shift position. Thus after a time t the two vectors will be aligned along the y-axis 180° away from the chemical shift mean and this will give rise to an inverted though decoupled signal in the spectrum. This general case may be applied to other multiplet components of the form AX_n where n is odd, though the outer vectors will have made several revolutions in the rotating frame but will finally rest along the $-y$-axis to give the inverted decoupled spectrum. In the case where n is even in a AX_n system, all the vector components will be in phase with the mean chemical shift position when the refocussing pulse is applied. Thus when the decoupler is turned on this will be maintained and a normally phased decoupled signal will appear.

Thus in the GASPE sequence, echo-modulation is employed to simplify the interpretation of resonances by altering the phase of selected signals in the final spectrum[86]. A particular ^{13}C spin-echo will be

phase-modulated *via* its C-H coupling. This phase-modulation will discriminate between carbon signals on the basis of even or odd numbers of attached protons. The modulation is induced by interrupting the decoupler (gating the decoupler, see below) for a precise period length $\frac{1}{J}$ which is related to the reciprocal of the appropriate coupling constant. Therefore these experiments require the presence of a limited and predictable set of coupling constants[86]. For example, an average value for ^{1}J (C,H) is about 140-145 Hz and thus a choice of a value of $(\frac{1}{J}) \approx 7$ msec. would reflect this. With this interval the phases of the, say, odd-proton carbons (CH and CH_3) will be opposite to those of the even-proton carbons (CH_2 and $-\overset{|}{\underset{|}{C}}-$). For the experimental work in this thesis a preparation period of 3 T_1 seemed adequate for relaxation between transients. A typical transformed spectrum is shown in Fig. 1.5.-10.

FIG. 1.5-10 A 1D $^{13}C\{^{1}H\}$ normal [A] and a GASPE $^{13}C\{^{1}H\}$ [B] spectrum of 2-chloronorbornane.

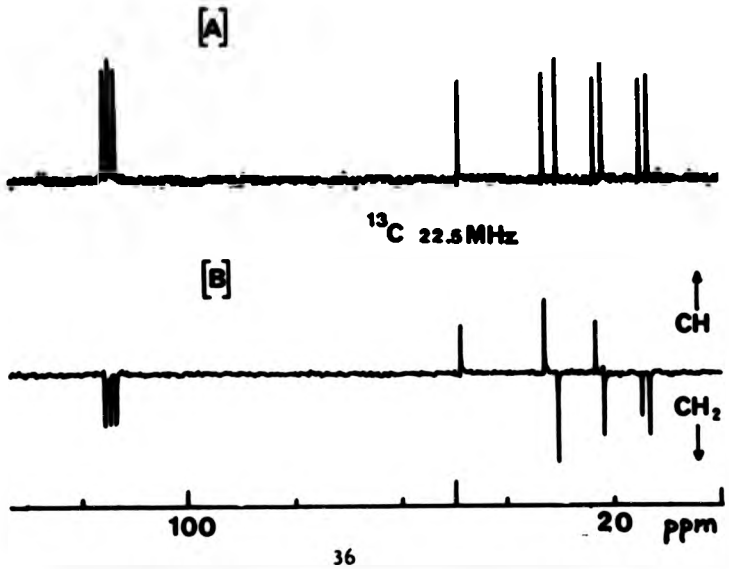

Alternatively the experiment may be performed by having the decoupler on during the period before the π pulse has been applied, off in the τ period following it, and on during acquisition. This however requires more slightly sophisticated hardware[87]. Both methods result in similar theoretical arguments and spectra.

Gated Decoupling

Because pulsed NMR data is acquired in the time domain it is possible to use gated decoupling to reject or to retain the NOE at will, according to conditions before and after the exciting R F pulse. This can be thought of as having two distinct time periods to apply decoupling as shown in Fig. 1.5-11.

FIG. 1.5-11 The Two Periods for Gated Decoupling

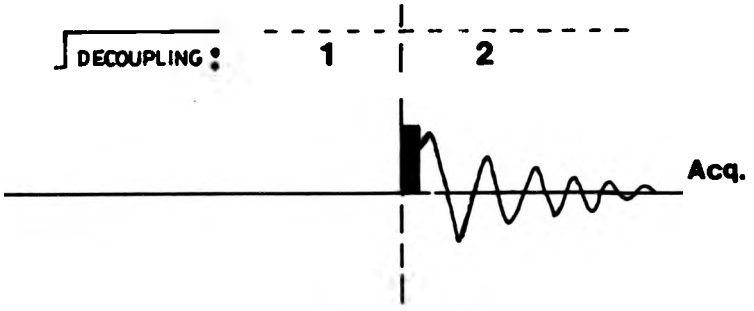

In a normal experiment, e.g. $^{13}C(^{1}H)$, the decoupler is on throughout periods 1 and 2 so that the decoupled spectrum enjoys NOE enhancement. If the decoupler is turned off during the period 2, a proton-coupled spectrum will be obtained because the decoupler response is rapid but owing to the relative slowness of the relaxation processes the NOE will still be present. This will apply on subsequent scans if period 1 is sufficiently long enough to allow proton saturation to occur. However if the decoupler is on during period 2 and off during period 1, a

decoupled spectrum without NOE will be obtained. Here, insufficient time is available for the protons to become saturated. In this case though, period 1 must be long enough to allow the protons to be able to return to equilibrium, ca. 10 T_1 (H), after their partial saturation during period 2. These two techniques, which are called gated and inverse-gated decoupling, are provided as standard on most NMR spectrometers[88].

1.5.2 NMR with Two Frequency Dimensions (2D-NMR)

Two-dimensional NMR: experiments in which the resulting spectrum contains two separate frequency axes in addition to the vertical intensity co-ordinate were suggested by Jeener[8] in 1971, and the method was implemented by Ernst[81,89] in 1976. The idea is based upon performing a series of spin-echo or other experiments associated with a variable time interval t_1 which is incremented systematically between successive experiments to create a set of free induction decays, each with a parameter t_2 as its running time variable. A 2D Fourier transformation is performed on the data set (see Section 1.6) and the resulting two-dimensional spectrum can then be shown as a montage in which the F_2 axis corresponds to the dispersion obtained in a normal one-dimensional experiment. The relationship of signals to the two axes can give many useful correlations of coupling constants with chemical shifts, or of the shieldings of different nuclear species. Very many different types of 2D experiments and pulsing schemes have been employed to obtain or highlight a particular phenomenon, mainly with the ^1H and/or ^{13}C in mind. For example, mapping of proton-proton coupling via Double Quantum Coherence[90] and elucidation of chemical exchange networks by 2D ^{13}C NMR spectroscopy is now possible[91]. Also a number of applications to ^{31}P and ^{15}N nuclei have been reported. A nice example has been reported

using 2D $^{15}N/^{1}H$ correlation for conformational analysis of Gramicidin A[92].

The experimental pulse format used will limit what the final 2D spectrum will contain. In general however, most of the 2D NMR experiments can be considered as a partitioning of the time axis into distinct periods as previously mentioned for 1D NMR in Fig. 1.5-1. These may now define the two time intervals t_1 (the evolution period) and t_2 (the detection period) of the time function $S(t_1,t_2)$.

With this in mind, it is now however probably easiest to understand the ideas of 2D NMR by reference in specific examples.

1.5.2.1 *J*-Spectroscopy

J-spectroscopy has come to the fore in organo-phosphorus chemistry as a viable sorting technique enabling a direct and unambiguous determination of both coupling constants and chemical shifts. Serious signal overlap in systems with more than two or three spins can be eliminated in the 2D spectrum, by spreading along two axes - chemical shifts along F_2 and spin-spin couplings along F_1. Though many different pulse sequences have now been created to elucidate heteronuclear and homonuclear coupled spin-systems most of these stem from the original Hahn sequence[1] using a standard (90° - $\frac{1}{2}$ - 180° - $\frac{1}{2}$ - acquire) experiment to create the spin-echo. A typical example is shown in Fig. 1.5-12.

FIG. 1.5-12 The Basic Scheme for J-Spectroscopy for ^{13}C Irradiation With Evolution (t_1) and Detection (t_2) Periods

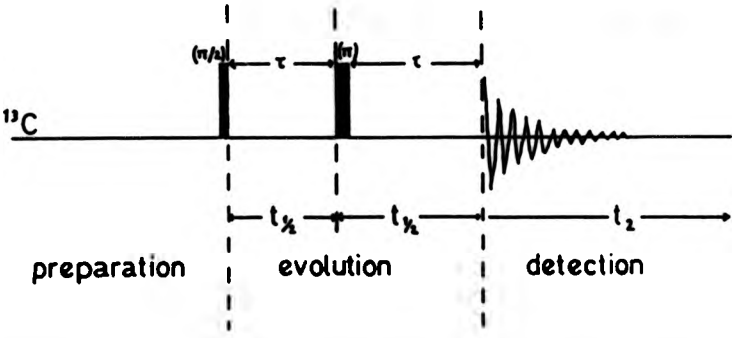

If we assume the case when coupling between all nuclei is weak and relaxation effects can be neglected we can consider this experiment on a homonuclear AX spin system in the rotating frame. In this case the 180° refocussing pulse has two effects: not only does it generate the spin-echo, it also inverts the X-spin thereby interchanging the labelling of the two A-spin states so that at the time of echo formation the two A-vectors are not completely refocussed even though the chemical shifts and the effects of magnetic field inhomogeneity are. Indeed, the signal obtained at the peak of the echo (i.e. at time 2τ will have an intensity which varies as a sinusoidal function of τ, and a series of experiments for a succession of values of τ will yield a data set (one point for each τ) which may be Fourier transformed with respect to τ to give a so-called J-spectrum consisting of a pair of lines at $\pm$ J(AX)/2 centred about zero frequency. Exactly the same arguments can be applied to the behaviour of the X-spins, and they will give an identical J-spectrum; since only the first point of each echo is sampled there will be no discrimination of precessional frequencies in the FID and the J-spectrum will be one-dimensional with the components due to A- and X- exactly superposed[85]. Note also that the lines of J-spectra should be very sharp as magnetic field inhomogeneity effects have been refocussed at time 2τ when the echo is sampled, and only true T_2 relaxation should remain. For first-order homonuclear systems of several spins the J-spectrum will be a number of pairs of lines, each symmetrical about zero frequency and giving the corresponding coupling constant directly.

In practice the spin-echo continues to be available for sampling after time 2τ since it is just like a normal free induction decay. Consequently, the behaviour of each individual line of the normal spectrum can be studied as a function of τ (which now must be referred to as t_1) by transforming each individual echo with respect to the running time

variable t_2 in the usual way. Thus in effect a separate J-spectrum is obtained for each line of the 1D spectrum, and a stacked plot of all the spectra (including the many traces that will have no signal at all) gives the full 2D spectrum. A refinement is that by suitably manipulating the real and imaginary parts of the spectra from the double Fourier transformation it is possible to obtain only one line (rather than a pair) for each coupling associated with a particular line of the 1D spectrum.

The 2D J-resolved spectrum of a homonuclear AX spin system is shown graphically in Fig. 1.5-13. It has four lines (black crosses) with co-ordinates $\nu_A \pm J/2$ and $\nu_X \pm J/2$ in the F_2 dimension, and $\pm J/2$

FIG. 1.5-13 A Graphical Representation of a 2D J-resolved Spectrum for a AX Spin System.

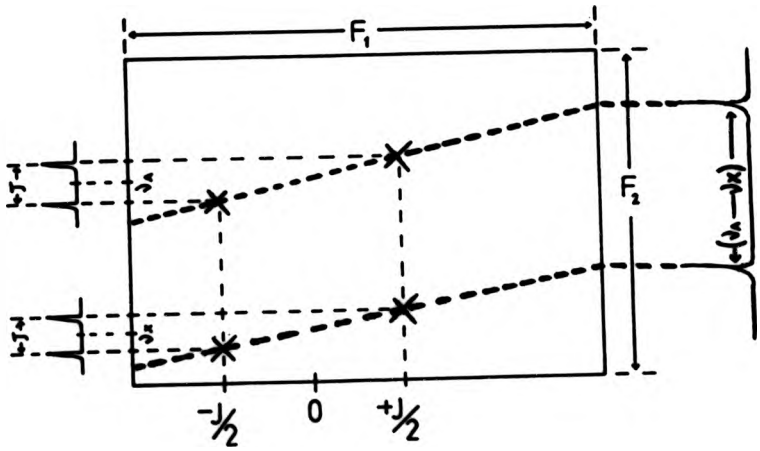

in the F_1 dimension, thus providing a separation of splittings due to spin couplings and those due to chemical shift differences. A straightforward projection onto the F_2 (vertical) axis gives the normal 1D spectrum with full coupling constant and chemical shift dispersion as shown at the top of the diagram, while a projection onto the F_1 axis would give a two-line J-spectrum. An important feature is that the line separations due to coupling constants are identical in the two dimensions so that a 45° projection leads to one component of each J-doublet being superimposed upon the other, and only one line is obtained for each chemical shift position. This is shown in red in Fig. 1.5-13 and it may be noted that although the peaks have been moved sideways their relative separations have been maintained. Thus, the effect of homonuclear broadband decoupling has been achieved[88]. This is a completely general result provided that any extra lines due to second order features are weak, and shifts of lines from their first-order positions are not much more than the line width; the simplification that it can bring about in complex spectra can be very useful. Also in the cases where overlapping arises it is possible to select individual multiplets by taking cross-sections of the complete 2D spectrum. An important feature of this experiment is that homonuclear couplings well in the excess of 100 Hz have been removed in compounds including metal complexes[93]. This would be difficult or impossible to achieve using conventional decoupling techniques[87]. A simple modification to the above experiment makes it suitable for heteronuclear systems. See Section 2.2.2.

In the case of ^{13}C observation with proton π pulses and the proton decoupling during the acquisition period, the resultant 2D spectra have ^{13}C chemical shifts in the F_2 dimension, and proton-coupled ^{13}C multiplets in F_1. The most used versions on the pulse sequences for 2J J-spectroscopy are the four shown in Figs. 1.5-14.

FIG. 1.5-14 Pulse Sequences for 2D J-spectroscopy

[A] and [B] proton flip methods
[C] and [D] gated decoupling methods

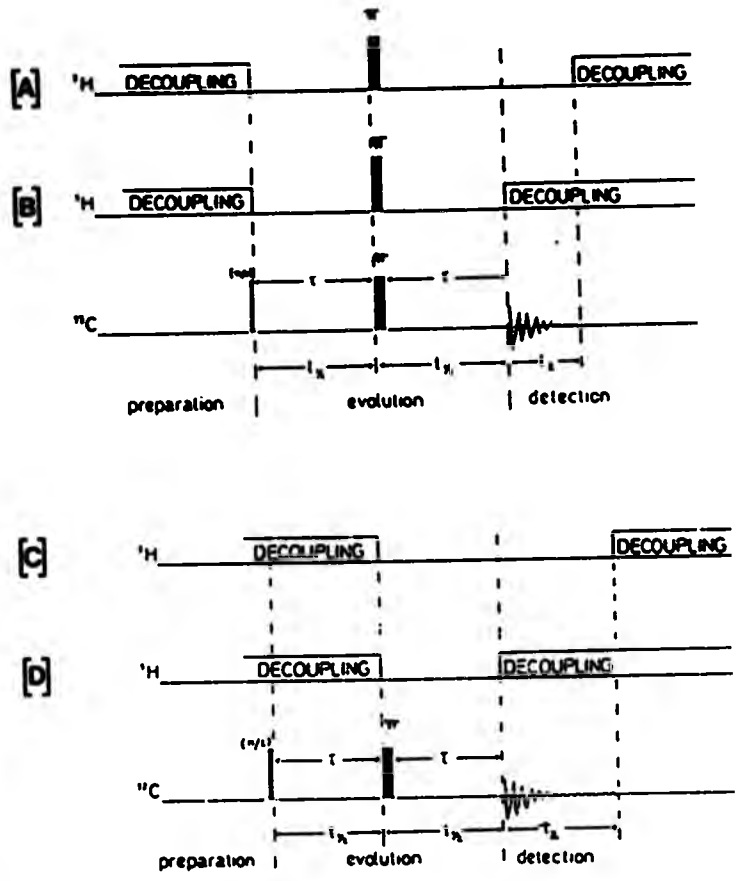

In Fig. 1.5-14[A] and [B] are shown so-called proton flip experiments. A π pulse is applied simultaneously to both the ^{13}C and ^{1}H spins inverting both the spin populations together. With coupling active in the whole evolution period, J-modulation is allowed for the whole period and thus good resolution may be achieved. The sequences in Fig.1.5-14[C] and [D] show the alternative approach, the so-called gated decoupler

versions, as previously mentioned in Section 1.5.1.3. Here proton noise decoupling is applied for half of the echo time t_1. This can be applied in the first or last portion of the echo as they give similar results. In this case coupling is only active for half of the evolution period, and hence J-modulation will be reduced to half as well. In this sequence proton decoupling prevents the refocusing of the ^{13}C-X multiplets, whereas without decoupling refocusing would occur. In both types of sequence parts [B,D] show ^{13}C as the detected nucleus to be decoupled during the detection period and thus only chemical shift information along F_2 will occur. This is shown in red in Fig. 1.5-43. In parts [A,C] the sequences show the decoupler to be off during the detection period, hence the F_2 axis will also contain coupling information. This experiment is also of value in ^{31}P NMR, although the presence of homonuclear coupling can cause problems[94]. The method however has clear potential for other heteronuclear combinations and a new sequence is in Section 2.2.2 which describes the use of the 2D J-resolved experiment where ^{13}C chemical shifts are correlated with ^{31}P-^{13}C coupling constants with proton decoupling in both dimensions.

Though 2D J-spectroscopy is very useful, one has to be aware of a few inherent problems with the technique and hence take steps to minimize these difficulties. For example, systems which are not first order produce multiplets with asymmetry in their spectra. Hence it is important to be able to distinguish between negative and positive frequency components. To achieve this, proper linear combinations of the four quadrants resulting from the 2D transformation must be used[95]. However in most commercial spectrometers quadrant manipulation is limited and the absorption-absorption quadrant is usually the only one available. This quadrant is chosen because it gives the most easily phased and best line shape and greatest resolution for the absorption signals. This is so only when the carrier frequency is placed in the centre of the spectral

width on the zero line in the F_2 axis. This also allows for more effective use of decoupling power[80]. Secondly, imperfections in the refocusing pulse may give rise to spurious signals known as phantoms and ghosts which lie askew of the line of symmetry of the particular multiplet[96]. These artifacts may be effectively suppressed by phase cycling the detection pulses with respect to both each other and to the receiver reference by an Exorcycle method[96]. The pattern of phases used is given in Table 1.5-1.

TABLE 1.5-1 Phase cycling sequence for 2D $^{13}C/^{1}H$ J-spectroscopy*

Cycle	Phase Angles (deg.)		
	90° Carbon pulse	180° Carbon pulse	Receiver ref.
1	0	0	0
2	0	90	180
3	0	180	0
4	0	270	180

* Taken from ref. 96

Thirdly, resolution along the F_1 axis which contains no chemical shift information (see Fig. 1.5-13) is determined by the number of t_1 values and hence the number of experiments performed in each stack. For high resolution in this F_1 dimension, small spectral windows or a great number of t_1 intervals must be used. Also digital filtering is not possible in this dimension so care must be taken to avoid foldback. For example, by restricting the digital resolution to 5-10 Hz in the F_1 dimension it is possible to avoid confusion from long-range ^{13}C-^{1}H couplings and thus readily determine the number of protons attached to each carbon on the basis of the one bond coupling[97].

1.5.2.2 2D Heteronuclear Shift Correlation

One of the more useful applications of two dimensional NMR spectroscopy for organo-phosphorus chemistry is the heteronuclear chemical shift correlation experiment. This technique was put forth by Maudsley and Ernst[88] and by Aue, Karhan and Ernst[89] and relies on an indirect approach. Chemical shift correlation is usually envisaged through the $^{13}C/^{1}H$ nuclei pair, though in principle any pair of nuclei may be used for the correlation experiment[80]. One nucleus is detected during acquisition and the magnetisation from the other nucleus of the pair is transferred to that detected nucleus through their spin-spin coupling interaction. The sequence thus identifies pairs of nuclei associated with chosen sizes of coupling, often selected to correspond to directly bonded atoms. Since the mechanism for transfer is through scalar coupling interaction, each of the different groups in the sample will give rise to an absorption on the correlation map. The chemical shift information for the non-detected nucleus is displayed along the t_1/F_1 dimension and the chemical shift information for the detected nucleus is displayed along the t_2/F_2 dimension.

1.5.2.2.1 $^{13}C/^{1}H$ Heteronuclear shift correlation

In the $^{13}C/^{1}H$ pair it is most convenient to detect the ^{13}C directly for the reasons which are given in Appendix 1. The basic experiment is used to relate ^{1}H chemical shifts to <u>known</u> ^{13}C chemical shifts by heteronuclear scalar spin-spin coupling mechanisms. The basic pulse sequence used to achieve this correlation is given in Fig. 1.5-15. Here, protons are indirectly detected <u>via</u> their free precession during the <u>t_1</u> evolution period and the extent of the ^{1}H precession is measured by the amount of magnetisation transferred to the carbon nuclei by the end of this period.

FIGURE 1.5-15 The Basic Pulse Scheme for 2D $^{13}C/^{1}H$ Heteronuclear Shift Correlation

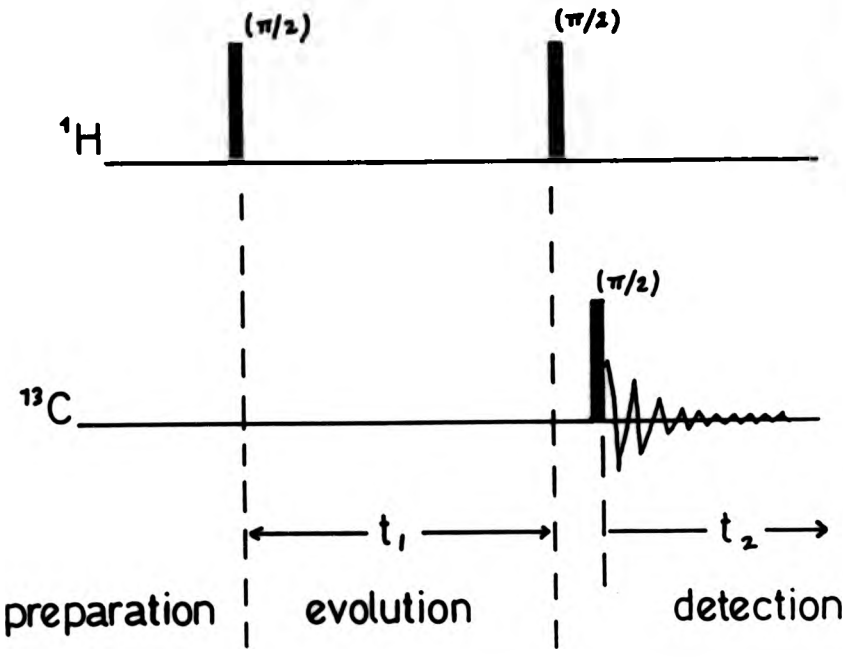

Magnetisation Transfer

For an isolated ^{13}C-^{1}H spin system heteronuclear pair the energy level diagram is shown in Fig. 1.5-16.

Initially the spin populations are at equilibrium through the Boltzman distribution mechanism. The corresponding populations of the energy levels may be represented by the numbers in the brackets [], reflecting that $^{13}C\gamma = 1/4\ ^{1}H\gamma^{100}$. This is shown in Fig. 1.5-16 (A). A population inversion is created selectively so that only one of the proton transitions is affected. This is shown in Fig. 1.5-16 (B) and as can be seen the ^{13}C transition between $H_\alpha C_\alpha$ and $H_\beta C_\beta$ experiences a five-fold increase in intensity, while that between $H_\beta C_\alpha$ and $H_\beta C_\beta$

FIGURE 1.5 -16 An Energy Level Diagram with the Associated Wave Function Combinations for an Isolated ^{13}C-^{1}H Spin-System*

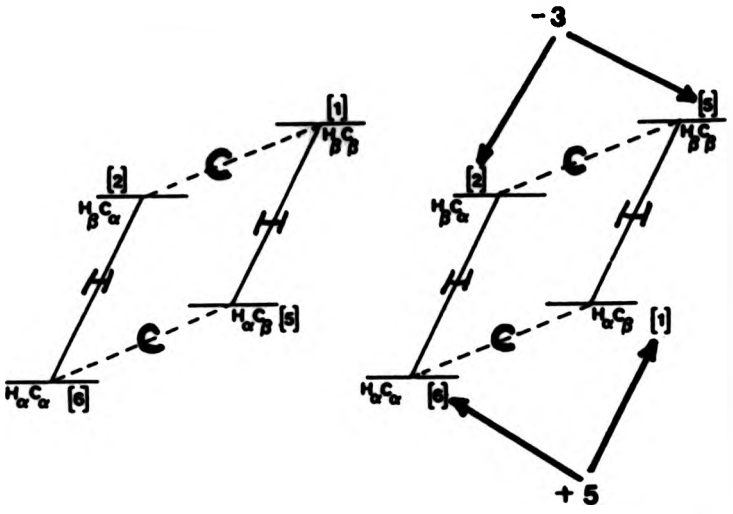

(a) Relative spin populations [] at Boltzmann equilibrium.

(b) Relative spin populations [] after selective population transfer

* taken from ref. 99

experiences a three-fold inverted increase in intensity. This is known as a selective population transfer[101,102]. This effect is achieved in the two-dimensional experiment by the sequence given in Fig. 1.5-15 which effects selective population inversions for all the resonances in the proton spectrum attached to the carbon nucleus. As stated previously, the length of the t_1 evolution period will determine the amount of population inversion which will occur. Fig. 1.5 -17 represents the effect of population on the t_1 interval.

FIGURE 1.5-17 A Vector Representation in Terms of Spin Populations of an Isolated $J(^{13}C,^{1}H)$ for Magnetization Transfer

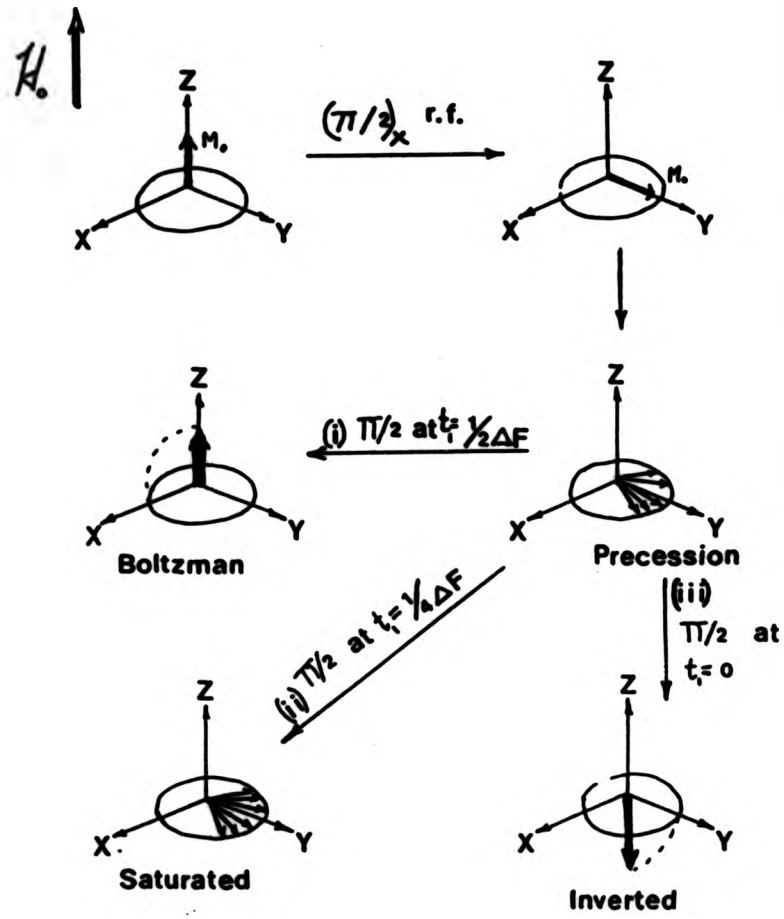

H_0 = magnetic field direction

M_0 = the magnitude of vector M

ΔF = the offset difference between a proton resonance and the proton transmitter frequency

As in the shift correlation sequence in Fig. 1.5-15 a $\frac{\pi}{2}$ pulse is applied to the protons. This will create transverse magnetisation in the usual way. Precession of these vectors is allowed for a period of t_1, after which a second $\frac{\pi}{2}$ pulse is applied. If the t_1 evolution period is long enough for a 180° precession to occur, the effect of the second $\frac{\pi}{2}$ pulse will be to return the vector to the +z axis. This corresponds to Fig. 1.5-17 (i) and is comparable to the Boltzman equilibrium population. If on the other hand, the t_1 evolution period allows the transverse magnetisation vectors to precess through 90°, the second pulse will have no effect and the vectors will remain in the x-y plane. In this case there will be zero z-magnetisation. This is shown in Fig. 1.5-17 (ii). Thirdly, if no precession is allowed, i.e. no t_1 evolution period, there will effectively have been a 180° pulse which will have inverted the spin populations to the -z-axis. This is shown in Fig. 1.5-17 (iii). For intermediate timings, population inversion is incomplete and cosine modulations will occur as a function of the time t_1. As a consequence of this, the two ^{13}C transitions, which share a common energy level with the protons involved, will also have their z-magnetisation affected and thus be sensitive to these changes in modulation. A $\frac{\pi}{2}$ ^{13}C pulse is then applied to read the population changes. To achieve better S/N in the transformed spectrum the experiment may be repeated many times. A delay time of ca. 5 T_1 to 10 T_1, where T_1 is the longitudinal relaxation time of the protons, is in principle necessary between scans to provide proper relaxation, however in most cases 1.3 T_1 is adequate and indeed may give optimal sensitivity[103].

The 2D $^{13}C/^{1}H$ shift correlation spectrum of an isolated ^{13}C-^{1}H spin system is illustrated graphically in Fig. 1.5-18.

FIGURE 1.5-18 A Schematic Representation of a Heteronuclear Shift Correlation for an Isolated AX Spin System

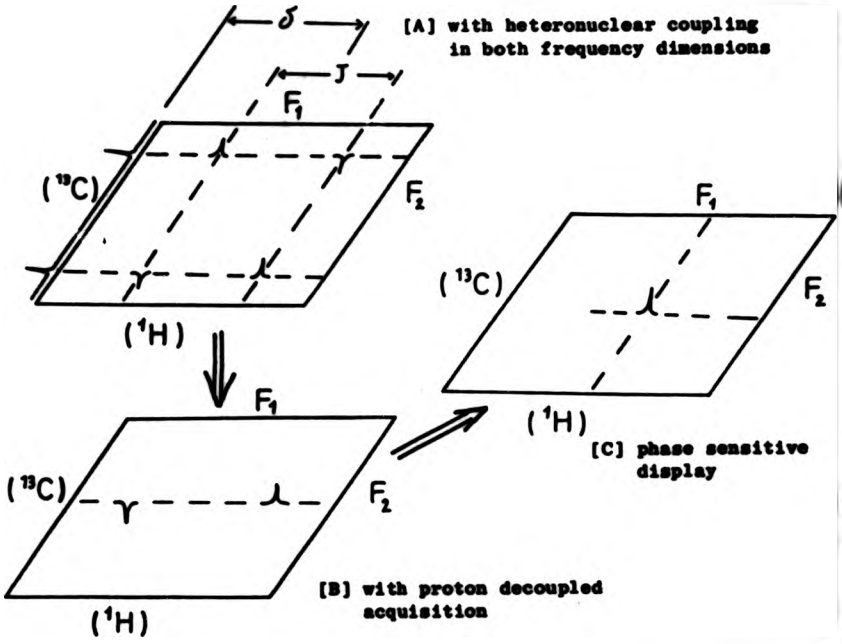

2D Fourier transformation with respect to t_1 and t_2 results in a 2D spectrum. As seen in Fig. 1.5-18[A] doublets occur in the F_1 dimension as $\delta H = \pm \frac{1}{2} J$. Their signals are doubled since both carbon transitions will be detected. There is no net magnetisation transfer and thus the two signals are of opposite phase and have equal amounts of positive and negative intensity. In order to simplify the resulting spectra the protons may be decoupled during acquisition of the ^{13}C signal. However if decoupling is started immediately after the $\frac{\pi}{2}$ ^{13}C pulse, the modulated anti-phase signals would mutually cancel. This can be avoided by delaying decoupling by a time $\Delta_2 = \frac{1}{2J}$ after the $\frac{\pi}{2}$ ^{13}C pulse, so that the ^{13}C vectors are parallel again, and an additive signal at the ^{13}C frequency can be detected. The result is shown in

Fig. 1.5-18[B]. A further simplification is to use ^{13}C decoupling during the evolution period. This may be achieved by applying a π ^{13}C pulse at the midpoint of t_1, which would cause the precessing magnetisation vectors to refocus at the end of the evolution period. Also a small delay $\Delta_1 = \frac{1}{2J}$ is inserted, where no ^{13}C decoupling is applied, so that detection of the magnetisation will be optimized. This result is shown in Fig. 1.5-18[C]. This required condition $\Delta_1 = \frac{1}{2J}$ also has the effect of minimising signals that originate through long-range C-H coupling interactions[98,99]. In this case their magnetisation vectors would not be able to precess in time and being in antiphase would mutually cancel.

CH_2 and CH_3 groups

For $^{13}CH_2$ and $^{13}CH_3$ groups, similar results may be obtained as for the isolated ^{13}CH group and hence the same sequence may be used with decoupling during both evolution and detection periods. The optimum choice for Δ_1 still remains at $\frac{1}{2J}$, because it depends only upon the precessional rate of the two proton vectors. However, the choice for the Δ_2 value will be different as it is dependent upon not only the size of the coupling J but also the number of the coupled protons. These differences are shown in Fig. 1.5-19.

Thus to avoid mutual cancellation of out-of-phase signals a compromise value of $\Delta_2 = \frac{0.3}{J}$ to cater for all CH, CH_2, CH_3 groups is used. Since a relatively narrow range of J(C,H) is used this presents no special problem when one-bond ^{13}C couplings are of interest[10,11,111]. However for ^{31}P, because of the wide range of values of $^nJ(^{31}P,^1H)$ in structures of real chemical interest, its use will probably be limited despite the attractions of achieving $^{31}P/^1H$ chemical shift correlations.

FIGURE 1.5-19 The Magnitude I *vs* Δ_2 Dependence for a Particular $^{13}C/^{1}H_n$ Group*

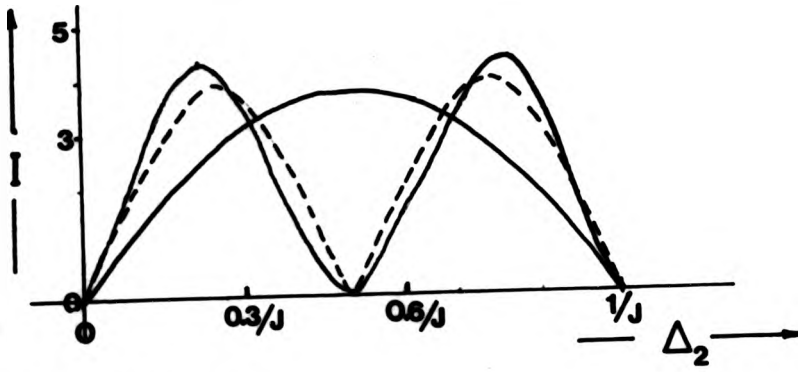

where CH ——

CH_2 – – –

CH_3 ———

* taken from ref. 80

The 2D $^{13}C/^{1}H$ Heteronuclear Shift Correlation Experiment

The actual pulse sequence used to achieve the $^{13}C/^{1}H$ chemical shift correlation experiment was that adapted from Bax[80] and the sequence is given in Fig. 1.5-20. Heteronuclear decoupling is achieved in each dimension, although if desired can be omitted in either or both. By phase cycling both the second $\frac{\pi}{2}$ ^{1}H pulse and the $\frac{\pi}{2}$ ^{13}C pulse by the method shown in Table 1.5-2, quadrature detection in both dimensions may be achieved.

FIGURE 1.8-20 The 2D $^{13}C/^{1}H$ Pulse Sequence for Heteronuclear Shift Correlation Experiment

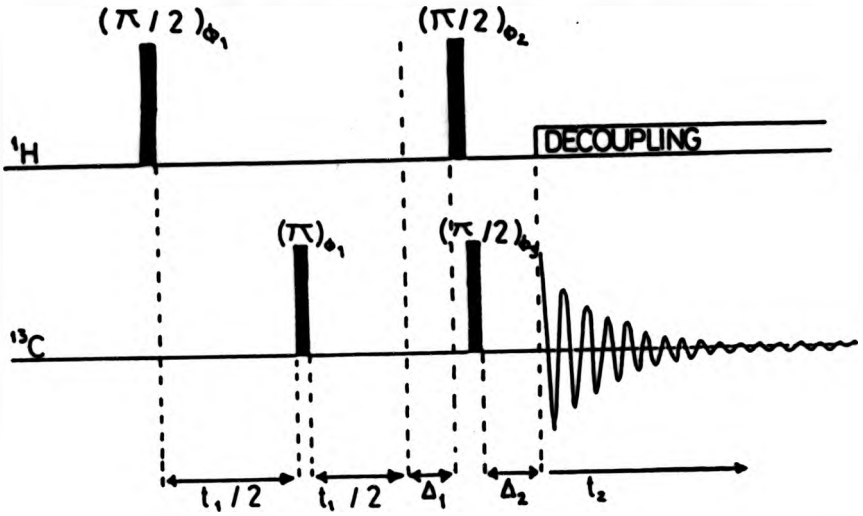

TABLE 1.8-2 Phase Cycling for $^{13}C^{1}H$ Heteronuclear Shift Correlation Experiment*

Cycle	Proton Pulse	Carbon Pulse
1	+x	+x
2	+y	-y
3	-x	-x
4	-y	+y

* Taken from ref. 80

In order to remove phase errors from the quadrature detection system, the whole four step experiment may be also cycled again four times. This may be achieved by increasing all the phases of the receiver and R F pulses each time by 90°[80]. Due to software limitations of the Jeol FX 90 Q spectrometer, a modified version of this full cycling procedure was used.

The proton pulse is set in the middle of the spectral width in the F_1 dimension. This allows the use of less R F decoupler power to decouple the ^1H region. The minimum acquisition frequency along the t_1 axis should be twice that of the ^1H spectral width to avoid folding. By setting the ^1H transmitter frequency at the centre of the ^1H region of interest, the sampling frequency may be halved and the size of the data matrices may be kept to a minimum. This will achieve optimum digital resolution in minimum time and in minimum data storage space.

The data matrices used need not be square, and indeed it is common to use many points (1024 - 4096) in the t_2/F_2 dimension corresponding to the relatively fine digitisation required of a normal NMR spectrum, and fewer points (32 - 256) in the t_1/F_1 dimension corresponding to relatively coarse digitisation and of course a smaller number of original experiments.

The 2D $^{13}C/^1H$ Heteronuclear Shift Correlation Experiment with Homonuclear Broadband Decoupling

The 2D $^{13}C/^1H$ spectra obtained using the sequence in Fig. 1.5-20 still retains splittings in the proton F_1 dimension due to homonuclear proton coupling. This is often an undesirable complication if the main objective is to determine accurate proton chemical shifts from corresponding slices arising from chosen ^{13}C resonances. It can however be avoided by adding extra pulses to the sequence as suggested by Bax[90], and an adaptation is shown in Fig. 1.5-21.

In this sequence, the π ^{13}C pulse in the preceding sequence (Fig. 1.5-20) is replaced by a pulse train which has different effects on those protons that are not directly attached to a ^{13}C nucleus from those which are. This pulse train is shown in Fig. 1.5-22 where J is the magnitude of the heteronuclear coupling constant in hertz.

FIGURE 1.5-21 The 2D $^{13}C/^{1}H$ Pulse Sequence for Heteronuclear Shift Correlation Experiment with Homonuclear Broadband Decoupling

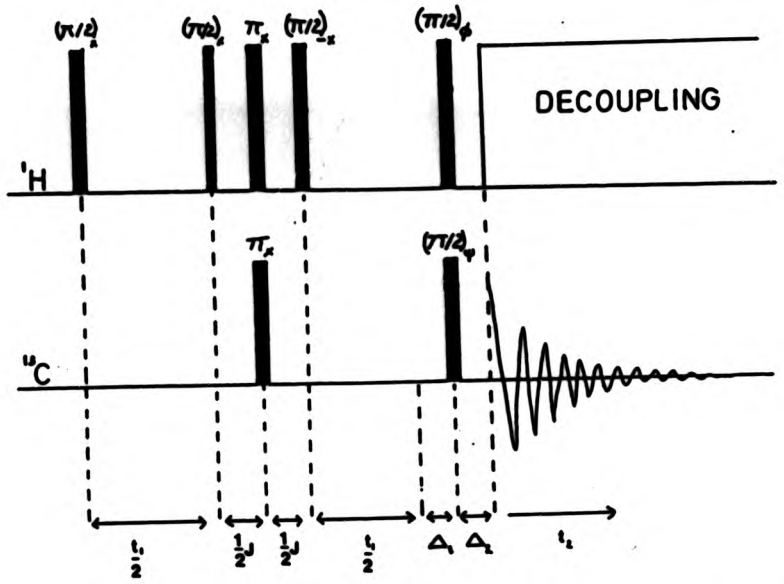

FIG. 1.5-22 The Pulse Train for Broadband Homonuclear Decoupling

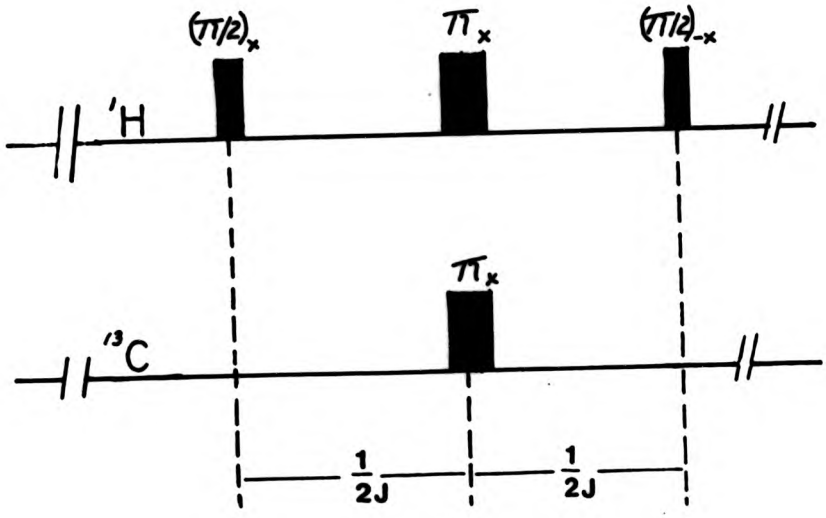

With this pulse train, protons which are not directly attached to the observed ^{13}C nucleus experience an effect as if a nonselective 180° pulse were applied and are put out of phase. However, protons which are directly bonded to the particular carbon are left unaffected and are thus decoupled from the non-bonded ones. For example, let us consider two protons, hydrogen H_A bonded directly to $^{13}C_X$, and H_B not directly bonded to $^{13}C_X$ but coupled indirectly to H_A, as in Fig. 1.5-23.

FIGURE. 1.5-23.

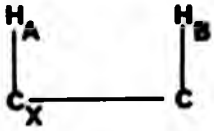

The effect of the pulse train will change the spin state of H_B, but will not affect the transverse magnetization of H_A. The pulse train is applied in the centre of the evolution period so that there will be no overall effect of coupling between H_A and H_B at the end of the evolution period[103]. Because the H_A nucleus is coupled in the $\underline{m}$ = +1.2 and $\underline{m}$ = -1/2 spin states equally for a period of $\underline{t_{1/2}}$ the position of the H_A magnetization vector in the transverse phase depends only on the chemical shift $\underline{\delta_A}$ and the length of the evolution period $\underline{t_1}$.

The magnetization of H_A is then transferred to its directly coupled ^{13}C nucleus ($^{13}C_X$) by way of the normal read pulse[80,103] and thus the observed ^{13}C signal will be modulated by the chemical shift $\underline{\delta_A}$ only. Broadband heteronuclear proton decoupling is turned on during acquisition ($\underline{t_2}$) and the 2D-Ft will give a single resonance at $(F_1,F_2) = (\delta_A,\delta_X)$ with no homonuclear proton splitting appearing in the F_1 dimension. However for inequivalent methylene resonances where coupling arises from different hydrogens their transfer of magnetization will be

different and hence coupling will still exist and an AB quartet will appear on the corresponding data slice. This is shown in Fig. 2.4-7 For this pulse train to be effective the estimation of J must be accurate to within 10%[102]. The whole sequence (Fig. 1.5-23) may be phase cycled as for the coupled heteronuclear $^{13}C/^{1}H$ shift correlation sequence to remove pulse errors and achieve quadrature detection.

An important application of this sequence in the present work arises because for phosphorus compounds it is a straightforward matter to use it to measure values of $J(^{31}P,^{1}H)$, together with the sign relative to that of the corresponding $J(^{31}P,^{13}C)$, even when the normal proton spectrum is highly second-order and/or overlapped. This is demonstrated in Section 2.2.

1.6 Data Manipulation of the 2D Fourier Transformation

The 2D Fourier transform is expressed mathematically as a product of two manipulations of the data associated with the two time intervals t_1 and t_2. As shown in Fig. 1.6-1, two methods of performing a 2D Fourier transformation are possible.

FIGURE 1.6-1 Methods of Double Fourier Transforming an Array

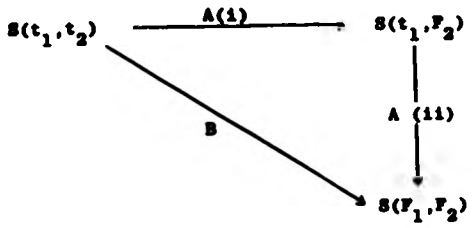

By route B the raw data set $S(t_1,t_2)$ is stored in bulk in the computer memory as a set of FIDs and a 2D Fourier transform is performed all at once to yield the two frequency dimensional spectrum $S(F_1,F_2)$. By route A, as achieved by the Jeol FX 90 Q, the 2D data is transformed in two steps. As the 2D experiments are based on a series of spin-echo like experiments with an associated variable time interval t_1, this interval is systematically incremented for the next experiment of the stack to create a set of FIDs which contain the t_2 parameter as their running time variable. Each of the individual FIDs is then transformed with a proper exponential or other weighting function. This yields a set of spectra which vary as a function of t_1. At this stage the information is stored as phase or amplitude modulations of the F_2 axis which have resulted from taking linear combinations of absorption and dispersion component information and comprises a $S(t_1,F_2)$ data set.

The second Fourier Transformation (with respect to t_1) is then performed on each one of these using one data point from each of the spectra and the data are stored in bulk memory as a function of the two frequency parameters $S(F_1,F_2)$. This procedure is <u>equivalent</u> to performing a double Fourier transformation on the original data set. Fig. 1.6-2 shows the FIDs of a sample of triethyl phosphine resulting from [A] a 1D Fourier transformation and [B] a 2D Fourier transformation. As with the first transform, the second yields again both absorption and dispersion terms resulting in an array consisting of four quadrants: absorption-absorption; absorption-dispersion; dispersion-absorption; and dispersion-dispersion. Theoretically it would be possible to take linear combinations of these four quadrants to optimise phasing along both axes[95] for a particular experiment, however the normal commercial NMR spectrometer is usually set up so that only the absorption-absorption quadrant is used. This may be done as the information content, for symmetry reasons, is the same in all four quadrants. Thus

the resulting 2D spectrum can then be displayed as a montage in which the F_2 axis corresponds to the dispersion obtained in a normal 1D experiment. The F_1 dimension will then contain other information according to the particular experiment actually performed and the correlation between the two axes will reflect this.

FIGURE 1.6-2 Comparison of the FID Resulting from a 1D and a 2D Pt for a Sample of Triethyl Phosphine

1.7 Line Shapes in 2D Spectra

A transient signal usually decays exponentially and this leads to resonances with a Lorentzian line shape in liquid NMR. The width of the line may be changed by using different exponential filtering but the line shape will still remain Lorentzian. In the case of liquid 2D NMR spectroscopy the intensity surface would be assumed to be a four pointed star pattern[104] which would reflect that this absorption has been obtained by a 2D transformation of the two time-domain signals and that they are both Lorentzian in shape. See Fig. 1.7-1

FIGURE 1.7-1 A Schematic Representation of an Absolute Value Lorentzian Line Shape

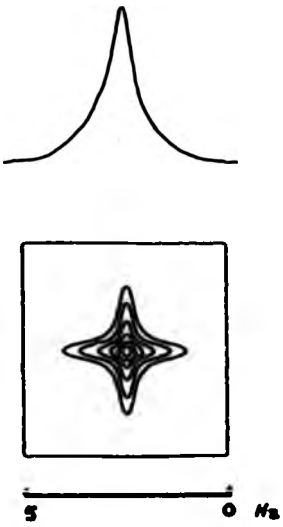

This seems to hold true for simple isolated examples, however, most signals are affected by modulation effects and the resulting complicated line shape in a 2D spectrum when this occurs is said to have a phase twist[95,99].

1.8 Filtering and Exponential Weighting

The absorption-absorption quadrant as previously mentioned is the most desirable quadrant for high resolution work because all the resonances are absorptions. However, in any quadrant, phase anomalies resulting from modulation effects (phase twist) make it difficult to set the phase in all sections in the spectrum. $S(F_1,F_2)$ may overlap in both dimensions or in one dimension and where there is an overlap, the interference will result in a phase twist. To circumvent this problem various display modes can be used to plot the full 2D spectrum.

A power mode which is expressed as the square of the normal phase sensitive mode allows phasing over all the plot. However, it does have the disadvantage of broadening the line shapes where overlapping resonances occur because dispersion as well as absorption components are squared in this function. Also as the intensities are squared, large intensity distortions may occur. Thus an absolute value mode, which is described as the square root of the power spectrum mode, is preferred as the signals are always positive and in this mode intensity distortions do not exist. This mode however, slightly degrades the resolution and gives rise to enhanced tails on the signal.

For individual cross-sections, a phase sensitive mode is possible as the signal can usually be phased satisfactorily. Also an exponential weighting function may be applied to the FID of the particular slice to increase the resolution and definition of the absorptions involved. This is especially useful in $^{13}C/^{1}H$ shift correlation work where J(H,H) coupling is present in the F_2 dimension. An example is shown in Fig. 1.8-1 of an inequivalent CH_2 group with different weightings applied to the FIDs. The resulting transformed AB quartets are also shown. As can be seen, fine structure may be enhanced with the proper choice of weighting functions.

FIGURE 1.8-1 The Effect of Exponential Weighting on the FID of the Designated C_3 Carbon 90° Cross-section in a Sample of 2-norbornyl Diphenyl Phosphine.

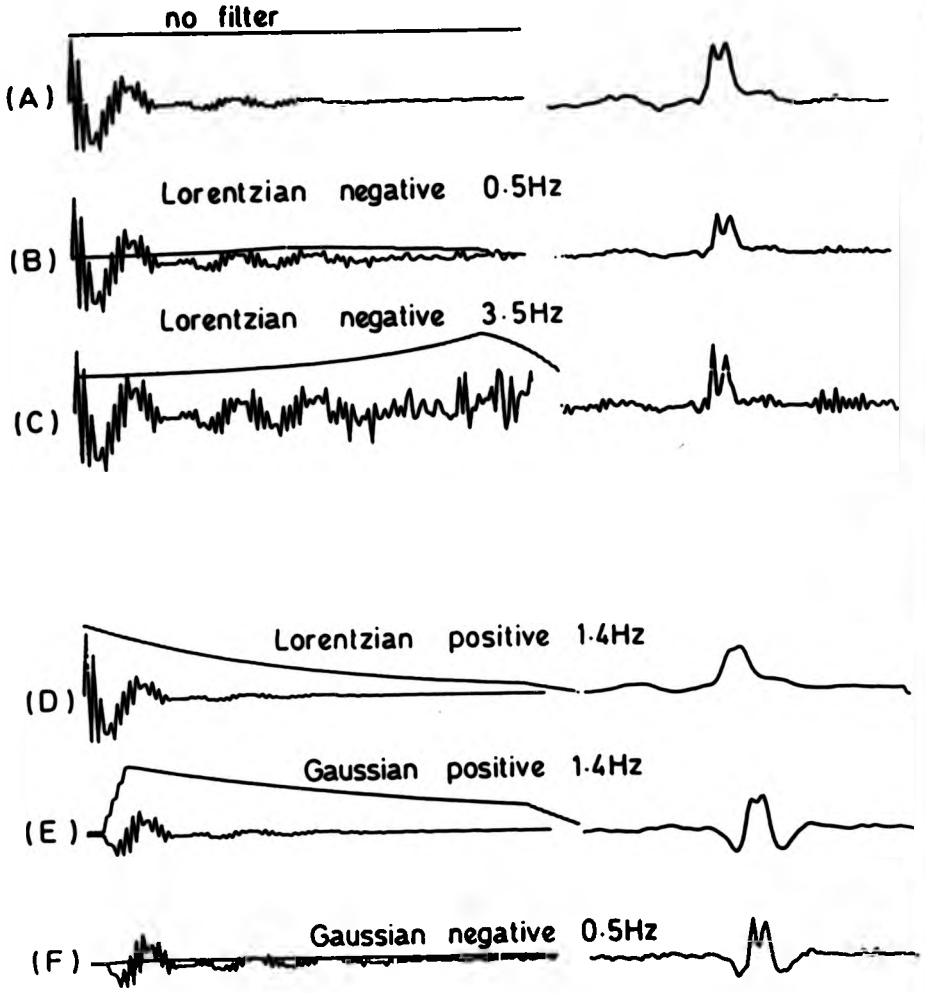

1.9 Graphical Presentation of 2D NMR Spectra

Two ways of presenting the 2D spectral map are: the Stack Plot (Fig. 1.9-1) and the Contour Plot (Fig. 1.9-2).

1.9.1 The Stack Plot

A stack plot is a representational graph composed by: incrementing values of one frequency dimension, and plotting it against another function of the other frequency dimension. The intensity of the absorption signal gives the third dimension and hence an overall 3-Dimensional surface. It is usually plotted askew to allow peaks behind other resonance peaks to be seen. Also whitewash[106] routines are employed to blot out the hidden lines to give a clearer impression of all resonances.

1.9.2 The Contour Plot

The contour plot is basically a downward view of a stack plot whereby concentrations of stars or nodes represent absorption signals on the grid surface. Nodes which have greater concentration of lines indicate strong absorption signals and those with less are of smaller intensity. An overall threshold is set manually as a whitewash to rid the background noise to present a clearer picture. Care however must be taken so as to not mistakenly lose useful or significant data. This is shown in Fig. 1.9-2.

Fig. 1.9-1 [A] A 2D J- Resolved ^1H Stack Plot of Ethyl acetate
[B] A 45° Projection taken from the Stack Plot

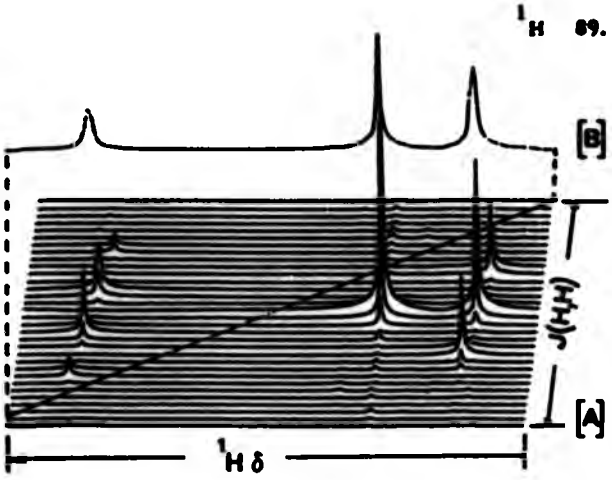

Fig. 1.9-2 A 2D J- Resolved ^1H Contour Plot of a Simple Benzoate

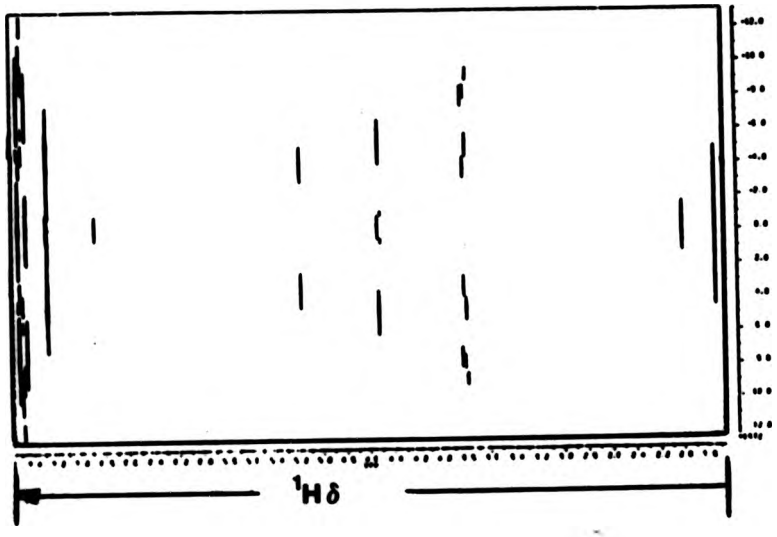

1.9.3 Cross-sections and Data Slices

In many chemical applications it is not necessary to perform a complete spectral transformation. Instead it is possible to take partial plots known as cross-sections in which the individual data slices can contain most of the desired information. In $^{13}C/^{1}H$ shift correlation plots cross-sections are usually taken parallel to the F_1 axis through the particular chosen peak maxima of interest. The F_2 dimension is examined along the row to retrieve the couplings and the chemical shifts associated with that peak in the F_1 dimension. For particular cross-sections or projections the phase-sensitive mode is favoured as it is usually possible to phase the individual absorptions in the slice, and the mode gives greater sensitivity, higher resolution, and a line shape closer to Lorentzian than the absolute value mode. An example of this is shown in Fig. 2.1-8.

1.9.4 Projections

In J-spectroscopy, a 2D array projection is calculated by integrating the intensity of the cross section through the diagonal which bisects the F_1 and F_2 axes. This is said to be a 45° projection. This is shown in Fig. 1.9-1

1.10 Optional Ways of Performing a 2D Experiment

The now most common way to create a 2D experiment is to use a Time-Space method whereby a 2D spectrum $S(F_1,F_2)$ is obtained after a two dimensional Fourier transformation of the time function $S(t_1,t_2)$ as described above. This however, is not the only way in which a 2D experiment may be performed. Several fundamental schemes can be used to generate a signal as a function of the two frequency variables $S(F_1,F_2)$ of which some are:

(a) The frequency space experiment

Two frequencies F_1 and F_2 are applied simultaneously and the response is measured as a function of both frequencies.

(b) The stochastic resonance experiment

A system is perturbed by white noise to give a stochastic response. The higher cross correlation functions can be computed between the input and output noise and their Fourier transform may produce 2D and higher order spectra.

(c) The mixed frequency space time experiment

While observing the FID in a Fourier experiment as a function of a time period t_2, the system is strongly perturbed by a frequency in F_2. Fourier transformation of the FID and repeating for various F_2 frequencies generates a 2D double resonance spectrum.

References - Chapter 1

1. R.R. Ernst, W.A. Anderson Rev. Sci. Instrum. 37, 93 (1966).
2. R.L. Vold, J.S. Waugh, M.P. Klein, D.E. Phelps J. Chem. Phys. 48, 3831 (1968).
3. H.Y. Carr, E.M. Purcell Phys. Rev. 94, 630 (1954).
4. E.D. Becker, J.A. Ferretti, T.C. Farrar J. Amer. Chem. Soc. 91, 7784 (1969).
5. G.A. Morris, R. Freeman ibid. 101, 760 (1979).
6. J. Dadok, R.F. Sprecher J. Magn. Reson. 13, 243 (1974).
7. L. Muller ibid. 28, 301 (1979).
8. J. Jeener Ampere International Summer School II, Basko, Poje, Yugoslavia (1971).
9. R.R. Ernst VIth International Conference on Magnetic Resonance in Biological Systems, Kanderstag (Sept. 1974).
10. V. Rutar, T.C. Wong J. Magn. Reson. 60, 333 (1984).
11. M.R. Bendall, D.T. Pegg ibid. 53, 144 (1983).
12. M.A. Phillippi, R.J. Wiersema, J.R. Brainard, R.E. London J. Amer. Chem. Soc. 104, 7333 (1982).
13. J. Jeener, B.H. Meir, P. Bachman, R.R. Ernst J. Chem. Phys. 71, 4546 (1979).
14. C. Altona, M. Sandaralingam J. Amer. Chem. Soc. 92, 1995 (1970).
15. L.D. Quin, M.J. Gallagher, G.T. Cunkle, D.B. Chesnut ibid. 102, 3136 (1980).
16. L.D. Quin, L.B. Littlefield J. Org. Chem. 43, 3508 (1978).
17. L.B. Littlefield, L.D. Quin Org. Magn. Reson. 12, 198 (1979).
18. D.G. Gorenstein J. Amer. Chem. Soc. 99, 2254 (1977).
19. R.B. Wetzel, G.L. Kenyon J. Amer. Chem. Soc. 94, 9230 (1972).
20. M. Lauer, O. Samuel, H.B. Kagan J. Organometal. Chem. 177, 309 (1979).
21. R.B. Wetzel, G.L. Kenyon Chem. Commun. 287 (1973).
22. R.B. Wetzel, G.L. Kenyon J. Amer. Chem. Soc. 96, 5189 (1974).
23. J. Thiem, B. Meyer Org. Magn. Reson. 11, 50 (1978).
24. G.W. Buchanan, C. Benezra Can. J. Chem. 54, 231 (1976).

25. K.A. Mesch, L.D. Quin Tetrahedron Lett. 21, 4791 (1980).

26. G.W. Buchanan, F.G. Morin Can. J. Chem. 55, 2285 (1977).

27. J. Thiem, B. Meyer Tetrahedron 3573 (1977).

28. C. Beneszra J. Amer. Chem. Soc. 95, 6890 (1973).

29. H.J. Callot, C. Beneszra Can. J. Chem. 48, 3362 (1970).

30. L. Evely, L.D. Hall, P.E. Steiner, D.H. Stokes Org. Magn. Reson. 5, 141 (1973).

31. P. Laszlo, P. von R. Schleyer J. Amer. Chem. Soc. 86, 1171 (1964).

32. E.J. Cremlyn, E.N. Kilem, N. Akhtar Phos. and Sulphur 7, 257 (1979).

33. W. Barns, D. Grant, M.A. McKervey, G. Step J. Chem. Soc. Perkin I, 234 (1976).

34. D.H. Williams, I. Fleming Spectroscopic Methods in Organic Chemistry 2nd ed. McGraw-Hill London 77, (1973).

35. D. Shaw FT NMR Spectroscopy Elsevier 125 (1976).

36. W. McFarlane S.E.R.C. Summer School NMR Spectroscopy Runner House, University of Sheffield 6, (1983).

37. P.W. Nicholls Ann. Reports on NMR Spectros. 6C, 1 (1977).

38. P.J. Smith, A.P. Tupciauskas Ann. Reports on NMR Spectros. 8, 291 (1978).

39. J.B. Lambert, L.G. Greifenstein J. Amer. Chem. Soc. 96, 5130 (1974).

40. R.D. Bertrand, D.M. Grant, E.L. Allred, J.C. Hinshaw, A.B. Strong ibid. 94, 996 (1972).

41. M.M. Crutchfield, C.H. Dungan, J.H. Letcher, V. Mark, J.R. Van Topics in Phosphorus Chemistry 5, 1 (1967).

42. D.G. Gorenstein Progress in NMR Spectros. 16, 1 (1983).

43. I.I. Raki, N.F. Ramsey, J. Schwinger Rev. Mod. Phys. 26, 167 (1954).

44. A. Saika, C.P. Slichter J. Chem. Phys. 22, 26 (1954).

45. G. Mavel Ann Reports on NMR Spectros. 5B, 1 (1973).

46. H.S. Gutowsky, J. Larman J. Amer. Chem. Soc. 87, 3815 (1965).

47. S.O. Grim, W. McFarlane, E.F. Davidoff J. Org. Chem. 32, 781 (1967).

48. S.O. Grim, W. McFarlane Nature 208 995 (1965).

49. L.D. Quin, J.J. Breen Org. Magn. Reson. 5, 17 (1973).

50. J.B. Lambert, A.R. Vagenas Org. Magn. Reson. 17, 265 (1981).

51. a) J.H. Letcher, J.R. van Wazer Topics in Phos. Chem. 5, 75 (1967).
b) J.H. Letcher, J.R. van Wazer J. Chem. Phys. 44, 815 (1966).

52. D. Purdela J. Magn. Reson. 5, 23 (1971).

53. M. Rajumaan, J. Simon Org. Magn. Reson. 7, 334 (1975).

54. T.A. Albright, M.D. Gordon, W.J. Freeman, E.E. Schweiner J. Amer. Chem. Soc. 98, 6249 (1976).

55. J. Kowalewski Ann. Reports on NMR Spectros. 12, 82 (1982).

56. J.M. Murrell Prog. in NMR Spectros. 6, 1 (1971).

57. J.A. Pople, D.P. Santry Mol. Phys. 8, 1 (1964).

58. N.F. Ramsey Phys. Rev. 91, 303 (1953).

59. H.M. McConnell J. Chem. Phys. 24, 460 (1956).

60. M. Karplus, D.M. Anderson ibid. 30, 6 (1959).

61. M. Karplus, ibid. 30, 11 (1959).

62. M. Banfield, D.M. Grant Advances in Magn. Reson. 1, 149 (1965).

63. M.A. Cherniak Notes of Chemical Physics Brock University, St. Catherines, Canada, 184 (1970).

64. C.J. Jameson, H.S. Gutowsky J. Chem. Phys. 51, 2790 (1969).

65. M.A. Bent Chem. Rev. 61, 275 (1961).

66. J.E. Huheey J. Chem. Phys. 45, 405 (1966).

67. L.D. Quin, L.B. Littlefield J. Org. Chem. 43, 3508 (1978).

68. R.R. Dean, W. McFarlane Mol. Phys. 12, 289, 364 (1967).

69. W. McFarlane Proc. Roy. Soc. A, 306, 185 (1968).

70. C.E. Griffin, M. Gordon J. Organometal. Chem. 3, 414 (1965).

71. D. Hagnaire, J.B. Robert, J. Verrier Chem. Comm. 819 (1967).

72. M. Karplus J. Amer. Chem. Soc. 85, 2890 (1963).

73. G.W. Buchanan, J.M. Bowen Can. J. Chem. 55, 604 (1977).

74. D. Doddrell, I. Barfitt, W. Kitching, M. Bullpitt, C. Lee, E.J. Mynott, J.L. Cansidine, H.G. Kuivila, R.H. Sarma J. Amer. Chem. Soc. 96, 1640 (1974).

75. P.F. Barron, D. Doddrell, W. Kitching J. of Organometallic Chemistry 132, 381 (1977).

76. L.M. Jackman, S. Sternhell Applications of NMR Spectros. in Organic Chemistry 2nd edit. Pergamon Press, London 5, 315 (1969).

77. N.D. Vissier, J.P. Oliver J. of Magn. Reson. 2, 117 (1970).

78. R. Benn, H. Gunther Angew. Chem. Int. Ed. Engl. 22, 350 (1983).

79. D.L. Turner Prog. in NMR Spectros. 17, 281 (1985).

80. A. Bax Two-Dimensional NMR in Liquids Delft University Press, Delft, R. Reidel Pub. (1982).

81. R.R. Ernst, W.P. Aue, P. Bachmann, J. Karhan, A. Kumar, L. Muller Two-Dimensional NMR Spectros, Magnetic Resonance in Condensed Matter - Recent Developments, Proc. Ampere Int. Summer School. 4th, 89 (1976).

82. W.P. Aue, E. Bartholdi, R.R. Ernst J. Chem. Phys. 64, 2229 (1976).

83. F. Bloch Phys. Rev. 70. 460 (1946).

84. a) E.L. Hahn, D.E. Maxwell Phys. Rev. 88, 1070 (1952).
b) E.L. Hahn ibid 80. 580 (1950).

85. R. Freeman, H.D.W. Hill Dynamic NMR Spectros. L.M. Jackman, F.A. Cotton, Ed. Academic Press, New York, 131 (1975).

86. C.J. Turner Prog. in NMR Spectros. 16, 311 (1984).

87. W. McFarlane private communication

88. R. Freeman, H.D.W. Hill J. Magn. Reson. 5, 278 (1971).

89. W.P. Aue, J. Karhan, R.R. Ernst J. Chem. Phys. 64,4226 (1976).

90. A. Bax, R. Freeman, T.A. Frenkiel, M.H. Levitt J. Magn. Reson. 43, 478 (1981).

91. Y. Huang, S. Macura, R.R. Ernst J. Amer. Chem. Soc. 103, 5327 (1981).

92. G.E. Hawkes, L.Y. Lian, E.W. Randall J. Magn. Reson. 56, 539 (1984).

93. I.J. Colquhoun, W. McFarlane J. Chem. Soc. Chem. Comm. 484 (1981).

94. P.H. Bolton, G. Bodenhausen J. Amer. Chem. Soc. 101, 1080 (1979).

95. G. Bocknhausen, R. Freeman, R. Niedermeyer, D.L. Turner J. Magn. Reson. 26, 133 (1977).

96. G. Bodenhausen, R. Freeman, D.L. Turner J. Magn. Reson. 27, 511 (1977).

97. L. Muller, A. Kumar, R.R. Ernst J. Chem. Phys. 63, 5490 (1975).

98. A.A. Maudsley, R.R. Ernst Chem. Phys. Lett. 50, 368 (1977).

99. R. Freeman Proc. R. Soc. London A373. 149 (1980).

100. R. Freeman, G.A. Morris Bull. of Magn. Reson. 1, 1,5 (1979).

101. K.G.R. Pachler, P.L. Wessels J. Magn. Reson. 12, 337 (1973).

102. S. Sørensen, R.S. Hansen, H.J. Jakobsen J. Magn. Reson. 14, 243 (1974).

103. J.S. Waugh J. Mol. Spectrosc. 35, 298 (1970).

104. G. Bodenhausen, R. Freeman J. Magn. Reson. 28, 471 (1977).

105. K. Hikichi, H. Chuchi Jeol News 18 A.1 2 (23), (1983).

CHAPTER 2

DATA AND INTERPRETATION

General: For the organo-metallic chemist, NMR spectroscopy is an invaluable technique in providing information on chemical backbone framework connectivities and yielding stereochemical relationships and their influences on the various properties. The use of phosphorus in conjunction with carbon and hydrogen data and the relationships between them *via* coupling - $^{n}J(P,C)$ and $^{n}J(P,H)$, gives a handle that is very sensitive to environmental surroundings. In particular, the value of Karplus and similar relations for deriving details of molecular configuration and conformation from coupling constants is well known. The method is established for proton-proton coupling, but it has also been extended for other couplings to include $^{n}J(^{31}\underline{P}\text{-}O\text{-}\underline{C})$, $^{n}J(^{31}P,C)$ and also $^{n}J(^{31}P,H)$[1-3]. For the measurement of $^{1}J(P,C)$ or $^{2}J(\underline{P}\text{-}O\text{-}\underline{C})$ in most cases, one usually only has to run the standard $^{13}C\{^{1}H\}$ spectrum to retrieve the first order coupling data arising from the (C,P_{α}) and (C,P_{β}) pairs. However in more overcrowded situations where overlap and perhaps masking of one of the pairs occur, more detailed analysis and experiments may be required. However, of these relationships the $^{31}P\text{-}^{1}H$ combination is the most sensitive to environment and hence has greatest potential for observing subtle changes in conformation and structure. Unfortunately in many organo-phosphorus compounds of interest, the proton spectrum is so complicated and/or tightly coupled that determining $^{n}J(P,H)$ is far from easy, even at high fields, and here is demonstrated an alternative approach. This is to use two-dimensional $^{13}C/^{1}H$ chemical shift correlation spectroscopy. In these experiments, one obtains the proton parameters indirectly and in many cases it is possible to read off the

required values of $^{n}J(P,H)$ immediately from appropriate cross-sections of the spectra. Through this correlation, the procedure also allows back checking via $^{n}J(P,H)$ to verify initial ^{13}C NMR assignments.

2.1 Examples of 2D NMR Analysis

In order to understand fully the technique, it is useful to consider first a simple compound without the complication produced by the presence of phosphorus as most of the data for the individual compounds shown in this thesis are derived from non-trivial NMR spectra. This may be also used as a vehicle to show clearly the systematic approach taken in elucidating the chemical shifts and the verification of their assignments, the measurement of coupling constants for particular nuclei, and the way in which 1D NMR may be complemented by 2D NMR analysis. The method will be illustrated by applying it to a simple bicyclic precursor, exo 7-bromo norcarn-2-one (C_7H_9Br) as shown in Structure 5.

2.2.1 Calculation of Chemical NMR Data for Exo 7-bromo norcarn-2-one

Structure 5

A ^{13}C NMR spectrum is shown in Fig. 2.1-1[A] and its assignment is given in Table 2.1-1 being aided by Muranaka et al[4]. Use of the 1D GASPE pulse sequence[5] for ^{13}C to confirm and differentiate assignments between the ^{13}CH, $^{13}CH_2$, $^{13}CH_3$ and quarternary carbons may be employed at this stage. In this case only $^{13}CH_2$, $^{13}CHBr$ and ^{13}CH groups are involved and this refinement is not really needed.

Fig. 2.1-1 A $^{13}C\{^{1}H\}$ [A] and a ^{1}H [B] NMR Spectrum of exo 7-bromo norcarn-2-ene

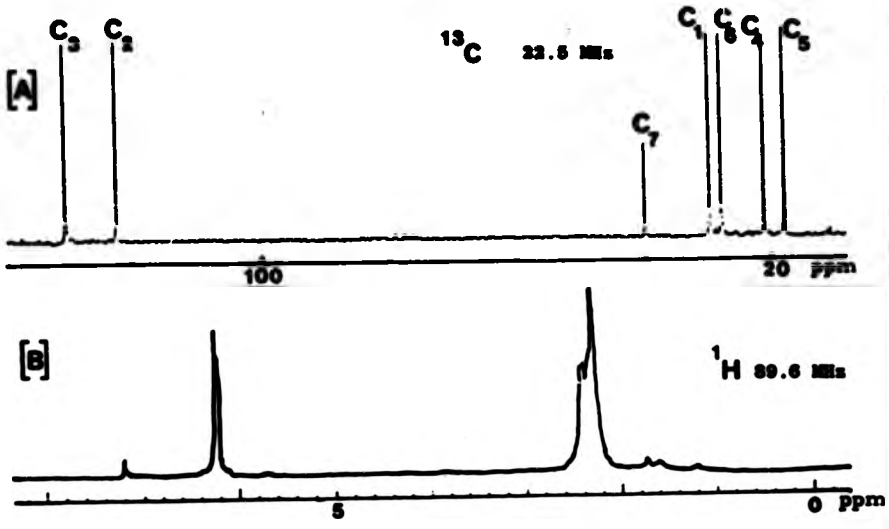

Table 2.1-1 ^{13}C NMR Chemical Shift Data for exo 7-bromo norcarn-2-ene

Carbon Number	^{13}C Chemical Shift (δ/ppm)[a]	
	Experimental	Literature [b]
C_1	30.12	30.1
C_2	122.78	122.7
C_3	130.58	130.6
C_4	21.59	21.6
C_5	18.41	18.6
C_6	28.16	28.2
C_7	40.26	40.0

a Positive signs are to high frequency of TMS = 0.0 ppm in $CDCl_3$ as solvent.

b Taken from ref. (4).

The ^{1}H NMR spectrum is shown in Fig. 2.1-1[B]. In it the non-olefinic protons resonate over a range of only 0.8 ppm and so preclude any straightforward analysis. However, as the ^{13}C NMR spectrum is well dispersed and can be assigned, a 2D $^{13}C/^{1}H$ shift correlation experiment may be used to separate and assign the proton resonances. The particular sequence used was that adapted by Bax[6], as described in Section 1.5.2 and given in Fig. 1.5-20. As stated previously, the basic shift correlated sequence may be simplified and its sensitivity enhanced by the decoupling of protons during the detection period, and by effective decoupling of the ^{13}C during the evolution period. To achieve proton decoupling during detection, the decoupler is turned on at a time Δ_2 (0.3/J) after the $\pi/2$ ^{13}C read pulse, where the value of Δ_2 is a compromise for all CH and CH_2 groups in the sample. The values of Δ_1 = 3.8 msec and Δ_2 = 2.1 msec were chosen for this sample on the basis of an estimate of 145 Hz for $^{1}J(C,H)$. With these decoupling procedures implemented, the 2D montage will contain the $^{13}C(^{1}H)$ resonances lying along the F_2 axis and the ^{1}H resonances with their homonuclear splittings lying along the F_1 axis. This sequence allows any given ^{13}C resonance to be correlated with its directly bonded hydrogen(s) and their associated homonuclear proton couplings along its cross-section.

In order to reduce the size of the data array and thus optimise the digital resolution for the available number of data points, the spectral widths for both the ^{13}C and ^{1}H are kept to a minimum. For example in this case, the ^{13}C spectral width was taken from 17 ppm to 150 ppm (ca. 2900 Hz) and the ^{1}H spectral width was taken from 2.0 ppm to 6.6 ppm (ca. 450 Hz) which still includes all resonances, as seen in Fig. 2.1-1[B]. In fact, to obtain chemical information, a full 2D plot need not be done. Instead hydrogen F_1 cross-sections corresponding to the ^{13}C resonances in the F_2 dimension may be taken to retrieve the information. This is

shown in Fig. 2.1-2[B]. As can be seen this technique has greatly simplified the hydrogen spectrum as compared to the 1D spectrum and J(H,H) may be inferred from this data. If however only exact chemical shifts are required, J(H,H) coupling, as can be seen on slice C_3 in Fig. 2.1-2[B], can still present unnecessary complications in this determination. In this case, this same sequence is modified further[7] as described in Section 1.5.2, Fig. 1.5-21, and allows elimination of homonuclear proton coupling except within the same CH_2 group. In this sequence homonuclear decoupling is employed in both frequency dimensions. The 2D stack is set up in the usual way and the cross-sections are shown in Fig. 2.1-2[A]. As can be seen, exact ^1H chemical shifts may be easily read off without J(H,H) coupling in most cases.

It will be noted from Fig. 2.1-2[A] that this method also provides unequivocal identification of inequivalent proton couplings arising from

Fig 2.1-2 90° OXO Data Matrix Slices of a C/^{1}H Heteronuclear Shift Correlated 2D NMR Spectrum With :- a) ^{1}H Homonuclear Decoupled and b) ^{1}H Fully Coupled in the F_1 (^{1}H) Dimension

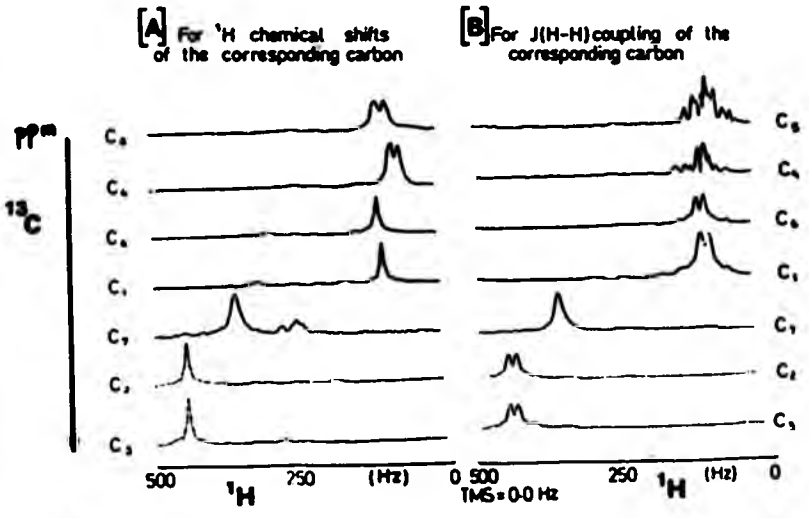

methylene groups. Calculation of the AB spin system is shown in Section 2.1.3. As a result, testing and back checking of the initial ^{13}C assignments is possible. Table 2.1-2 gives the results of the NMR experiments and analysis performed on the exo form of 7-bromo norcarn-2-ene.

Table 2.1-2 ^{1}H NMR Chemical Shift Data for exo 7-bromo norcarn-2-ene

Carbon Number	^{1}H Chemical Shift (δ/ppm) [a]
C_1	2.0
C_2	5.8
C_3	5.8
$C_4(H_1)$	1.9
$C_4(H_2)$	1.8
$C_5(H_1)$	1.5
$C_5(H_2)$	1.7
C_6	2.0
C_7	4.9

a Positive signs are to high frequency of TMS = 0.0 ppm in $CDCl_3$ as solvent.

2.1.2 The Determination of $^{n}J(P,H)$ for triethyl phosphine

The use of $^{13}C/^{1}H$ shift correlation sequences where homonuclear decoupling is employed in both frequency dimensions is especially valuable for compounds where another nucleus, say ^{31}P, is also coupled to a hydrogen and carbon. For example, in organophosphorus compounds where many of the signals in the ^{13}C spectrum are split into a doublet by $^{n}J(^{31}P,C)$, each line will yield its own proton cross-section in the 2D spectrum. The difference between the two proton resonance

frequencies from the corresponding slices of a particular carbon associated with P_α and P_β will be the $^nJ(P,H)$ and the <u>effective proton chemical shifts</u> of these signals will be given by $\delta H \pm 1/2\ J(^{31}P,H)$.

For example we can consider the simple compound triethyl phosphine. The $^{13}C\{^1H\}$ NMR spectrum in Fig. 2.1-3[A] shows the two carbon signals to be split by $^nJ(P,C)$; their assignments are known[8] and are given in Table 2.1-3. At 90 MHz the hydrogen spectrum, Fig. 2.1-3[B], shows the expected complex $(A_9B_2)_3X$ spin system. In order to assign $^nJ(P,H)$ and δH, a 2D $^{13}C/^1H$ shift correlation experiment was run. The corresponding cross-sections taken from the F_1 dimension show the homonuclear proton resonances arising from these four ^{13}C resonances in the F_2 dimension given in Fig. 2.1-4. The differences between the two hydrogen resonances

Fig. 2.1-3[A] $A^{13}C\{^1H\}$ NMR Spectrum of Triethyl Phosphine

Fig. 2.1-3[B] A ^{1}H NMR Spectrum and Expansion of Triethyl Phosphine

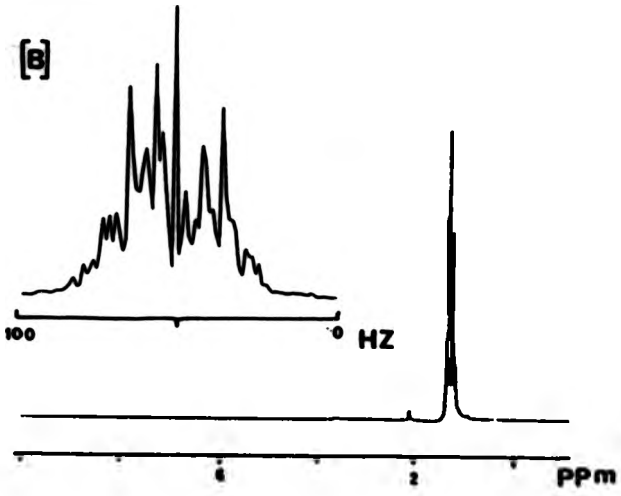

in Hertz along the F_1 axis will be the value for the J(P,H) and the proton chemical shift will be $\delta H \pm \frac{1}{2}J(P,H)$. This is portrayed in the expansion for the C_2 carbon in Fig. 2.1-4[B]. It should be also noted that the shift correlation experiment is sensitive to relative signs of couplings. As can be seen in this figure where the F_1 axis is plotted from high frequency to low frequency, the determination also gives the relative signs of $^{n}J(P,H)$ and $^{n-1}J(P,C)$ for each CH pair. If an absolute sign could be determined via Multiple Resonance techniques, then the true sign, positive or negative could be assigned to these. In this case, Fig. 2.1-4[A] shows that both $^{n}J(P,H)$ are of the same

Fig. 2.1-4[A] 90° Cross sections of a 2D $^{13}C/^{1}H$ Shift Correlation Experiment of triethyl phosphine

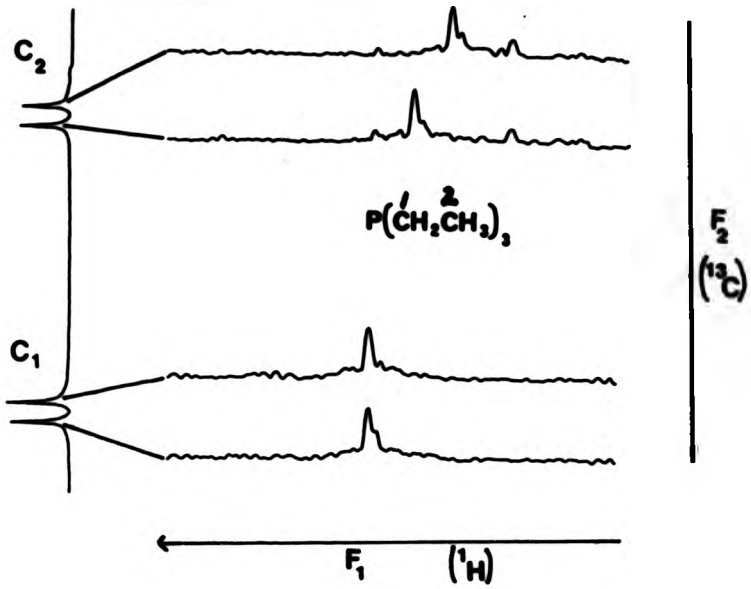

[B] An Expansion of CH_3 Carbon Slices

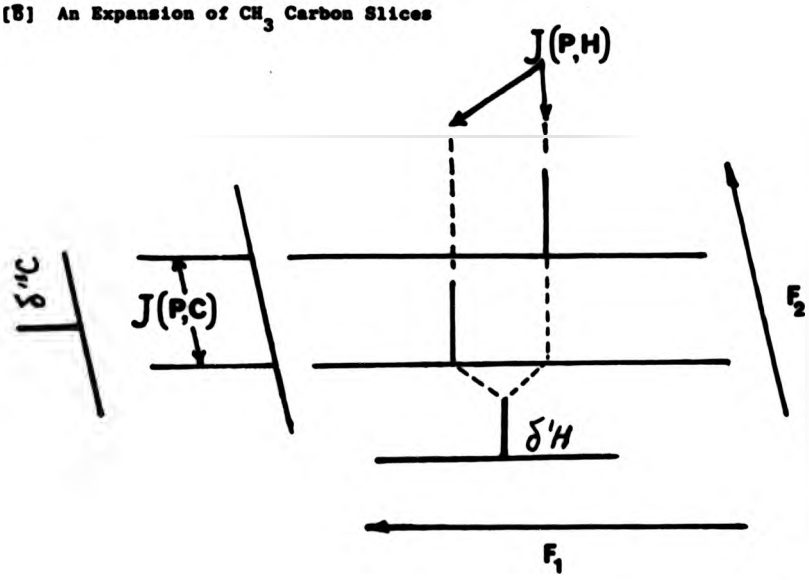

sign. The calculated ^{1}H, ^{13}C and ^{31}P chemical shifts and $^{2}J(P,C)$ and $^{2}J(P,H)$ values are given with the literature values in Table 2.1-3.

Table 2.1-3 NMR Data for triethyl phosphine

Nucleus		Experimental	Literature*
$\delta^{31}P$ [a]		-20.0	-20.1
$\delta\,^{13}C$ [b]	CH_2	19.8	-
	CH_3	10.5	-
$\delta\,^{1}H$ [b]	CH_2	1.5	1.6
	CH_3	1.2	1.2
$J(P,H)$ [c]	CH_2	0.6	(-) 0.5
	CH_3	13.5	13.8
$J(P,C)$ [c]	CH_2	0.8	0±4
	CH_3	14.0	14.1

a Positive signs are high frequency to 85% H_3PO_4 = 0.0 ppm

b Positive signs are high frequency to TMS = 0.0 ppm

c in Hertz

* taken from ref (8) & (61)

2.1.3 Determination of $^{2}J(P,H)$ and $\delta\,^{1}H$ for Inequivalent Hydrogens on a Carbon (CH_2)

In the modified Bax sequence[7] where homonuclear decoupling is effected in the F_1 dimension, a single hydrogen resonance will be simplified to a single line in most cases. However in the situation where the hydrogens that are attached to the same carbon are inequivalent, because of the coupling $^{2}J(H,H)$ = ca. 12 Hz, a two spin AB system will arise. This is because the homonuclear decoupling pulse train inserted

in the middle of the 2D sequence affects both protons equally and therefore there can be no mutual decoupling. Hence the corresponding data slice with this second order effect will have to be analysed as a complex spectrum.

2.1.3.1 Analysis of an AB system

For the general two-spin (I = 1/2) case, there are four possible allowed transitions. Three parameters may be obtained from the spectrum, i.e. ν_A, ν_B and J(A,B). In the general case the AB spectrum may be represented by Fig. 2.1-6 and its energy levels and transition frequencies are given in Table 2.1-4 where $\delta = \nu_A - \nu_B$ and $2C = [\delta^2 + J(A,B)^2]^{1/2}$.

Table 2.1-4 Energy Levels and Transition Frequencies for Two Nuclei (AB)

Line (n)	Energy Levels	Transition	Frequency	Relative Intensity
1	$\frac{\nu_A + \nu_B}{2} + \frac{J_{AB}}{4}$	$E_3 \rightarrow E_1$	$C + \frac{J_{AB}}{2}$	$1 - \frac{J}{2C}$
2	$\frac{1}{2}\left[(\nu_A - \nu_B)^2 + J_{AB}^2\right]^{\frac{1}{2}} - \frac{J_{AB}}{4}$	$E_2 \rightarrow E_1$	$-C + \frac{J_{AB}}{2}$	$1 + \frac{J}{2C}$
3	$-\frac{1}{2}\left[(\nu_A - \nu_B)^2 + J_{AB}^2\right]^{\frac{1}{2}} - \frac{J_{AB}}{4}$	$E_4 \rightarrow E_2$	$C - \frac{J_{AB}}{2}$	$1 + \frac{J}{2C}$
4	$\frac{-(\nu_A + \nu_B)}{2} + \frac{J_{AB}}{4}$	$E_4 \rightarrow E_3$	$-C - \frac{J_{AB}}{2}$	$1 - \frac{J}{2C}$

If we consider the example of a 2D $^{13}C/^{1}H$ shift correlated cross-section from the C_3 resonance of exo 2-bromo norbornane shown in Fig. 2.1-5, we may use the numberings from Fig. 2.1-6 and apply them to calculate this AB spectrum.

Fig. 2.1-5 90° Cross-sections taken along the F_1 (^1H) Dimension from a 2D $^{13}C/^1H$ shift correlated spectrum for a sample of <u>exo</u> 2-bromo norbornane

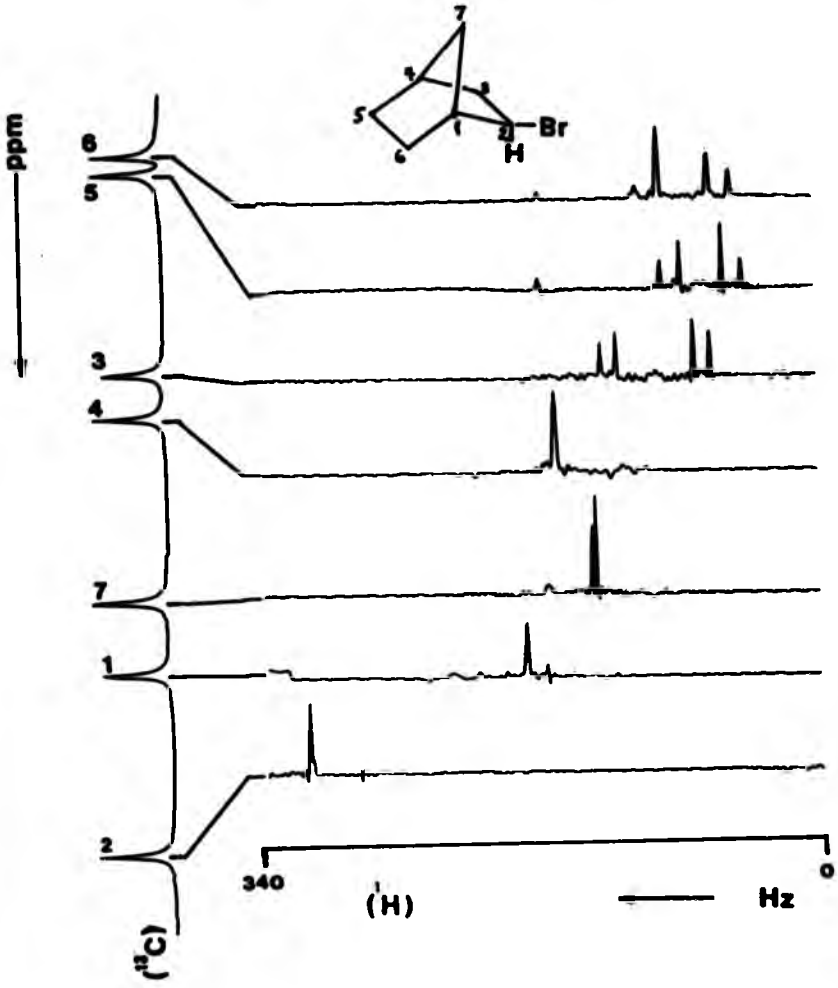

Fig. 2.1-6 An AB spectrum of the C_3 hydrogens in exo 2-bromo norbornane

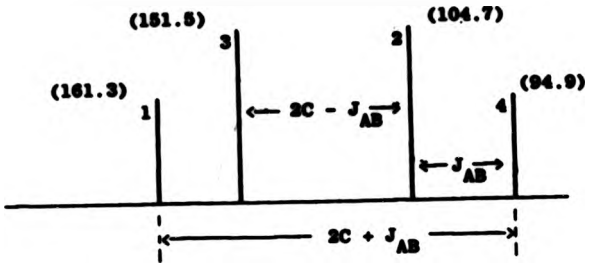

Using Fig. 2.1-6:

$|J| = 1\text{-}3 = 2\text{-}4$

$= 161.3 - 151.5 = 104.7 - 94.9$

$\boxed{|J| = 9.8 \text{ Hz}}$

$\delta^2 = (\nu_A - \nu_B)^2 = 4C^2 - J^2$

$\delta = \nu_A - \nu_B = (4C^2 - J^2)^{\frac{1}{2}}$

$\delta = [(2C - J)(2C + J)]^{\frac{1}{2}}$

$\delta = [(3 - 2)(1 - 4)]^{\frac{1}{2}}$

substituting values we get:

$\delta = [(151.5 - 104.7)(161.3 - 94.9)]^{\frac{1}{2}}$

$\boxed{\delta = 55.74}$

$\nu_A + \nu_B = (3 + 2) = (1 + 4)$

$= (151.5 + 104.7)$ $\boxed{\nu_A + \nu_B = 256.2}$

$(\nu_A - \nu_B) + (\nu_A + \nu_B) = 55.74 + 256.2$

$2\nu_A = 311.9$ $\boxed{\nu_A = 155.9}$

$\nu_B = 256.2 - 155.9$ $\boxed{\nu_B = 100.3}$

2.1.3.2 2D Analysis of an ABX system

In the case where another nucleus, e.g. ^{31}P, is coupled to the hydrogen AB pair an ABX system results. However the two cross-sections which arise from the CP_α and the CP_β, are separated by the J(P,C) in the F_2 dimension. These result from the HP_α and the HP_β components. Here each slice will contain half of the AB part of the ABX system corresponding to opposite spin states of X. This is most easily shown by considering Fig. 2.1-7 for a C_5H in a sample of 2-norbornyl dichloro phosphine taken from the 2D 90° cross sections from Fig. 2.2-6, in Section 2.2. Here the two cross-sections arising from $^{13}CP_\alpha$ and $^{13}CP_\beta$ components give respectively the $^1HP_\alpha$ and the $^1HP_\beta$ components in part [A]. Calculations of the AB systems are done individually for each of the slices to produce the stick diagram in part [B]. Subtraction of effective chemical shifts from the two diagrams, shown in red in part [B], will give the two coupling constants $J(H_A,P)$ and $J(H_B,P)$. Part [C] shows the evaluation of the two chemical shifts of δ_A and δ_B which are equal to $\pm \frac{1}{2} J(P,H_A)$ and $\pm \frac{1}{2} J(P,H_B)$ respectively.

Fig. 2.1-7 Schematic diagram and calculation of a ABX spectrum from a 2D cross-section of exo 2-norbornyl dichloro phosphine

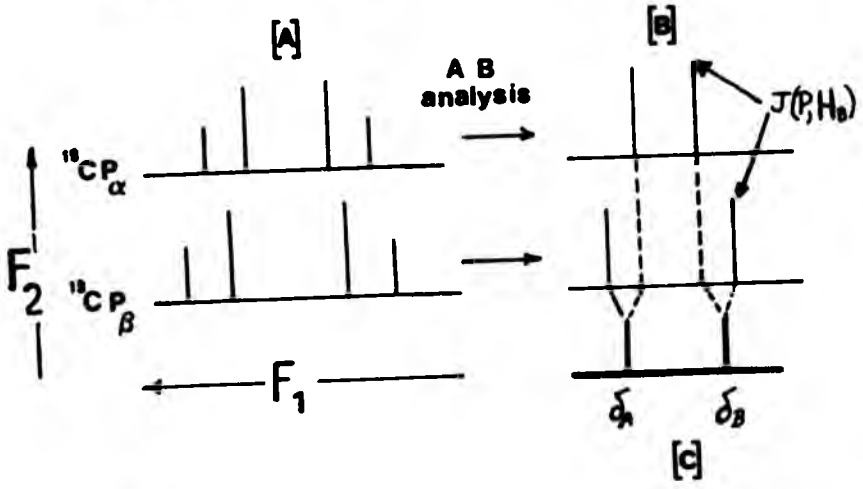

[X] Bicyclic Structures - Norbornanes

As previously mentioned in Section 1.3, bicyclic molecules such as substituted norbornanes, are regarded as a rigid system due to limited pseudorotation of their torsion angles. In cages such as these, it is possible to determine P-C and P-H couplings over a number of bonds. In this context, it then should be possible to examine the influence of phosphorus, by changing the phosphorus substituents on the cyclic ring so as to vary the phosphorus environment. The differences may then be monitored by examining and comparing the carbon and hydrogen chemical shifts together with the $^{n}J(P,C)$ and the more sensitive $^{n}J(P,H)$ coupling constants for a range of different derivatives. Previous examinations of a few of these phosphorus-cage systems by 1D NMR methods has allowed determination of the phosphorus and some of the carbon chemical shift data and some $^{n}J(P,C)$. However with the use of 2D NMR analysis calculation of most carbon and hydrogen chemical shifts and $^{n}J(P,C)$ and $^{n}J(P,H)$ should be possible.

3.2 2-Norbornyl Phosphorus Derivatives

For the 2-norbornyl phosphorus derivatives, a mixture of exo and endo isomers is usually produced. However these are often obtained in low yield and are waxy air-sensitive oils, and isolation and/or separation of single isomers was extremely difficult and in most cases not attempted as relatively large quantities were needed for the 2D NMR analysis. Thus a mixture of exo and endo isomers of a derivative were analysed together in their corresponding reaction ratios. Overall the exo isomer is formed preferentially in these systems with an exo: endo ratio in most cases of 2:1 or more. This then gave a way of unambiguous assignment between the two isomers as the exo isomer has

greater intensities, especially visible in the ^{31}P and the ^{13}C NMR spectra. An example is shown in Fig. 2.2-1.

Fig. 2.2-1 ^{31}P [A] and ^{13}C [B] NMR spectra of exo and endo 2-norbornyl dibromo phosphines

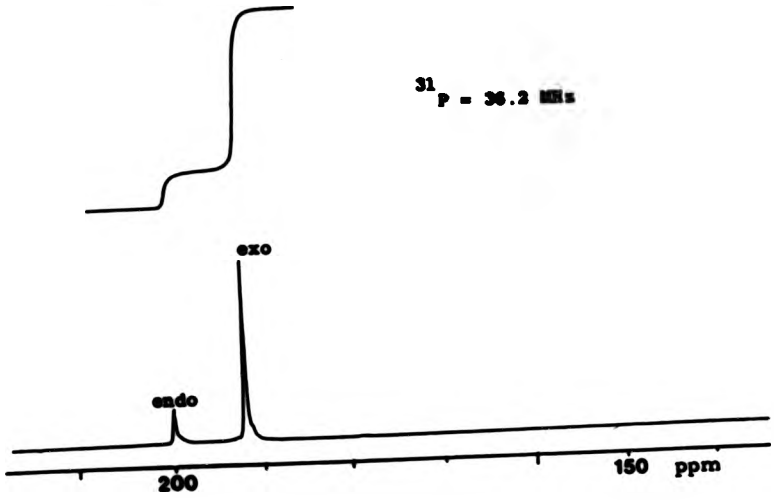

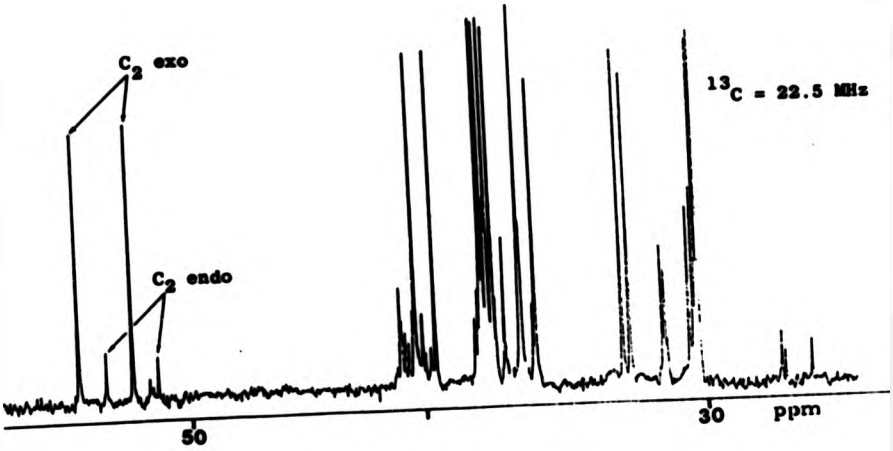

The basis of interpretation as to whether the isomer was exo or endo relied upon the arguments put forth by Quin[10-14]. Here it was suggested that exo preference may be explained by the fact that there is less crowding from the C_7 hydrogen group and hence less steric hindrance and thus the greater ability to accommodate substituents. Whereas in the endo isomer, greater steric crowding is produced by the C_6 hydrogen, which is physically much closer to the C_2 substituent site. An example of this can be seen in Structure 6. Similarly, a phosphorus

Structure 6

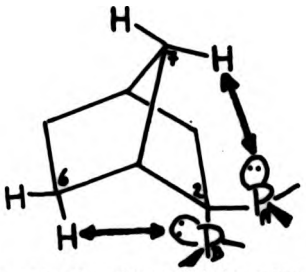

substituent P_B at the endo C_2 site will be very restricted by C_6. However if a phosphorus substituent P_A was situated in the exo site the C_6 would be less affected. This steric crowding behaviour is well known for ^{13}C nuclei and this was shown in the case for the chemical shift data for the 2-methyl isomers when compared to norbornane[10]. See Table 2.2-1. Quin[10] states that steric crowding of the phosphorus by γ carbons causes similar shifts as seen for ^{13}C signals. The analysis was checked by preparing some of the same compounds as Quin[10] and measuring their ^{31}P and ^{13}C chemical shifts. These are tabulated in Tables 2.2-2 and 2.2-3. As can be seen, no major discrepancies are noted, so it was presumed that this assignment was correct. This interpretation thus formed a basis to interpret and assign the isomers of new derivatives.

Table 2.2-1 Chemical shift data for exo, endo isomers of 2-methyl norbornane and norbornane*

Carbon Position	δ/ppm		
	2-methyl norbornane		norbornane
	methyl exo	methyl endo	
C_1	42.5	-	36.8
C_2	36.8	36.6	30.1
C_3	40.2	38.9	30.1
C_4	37.5	35.2	36.8
C_5	29.0	30.6	30.1
C_6	30.3	29.4	30.1
C_7	35.0	40.7	38.7
Me	22.3	17.4	-

* Taken from ref. (10)

Table 2.2-2 Comparison of ^{31}P NMR chemical shifts and reaction ratios in some 2-norbornyl phosphorus derivatives

P Substituent	δ/ppm [a]				exo:endo ratio	
	exo		endo			
	expt.	Lit.*	expt.	Lit.*	expt.	Lit.*
$-PCl_2$	+186.0	+187.5	+194.8	+196.8	-8.8	-9.3
-PClBr	+183.9	+183.9	+191.7	+191.3	-7.8	-7.4
$-P(MeO)_2$	+183.5	+185.3	+190.0	+192.4	-6.5	-7.1

a in ppm, positive to high frequency of 85% H_3PO_4 = 0.0 ppm.
b taken from ref (10)

Table 2.2-3 Comparison of ^{13}C NMR chemical shifts of some 2-norbornyl phosphorus derivatives

Carbon Position	δ/ppm											
	PR_2 = $-PCl_2$				-PClBr				$-P(OMe)_2$			
	exo		endo		exo		endo		exo		endo	
	a	b	a	b	a	b	a	b	a	b	a	b
C_1	39.98	38.5	39.82	39.4	39.98	39.7	41.68	-	-	-	38.50	-
C_2	54.90	54.5	53.80	53.4	53.20	53.1	52.06	51.9	44.30	44.3	42.65	42.7
C_3	33.50	33.1	33.78	33.3	35.58	35.4	35.08	-	31.35	30.4	30.80	-
C_4	37.36	37.0	37.41	-	37.57	37.1	37.62	-	-	-	-	-
C_5	28.93	28.4	29.98	29.5	28.48	28.3	30.12	29.7	29.50	29.5	30.20	29.6
C_6	31.67	31.2	25.22	24.8	31.52	32.2	25.16	24.1	32.40	31.5	26.75	25.8
C_7	37.54	37.0	40.91	40.5	37.13	37.1	45.07	40.06	38.95	-	41.17	40.7

a = experimental value

b = literature value from ref (10)

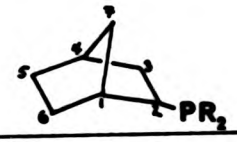

16

2.2.1 Selective Phosphorus and Hydrogen Broadband Decoupling of ^{13}C NMR Spectra

In the few cases where ^{13} signals could not be readily demonstrated to belong to the exo or the endo isomer, $^{13}C\{^{13}P$ sel, $^{1}H\}$ decoupling experiments were performed. These were achieved by irradiating at the ^{31}P frequency at one of the phosphorus isomers and comparing the resulting spectrum to the normal $^{13}C\{^{1}H\}$ spectrum on the same spectral width. Then the phosphorus resonance of the other isomer was irradiated and this spectrum was also compared to the normal $^{13}C\{^{1}H\}$ spectrum. It was feasible to do this because the phosphorus chemical shift difference between the two exo/endo isomers, as can be estimated from Table 2.2-4, was about 6 ppm, which at ^{31}P resonance frequency of 36.2 MHz, is about 200 Hz apart. For samples where the chemical shift differences were smaller, less than say 4 ppm (ca. 150 Hz), the separation was not as good. However it was still possible to detect the ^{13}C enhanced signals arising from the ^{31}P-irradiated isomer. Fig. 2.2-2 shows an example of exo and endo 2-norbornyl bis(diethylamino) phosphines, in an exo:endo ratio of 2:1, where the chemical shift differences between the exo/endo phosphorus isomer resonances was only 2.1 ppm (ca. 76 Hz). Here the red markings show two couplings arising from the endo isomer. The green marking shows coupling from the exo isomer.

2.2.2 A Pulse Sequence for a 2D $^{13}C\{^{31}P,^{1}H\}$ vs J(P,C) $\{^{1}H\}$ J-resolved Experiment

In systems such as the norbornyl cages, many ^{13}C resonances from both exo and endo isomers absorb in a small chemical shift range and extensive overlap may result. To alleviate this particular problem we propose the use of a two-dimensional J-resolved experiment. The two dimensionality of this technique will allow separations of these overlapped carbon resonances if a $^{13}C\{^{31}P,^{1}H\}$ vs J(P,C) $\{^{1}H\}$ format is used.

Fig. 2.2-2 ^{13}C NMR Spectra of a Mixture of exo and endo 2-norbornyl bis(diethylamino) Phosphines Subjected to Selective Phosphorus Irradiation

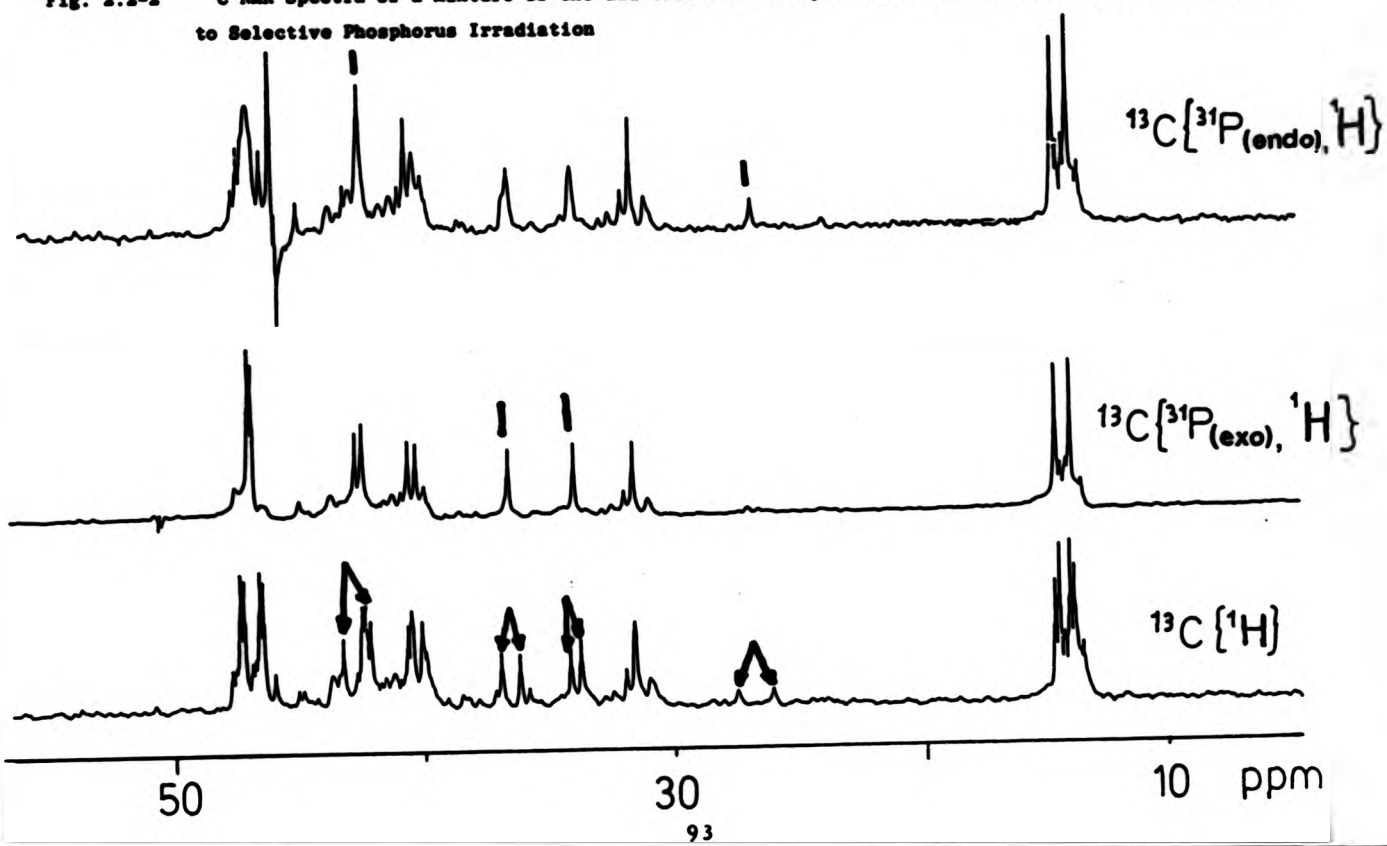

Here the $^{13}C\{^{31}P\}$ spectrum will lie along the F_2 axis and the corresponding $^nJ(P,C)$ will be along the F_1 dimension. ^1H decoupling is effected along both axes. The basic experiment is that of a spin-echo and the sequence is shown in Fig. 2.2-3. If this sequence is compared

Fig. 2.2-3 The 2D Pulse Sequence for $^{13}C\{^{31}P\}$ vs J(P,C) J-resolved Experiment with Broadband Decoupling in Both Dimensions

Note: ^1H decoupling occurs in both dimensions

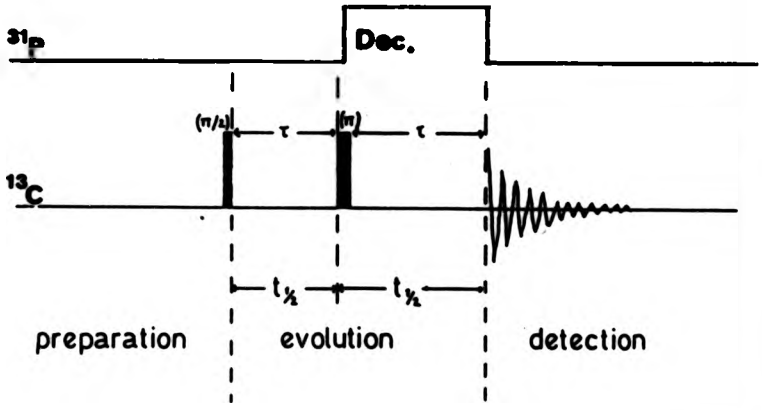

with the ^{13}C vs $J(^{13}C-^1H)$ J-resolved sequence in Fig. 1.5-14[B], it will be seen that a simple but useful modification has been made to encompass the heteronuclear $^{31}P-^{13}C$ system. This is to gate the interval just previous to the refocussing pulse which is applied to the ^{13}C observed spins. This will allow an interchange of the spin labels associated with the different spin states of the phosphorus. Thus when this occurs, the F_1 dimension will contain the heteronuclear coupling constants $J(^{31}P-^{13}C)$. Proton decoupling is kept on all the time to allow decoupling along both axes. The two-dimensional spectrum is

Fig. 2.2-4[A] A 2D $^{13}C\{^{31}P,^{1}H\}$ /J(P,C) $\{^{1}H\}$ Stack Plot and
[B] A $^{13}C\{^{1}H\}$ NMR of exo 2-norbornyl dichloro phosphine

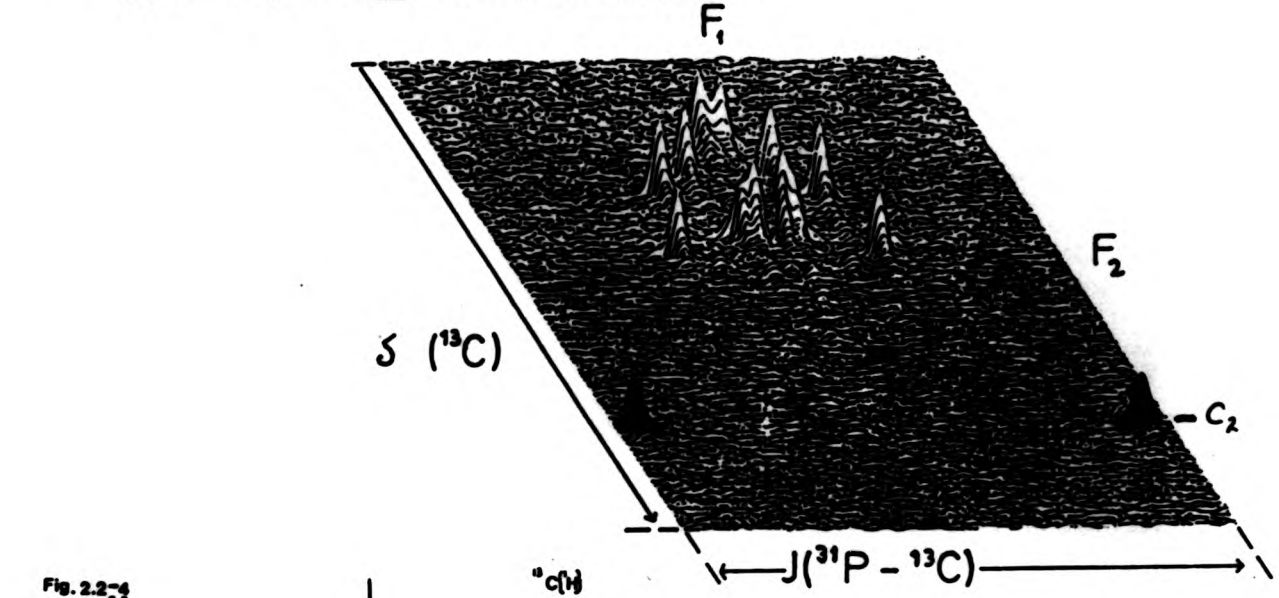

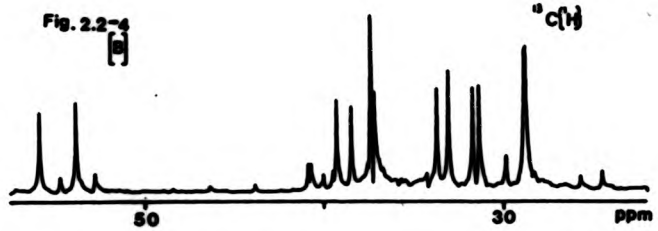

achieved in the normal way, as discussed in Section 1.5.2, and an example of a 2D stack plot is shown in Fig. 2.2-4[A] on a sample of exo and endo 2-norbornyl dichloro phosphines. The normal ^{13}C spectrum for the same sample is shown below it, in Fig. 2.2-4[B]. J(P,C) couplings for each associated carbon can be easily isolated by taking data slices along the F_1 dimension on the F_2 resonance or virtually, as can be seen, can be read off the stack plot. Also projections may be taken along the F_2 axis to yield the $^{13}C\{^{31}P,^{1}H\}$ decoupled spectrum. Hence, this is a powerful technique as it allows easy clarification of initial assignments through coupling magnitudes for mixtures of isomers which are undeterminable by 1D attack.

2.2.3 ^{31}P NMR Data of the 2-norbornyl Phosphorus Derivatives

The NMR data for the various prepared 2-norbornyl phosphorus derivatives are given in Table 2.2-4. Generally, the ^{31}P chemical shift table seems to reflect the overall trends expected for phosphorus chemical shift data in terms of the effects of different substituents. For example, going from $-PCl_2$, to $-P(NMe_2)_2$, to PPh_2, to $-PMe_2$, these substituents show the chemical shift to move to lower frequency. However, difficulty arises when one tries to interpret differences between exo and endo isomers for a range of compounds. For example, for some substituents such as $-PMe_2$, and $-P(S)Me_2$, the value of $[\delta_{exo-endo}]$ is +4.0 and +2.0 respectively, suggesting that the greater crowding at the endo position produces a shift to lower frequency compared with the exo isomers. On the other hand, other substituents such as the series $-PCl_2$, $-PBrCl$, $-PBr_2$, $-P(OMe)_2$, and $-P(O)(OMe)_2$ indicate the opposite to be true. These differences in $[\delta_{exo-endo}]$ have led Quin et al[10] to propose a second effect to be at work: namely geometrical factors which arise from subtle molecular differences related to parameters such as

Table 2.2-4 ^{31}P NMR Chemical Shifts of Some 2-Norbornyl/ Phosphorus Compounds

Substituent R =	2-norboryal-R			Ratio	Preparation
	Exo	Endo	$\delta_{Exo-Endo}$	Exo:Endo	Number
P(III)					
PBr_2	193.4	201.2	-7.8	4:1	[11]
PClBr	183.8	191.7	-7.9	5:1	[12]
PCl_2 [a]	186.0	194.8	-8.8	4:1	[13]
$P(OMe)_2$	183.5	190.0	-6.5	4:1	[17]
$-O-PCl_2$ [a]	175.6	-	-	-	[24]
PPhCl	97.6	102.3	-4.8	2:1	[18]
$P(NEt_2)_2$ [b]	91.9	94.0	-2.1	3:1	[15]
PClPh	82.9	87.6	-4.7	2:1	[18]
	51.6	54.6	-3.0	3:1	[21]
	47.8	50.7	-2.9	2:1	[19]
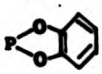	48.6	49.8	-1.2	2:1	[20]
PPh_2	-7.5+	-11.5+	+4.0	1:1	[14]
PMe_2 [a]	-43.4+	-47.4+	+4.0	2:1	[16]
P(V)					
$P(S)Me_2$	42.1	40.1	+2.0	2:1	[24]
$P(O)OMe)_2$	28.9	29.7	-0.8	2.3	[22]
$P(O)(OPh)_2$	12.0	8.9	+3.1	2.3	[23]

+ negative signs are low frequency of H_3PO_4 = 0.0 ppm; in C_6D_6 solvent except where noted

a in $CDCl_3$

b in CD_2Cl_2

bond and torsion angles, and bond lengths. In the case of the 2-norbornyl substituents, different ^{31}P shift effects at the exo or endo positions seem to show a combination of both.

To try to understand the reason as to why both contributions may be possible, one has to consider the detailed structure of the system. As there has been very limited work in this area of chemistry and as these air-sensitive compounds do not lend themselves very easily to crystal structure determinations, very few have been done. The most useful one, that of exo N-(2-norbornyl) benzamide[10,15] has been used as a basis for calculation of angles and to visualize the torsion angle dependence. In the endo isomer the torsion angle between the C_1 hydrogen and the endo phosphorus at position C_2 is twice that which occurs when the phosphorus is in the C_2 exo position, (i.e. in the exo isomer). Thus lower frequency shifts associated with the exo isomer may be the result of greater proximity to this γ C_1 hydrogen.

However, the [$\delta_{exo-endo}$] column in Table 2.2-4 reflects that if there is a second geometric interaction then both interactions are active together. For example, steric compression effects dominate for $-PMe_2$, $-P(O)(OPh)_2$ and $-P(S)Me_2$ substituents whereas for $-PCl_2$, $-PBr_2$, and $-P(NMe_2)_2$ the second geometrical effect seems to prevail. For $-P(O)(OMe)_2$ and 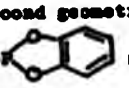 groups there is a balance between the two effects. It is not clear from this data which effect dominates the other. This table also seems to reflect that for most substituents the geometric effect is the one most likely to predominate.

2.2.4 ^{13}C NMR and ^{1}H NMR Data

The ^{13}C and ^{1}H NMR data are given in Tables 2.2-5 to 2.2-18(A). As the compounds used in this thesis have complicated structures with all carbons coupled to phosphorus and are obtained as exo:endo mixtures,

great care was needed in the assignment of the particular carbon in question. Differentiation between the exo and the endo isomers usually presented no problem as different intensity proportions made it fairly easy to identify the carbons belonging to a particular isomer. In the cases where overlap made identification difficult, a decoupling technique could be used whereby the exo or endo phosphorus resonance could be selectively decoupled. The resulting ^{13}C spectrum could be compared with the normal ^{13}C spectrum, as described in Section 2.3.1.1 to identify by the absence of coupling which signals belonged to the decoupled isomer. Also higher magnetic field strengths corresponding to spectra at 50.3 MHz and 62.9 MHz, could be used to yield a greater peak separation and hence alleviate the problem of overlapping signals.

Differentiation between CH and CH_2 carbons was effected by use of the 1D GASPE sequence, as described in Section 1.5.1. Comparisons with other ^{13}C NMR data from similar compounds and those prepared by Bensera[9], Quin[10] and Theim[12] were used to confirm these assignments. Differentiation between the different CHs and CH_2s were made by all of the above-mentioned techniques and by use of the magnitude of the $^{n}J(P,C)$ to separate these groups.

Some of the compounds presented their own peculiarities and a short explanation is given. However in order to show how these data tables were produced, a full analysis is given for the first compound mixture: namely exo and endo 2-norbornyl dichloro phosphines [13].

Exo and Endo 2-norbornyl dichloro phosphines [13]

A ^{31}P NMR spectrum revealed an exo:endo mixture ratio of ca. 4:1 as shown in Fig. 2.2-5[A]. The ^{13}C spectrum, in Fig. 2.2-5[B], was assigned with the aid of Quin's previous work[10]. The GASPE sequence was used to distinguish between the CH and CH_2 groups and partially confirmed the initial ^{13}C assignments. A 2D J-resolved $^{13}C(^{31}P)$ vs $^{n}J(P,C)$ experiment

was performed to clarify some of the overlapping couplings originating from particularly chosen ^{13}C resonances, as described previously in Fig. 2.2-4. With this experiment clear interpretation of ^{13}C NMR chemical shifts could be made as here all the P-C couplings lie along the F_1 dimension while a $^{13}C\{^{31}P,^{1}H\}$ spectrum lies along the F_2. Hence the determination of the values of $^{n}J(P,C)$ became the simple task of reading off the coupling constants by taking data slices along the F_1 dimension of the appropriate assigned carbon in the 2D J-spectrum.

Fig. 2.2-5 A ^{31}P [A] and a $^{13}C\{^{1}H\}$ [B] NMR Spectrum of exo,endo 2-norbornyl dichloro phosphines

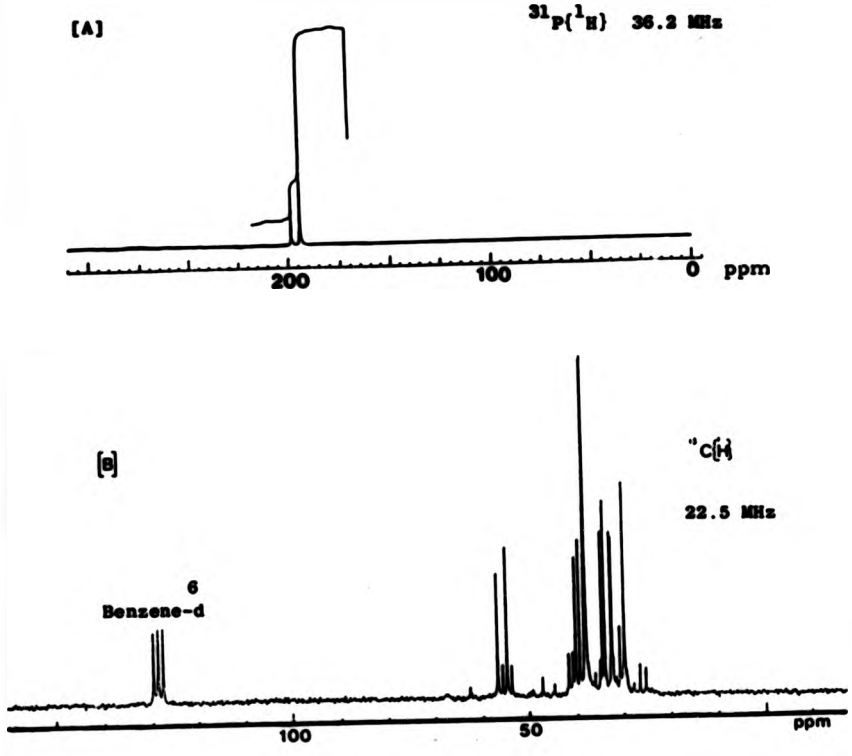

Fig. 2.2-6 Hydrogen Resonances in the 90° cross sections of the F_1 Dimension which correspond to the carbon signals in the F_2 Dimension

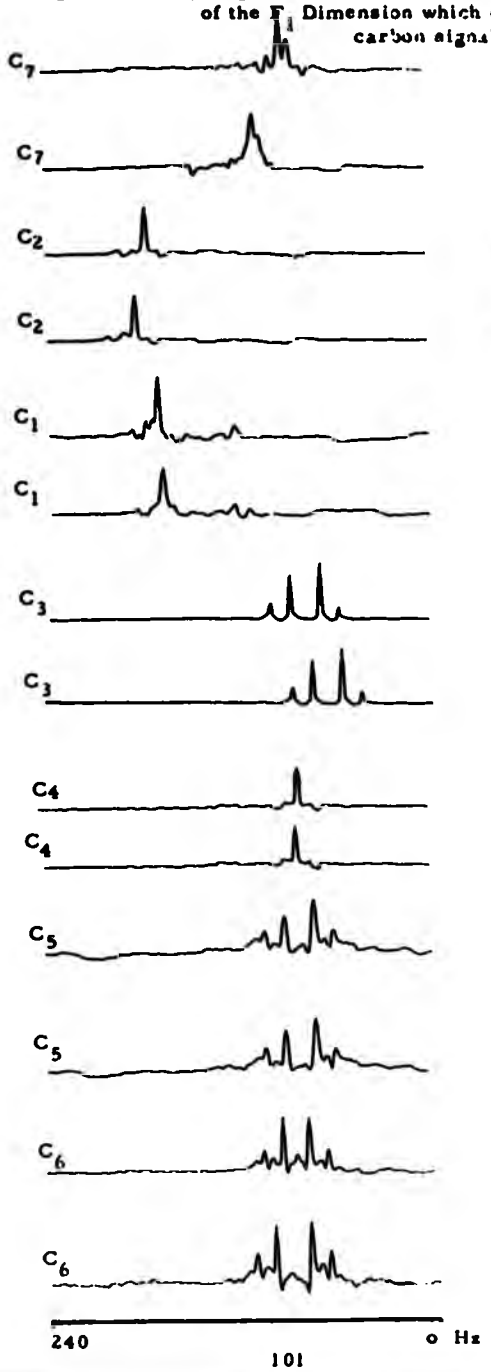

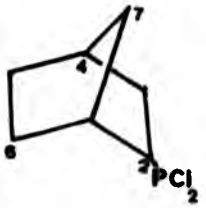

EXO

To determine the ^{1}H chemical shifts of the two isomers, a 2D $^{13}C/^{1}H$ shift correlated experiment was performed with homonuclear broadband decoupling in both dimensions (Section 1.5.2.2, Fig. 1.5-21). The data array was chosen to have minimum spectral widths in both the carbon and hydrogen spectra subject to containing all the necessary resonances. This was done to optimise the digital resolution in the F_1 and F_2 dimensions and to minimise the computation time, by using the minimum number of data points in each dimension. The hydrogen resonances in the data slices of the F_1 dimension which correspond to the carbon signals in the F_2 are shown in Fig. 2.2-6. For the C_1, C_4 and C_2 signals the hydrogen chemical shifts may be readily determined by taking the mean of the $CP_{\underline{\alpha}}$ and the $CP_{\underline{\beta}}$ slices in the F_1 dimension. Also the difference here is the J(P,H) coupling. For slices arising from carbons C_3, C_5, C_6 and C_7, AB quartets are shown, demonstrating coupling between inequivalent hydrogens in a CH_2 group. (This then allows a further check as to the assignment of the particular carbon and hydrogen.) Complex analysis as outlined in Section 2.1.3.2 was individually performed on each $CP_{\underline{\alpha}}$ and $CP_{\underline{\beta}}$ slice. This yielded two effective hydrogen chemical shifts, H_A and H_B, for each of the $CP_{\underline{\alpha}}$ and $CP_{\underline{\beta}}$ slices. Then the difference between $\underline{\delta}^{eff}(P_{\underline{\alpha}}H_A)$ and $\underline{\delta}^{eff}(P_{\underline{\beta}}H_A)$ will be the J(P,H) coupling for H_A and the true chemical shift will be the mean frequency between these $P_{\underline{\alpha}}H_A$ and $P_{\underline{\beta}}H_A$ resonances along the F_1 dimension. Likewise calculation of $J(P,H_B)$ and δ_B is performed. A sample calculation was previously shown in Fig. 2.1-7 for the C_3 carbon of this sample.

Exo and Endo 2-carbonyl dibromo phosphines [11]

The ^{13}C NMR spectrum is shown in Fig. 2.2-7[A]. As can be seen, in these very complex systems even though intensity differences exist between exo and endo isomers, there is still difficulty in proper assignment of ^{13}C spectra. This is largely because apart from the $^{13}C_2$

resonance the chemical shift range of the norbornyl system is only ca. 15 ppm. A convenient solution to this was the use of the GASPE sequence, described in Section 1.5.1.3, to distinguish between ^{13}CH and $^{13}CH_2$ groups in the bicyclic ring. The resulting spectrum is shown in Fig. 2.2-7[B]. Here the CHs are emission phased and the CH_2s are absorption phased.

Fig. 2.2-7 A 1D $^{13}C\{^1H\}$ normal [A] and a GASPE [B] NMR Spectrum of exo, endo 2-norbornyl dibromo phosphines

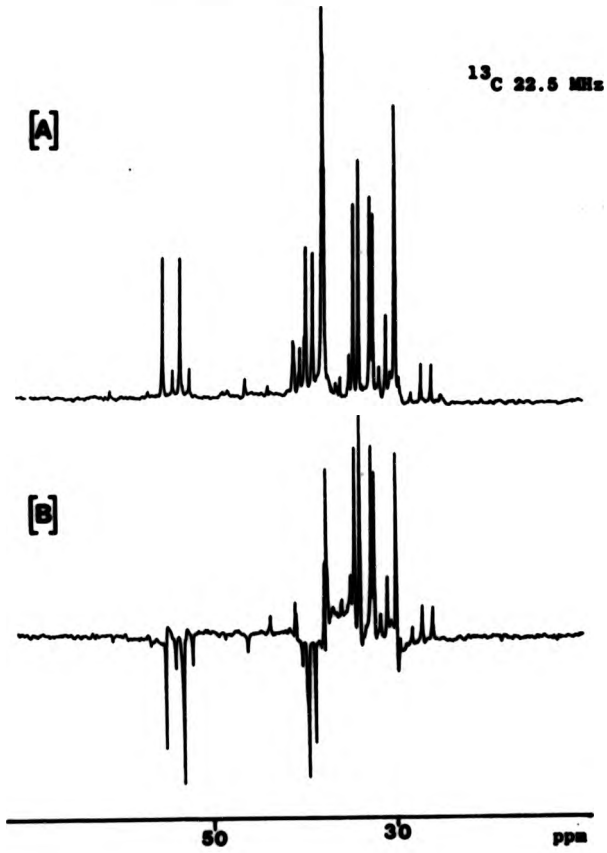

The ^{1}H chemical shifts were determined by use of a 2D $^{13}C/^{1}H$ heteronuclear shift correlation sequence as described in Section 1.5.2.2, Fig. 1.5-21. Each ^{13}C signal is split into doublets by $^{n}J(^{31}P,C)$ and each line yields its <u>own</u> proton cross-section in the 2D spectrum. The effective proton chemical shifts are now given by $\delta(H) = \pm \frac{1}{2}J(^{31}P,H)$ and this is shown for the <u>exo</u> isomer in Fig. 2.2-8[A]. The 2D Stack Plot is shown in Fig. 2.2-8[B]. Data resulted from such experiments performed on a mixture of <u>exo</u> and <u>endo</u> forms. As can be seen from Fig. 2.2-8, identification of inequivalent methylene groups is easy. The values of $^{n}J(P,H)$ were determined by taking the appropriate difference between their respective dimensional data slices.

<u>Exo and Endo 2-norbornyl bromochloro phosphines [12]</u>

The ^{31}P NMR spectrum is expected to have four lines arising from the <u>R exo</u> and <u>endo</u> forms and the <u>S exo</u> and <u>endo</u> forms as shown in Structure 7 as the phosphorus atom should be chiral. However, the ^{31}P

Structure 7

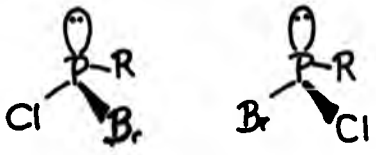

NMR spectrum shown in Fig. 2.2-9[A] suggests that only two forms in an <u>exo</u>:<u>endo</u> ratio of 5:1 exist. It is possible that the chlorine and bromine are not dissimilar enough to promote effective chirality on the phosphorus. ^{13}C NMR evidence supports this premise as only two major isomers - one <u>exo</u> and one <u>endo</u> - are present. This is shown in Fig. 2.2-9[B]. ^{13}C assignments were determined on this basis by use of the GASPE pulse sequence and by comparison with compounds [11] and [13] and with similar compounds prepared by Quin[10]. A 2D $^{13}C/^{1}H$ heteronuclear

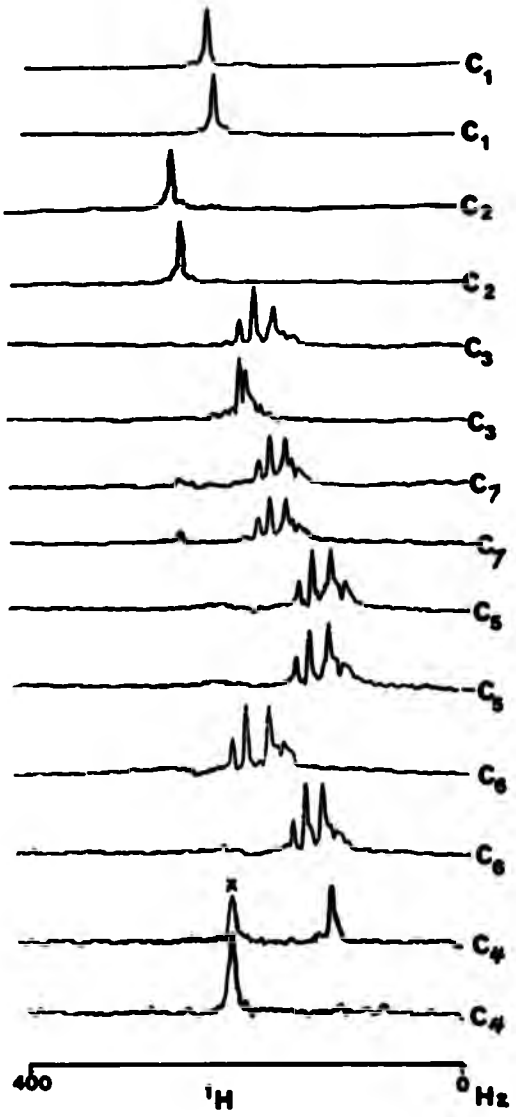

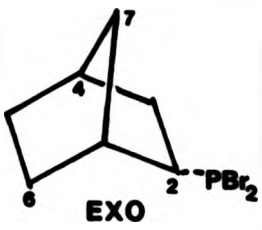

Fig. 2.2-8[A]
90° OXQ Data Matrix Slices of a $^{13}C/^{1}H$ Heteronuclear Shift Correlated 2D NMR Spectrum of exo 2-norbornyl dibromophosphine

Fig. 2.2-8[B] A $^{13}C/^{1}H$ shift correlation 2D Stack Plot of 2-norbornyl dibromo phosphine

^{13}C = 22·5 mHz
^{1}H = 89·56mHz

2048 x 256 data matrix

in Ben^{6}d 1 : 1

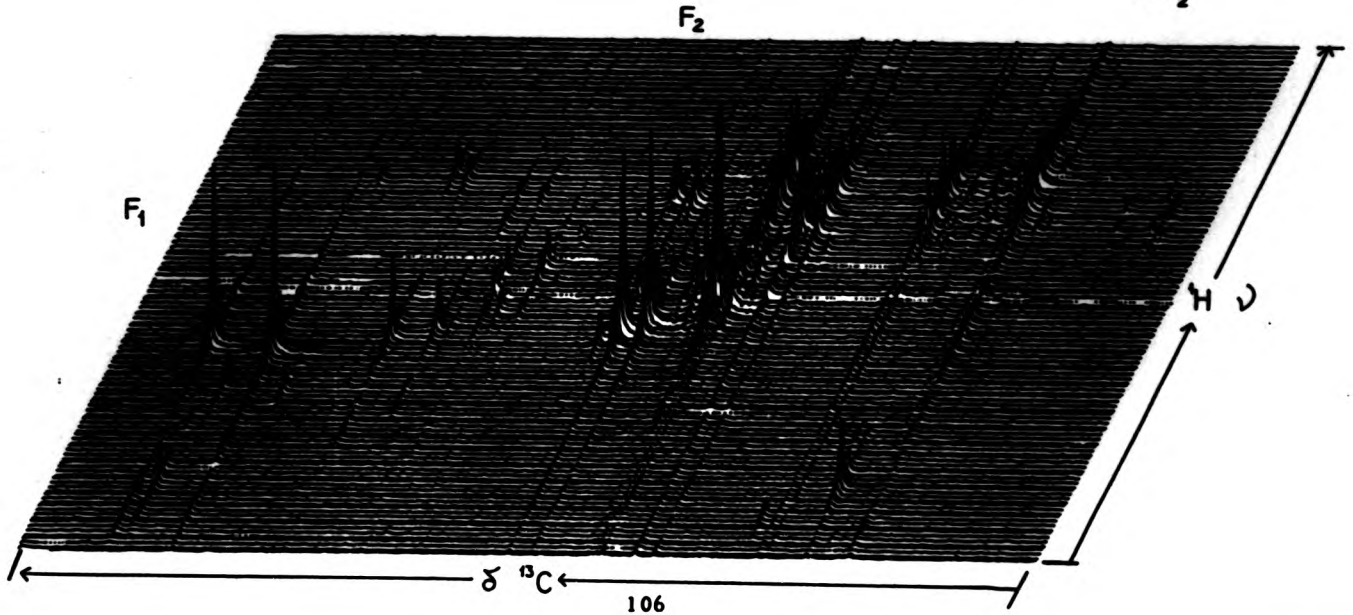

shift correlation experiment yielded the hydrogen chemical shifts and the values of $^{n}J(P,H)$. Due to the instability of the compound at room temperature and low proportions of the endo form in the mixture, only limited hydrogen analysis was possible for this isomer.

Fig. 2.2-9 A ^{31}P[A] and $^{13}C\{^{1}H\}$ [B] NMR Spectrum of a mixture of exo, endo 2-norbornyl bromochloro phosphines

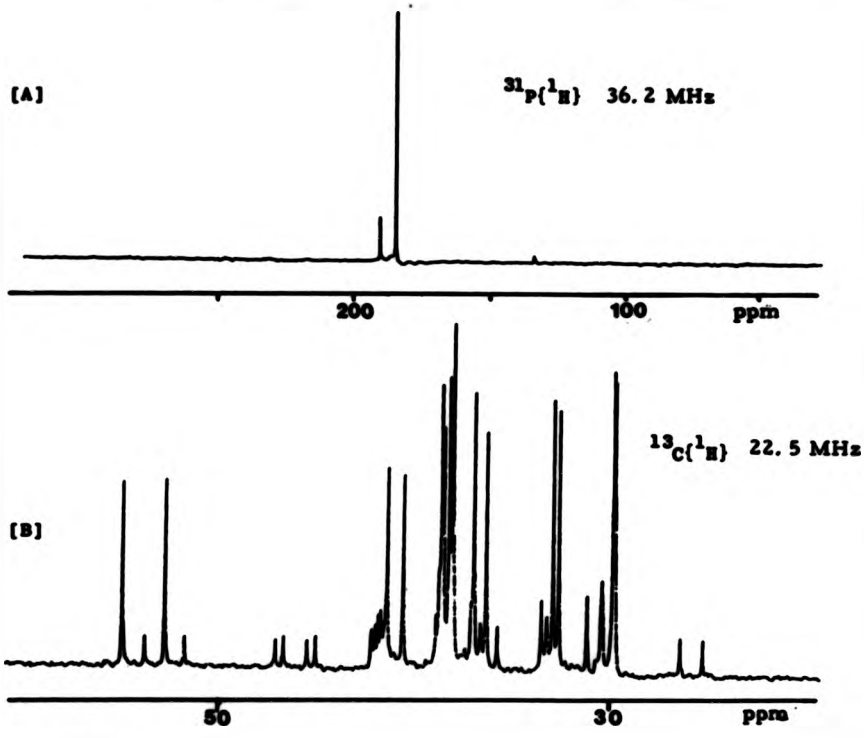

Exo and Endo 2-norbornyl dimethyl phosphites (17)

In the $-P(OMe)_2$ derivative the two methoxy carbons attached to the phosphorus atom are rendered non-equivalent by chirality at the norbornyl C_2 carbon, and separate doublets are seen for each methoxy group of the exo and the endo isomers. Hence eight lines are expected in the ^{13}C spectrum. The peak separation is small however and only four lines can

be resolved at 22.5 MHz. This is shown in Fig. 2.2-10[A]. A 62.9 MHz ^{13}C spectrum was obtained and at this field strength the four exo signals are clearly shown and three of the four endo signals can be seen. This expansion is included in Fig. 2.2-10[B]. ^{13}C assignments were made on the basis of comparison with results obtained by Quin[10] and were checked by use of the GASPE pulse sequence. $^{n}J(P,C)$ were deduced from the 1D ^{13}C spectrum. A $^{13}C/^{1}H$ 2D shift correlation experiment yielded the ^{1}H chemical shifts and the values of $^{n}J(P,H)$ for the compound.

Fig. 2.2-10 [A] A $^{13}C(^{1}H)$ NMR spectrum of a mixture of exo, endo 2-norbornyl dimethyl phosphites at 22.5 MHz and [B] An expansion of the Methoxy region at 62.5 MHz

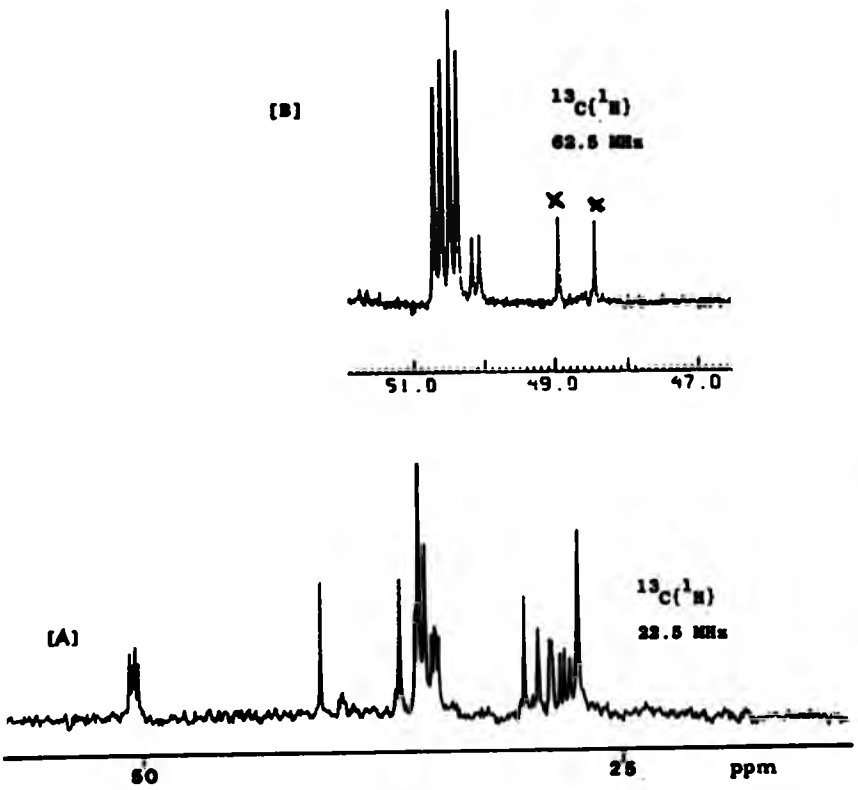

Exo 2-norbornyl phosphonic dichloride [24]

Only the exo product, though unstable, was formed when phosphorus trichloride was reacted with exo norborn-2-ol. This suggests that the bulky substituent, though highly confined, would have a less restricted rotation in the exo position and as a result the reaction is stereo-specific. Due to the instability of this compound at room temperature, only ^{13}C analysis could be performed. A GASPE sequence was used to differentiate between the CH and the CH_2 resonances and a $^{13}C\{^{31}P,^{1}H\}$ double resonance spectrum allowed assignment and estimation of the values of J(P,C). Comparison with other similar samples resulted in the proposed ^{13}C assignments.

Exo and Endo 2-norbornyl bis(diethylamino) phosphines [16]

In the $-P(NEt_2)_2$ derivative, the two diethylamino groups are non-equivalent, due to chirality at the norbornyl C_2 carbon, and separate doublets are seen for each of the methylene and methyl carbons of both the exo and endo isomers. This can be illustrated as mirror image isomers in Structure 8. Hence eight lines are expected for each of the

Structure 8

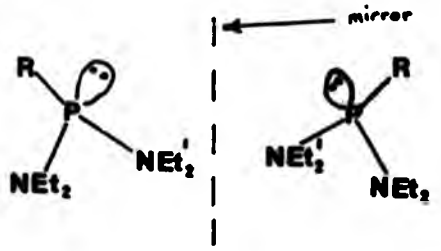

CH_2 and CH_3 groups in the ^{13}C NMR spectrum. As the resonances of the CH_2 and the CH_3 groups occur within a small chemical shift range and the peak separations are small, selective phosphorus decoupling experiments were performed to separate the signals (the exo from the endo isomer) as previously demonstrated in Section 2.2.1, Fig. 2.2-2. A GASPE experiment was performed on the ^{13}C spectrum to assign the CH_2 and CH

groups in the norbornyl ring. A 62.9 MHz ^{13}C NMR spectrum allowed final separation of the diethylamino chemical shifts and determination of the associated coupling constants.

As can be seen in Fig. 2.2-11 the 1D ^{1}H spectrum allows no feasible assignments of any proton chemical shifts. Hence a 2D $^{13}C/^{1}H$ shift correlation experiment with homonuclear broadband decoupling in both dimensions was undertaken to elucidate hydrogen chemical shifts and the values of $^{n}J(P,H)$.

Fig. 2.2-11 ^{1}H NMR Spectrum of <u>exo</u>, <u>endo</u> 2-norbornyl bis(diethylamino) phosphines

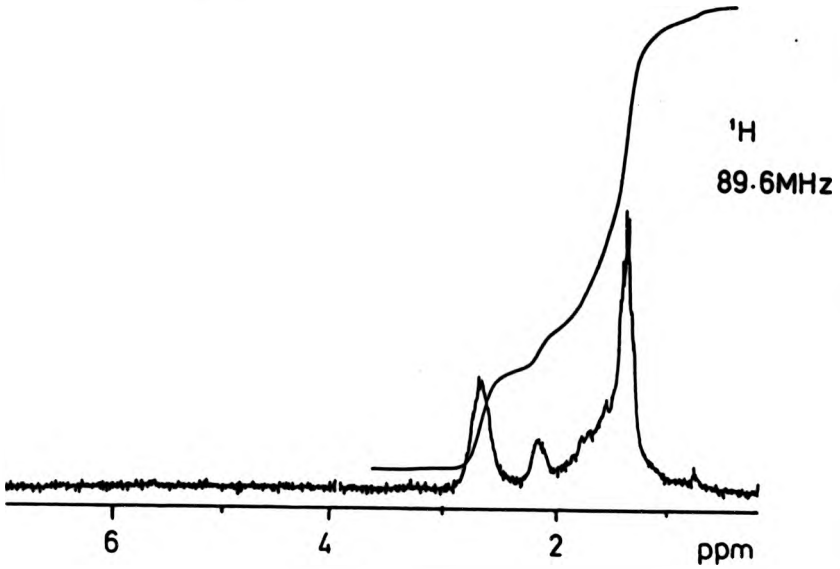

<u>Exo and Endo 2-norbornyl chloro phenyl phosphines [18]</u>

In Fig. 2.2-12 the ^{13}P NMR spectrum shows the four isomers from a reaction of dichloro phenyl phosphine with the 2-norbornyl Grignard reagent. This feature arises because the C_2 carbon on the norbornyl ring is chiral. This will give rise to both <u>R</u> and <u>S</u> <u>exo</u>, and <u>R</u> and <u>S</u> <u>endo</u> isomers. Attempted separation of the isomers proved unsuccessful

and hence only accurate ^{31}P chemical shifts could be obtained.

Fig. 2.2-12 ^{31}P NMR of a mixture of exo, endo 2-norbornyl chloro phenyl phosphines

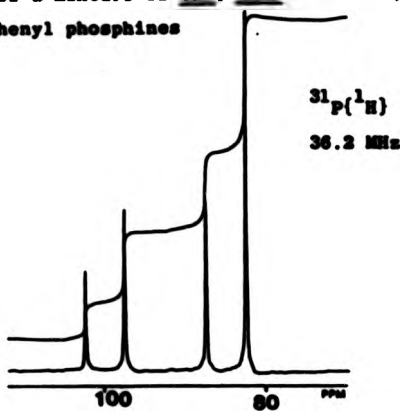

Exo and Endo 2-norbornyl 1.3-dithiol phospholanes [21]

The GASPE sequence was used to identify the CH and CH_2 resonances in the ^{13}C spectrum. Individual CH and CH_2 ^{13}C assignments were inferred by comparison with other similar compounds and with those prepared by Quin et al[10]. J(P,C) couplings were easily read off the ^{13}C spectrum and their magnitudes were compared with those of other compounds of this type. A $^{13}C/^{1}H$ shift correlation experiment was performed to give the related hydrogen chemical shifts and the associated values of $^{n}J(P,H)$. Data patterns are similar to those shown for other compounds of the series.

The effect of sulphur is to deshield the norbornyl ring and as can be seen an overall shift to high frequency of both the carbon and hydrogen chemical shifts results. This is reflected in the case of the C_2 carbon in the compound, as the ^{13}C resonance is at 48 ppm. The two methylene carbons C_8 in the five membered 1,3-dithiol phospholane ring show likewise a pronounced carbon shift of 56 ppm. This high frequency shift can be easily seen in the Stack Plot given in Fig. 2.2-13.

Fig. 2.2-13 A 2D Stack Plot from a $^{13}C/^{1}H$ Shift Correlated Experiment

^{13}C = 22.5MHz
^{1}H = 89.56MHz
2048 × 256 data matrix

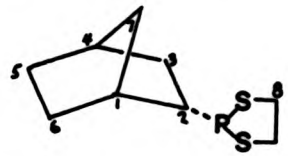

in Ben^{6}d 1;1

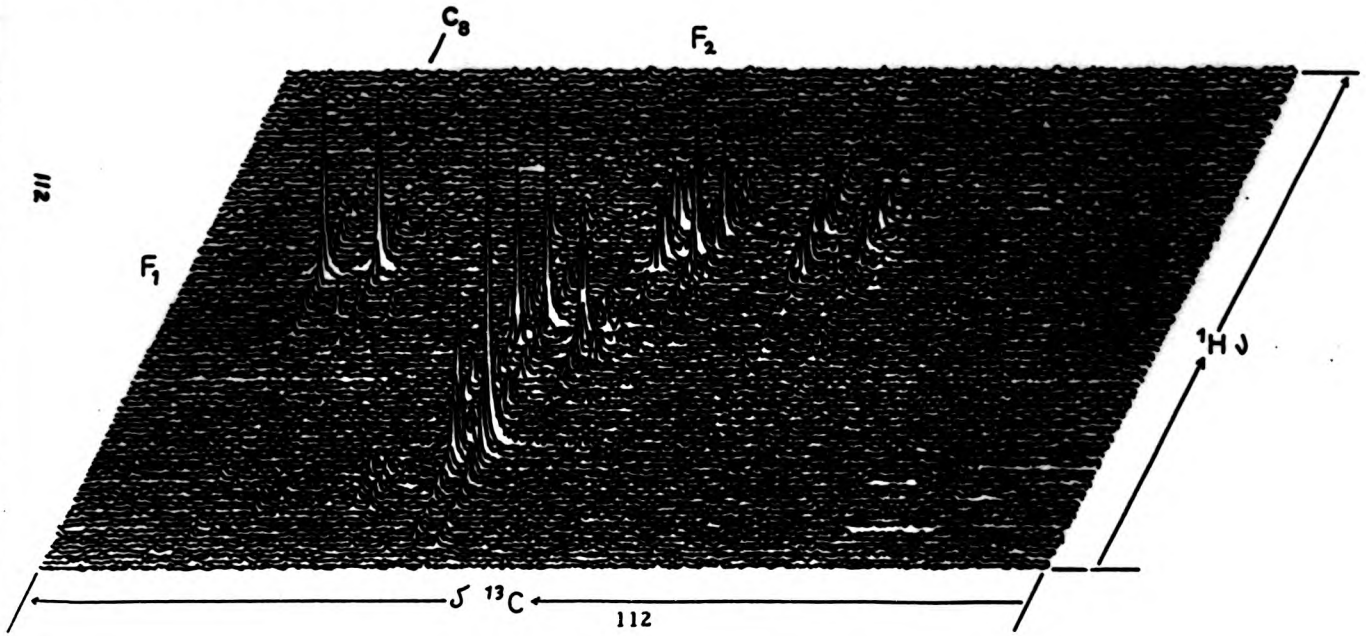

Exo and Endo 2-norbornyl 1,3 dioxaphospholanes [19]

and

Exo and Endo 2-norbornyl dioxa o-phenylene phospholes [20]

As with the 1,3-dithiol phospholane derivatives, the deshielding effect of the oxygen produces a shift to high frequency in both the carbon and hydrogen chemical shifts associated with the norbornyl ring for the two derivatives. In the case of the o-phenylene phospholane derivative, the aromatic ring has a stabilising effect upon the P-O-C ring and less deshielding is experienced by the phosphorus. The aromatic ring would also reduce the opportunity for the P-O-C ring to adopt a twist-envelope[16] conformation (shown in Structure 9) and the ring is probably stable and planar. ^{13}C assignments were assessed by comparing all six exo and endo: dioxa, dithiol, and o-phenylene derivatives, by use of the GASPE 1D technique, and by ^{13}C NMR experiments with selective phosphorus decoupling.

Structure 9

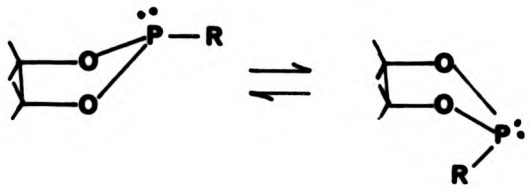

Exo and Endo 2-norbornyl diphenyl phosphines [14]

In the $-PPh_2$ derivative, the two phenyl groups attached to the phosphorus atom are non-equivalent, due to chirality at the norbornyl C_2 carbon, and separate doublets are expected for each of the aromatic carbons in each of the exo and endo isomers. Hence four pairs of doublets are expected for each of the aromatic carbons in the normal ^{13}C NMR spectrum. The peak separation is small however and even at

62.9 MHz, only the ipso-carbons are resolved. Other aromatic signals were in two unresolved clusters at 128.6 to 129.1 ppm and 133.2 to 134.3 ppm. The proposed ^{13}C and ^{1}H chemical shift and phosphorus coupling data result from 1D and 2D experiments.

Exo and Endo 2-norbornyl dimethyl phosphines [16]

Similar 1D NMR analyses were carried out as previously shown for the other derivatives in this series of compounds. Because of their great sensitivity to air, isolation of the compound was difficult and no 2D NMR analysis could be undertaken as sufficient material was unavailable. ^{13}C assignments were based on the same compound prepared by Quin et al[10] and the use of a 1D GASPE assign sequence supported this assignment. Since the C_2 position on the norbornyl ring is chiral, the two methyl groups attached to the phosphorus atom are non-equivalent. Thus for the $-PMe_2$ function, separate doublets are seen for each of the methyls of both exo and endo isomers in the carbon spectrum. The values of $^{n}J(P,C)$ were measured from the ^{13}C spectrum. The ^{1}H 1D spectrum revealed absorptions in the 0.9 to 2.3 ppm range though no isolated chemical shifts could be seen even at 200 MHz.

2.2.4.1 ^{13}C chemical shifts

Many systems have been devised in which one particular feature may make a dominant contribution to the overall screening constant, so that conclusions may be drawn to elucidate the mechanism of intramolecular substituent effects. In this respect, the choice of the observed nucleus is most critical. ^{13}C nuclei are extremely sensitive to the electronic environment which is reflected by their large chemical shift range, ca. 600 ppm. The advent of Fourier transform machines has made feasible the running super$^{\frac{1}{2}}$ quality routine ^{13}C NMR spectra, and

... continued on page 128

Table 2.2-6 ^{13}C and ^{1}H NMR Data of Exo, Endo 2-norbornyl dibromo phosphines [11]

[A] Chemical Shifts

Carbon Position	$\delta\ ^{13}C$/ppm			$\delta\ ^{1}H$/ppm			
	Phosphorus Position			Phosphorus Position Exo, Hydrogens:		Endo, Hydrogens:	
	Exo	Endo	δ-δ	Exo	Endo	Exo	Endo
C_1	40.75	41.06	-0.31	NA	1.58	1.54	NA
C_2	54.97	53.67	1.30	NA	2.82	3.15	NA
C_3	36.43	37.03	-0.6	1.52	1.73	2.12	1.41
C_4	37.99	38.35	-0.36	NA	2.48	2.41	NA
C_5	29.34	30.77	-1.43	1.61	1.31	3.93	3.93
C_6	32.36	27.13	5.23	1.74	1.40	1.64	1.18
C_7	38.60	41.72	-3.12	2.26	2.71	1.42	1.63

[B] $^{n}J(P,X)$

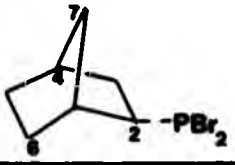

Carbon Position	$^{n}J(P,C)$/Hz		$^{n}J(P,H)$/Hz			
	Phosphorus Position		Phosphorus Position Exo, Hydrogens:		Endo, Hydrogens:	
	Exo	Endo	Exo	Endo	Exo	Endo
C_1	18.06	11.42	NA	3.1	6.3	NA
C_2	51.18	48.58	NA	3.1	6.3	NA
C_3	11.43	16.79	6.9	10.9	3.4	6.0
C_4	2.74	4.29	NA	1.6	0.4	NA
C_5	1.95	2.73	0.0	0.0	0.5	0.0
C_6	9.03	27.34	0.1	0.3	0.4	4.7
C_7	2.93	1.56	7.8	6.2	0.6	0.2

Table 2.2-6 ^{13}C and ^{1}H NMR Data of Exo, Endo 2-norbornyl bromochloro phosphines [12]

[A] Chemical Shifts

Carbon Position	$\delta\ ^{13}C$/ppm			$\delta\ ^{1}H$/ppm			
	Phosphorus Position			Phosphorus Position Exo, Hydrogens:		Endo, Hydrogens:	
	Exo	Endo	Δ-Δ	Exo	Endo	Exo	Endo
C_1	39.98	41.68	-1.70	NA	2.30	2.32	NA
C_2	53.20	52.06	1.14	NA	2.50	2.85	NA
C_3	35.58	35.08	0.50	1.42	1.0	-	-
C_4	37.57	37.62	-0.05	2.06	NA	2.06	NA
C_5	28.48	30.12	-1.64	1.25	0.94	-	-
C_6	31.52	25.16	6.36	1.34	1.03	-	-
C_7	37.13	45.07	-9.94	1.15	0.89	-	-

[B] $^{n}J(P,X)$

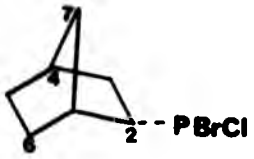

Carbon Position	$^{n}J(P,C)$/Hz		$^{n}J(P,H)$/Hz			
	Phosphorus Position		Phosphorus Position Exo, Hydrogens:		Endo, Hydrogens:	
	Exo	Endo	Exo	Endo	Exo	Endo
C_1	18.0	7.57	NA	7.0	6.3	NA
C_2	51.52	48.83	NA	6.7	6.3	NA
C_3	14.6	20.02	2.0	5.9	-	-
C_4	3.75	3.94	0.4	NA	0.3	NA
C_5	2.10	0.25	1.5	0.6	-	-
C_6	7.30	27.09	0.6	0.2	-	-
C_7	8.79	4.64	1.6	0.8	-	-

Table 2.2-7 ^{13}C and ^{1}H NMR Data of Exo, Endo 2-norbornyl dichloro phosphines [13]

[A] Chemical Shifts

Carbon Position	δ ^{13}C/ppm			δ ^{1}H/ppm			
	Phosphorus Position			Phosphorus Position Exo,Hydrogens:		Endo,Hydrogens:	
	Exo	Endo	Δ-Δ	Exo	Endo	Exo	Endo
1	38.96	39.92	0.85	NA	2.29	2.38	NA
2	84.90	83.80	1.10	NA	2.15	2.48	NA
3	33.80	33.78	-0.28	1.37	1.38	1.41	1.42
4	37.36	37.41	-0.05	NA	-	2.37	NA
5	28.93	29.98	-1.05	1.36	1.0	1.28	1.28
6	31.67	25.22	6.45	1.43	1.08	1.43	1.29
7	37.54	40.91	-3.37	1.12	1.12	1.18	1.0

[B] $^{n}J(P,X)$

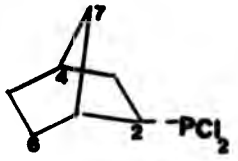

Carbon Position	$^{n}J(P,C)$/Hz		$^{n}J(P,H)$/Hz			
	Phosphorus Position		Phosphorus Position Exo,Hydrogens:		Endo,Hydrogens:	
	Exo	Endo	Exo	Endo	Exo	Endo
C_1	18.16	12.06	NA	7.3	3.0	NA
C_2	45.86	43.28	NA	2.4	3.9	NA
C_3	14.50	27.60	1.6	18.0	3.5	1.2
C_4	1.36	3.33	1.0	NA	0.0	NA
C_5	1.67	0.3	0.0	0.3	0.3	0.7
C_6	7.7	27.16	6.0	0.0	1.4	5.3
C_7	4.7	3.12	4.0	2.9	0.2	1.9

Table 2.2-6 ^{13}C and ^{1}H NMR Data of Exo, Endo 2-norbornyl dimethyl phosphites [17]

[A] Chemical Shifts

Carbon Position	δ ^{13}C/ppm			δ ^{1}H/ppm			
	Phosphorus Position			Phosphorus Position Exo, Hydrogens:		Endo, Hydrogens:	
	Exo	Endo	Δ-Δ	Exo	Endo	Exo	Endo
C_1	UR	38.5	-	US	NA	2.06	NA
C_2	44.30	42.65	1.65	NA	1.64	1.86	NA
C_3	31.35	30.80	0.55	1.42	1.20	1.08	1.44
C_4	UR	UR	-	US	NA	US	NA
C_5	29.80	30.20	-0.7	1.35	1.02	1.46	1.22
C_6	32.40	26.75	5.65	1.42	1.13	-	-
C_7	38.95	41.17	-2.22	1.38	1.0	2.15	2.26
(OMe) C_8	50.38	50.46	-0.08	3.24	NA	3.32	NA
(OMe') C_9	50.97	50.78	0.19	3.35	NA	3.30	NA

UR - unrecorded in cluster between 36-38 ppm
US - present in cluster between 2.02-2.2 ppm with J(P,H) <2 Hz

[B] $^{n}J(P,X)$

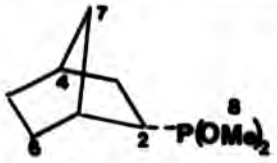

Carbon Position	$^{n}J(P,C)$/Hz		$^{n}J(P,H)$/Hz			
	Phosphorus Position		Phosphorus Position Exo, Hydrogens:		Endo, Hydrogens:	
	Exo	Endo	Exo	Endo	Exo	Endo
C_1	-	4.8	NA	-	6.0	NA
C_2	19.34	17.96	NA	19.1	17.9	NA
C_3	13.56	15.03	2.0	1.0	1.2	1.2
C_4	(2.5)	(1.5)	-	-	-	-
C_5	0.0	2.56	0.2	0.2	0.0	0.0
C_6	7.40	24.10	3.7	0.2	-	-
C_7	4.76	5.50	1.4	1.0	1.0	0.0
C_8	5.86	5.86	10.7	NA	10.7	NA
C_9	5.86	5.86	10.7	NA	10.7	NA

- Not reported
NA Not applicable

Table 2.2-9 ^{13}C and ^{1}H NMR Data of Exo, Endo 2-norbornyl bis (diethylamino) phosphines [15]

[A] Chemical Shifts

Carbon Position	$\delta\ ^{13}C$/ppm			$\delta\ ^{1}H$/ppm			
	Phosphorus Position			Phosphorus Position Exo, Hydrogens:		Endo, Hydrogens:	
	Exo	Endo	δ-Δ	Exo	Endo	Exo	Endo
C_1	39.66	39.85	-0.19	NA	1.70	1.76	NA
C_2	40.73	40.25	0.48	NA	2.04	2.08	NA
C_3	34.74	34.79	-0.05	1.61	1.03	1.13	1.16
C_4	37.81	37.86	-0.05	NA	2.16	2.16	NA
C_5	30.03	30.50	-0.47	1.32	1.03	1.31	1.46
C_6	32.55	26.41	6.14	1.52	1.17	1.26	2.07
C_7	38.56	38.27	0.29	2.06	2.69	1.68	1.32
C_8	43.86	44.17	-0.31	2.88	NA	2.90	NA
C_8'	43.49	43.74	-0.25	2.89	NA	2.90	NA
C_9	14.72	15.86	-1.14	0.92	NA	0.93	NA
C_9'	14.66	15.72	-1.06	0.90	NA	0.89	NA

[B] $^{n}J(P,X)$

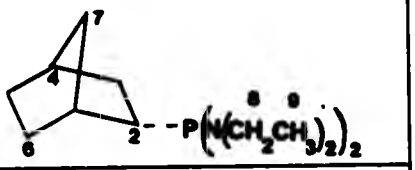

Carbon Position	$^{n}J(P,C)$/Hz		$^{n}J(P,H)$/Hz			
	Phosphorus Position		Phosphorus Position Exo, Hydrogens:		Endo, Hydrogens:	
	Exo	Endo	Exo	Endo	Exo	Endo
C_1	8.96	7.62	NA	4.2	5.9	NA
C_2	17.97	16.79	NA	7.4	6.9	NA
C_3	18.95	14.65	1.4	0.1	13.4	17.4
C_4	1.56	1.95	1.4	NA	0.1	NA
C_5	2.15	0.78	0.8	0.8	<0.2	<0.2
C_6	7.82	27.93	5.5	0.3	2.7	9.1
C_7	3.67	2.54	6.8	1.3	2.2	<0.2
C_8	15.04	15.04	7.8	NA	8.3	NA
C_8'	15.04	15.04	8.3	NA	8.3	NA
C_9	18.50	11.33	2.0	NA	3.4	NA
C_9'	18.50	11.33	0.9	NA	1.0	NA

Table 2.2-10 ^{13}C and ^{1}H NMR Data of Exo, Endo 2-norbornyl 1,3-dithiol phospholanes [21]

[A] Chemical Shifts

Carbon Position	$\delta\ ^{13}C$/ppm			$\delta\ ^{1}H$/ppm			
	Phosphorus Position			Phosphorus Position Exo, Hydrogens:		Endo, Hydrogens:	
	Exo	Endo	Δ-Δ exo endo	Exo	Endo	Exo	Endo
C_1	39.95	42.79	-2.85	NA	3.28	3.29	NA
C_2	47.46	48.03	-0.57	NA	1.50	1.51	NA
C_3	35.24	36.35	-1.10	1.20	1.12	1.08	1.46
C_4	37.96	37.54	0.42	2.18	NA	2.0	NA
C_5	29.69	30.52	-0.83	1.40	1.07	1.56	1.30
C_6	31.63	24.55	7.08	1.50	1.10	-	1.92
C_7	38.96	45.83	-5.86	3.91	2.24	1.15	1.54
C_8	56.89	56.71	0.81	1.30	NA	1.30	NA

[B] $^{n}J(P,X)$

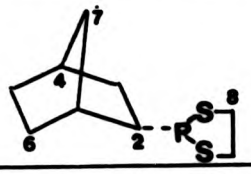

Carbon Position	$^{n}J(P,C)$/Hz		$^{n}J(P,H)$/Hz			
	Phosphorus Position		Phosphorus Position Exo, Hydrogens:		Endo, Hydrogens:	
	Exo	Endo	Exo	Endo	Exo	Endo
C_1	21.25	12.46	NA	0.8	1.6	NA
C_2	41.77	39.58	NA	4.7	4.2	NA
C_3	14.29	28.95	4.8	0.2	5.7	2.7
C_4	4.76	6.6	NA	0.2	0.6	NA
C_5	2.20	1.79	0.8	0.8	-	-
C_6	7.69	25.06	5.8	2.9	1.2	4.7
C_7	18.32	20.89	3.9	0.2	6.3	3.1
C_8	8.6	9.2				

Table 2.2-11 ^{13}C and ^{1}H NMR Data of Exo, Endo 2-norboryl 1,3-dioxaphospholanes [19]

[A] Chemical Shifts

Carbon Position	$\delta\ ^{13}C$/ppm			$\delta\ ^{1}H$/ppm			
	Phosphorus Position			Phosphorus Position Exo, Hydrogens :		Phosphorus Position Endo, Hydrogens:	
	Exo	Endo	Δ-Δ	Exo	Endo	Exo	Endo
C_1	36.69	42.80	-3.11	NA	3.12	3.06	NA
C_2	49.01	50.12	-1.11	NA	1.80	1.82	NA
C_3	35.00	36.12	-1.12	1.15	1.26	1.06	1.44
C_4	37.69	37.52	0.17	NA	2.16	2.45	NA
C_5	29.64	30.51	-0.87	1.45	1.10	1.49	1.30
C_6	32.68	28.46	4.22	1.53	1.10	1.48	1.92
C_7	40.08	46.24	-6.16	3.98	2.40	1.16	1.49
C_8	68.94	68.81	0.13	NA	2.52	2.48	NA

[B] $^{n}J(P,X)$

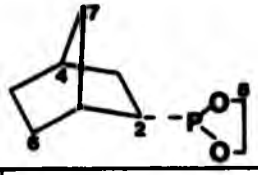

Carbon Position	$^{n}J(P,C)$/Hz		$^{n}J(P,H)$/Hz			
	Phosphorus Position		Phosphorus Position Exo, Hydrogens :		Phosphorus Position Endo, Hydrogens:	
	Exo	Endo	Exo	Endo	Exo	Endo
C_1	20.17	12.28	NA	1.0	1.6	NA
C_2	42.85	40.62	NA	4.6	4.5	NA
C_3	12.02	26.67	2.1	0.2	2.7	3.5
C_4	4.62	6.40	NA	0.6	0.3	NA
C_5	2.0	1.62	0.8	0.8	0.0	0.2
C_6	8.0	24.13	4.6	2.9	1.5	4.0
C_7	19.23	20.80	3.7	0.8	6.2	3.0
C_8	7.94	7.93				

Table 2.2-12 ^{13}C and ^{1}H NMR Data of Exo, Endo 2-norbornyl dioxa-o-phenylene phospholes [20]

[A] Chemical Shifts

Carbon Position	$\delta\ ^{13}C$/ppm			$\delta\ ^{1}H$/ppm			
	Phosphorus Position			Phosphorus Position Exo, Hydrogens :		Endo, Hydrogens:	
	Exo	Endo	$\delta_{exo}-\delta_{endo}$	Exo	Endo	Exo	Endo
C_1	39.76	40.51	-0.75	NA	3.08	3.06	NA
C_2	46.33	46.53	-0.25	NA	1.47	1.46	NA
C_3	31.94	32.08	-0.14	1.18	1.12	1.10	1.43
C_4	36.21	35.6	0.52	NA	2.60	2.78	NA
C_5	29.21	29.40	-0.19	1.20	1.16	1.22	1.26
C_6	30.13	25.56	4.57	1.36	1.26	1.42	1.89
C_7	39.66	45.73	-6.07	3.96	2.22	1.26	1.76

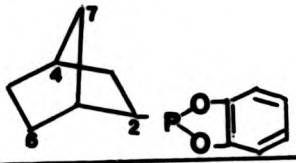

[B] $^{n}J(P,X)$

Carbon Position	$^{n}J(P,C)$/Hz		$^{n}J(P,H)$/Hz			
	Phosphorus Position		Phosphorus Position Exo, Hydrogens :		Endo, Hydrogens:	
	Exo	Endo	Exo	Endo	Exo	Endo
C_1	17.44	15.37	NA	1.1	1.6	NA
C_2	46.33	44.58	NA	4.8	4.7	NA
C_3	13.12	24.62	2.6	1.6	0.8	1.2
C_4	3.98	6.28	NA	1.0	0.8	NA
C_5	1.32	1.43	0.8	1.3	0.2	0.2
C_6	8.26	27.06	4.7	2.5	-	-
C_7	16.00	20.32	3.4	1.1	5.2	1.8

Table 2.2-13 ^{13}C and ^{1}H NMR Data of Exo, Endo 2-norbornyl diphenyl phosphines [14]

[A] Chemical Shifts

Carbon Position	$\delta\ ^{13}C$/ppm			$\delta\ ^{1}H$/ppm			
	Phosphorus Position			Phosphorus Position Exo, Hydrogens:		Endo, Hydrogens:	
	Exo	Endo	δ-A exo endo	Exo	Endo	Exo	Endo
C_1	40.20	40.38	-0.18	NA	2.42	2.44	NA
C_2	40.42	39.66	0.76	NA	2.14	2.88	NA
C_3	36.09	36.35	-0.26	1.63	1.56	1.76	1.47
C_4	37.86	37.99	-0.13	NA	2.55	2.56	NA
C_5	29.87	30.49	-0.62	1.41	1.70	1.71	1.47
C_6	32.03	25.84	6.19	1.51	1.75	1.60	2.42
C_7	40.21	46.77	-0.56	1.39	1.99	1.49	2.43
aromatics	128-129;	133-134;	139.6-140.7;		aromatics	6.8-7.4	ppm

[B] $^{n}J(P,X)$

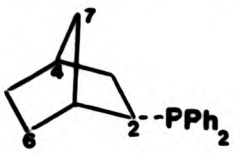

Carbon Position	$^{n}J(P,C)$/Hz		$^{n}J(P,H)$/Hz			
	Phosphorus Position		Phosphorus Position Exo, Hydrogens:		Endo, Hydrogens:	
	Exo	Endo	Exo	Endo	Exo	Endo
C_1	6.85	0.89	NA	1.8	0.0	NA
C_2	5.90	2.91	NA	9.6	12.1	NA
C_3	6.51	9.54	16.5	14.6	7.3	9.9
C_4	1.18	6.85	NA	0.9	0.0	NA
C_5	0.2	0.0	1.9	1.7	0.0	0.0
C_6	2.63	23.44	0.3	3.8	6.2	7.0
C_7	1.02	1.43	0.4	0.4	0.9	0.0
ipso	aromatic 15.8 Hz; 13.61 Hz					

Table 2.2-14 ^{13}C and ^{1}H NMR Data of Exo, Endo 2-norbornyl dimethyl phosphonodithioate [28]

[A] Chemical Shifts

Carbon Position	δ ^{13}C/ppm			δ ^{1}H/ppm			
	Phosphorus Position			Phosphorus Position Exo, Hydrogens:		Endo, Hydrogens:	
	Exo	Endo	Δ-δ	Exo	Endo	Exo	Endo
C_1	38.39	39.75	-1.36	NA	2.49	2.53	NA
C_2	43.96	42.53	1.43	NA	5.02	4.82	NA
C_3	32.47	30.53	1.94	2.78	2.75	2.82	2.41
C_4	36.41	37.51	-1.1	NA	2.42	2.51	NA
C_5	28.40	28.90	-0.5	UR	UR	UR	UR
C_6	31.93	23.95	7.96	UR	UR	UR	UR
C_7	36.86	41.89	-5.03	1.78	1.80	1.93	2.12
C_8	20.13	22.25	-2.12	NA	3.50 to 3.60	3.64 to 2.82	NA
$C_{8'}$	19.91	20.89	-0.98	NA			NA

[B] $^{n}J(P,X)$

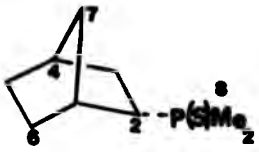

Carbon Position	$^{n}J(P,C)$/Hz		$^{n}J(P,H)$/Hz			
	Phosphorus Position		Phosphorus Position Exo, Hydrogens:		Endo, Hydrogens:	
	Exo	Endo	Exo	Endo	Exo	Endo
C_1	<0.2	2.02	NA	-	0.9	NA
C_2	54.21	55.48	NA			NA
C_3	3.62	<0.2	3.5	-	4.6	-
C_4	3.73	5.62	NA	(0.1)	(0.2)	NA
C_5	<0.2	<0.2	-	-	-	-
C_6	13.95	6.52	-	-	-	-
C_7	<0.2	12.87	-	6.2	-	3.1
C_8	53.9	54.63	NA	-	-	NA
$C_{8'}$	52.7	53.7	NA	-	-	NA

Table 2.2- 18 ^{13}C and ^{1}H NMR Data of Exo, Endo 2-norbornyl dimethyl phosphates [22]

[A] Chemical Shifts

Carbon Position	δ ^{13}C/ppm			δ ^{1}H/ppm			
	Phosphorus Position			Phosphorus Position Exo, Hydrogens :		Endo, Hydrogens:	
	Exo	Endo	Δ-Δ exo endo	Exo	Endo	Exo	Endo
C_1	49.36	52.05	-2.69	NA	2.52	2.50	NA
C_2	86.33	78.89	7.44	NA	4.75	4.17	NA
C_3	41.85	43.71	-1.86	-	-	2.73	2.38
C_4	42.04	41.44	0.60	NA	2.33	2.27	NA
C_5	27.48	28.12	-0.64	UR	UR	UR	UR
C_6	33.13	27.07	6.06	UR	UR	UR	UR
C_7	47.07	48.31	-1.24	1.69	1.78	1.89	2.06
C_8	58.48	58.79	-0.31	NA	3.57	3.65	NA
C_8'	58.97	57.24	0.73	NA	3.52	3.71	NA

UR unresolved cluster at 1.68-2.26 ppm
\- not reported

[B] $^{n}J(P,X)$

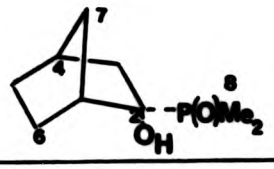

Carbon Position	$^{n}J(P,C)$/Hz		$^{n}J(P,H)$/Hz			
	Phosphorus Position		Phosphorus Position Exo, Hydrogens :		Endo, Hydrogens:	
	Exo	Endo	Exo	Endo	Exo	Endo
C_1	8.79	8.30	NA	9.37	0.2	NA
C_2	26.4	28.8	NA	0.8(OH)	1.1(OH)	NA
C_3	-	1.2	-	-	8.2	17.7
C_4	11.83	-	NA	0.0	-	NA
C_5	1.2	2.44	(0.0)	(0.0)	(0.0)	(0.0)
C_6	18.42	7.2	(0.1)	(0.0)	(0.1)	(0.0)
C_7	1.96	8.79	7.4	5.4	5.1	2.0
C_8	6.83	6.83	NA	10.9	9.4	NA
C_8'	7.81	7.81	NA	10.9	9.4	NA

Table 2.2-16 ^{13}C and ^{1}H NMR Data of Exo, Endo 2-norbornyl diphenyl phosphates [23]

[A] Chemical Shifts

Carbon Position	$\delta\ ^{13}C$/ppm			$\delta\ ^{1}H$/ppm			
	Phosphorus Position			Phosphorus Position Exo, Hydrogens :		Phosphorus Position Endo, Hydrogens:	
	Exo	Endo	Δ-Δ exo endo	Exo	Endo	Exo	Endo
C_1	52.17	54.00	-1.83	NA	3.14	3.09	NA
C_2	86.34	83.01	3.33	NA	4.89	4.96	NA
C_3	43.93	44.38	-0.45	2.08	1.10	2.08	1.21
C_4	44.01	43.57	0.44	NA	2.83	2.83	NA
C_5	30.14	31.06	-0.92	UR	UR	UR	UR
C_6	34.53	29.31	5.22	UR	UR	UR	UR
C_7	50.3	51.29	-0.99	1.64	1.48	2.01	2.09

UR - unresolved cluster at 1.9-2.25 ppm

[B] $^{n}J(P,X)$

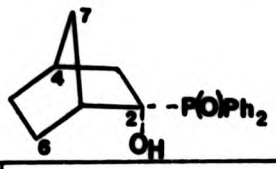

Carbon Position	$^{n}J(P,C)$/Hz		$^{n}J(P,H)$/Hz			
	Phosphorus Position		Phosphorus Position Exo, Hydrogens :		Phosphorus Position Endo, Hydrogens:	
	Exo	Endo	Exo	Endo	Exo	Endo
C_1	8.02	7.86	NA	5.4	0.5	NA
C_2	28.61	27.46	NA	0.8(OH)	1.2(OH)	NA
C_3	-	-	-	-	-	NA
C_4	-	-	NA	-	-	NA
C_5	0.8	1.0	0.0	0.0	0.0	0.0
C_6	3.96	7.96	0.0	0.0	0.0	0.0
C_7	2.10	3.29	12.6	5.0	6.3	8.3

Table 2.2-17 ^{13}C Chemical Shifts and J(P,C) Coupling Constants of exo-2-norbornyl phosphonic dichloride [24]

Carbon Position	δ ^{13}C/ppm	J(P,C)/Hz
C_1	42.13	1.5
C_2	89.96	10.6
C_3	36.15	6.6
C_4	33.15	6.6
C_5	25.63	<0.2
C_6	28.81	0.36
C_7	43.93	1.5

Table 2.2-18 ^{13}C Chemical Shifts and J(P,C) Coupling Constants of exo, endo 2-norbornyl dimethyl phosphines [16]

Carbon Position	δ ^{13}C/ppm			J(P,C)/Hz	
	Phosphorus Position		Δ - A exo-endo	Phosphorus Position	
	Exo	Endo		Exo	Endo
C_1	36.10	37.80	0.3	15.42	9.20
C_2	44.3	43.4	0.9	8.82	6.34
C_3	33.7	33.6	0.1	9.36	11.00
C_4	35.65	-	-	3.47	-
C_5	28.2	28.5	-0.3	0.0	0.0
C_6	30.7	23.6	7.1	6.28	22.83
C_7	35.0	42.2	-7.2	2.30	3.47
C_8	13.02	11.72	1.3	14.0	12.0
C_9	13.96	12.66	1.3	14.0	12.0

carbon shifts have been of great use in deciphering stereochemical problems in rigid bicyclic and many other systems.

It is convenient to analyse substituent steric effects for carbon chemical shifts by the use of $\underline{\alpha}$, β, γ, and $\underline{\delta}$ term effects, as similarly described in Section 1.4.1.2, equation [1.7], where the Greek letters refer to the position of the substituent relative to the ^{13}C nucleus that experiences the steric perturbation. These are shown in Structure 10[A] for a 2-substituted norbornyl ring where P represents the substituted phosphorus atom.

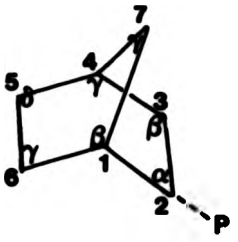

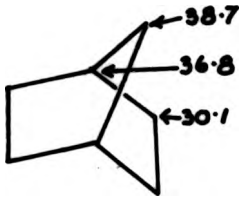

* in ppm, taken from ref. 9

Structure 10 [A] [B]

In comparing the carbon chemical shifts of 2-norbornyl phosphorus substituted derivatives (shown in Tables [A] of 2.2-5 to 2.2-18) it is interesting to use norbornane itself as a chemical shift standard (shown in Structure 10 [B]). The chemical shift differences for the individual carbons (in ppm with respect to norbornane) are compiled for the P(III) derivatives in Table 2.2-19.

^{13}C $\underline{\alpha}$-effects

Several workers[17-19] have measured $\underline{\alpha}$-substitutent effects on ^{13}C chemical shifts in simple alkanes and have interpreted their results in terms of electronegativity effects - at least for substituents composed of first row elements. Consideration of the results for 2-norbornyl

phosphorus derivatives presented here reveals consistent trends with substitution in terms of electronegative effects for the C_2 carbon. This is in accord with data from similar substituted phosphorus compounds given by Bensera[9] and Quin[10]. The α-effect of both exo and endo 2-substituents appears to be large in both P(III) and P(V) compounds. This is shown in a marked shift of the C_2 carbon well to high frequency of all the other carbon resonances in the ring and is also associated with a large value of $^{n}J(P,C)$. In most cases, the exo C_2 lies to higher frequency than the endo C_2 carbon. This is thought to arise because rotation is slightly less hindered in the exo form than in the endo form. A larger s-character effect would then be able to be localised in the electron pair and this may give a slightly larger compression effect which causes a stronger deshielding effect for the exo C_2 carbon. This is also exemplified by a slightly larger J(P,C) in the exo form. This interaction is indicated previously in Structure 6, Section 2.2.

When a more electronegative group, i.e. Cl, Br, etc, replaces a group on the phosphorus which is generating a sterically induced high frequency shift at the C_2 carbon, say $-P(NMe_2)_2$, the α-effect is always larger. Thus the observed chemical shift may be regarded as the sum of a normal α-effect plus the change in the steric shift. This steric shift may be influenced by the bulkiness of the substituent. For the 2-norbornyl phosphorus case, when one progresses from $-PMe_2$ to $-PPh_2$ to $-P(NEt_2)_2$ no distinct trends are shown by the C_2 carbon. This however may be due to insufficient data and thus the inability to see subtle differences in this area.

^{13}C β-effects

The two carbons C_1 or C_3 are in a β-position relative to the phosphorus substituent at C_2. As suggested by Quin[10] these carbons are shifted to higher frequency by this substituent effect. However,

Table 2.2-19 ^{13}C Substituent Chemical Shifts for 2-substituted Phosphorus (III) Norbornanes[a]

P(III) Substituents	Carbon Position						
	C_1 β	C_2 α	C_3 β	C_4 γ	C_5 δ	C_6 γ	C_7 γ
				(Phosphorus Exo)			
PBr_2	3.96	23.67	6.33	1.19	-0.76	2.36	-0.11
PCl_2	2.18	24.80	3.68	0.56	-1.17	1.57	-1.16
PClBr	3.18	23.10	5.48	-1.22	-1.62	1.42	-1.57
$P(NMe_2)_2$	-	14.2	1.25	-	-0.6	1.30	0.25
$P(NEt_2)_2$	2.86	10.63	4.64	1.01	-0.07	1.45	-0.14
	3.15	17.36	6.18	1.16	-0.41	1.53	0.33
	2.89	18.91	4.9	0.9	-0.5	2.58	1.3
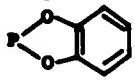	2.96	16.23	1.84	-0.6	-0.9	0.1	0.9
PPh_2	3.4	10.32	5.95	1.1	-0.2	1.93	1.5
PMe_2	1.3	14.2	3.6	-1.1	-1.9	0.6	-3.7
				(Phosphorus Endo)			
PBr_2	4.26	23.57	6.93	1.55	0.67	-2.97	3.02
PCl_2	3.02	23.72	3.40	0.61	-0.12	-4.68	2.21
PClBr	4.68	21.96	4.98	0.82	0.02	-4.94	6.37
$P(NMe_2)_2$	1.73	12.55	0.7	-	0.10	-3.35	2.47
$P(NEt_2)_2$	3.06	10.15	4.69	1.06	0.40	-3.69	-0.4
	5.14	17.93	6.25	0.74	0.42	-5.55	7.13
	6.0	20.02	6.02	0.7	0.4	-1.61	7.51
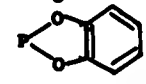	3.71	16.48	1.96	-1.2	-0.7	-4.5	7.0
PPh_2	3.58	9.56	6.25	1.19	0.31	-4.3	2.0
PMe_2	1.0	13.3	3.5	-	-1.6	-6.5	3.5

- not reported. a Substituent chemical shifts in ppm, relative to norbornane; a minus sign denotes a shift to low frequency on substitution

the C_3 carbon in all analysed derivatives show a greater deshielding than the C_1 carbon in the same isomer and hence lies to higher frequency than C_1. Comparing the two exo:endo isomers reveals that when the phosphorus is orientated in the exo position on C_2, a greater β-effect is seen for both C_1 and C_3 (shown in Table of 2.2-19). As the bulkiness of the substituent increases, smaller differences are seen between the exo C_1 carbon and the endo C_1 carbon. This is also true for the C_3 carbons. This may suggest a relationship between the compression of the phosphorus lone pair via bulky substituent groups and the β-effect. However, it may also be that the norbornyl ring undergoes slight distortion to accommodate these larger groups and that the difference in chemical shift between the isomers reflects this, rather than being a function of the substituent itself.

^{13}C γ-effects

The importance of steric interactions on ^{13}C chemical shifts has been verified in several studies[20-22]. This present study is no exception and the sterically influenced γ induced shifts are in most cases easily recognisable in the derivatives studied here. With a phosphorus substituent in the 2-position used as a starting point, there are three γ positions C_4, C_6 and C_7 which are relevant. The C_4 carbon position is far removed from the C_2 phosphorus position and hence little steric interaction is found. Accordingly deviations from the chemical shift in norbornane itself are small for both the P(III) and P(V) compounds. For the C_6 and C_7 carbons, the situation is very different and the more expected and sizeable γ steric shielding interactions occur.

When an endo substituent is introduced at C_2, a dramatic shift to low frequency occurs for C_6 (ca. 4 ppm). Here a large interaction, in

the form of steric crowding, occurs between the *endo* phosphorus group and C_6. This interaction (γ *gauche* orientation) produces an expected shift to low frequency. The data in Table 2.2-19 seems to suggest that larger substituents on the phosphorus atom cause a greater chemical shift difference. However, when the phosphorus group is orientated *exo* on C_2 this large interaction with C_6 is not seen. This suggests that the phosphorus groups are less hindered by C_6 in this position. For C_7 the opposite effect is seen. When the phosphorus group is positioned *exo* on C_2 a greater interaction occurs producing some negative chemical shifts for C_7 when there are larger substituents on the phosphorus atom. Whereas when the phosphorus is *endo*, C_7 is not affected and no chemical shifts to lower frequency are seen for this carbon. This then gives a good method of distinguishing between whether a phosphorus group is *exo* or *endo*. It should also be noticed that when a phosphorus substituent is added to a structure as

the ^{13}C chemical shifts in the cage, as expected, shift slightly to high frequency. In the 2-norbornyl system, this electronic effect can be seen greatest on C_6 when the substituents on the phosphorus atom are electronegative and the group is in the *exo* position.

2.2.4.2 ^1H Chemical shift data

The ^1H chemical shift data for the 2-norbornyl derivatives are presented in Tables [A] of 2.2-5 to 2.2-18. Individual hydrogen assignments were based on the ^{13}C assignments and these were correlated *via* the 2D shift correlation experiment. However, evaluation of the individual contributions to the total screening constant appears to be more complicated in the case of protons than for other nuclei that have been studied. Nevertheless pronounced proton shifts caused by van der

Waal's (steric) influences may be observed <u>via</u> 2D NMR even in congested circumstances.

It is convenient to analyse these proton 2-norbornyl phosphorus steric effects by comparing them with the proton chemical shifts of norbornane (given in Structure 11[A] and ... compiled in Table 3.2-20.)

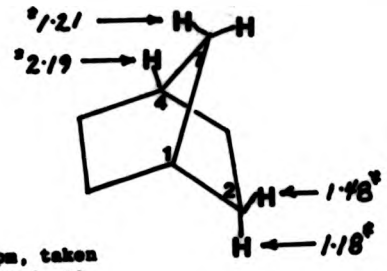

* in ppm, taken from ref. 40

[A]

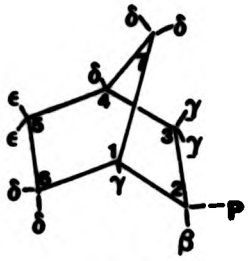

[B]

Structure 11

C_1 and C_4 hydrogens

For the C_4 hydrogen in P(III) and P(V) compounds, the C_2 phosphorus substituents have little or no effect on the chemical shift relative to norbornane. Comparison of <u>exo</u> and <u>endo</u> substitution again reveals no specific trends for this $\underline{\delta}$ effect. This is probably due to the great distance from the C_2 position. This is also supported by the lack or minimal amount of coupling as seen on the C_4 hydrogen, normally < 1 Hz. For the C_1 hydrogen, in both P(III) and P(V) derivatives the γ shielding effect varies from compound to compound. Differences between <u>exo</u> and <u>endo</u> isomers seem almost negligible and this suggests that H_1 does not contribute significantly to the interactions with the phosphorus group. The only notable difference is when the phosphorus substituent is bound in a ring as in compounds [19-21] which seems to produce some steric control and gives a high frequency shift of <u>ca</u>. 1 ppm for the C_1 hydrogen in both <u>exo</u> and <u>endo</u> isomers.

Table 2.2-20 ^{1}H Substituent Chemical Shifts for 2-Substituted Phosphorus (III) Norbornanes[a]

P(III) Substituents	H_1	H_2	Hydrogen Position					H_6exo	H_6endo	H_7syn	H_7anti
			H_3exo	H_3endo	H_4	H_5exo	H_5endo				
	γ	β	γ	γ	δ	ε	ε	δ	δ	δ	δ
			(Phosphorus EXO)								
PBr_2	-0.61	1.64	0.04	0.05	0.29	0.13	0.03	0.26	0.22	1.50	1.05
PBrCl	0.11	1.32	-0.06	-0.01	-0.13	-0.23	-0.24	-0.14	-0.15	-0.32	-0.06
PCl_2	0.10	0.97	-0.11	0.20	-	-0.12	-0.18	-0.07	-0.10	-0.09	-0.09
$P(OMe)_2$	-	0.46	-0.06	0.02	-	-0.13	-0.16	-0.06	-0.05	-0.21	-0.10
$P(NEt_2)_2$	-0.49	0.86	0.13	-0.15	-0.03	-0.16	-0.15	0.04	-0.01	0.85	1.48
	1.09	0.32	-0.28	-0.06	-0.01	-0.08	-0.11	0.02	-0.08	1.03	2.70
	0.93	0.62	-0.22	-0.03	-0.03	-0.03	-0.08	0.05	-0.08	1.19	2.77
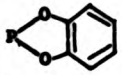	0.89	0.29	-0.30	-0.06	0.41	-0.28	-0.02	-0.12	0.08	1.01	2.75
PPh_2	0.23	0.96	0.15	0.38	0.36	-0.07	0.52	0.03	0.57	0.78	0.18

Continued

Table 2.2-20 Continued

P(III) Substituents	H_1 γ	H_2 β	Hydrogen Position					H_6exo δ	H_6endo δ	H_7syn δ	H_7anti δ
			H_3exo γ	H_3endo γ	H_4 δ	H_5exo ε	H_5endo ε				
			(Phosphorus ENDO)								
PBr_2	-0.65	1.67	0.64	0.23	0.22	2.45	2.78	0.16	0.00	0.42	0.21
PBrCl	0.13	1.37	-	-	-0.13	-	-	-	-	-	-
PCl_2	0.19	1.00	-0.07	0.24	0.18	-0.20	0.10	-0.07	0.11	-0.21	-0.03
$P(OMe)_2$	-0.13	0.38	-0.40	0.26	-	-0.02	0.04	-	-	1.07	0.94
$P(NEt_2)_2$	-0.93	0.60	-0.35	-0.02	-0.03	-0.17	0.28	-0.22	0.89	0.47	0.11
	1.10	0.03	-0.40	0.28	0.27	0.02	0.12	-	0.74	0.33	-0.06
	0.87	0.34	-0.42	0.26	0.26	0.01	0.12	0.00	-.74	0.28	-0.05
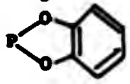	0.87	-0.02	-0.38	0.25	0.59	-0.26	0.06	0.06	0.71	0.55	0.05
PPh_2	0.35	1.40	0.28	0.29	0.37	0.23	0.29	0.12	1.24	1.22	0.28

- Not reported

a Substituent chemical shifts in ppm, relative to norbornane; a minus sign denotes a shift to low frequency on substitution.

Hydrogen on C_2

The proton on C_2 shows typical high frequency chemical shifts arising from deshielding effects for both P(III) and P(V) compounds. The more crowded endo isomer has the higher frequency signal for the C_2 hydrogen. This is in agreement with results for other 2-substituted norbornanes not containing phosphorus[23]. The value of $^2J(P,H)$ for the C_2 hydrogen in most cases are larger for the exo isomer for both the P(III) and P(V) derivatives.

Hydrogens on C_3

In norbornane, the chemical shifts are 1.48 ppm for the exo and 1.18 ppm for the endo C_3 hydrogen respectively. For all the phosphorus derivatives the C_3 hydrogen resonances occurred from 1.08 to 1.76 ppm. The steric influence on the γ effect was absent and the chemical shifts for an isomer pair were nearly identical. However, slight shifts to high frequency occurred for all isomers on the C_3 hydrogens which were in the same conformation as the phosphorus substituent. For example, the C_3 H endo hydrogen would be higher in chemical shift than the C_3 H exo hydrogen when the C_2 phosphorus substituent was in the endo position.

Hydrogens on C_5 and C_6

Due to great distances of the C_5 and C_6 hydrogens from the phosphorus on the C_2 position, little changes of any chemical significance are felt in either the exo or endo isomers. This is demonstrated for all isomers in the P(III) and P(V) compounds shown. However, in the case where the C_2 phosphorus substituent was endo a higher frequency chemical shift could be seen on the C_6 endo hydrogen when bulky groups were attached to the phosphorus.

Hydrogens on C_7

From Table 2.2-20, for P(III) derivatives the *syn* C_7 hydrogen showed a chemical shift difference of *ca.* 1 ppm for norbornane when the phosphorus substituent was in the *exo* position. The overall trend seems to be to higher frequency and is more apparent for bulky phosphorus substituents. This provided then a clear way of distinguishing and assigning the position of the phosphorus group. For P(V) species, this shift to high frequency was still apparent though the magnitude was much smaller.

2.2.4.3 Comparison of coupling constants in 2-norbornyl phosphorus derivatives

To extend and complement the information gathered from the chemical shift data for ^{31}P, ^{13}C and ^{1}H spin-spin coupling constants $^{n}J(P,C)$ and $^{n}J(P,H)$ were examined. In rigid bicyclic systems, such as the norbornyl ring, they have been shown to be invaluable as a basis for determining the stereochemical dependence of coupling constants[24]. This data is given in Table [B] of 2.2-5 to 2.2-18.

$^{1}J(P,C)$ One-bond spin-spin couplings

For P(III) compounds, the size of the coupling constant is dependent upon the particular α-effect associated with the substituent groups and the ability to concentrate *s*-character in the electron lone pair. With electronegative groups such as $-PCl_2$ and $-PBr_2$, values are from *ca.* 40-50 Hz, whereas with substituents that are more bulky like the $-PPh_2$ derivative, couplings of the order *ca.* 10-20 Hz are found for $^{1}J(P,C_2)$. Here, the couplings in the *exo* isomers of the P(III) compounds are found to be slightly larger than for the *endo* isomers.

For P(V) derivatives, few examples have been made and hence no real patterns can be drawn other than the one-bond coupling is large and in both of the cases the *exo* isomer has the largest coupling.

$^2J(P,X)$ Geminal Coupling Constants

$^2J(P,C)$

For P(III) compounds, the values of $^2J(P,C)$ are of larger magnitude for the endo isomers than the exo. This may suggest that ^2J is sterically controlled by the dihedral angle between the lone pair on the phosphorus and the β-carbons on the norbornyl ring. With steric control, small angles are associated with large couplings[10]. With this steric crowding, smaller angles in the endo position are also demonstrated when one compares the magnitudes of $^2J(P,C_3)$ and $^2J(P,C_1)$ in the ring. In all cases, $^2J(P,C_3)$ has the larger coupling magnitude, suggesting that the phosphorus electron pair is orientated towards the C_3 ring site as opposed to the C_1 site. In the exo isomers, the phosphorus lone pair orientation seems to be closer to the C_1 norbornyl ring site producing a larger associated coupling, i.e. $^2J(P,C_1) > {}^2J(P,C_3)$.

For larger substituents, i.e. $-PPh_2$ and $-P(NEt_2)_2$, couplings of smaller magnitude are found in both exo and endo isomers suggesting that the electron pair is orientated away from the norbornyl ring giving rise to small coupling to C_1 and to C_3.

For the two P(V) compounds, the phosphorus lone pair orientation seems to be nearer to the C_1 ring site, and hence gives rise to large couplings to C_1.

$^2J(P,H)$

Only one geminal coupling constant for the $^2J(P,H)$ is possible in the norbornyl ring. Here the magnitude of the coupling in the exo and endo isomers seem generally to depend on the particular phosphorus derivative involved. However for most cases, the exo isomer is associated with the larger two bond coupling. As one increases the bulk of the substituent groups on the phosphorus, as in the series $-PBr_2$, $-POMe_2$, $-P<\!\!\overset{S}{S}\!\!>$, and $-PPh_2$, the differences in magnitude lessen between the isomers.

$^{3}J(P,X)$ Vicinal Coupling Constants

It has been demonstrated[25-27] that for rigid bicyclic systems such as norbornanes, there is a definite relation between the magnitude of three-bond couplings $^{3}J(P,C)$ and more importantly $^{3}J(P,H)$ and the dihedral angle ϕ relating these atoms. These Karplus-type relationships are discussed in Section 3.3 and the magnitudes of the 2-norbornyl couplings are also discussed there.

Long Range Couplings

$^{n}J(P,C)$

The most commonly studied long range couplings are $^{n}J(H,H)$ but in the norbornyl ring, the values of $^{4}J(P,C_5)$ can be easily identified. In all the norbornyl compounds studied values were less than 3 Hz, and in themselves provide little chemical information, although the data suggests that perhaps slightly larger couplings occur when the phosphorus atom is in the exo position. As stated above the geminal coupling, $^{2}J(P,C)$, suggests that the electron lone pair on the phosphorus orientates itself closer to the C_1 carbon on the norbornyl ring when the phosphorus is exo. This larger coupling might then be justified if the $J(P\text{-}C_2\text{-}C_1\text{-}C_6\text{-}C_5)$ coupling pathway is chosen.

$^{n}J(P,H)$

Long range values of $^{n}J(P,H)$ were determined between the hydrogen on carbons C_4, C_5, C_6 and C_7. The values of $^{n}J(P,H)$ for protons on C_6 and C_4 are very small due to their great distances from the phosphorus atom. These are shown mainly for novelty value and as examples of $^{4}J(P,H)$ and $^{5}J(P,H)$. However, the values of $^{4}J(P,H)$ to the protons of carbon C_6 and C_7 lead to some chemically significant results. When a phosphorus substituent is endo the C_6 endo hydrogen shows a large $^{4}J(P,H)$, ca. 4-9 Hz, in all cases. The phosphorus electron lone pair may apply steric crowding to the C_6 endo hydrogen making the angle

proximity smaller than usually expected for $^4J(P,H)$. The C_6 exo hydrogen, however is orientated away from the phosphorus and hence has a characteristically small coupling. When the phosphorus substituent is in the exo position, the C_7 syn hydrogen then becomes sterically crowded and, in all the norbornyl derivatives, shows an increase in coupling magnitude. However, when the phosphorus is in the endo position no effect is seen. Hence accurate identification may be made as to the orientation of the phosphorus, whether exo or endo by the simple comparison between these two values of $^4J(P,H)$.

2.3 7-Norbornenyl Phosphorus Derivatives

Some 7-norbornenyl phosphorus derivatives (shown in Structure 12) were synthesised to extend the preliminary relationships which have been derived in the study of the 2-norbornyl phosphorus system. This part of the work covered the dependence of $^{n}J(P,C)$ and $^{n}J(P,H)$ couplings on dihedral angles, and the effect of phosphorus on the chemical shifts of the ^{1}H and ^{13}C nuclei in the bicyclic cage. The 7-norbornenyl cage system can also be considered as a rigid structure, or at least to be limited to a form of pseudorotation[10]. Hence it is anticipated that similar steric crowding effects on chemical shifts should be apparent.

Structure 12

Initial work by Quin[28,29], Grutzner[23] and others[30-38] has shown steric compression effects of the substituent X on ^{13}C chemical shifts. However, few examples have been studied which involve this particular system. To test these initial observations a series of derivatives was prepared by changing the phosphorus environment at the seven position on the norbornenyl ring. These differences were then monitored by examining and comparing chemical shifts and coupling constants by the 1D and 2D NMR methods previously outlined in Section 2.1.

Synthesis by routes [26] to [36] (see Experimental, Chapter 4) gave a mixture of <u>syn</u> and <u>anti</u> isomers and these were analysed together in their reaction ratios. The <u>anti</u> isomer is preferred in most of the reactions, as shown in Table 2.3-2.

In Structure 12[A] the phosphorus substitution is on the *syn* position of norbornylene. In this position the phosphorus atom is much less crowded and in a very different environment than when it is in the *anti* (12[B]), or in the *exo* or *endo* 2-norbornyl isomer. This feature arises because in the *syn* form, the phosphorus can experience interaction only from a hydrogen on the sp^2 hybridized C_2/C_3 whereas for the *anti* and the other *exo*,*endo* phosphorus substituent positions there can be interaction with *gauche* hydrogens on the sp^3 hybridized C_5/C_6. In addition, when in the *syn* position, the phosphorus may be subject to long range diamagnetic anisotropic effects from the double bond. With this great difference between the two isomers, and because of the plane of symmetry in the structure, NMR analysis for these derivatives was in most cases straightforward. Differentiation between *syn* and *anti* isomers was achieved by various methods. As already noted in the method of preparation, considerably more of the *anti* isomer was formed than of the *syn*. This made it possible to distinguish between the isomers by intensity differences in the phosphorus and carbon spectra. Comparison of the P-C couplings for the sp^2 carbon also permitted the distinction between the two isomers. A few of the compounds produced by Quin[28] were prepared again, and the ^{13}C chemical shifts are given in Table 2.3-1.

Assignments were also correlated with the 7-halonorbornene starting materials and other 7-substituted norbornenyl derivatives given by Stothers *et al*[39] and by others[41]. Their ^{13}C NMR chemical shifts are also presented in Table 2.3-1. As can be seen no major discrepancies are noted so it was presumed that this process of assignment was correct and this argument was used as a basis to interpret and assign other new compounds. In the few cases where ^{13}C signals could not be easily identified as belonging to the *syn* or the *anti* isomers, a selective

phosphorus decoupling experiment was performed. This was achieved by the method outlined in Section 2.2.1.

TABLE 2.2-1 Comparison of ^{13}C NMR Chemical Shifts of Some 7-substituted Norbornenyl Derivatives[a]

Substituent n =	$C_{1,4}$ expt.	$C_{1,4}$ lit	$C_{2,3}$ expt.	$C_{2,3}$ lit	$C_{5,6}$ expt.	$C_{5,6}$ lit	C_7 expt.	C_7 lit
 syn								
Cl_2P	43.96	-	134.72	134.8	24.92	25.5	76.26	76.7
Me_2P	44.12	-	133.82	133.9	24.30	24.3	66.46	66.8
 anti								
Cl_2P	43.92	44.0	136.65	136.6	22.10	22.1	71.20	71.20
Me_2P	44.09	44.1	137.26	137.3	21.6	22.8	64.5	64.5
Miscellaneous								
	49.30	44.3	132.62	132.8	22.7	22.7	65.72	66.0
	41.95	41.95	135.35	135.2	24.70	24.6	48.67	48.5
	55.61	55.61	104.32	104.3	28.42	28.4	128.37	129.17
	45.60	45.6	134.5	134.8	21.3	21.3	82.53	82.5

- not reported

a taken from refs. 28, 29, 39, 40 in ppm, TMS = 0.0 ppm

2.3.1 ^{31}P NMR Data of the 7-norbornenyl Phosphorus Derivatives

TABLE 2.3-2 ^{31}P NMR Chemical Shifts of Some Prepared 7-norbornenyl Phosphorus Compounds

Substituent n =	7-Norbornenyl-n [a]			Reaction Ratio syn:anti	Preparation Number
	syn	anti	Δδ [δsyn−anti]		
P(III)					
- PBr_2	202.2	195.8	+6.4	1:5	[26]
- PClBr	196.9	190.9	+6.0	1:4	[27]
- PCl_2	197.4	190.5	+6.9	1:4	[28]
- $PPhCl$	104.3	96.3	+8.0	1:2	[29]
- $P(NEt_2)_2$	96.2	93.8	+2.4	1:2	[30]
- $PClPh$	84.62	76.64	+8.0	1:2	[29]
- 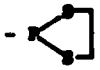	49.8	47.1	+2.7	1:2	[31]
- 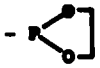	46.1	43.5	+2.6	1:2	[32]
- PPh_2	-10.7	-8.9	-1.8	2:1	[33]
- PMe_2	-61.8	-60.1	-1.7	2:1	[34]
Substituent R = 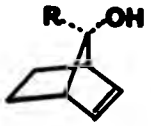					
- $P(O)(OMe)_2$	33.3	29.0	+4.2	1:2	[35]
- $P(O)(OPh)_2$	11.00	6.8	+4.2	1:2	[36]

a in ppm, positive to high frequency from H_3PO_4 = 0.0 ppm

The NMR data for the various 7-norbornenyl phosphorus derivatives are given in Table 2.3-2. Here again as previously noted, the overall trends for ^{31}P chemical shift data are substantiated, and the norbornenyl group has no seriously perturbing effect (cf. Table 1.4-3, Chapter 1). Increasing the electronegativity of the phosphorus substituent deshields the phosphorus and a shift to higher frequency results. Difficulty arises when one tries to interpret the differences between syn and anti isomers for a range of compounds. For example, with electronegative groups such as $-PBr_2$, $-PCl_2$, -PClBr, and -PPhCl, large differences occur between syn and anti isomers [$\delta_{syn-anti}$] = +6.4, +6.9, +6.0, and +8.0 ppm respectively where the syn isomer is to higher frequency. This may be explained by considering the loss of steric strain in moving from the anti to the less crowded syn position. This could cause a marked net deshielding effect and hence as expected the syn isomer is to high frequency of the anti. However, the diamagnetic effect of the double bond which shields the phosphorus atom would cause an opposite effect. The ^{31}P data here suggests that if in fact the diamagnetic effect occurs (this would arise through interaction of the phosphorus lone pair with the secondary magnetic field associated with circulation of the π-electrons above and below the plane of the olefinic carbons[29]), it must be appreciably reduced by electronegative substituents. Whereas for other substituents in the series, such as $-P$  , $-P$  , $-PPh_2$, and $-PMe_2$, smaller differences between the syn and anti are seen, and indeed reversal may occur in [$\delta_{syn-anti}$] (i.e. +2.7, +2.6, -1.8, -1.7 ppm). Here according to Quin[29] this apparent difficulty for the $-PMe_2$ group (and the $-PPh_2$ group) is explained by suggesting that the behaviour is similar to that of a methyl group in the 7-position of norborn-2-ene as studied by Grutzner et al[23]. In these cases the shielding effect arising from the 2,3 double bond is greater, so what we actually see is an averaged value between the two effects. On the

one hand, deshielding occurs as the substituent moves from the anti to the syn position and hence [$\delta_{syn-anti}$] is positive. On the other hand, this effect is minimised by the interaction between the phosphorus non-bonded electron lone pair and the 2,3 double bond when the phosphorus is in the syn position. This will give a greater shift to low frequency and would produce a negative [$\delta_{syn-anti}$]. It is proposed that other compounds where the [$\delta_{syn-anti}$] is small or negative may be behaving similarly.

Other attempts have been made to explain similar conformational effects. Corenstein[42] has proposed that slight bond angle distortions to alleviate strain might occur. This strain which may be introduced by accommodation of say a larger substituent, could be partially relieved if the internal $C_1-C_7-C_4$ angle could be decreased. This would allow the hybridization of the phosphorus atom to be closer to p^3 and hence hold greater p-character in its electron lone pair. This would act to shield the phosphorus atom and a lower frequency shift would be expected. In this system, very little ring distortion is likely and thus very large substituent groups would be needed to put enough pressure on the phosphorus to cause any deformation of the ring. This may only be a small contributing factor for groups such as $-PPh_2$ and $-PMe_2$. However, to determine the amount of any such contribution would require the analysis of many compounds in this series. Obviously this situation is far from straightforward and the balance adopted between these opposing effects to give a net effect is not well understood. However, the new data presented here seems to be in agreement with Quin's hypothesis, where the 2,3 double bond may be the controlling factor in this system for non-electronegative substituents[28,29]. This occurs because the π-electron clouds of the double bond are large and essentially restrict the phosphorus atom. This may play a contributing factor in the question as to why anti formation from both syn and anti

starting material seems preferred in most cases. This data also suggests that the ring distortion is minimal for most compounds of this type.

2.3.2 ^{13}C NMR and ^{1}H NMR Data

The ^{13}C and ^{1}H NMR data are given in Tables 2.3-3 to 2.3-10. In most cases the analysis of these systems is complex but straightforward and needs no explanation. Some cases however present their own particular difficulties, and thus a short note is given with the corresponding data table. In order to show how these data tables were produced a full analysis is given for a typical compound mixture: namely syn and anti 7-norbornenyl dichlorophosphines.

Syn and Anti 7-norbornenyl dichlorophosphines [28]

A ^{31}P NMR spectrum revealed a syn:anti ratio of ca. 1:4, as shown in Fig. 2.3-1. The ^{13}C spectrum was assigned with the aid of Quin's previous work[29] and is tabulated in Table 2.3-1. In this ring system separation between the CH and CH_2 groups is well defined and use of GASPE or other assignment sequences was unnecessary. The values of $^{n}J(P,C)$ could be easily read off the $^{13}C\{^{1}H\}$ spectrum and are shown in Table 2.3-6[B]. To determine the ^{1}H chemical shifts of the two isomers, a 2D $^{13}C/^{1}H$ shift correlated experiment was performed with homonuclear broadband decoupling in both dimensions (Section 1.5.2.2). In these symmetric molecules for the C_1/C_4, C_2/C_3, and C_7 signals, the hydrogen chemical shifts may be readily determined by taking the mean of the CP_{α} and CP_{β} slices in the F_1 dimension. Also the difference between these is the P-H coupling. For the C_5/C_6 slices, AB quartets are obtained, demonstrating the coupling between the inequivalent hydrogens in a CH_2 group. Complex analysis as outlined in Section 2.1.3.2 was performed on each CP_{α} and CP_{β} slice. This yielded two effective

hydrogen chemical shifts δH_A and δH_B for each of the $CP_{\underline{\alpha}}$ and $CP_{\underline{\beta}}$ slices. The differences between these effective chemical shifts for each of H_A and H_B will be the P-H coupling and the <u>true</u> chemical shift will be the mean frequency between $P_{\underline{\alpha}}(\delta H_A)$ and $P_{\underline{\beta}}(\delta H_A)$ (and $P_{\underline{\alpha}}(\delta H_B)$ and $P_{\underline{\beta}}(\delta H_B)$ respectively).

FIG. 2.3-1 ^{31}P NMR Spectrum of a Mixture of <u>syn</u>,<u>anti</u> 7-norbornenyl dichloro phosphines

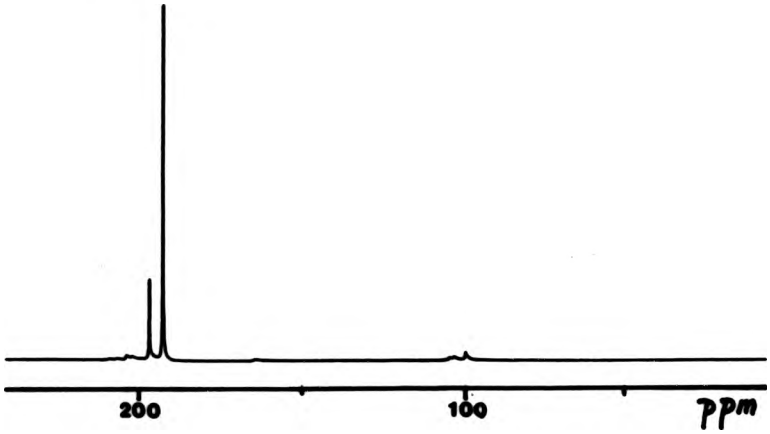

<u>Syn and Anti 7-norbornenyl bromo chloro phosphines [27]</u>

As for the 2-norbornyl adduct (Section 2.2.1), the ^{31}P NMR spectrum is expected to have four lines arising from the <u>R</u> and <u>S</u> <u>syn</u> and the <u>R</u> and <u>S</u> <u>anti</u> forms as the phosphorus atom should be chiral. However, also as with the 2-norbornyl derivative, the phosphorus spectrum suggests that only two forms - one <u>syn</u> and one <u>anti</u> in a ratio of 1:4 are present. The ^{13}C NMR evidence supports this as again only two major isomers are seen in a similar ratio. Thus when considering both the 2-norbornyl and 7-norbornenyl cases it seems that the bromine and chlorine are not dissimilar enough to promote effective chirality at the phosphorus atom.

Syn and Anti 7-norbornenyl chloro phenyl phosphines [29]

The ^{31}P NMR spectrum showed four isomers from the reaction of dichloro phenyl phosphine with the 7-norbornenyl Grignard reagent. This feature arises because the phosphorus is assuming chirality where the non-bonded electron pair may be regarded as the fourth substituent. This will give rise to both R and S syn, and R and S anti isomers. Attempted separation of these isomers proved unsuccessful and hence only accurate ^{31}P chemical shifts can be reported as shown in Table 2.3-2.

Key for Tables 2.3-3 to 2.3-10	
NA	not applicable position
( )	estimated
-	not reported

TABLE 2.3-3 ^{13}C NMR Data of Syn and Anti 7-norbornenyl dimethyl phosphines [34]

Carbon Position	$\delta\ ^{13}C$/ppm			$^{n}J(P,C)$/Hz	
	Phosphorus Position			Phosphorus Position	
	Syn	Anti	Δ - Δ syn anti	Syn	Anti
C_1/C_4	44.12	44.09	0.03	5.2	12.0
C_2/C_3	133.82	137.26	-3.44	3.7	6.0
C_5/C_6	24.30	—	2.70	2.6	8.6
C_7	66.46	64.50	1.96	6.1	12.2
C_8	14.46	12.82	1.64	12.5	12.7
For P-Me $^{3}J(P,H)$ ≈ 2.8 Hz for phosphorus syn ≈ 2.6 Hz for phosphorus anti					

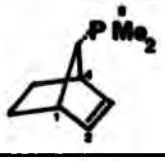

TABLE 2.3-4 ^{13}C and ^{1}H NMR Data of Syn, Anti 7-norbornenyl Dibromo Phosphines [26]

[A] Chemical Shifts

Carbon Position	$\delta\ ^{13}C$/ppm			$\delta\ ^{1}H$/ppm			
	Phosphorus Position			Phosphorus Position Syn		Anti	
	Syn	Anti	Δ - Δ Syn-Anti	Hydrogen Exo	Endo	Hydrogen Exo	Endo
C_1/C_4	45.05	44.96	0.09	3.12	NA	3.06	NA
C_2/C_3	136.68	138.70	-2.02	6.02	NA	NA	6.16
C_5/C_6	28.88	26.65	2.23	1.89	1.96	1.87	1.43
C_7	76.05	70.6	5.45	3.40	NA	2.84	NA

[B] $^{n}J(^{31}P,X)$

Carbon Position	$^{n}J(P,C)$/Hz		$^{n}J(P,H)$/Hz			
	Phosphorus Position		Phosphorus Position Syn		Anti	
	Syn	Anti	Hydrogen Exo	Endo	Hydrogen Exo	Endo
C_1/C_4	10.6	14.4	5.1	NA	5.3	NA
C_2/C_3	4.8	4.5	2.7	NA	NA	1.8
C_5/C_6	6.9	12.6	1.6	1.8	3.7	3.4
C_7	41.7	48.8	6.9	NA	7.3	NA

TABLE 2.3-5 ^{13}C and ^{1}H NMR Data of Syn, Anti 7-norbornenyl Bromo Chloro Phosphines [27]

[A] Chemical Shifts

Carbon Position	δ ^{13}C/ppm			δ ^{1}H/ppm			
	Phosphorus Position			Phosphorus Position Syn		Anti	
	Syn	Anti	Δ = Δ Syn-Anti	Hydrogen Exo	Endo	Hydrogen Exo	Endo
C_1/C_4	44.16	44.13	0.03	2.96	NA	2.92	NA
C_2/C_3	134.70	136.66	-1.96	5.89	NA	NA	6.18
C_5/C_6	24.86	22.11	2.75	1.57	1.67	1.02	1.32
C_7	74.56	69.58	4.96	2.63	NA	2.32	NA

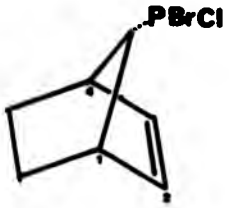

[B] $^{n}J(^{31}P,X)$

Carbon Position	$^{n}J(P,C)$/Hz		$^{n}J(P,H)$/Hz			
	Phosphorus Position		Phosphorus Position Syn		Anti	
	Syn	Anti	Hydrogen Exo	Endo	Hydrogen Exo	Endo
C_1/C_4	11.0	14.6	5.0	NA	5.8	NA
C_2/C_3	6.9	6.8	3.1	NA	NA	1.6
C_5/C_6	6.9	12.8	1.5	1.5	3.4	(3.0)
C_7	48.2	50.6	5.6	NA	6.0	NA

TABLE 2.3-6 ^{13}C and ^{1}H NMR Data of Syn, Anti 7-norbornenyl Dichloro Phosphines [28]

[A] Chemical Shifts

Carbon Position	$\delta\ ^{13}C$/ppm			$\delta\ ^{1}H$/ppm			
	Phosphorus Position			Phosphorus Position Syn		Anti	
	Syn	Anti	Δ - Δ Syn-Anti	Hydrogen Exo	Endo	Exo	Endo
C_1/C_4	43.96	43.92	0.04	2.96	NA	2.94	NA
C_2/C_3	134.72	136.65	-1.93	5.93	NA	NA	6.08
C_5/C_6	24.92	22.10	2.82	1.78	1.96	1.87	1.42
C_7	76.26	71.20	5.06	2.40	NA	2.16	NA

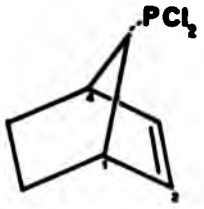

[B] $^{n}J(^{31}P,X)$

Carbon Position	$^{n}J(P,C)$/Hz		$^{n}J(P,H)$/Hz			
	Phosphorus Position		Phosphorus Position Syn		Anti	
	Syn	Anti	Hydrogen Exo	Endo	Exo	Endo
C_1/C_4	(10.8)	14.5	(5.3)	NA	(5.6)	NA
C_2/C_3	6.7	6.2	2.6	NA	NA	1.8
C_5/C_6	6.8	10.0	1.4	1.6	3.5	3.2
C_7	40.3	47.6	5.9	NA	6.1	NA

TABLE 2.3-7 ^{13}C and ^{1}H NMR Data of Syn, Anti 7-norbornenyl Bis Diethylamino Phosphines [30]

[A] Chemical Shifts

Carbon Position	δ ^{13}C/ppm			δ ^{1}H/ppm			
	Phosphorus Position			Phosphorus Position Syn		Anti	
	Syn	Anti	Δ - Δ Syn-Anti	Hydrogen Exo	Endo	Hydrogen Exo	Endo
C_1/C_4	45.84	45.80	0.04	2.86	NA	2.87	NA
C_2/C_3	133.96	134.97	-2.01	6.10	NA	NA	6.20
C_5/C_6	24.86	22.13	2.73	1.36	1.41	1.12	0.94
C_7	65.34	63.36	1.98	2.12	NA	2.06	NA
C_8	43.85	44.16	-0.31	2.98	NA	2.87	NA
C_9	14.64	15.84	-1.2	0.94	NA	0.89	NA

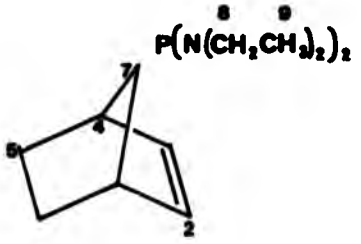

[B] $^{n}J(^{31}P,X)$

Carbon Position	$^{n}J(P,C)$/Hz		$^{n}J(P,H)$/Hz			
	Phosphorus Position		Phosphorus Position Syn		Anti	
	Syn	Anti	Hydrogen Exo	Endo	Hydrogen Exo	Endo
C_1/C_4	9.3	15.9	3.8	NA	3.8	NA
C_2/C_3	4.5	4.6	2.6	NA	NA	1.2
C_5/C_6	4.2	8.6	1.8	1.9	3.2	3.0
C_7	34.2	30.6	4.9	NA	5.0	NA
C_8	15.0	15.0	8.20	NA	8.21	NA
C_9	11.4	11.4	0.98	NA	0.94	NA

TABLE 2.3-8 ^{13}C and ^{1}H NMR Data of Syn, Anti 7-norbornenyl 1,3-dithol Phospholanes [31]

[A] Chemical Shifts

Carbon Position	$\delta\ ^{13}C$/ppm			$\delta\ ^{1}H$/ppm			
	Phosphorus Position			Phosphorus Position Syn		Anti	
	Syn	Anti	Δ - Δ Syn-Anti	Hydrogen Exo	Endo	Exo	Endo
C_1/C_4	44.02	43.96	0.06	3.60	NA	2.99	NA
C_2/C_3	132.26	134.26	-2.0	5.56	NA	NA	5.89
C_5/C_6	24.78	21.96	2.82	2.55	2.15	1.83	1.54
C_7	74.10	72.10	2.0	1.67	NA	1.64	NA
C_8	57.82	57.58	0.24	NA	(0.6—▸1.3)		NA

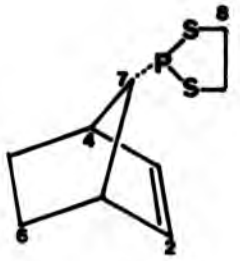

[B] $^{n}J(^{31}P,X)$

Carbon Position	$^{n}J(P,C)$/Hz		$^{n}J(P,H)$/Hz			
	Phosphorus Position		Phosphorus Position Syn		Anti	
	Syn	Anti	Hydrogen Exo	Endo	Exo	Endo
C_1/C_4	10.6	13.3	3.9	NA	4.2	NA
C_2/C_3	5.7	5.3	-	NA	NA	1.6
C_5/C_6	4.1	9.0	1.7	1.8	2.5	(3.0)
C_7	40.3	42.4	4.04	NA	4.18	NA
C_8	8.8	8.6	-	NA	-	NA

TABLE 2.3-9 ^{13}C and ^{1}H NMR Data of Syn, Anti 7-norbornenyl 1,3-dioxa phospholanes [32]

[A] Chemical Shifts

Carbon Position	δ ^{13}C/ppm			δ ^{1}H/ppm			
	Phosphorus Position			Phosphorus Position Syn		Anti	
	Syn	Anti	Δ = Syn-Anti	Hydrogen Exo	Endo	Hydrogen Exo	Endo
C_1/C_4	44.12	44.08	0.04	3.17	NA	3.09	NA
C_2/C_3	132.35	133.85	-1.06	5.56	NA	NA	5.49
C_5/C_6	24.82	22.02	2.8	2.27	-	1.71	1.52
C_7	68.72	66.76	1.96	1.29	NA	1.22	NA
C_8	68.96	68.84	0.12	NA	(2.2 –	2.6)	NA

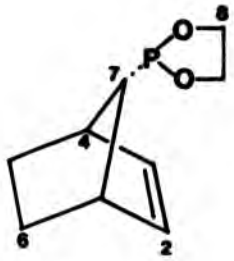

[B] $^{n}J(^{31}P,X)$

Carbon Position	$^{n}J(P,C)$/Hz		$^{n}J(P,H)$/Hz			
	Phosphorus Position		Phosphorus Position Syn		Anti	
	Syn	Anti	Hydrogen Exo	Endo	Hydrogen Exo	Endo
C_1/C_4	10.0	13.1	3.6	NA	4.0	NA
C_2/C_3	5.6	6.1	2.0	NA	NA	1.3
C_5/C_6	4.8	9.0	2.0	-	2.4	2.3
C_7	38.6	40.3	4.0	NA	4.5	NA
C_8	8.0	8.0	(4.0 →	9.0)	(8.8)	10.98

TABLE 2.3-10 ^{13}C and ^{1}H NMR Data of Syn, Anti 7-norbornenyl Diphenyl Phosphines [33]

[A] Chemical Shifts

Carbon Position	δ ^{13}C/ppm			δ ^{1}H/ppm			
	Phosphorus Position			Phosphorus Position Syn		Anti	
	Syn	Anti	Δ = Δ Syn-Anti	Hydrogen Exo	Endo	Hydrogen Exo	Endo
C_1/C_4	44.30	42.58	1.72	2.94	NA	2.97	NA
C_2/C_3	133.52	136.46	-2.94	5.62	NA	NA	5.86
C_5/C_6	23.26	19.42	3.84	1.96	1.65	1.04	1.58
C_7	56.32	54.22	2.1	2.95	NA	2.23	NA
aromatics	: 126	- 135 p	m		7.7 - 7.8	ppm	

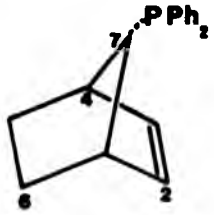

[B] $^{n}J(^{31}P,X)$

Carbon Position	$^{n}J(P,C)$/Hz		$^{n}J(P,H)$/Hz			
	Phosphorus Position		Phosphorus Position Syn		Anti	
	Syn	Anti	Hydrogen Exo	Endo	Hydrogen Exo	Endo
C_1/C_4	6.0	12.8	6.4	NA	6.5	NA
C_2/C_3	4.1	4.3	2.1	NA	NA	(0.9)
C_5/C_6	5.6	8.1	0.8	(0.9)	2.9	2.9
C_7	24.0	28.0	2.7	NA	2.7	NA

2.3.2.1 ^{13}C Chemical Shifts

^{13}C spectra were obtained on norbornenes with different phosphorus substituents in the 7-position resulting in both syn and anti derivatives. Again, as in the 2-norbornyl derivatives, ^{13}C chemical shift data are extremely useful in solving stereochemical problems in these rigid bicyclic systems. For convenience α, β, and γ term effects will be used to describe the pattern of chemical shifts as outlined previously (Section 1.4.1.2, equation [1.7]). These refer to the substituent positions relative to the ^{13}C nucleus that experiences the steric perturbation (Structure 13[A]).

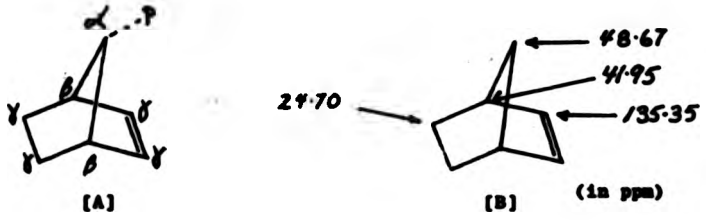

Structure 13

In comparing the carbon chemical shifts of norbornenyl derivatives with a phosphorus substituent in the 7-position it is useful to use norborn-2-ene itself as a chemical shift standard. The ^{13}C chemical shifts of norborn-2-ene relative to TMS are shown in Structure 13[B] and the individual carbon chemical shifts for all of the P(III) derivatives are compiled in Table 2.3-11.

TABLE 2.3-11 ^{13}C Substituent Chemical Shifts for 7-substituted Norborn-2-enes [a]

P(III) Substituents	Carbon Position			
	C_1/C_4 β	C_2/C_3 γ	C_5/C_6 γ	C_7 α
			Phosphorus Syn	
$-PBr_2$	3.1	1.3	4.2	27.4
$-PCl_2$	2.0	-0.6	0.2	27.6
-PBrCl	2.2	-0.7	0.2	25.9
$-P(NEt_2)_2$	3.9	-2.4	0.16	16.7
	2.1	-3.1	0.1	25.4
	2.2	-3.0	0.1	20.0
$-PPh_2$	2.4	-1.8	-1.4	7.7
$-PMe_2$	2.2	-1.5	-0.4	17.8
			Phosphorus Anti	
$-PBr_2$	3.0	3.4	1.95	21.9
$-PCl_2$	2.0	1.3	-2.6	22.5
-PBrCl	2.2	1.3	-2.6	20.9
$-P(NEt_2)_2$	3.9	-0.4	-2.57	14.7
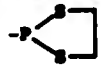	2.0	-1.1	-2.7	23.4
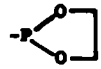	2.1	-1.5	-2.7	18.1
$-PPh_2$	0.6	1.1	-5.28	5.6
$-PMe_2$	2.1	1.91	-3.1	19.8

- not reported

a substituent chemical shifts in ppm, relative to norborn-2-ene; a minus sign denotes a shift to low frequency on substitution.

^{13}C α-effects

From Tables [A] of 2.3-3 to 2.3-10 and also 2.3-11, it can be seen that the α-effect on the C_7 carbon produced by the phosphorus group shows a pronounced shift to high frequency from C_7 in norborn-2-ene itself. This appears to be true for both syn and anti isomers of the P(III) derivatives. The largest increases for C_7 are seen for phosphorus substituents that are more electronegative such as $-PBr_2$ and $-PCl_2$. An α-effect can be seen of ca. 27 ppm for these derivatives. As one increases the bulkiness of the substituent on the phosphorus atom a decrease in the extent of shift to high frequency occurs. For example in the series $-PBr_2$, $-P\langle_{S}^{S}\rangle$, $-P(NEt_2)_2$, the α-effect decreases from +27.4, +25.4 to +16.7 ppm for C_7. These α-effects are in accord with data from similar 7-substituted norbornane compounds in Table 2.3-1. It also suggests that there is no ring distortion and that the bond between the phosphorus atom and the α-carbon in the ring can be considered normal. When comparing syn and anti isomers of the same substituted derivative, in all cases the shift for the syn isomer lies substantially to higher frequency than for the anti isomer. This is thought to occur because when moving to the syn position from the anti, rotation of the phosphorus atom is less hindered as the phosphorus atom is in a less confined structure.

^{13}C β-effects

In the 7-norbornenyl derivatives both C_1 and C_4 are in a β-position relative to the phosphorus substituent at C_7. As suggested by Quin[20] from similar compounds, the resonances of these carbons should be shifted to higher frequency by this substituent effect. This argument is reinforced by the present observations as in all cases the derivatives show some steric control by phosphorus, and a resulting shift to high frequency occurs (ca 2 ppm from norborn-2-ene). However differences

are small when electronegative or larger substituents on the phosphorus are changed. For example only a 0.1 ppm difference is seen between the $-PCl_2$ and the $-PMe_2$ anti substituent. Here also, no or only slight differences are noted when the syn and anti isomers for the same derivatives are compared. This suggests that the rigidity of this bicyclic ring does not allow the C_1/C_4 carbon to respond to small differences.

^{13}C γ-effects

Interestingly, the sp^2 hybridized carbons C_2/C_3 and the sp^3 hybridized carbons C_5/C_6 are positioned so that both could be influenced by the γ-effects from the phosphorus on C_7. From Tables [A] of 2.2-3 to 2.2-10 steric control is shown only if the phosphorus is in the position syn relative to the carbon of interest (γ-periplanar). For example in syn 7-norbornenyl dichloro phosphine, the C_2/C_3 carbons show the γ-effect and a shift to lower frequency with respect to the corresponding carbons in 2-norbornene results (ca. 1 ppm). However, for the C_5/C_6 carbons, no γ-effect is seen and in fact a slight shift to higher frequency occurs (ca. 1.2 ppm). Conversely in the anti derivative, the C_5/C_6 sp^3 hybridized carbons show the steric γ-effect and the C_2/C_3 sp^3 hybridized carbons do not. This result is more or less displayed for all the P(III) derivatives studied. This feature also allows for easy identification of the syn and anti isomer pairs. Differences in these γ-antiperiplanar and γ-periplanar effects have been commonly noted by Eliel et al[43] and others[44-46] in similar non-phosphorus compounds. It has been suggested that an explanation which depends upon steric compression effects is possible, though a composite of factors may play the major part.

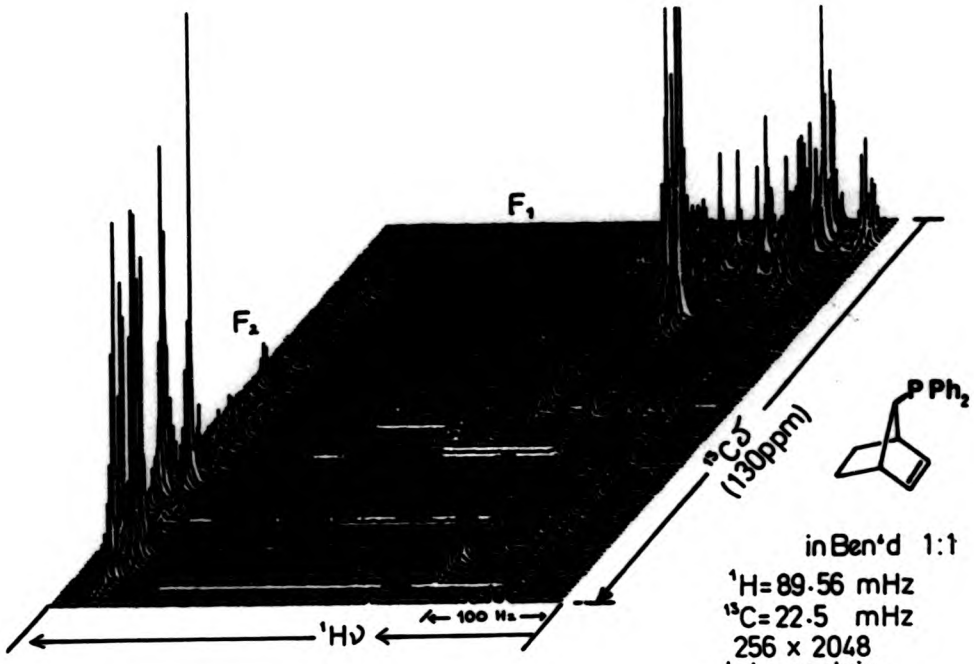

Fig 2.3-2 A 2D $^{13}C/^{1}H$ Shift Correlated Stack Plot of Syn-7-Diphenyl Phosphonous Norbor-2-ene

2.3.3.2 ^{1}H Chemical Shifts

Initial structural assignments, as stated previously, were made on the basis of phosphorus and carbon chemical shift data. These assignments were then correlated by a 2D $^{13}C/^{1}H$ shift correlation NMR experiment to allow assignment and determination of the individual hydrogen resonances. For example, Fig. 2.3-2 shows a Stack Plot of a 2D $^{13}C/^{1}H$ Shift Correlated experiment of Syn 7-norbornenyl diphenyl phosphine. Here data slices along a particular assigned carbon of interest may be taken to allow easy determination and assignment of its associated hydrogens. Such ^{1}H chemical shift data have been shown to be useful in determining structural features in similar rigid bicyclic systems. For example, Fraser[47] utilised the fact that the 5,6-exo protons in norborn-2-ene derivatives are shifted to high frequency relative to the corresponding isomeric 5,6-endo ring protons, and hence established the configuration of these protons in norbornenes bearing substituents in the C_5/C_6 ring positions. The resulting proton shieldings for norborn-2-ene are shown in Structure 14[B].

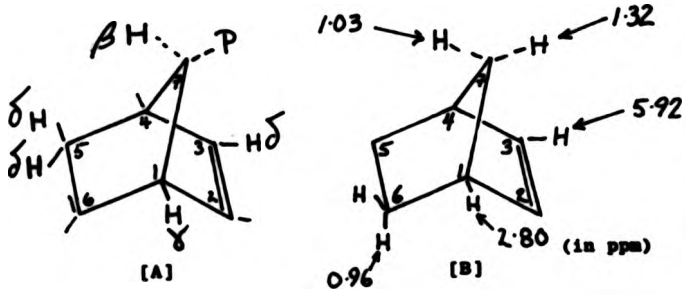

Structure 14

This method which was used to confirm the structure of norborn-2-ene, by measuring the differences in proton chemical shifts, was extended to distinguish norborn-2-enes bearing substituents other than hydrogen in the C_5/C_6 positions[48]. In other bicyclic structures such as norbornanes, the exo ring protons are similarly shifted to high frequency

relative to the endo ring protons and the differences are of the order of 0.3 ppm[49]. By extension of this method it was hoped that the measurement of ^1H chemical shift differences would allow effective correlations in assigning stereochemistry in the 7-substituted ring systems bearing a variety of phosphorus substituents. The distance away from the phosphorus substituent are represented as described in Section 1.4.1.2 and are shown in Structure 14[A]. To analyse these proton steric effects arising from the phosphorus atom substituent on the C_7-$\underline{\alpha}$ carbon, it is convenient to compare them with the ^1H chemical shifts of norborn-2-ene given in Structure 14[B]. Table 2.3-12 shows the compilation of these effects for the different hydrogens in the cage for all P(III) derivatives.

β-effects on the Hydrogen on C_7

In Tables [A] of 2.3-3 to 2.3-10 for P(III) derivatives, the hydrogen on C_7 shows an increase in chemical shift of 0.2 to 2.4 ppm to high frequency when C_7 carries a phosphorus substituent. As one increases the size of the phosphorus substituent, this increase in proton chemical shift becomes greater. For example, moving from -P<S,S> to $-P(NEt_2)_2$ to $-PPh_2$ causes the $\underline{\delta}(H_7)$ to increase from 1.67 to 2.12 and then to 2.95 ppm for the syn derivative, and the anti derivative behaves similarly. Also for an increase in electronegativity of the phosphorus substituent, there is a corresponding increase in $\underline{\delta}(H_7)$. In most cases $\underline{\delta}(H_7)$ in the syn isomer is to high frequency of that in the anti (Table 2.3-12). This tends to suggest that when the phosphorus substituent is orientated on the less hindered side of the ring, a less dominant effect is felt by H_7 from this substituent. The extent of shift difference between the syn and the anti isomers seems to be dependent upon the particular substituent and no general trends can be deduced at this stage.

TABLE 2.3-12 ^{1}H Substituent Chemical Shifts for 7-substituted Norbor-2-enes.

P(III) Substituents	Hydrogen Position				
	H_1/H_4 γ	H_2/H_3 δ	H_5/H_6 δ_{exo}	H_5/H_6 δ_{endo}	H_7 β
			Phosphorus Syn		
$-PBr_2$	0.3	0.1	0.3	1.0	2.4
$-PCl_2$	0 2	0.0	0.8	1.0	1.4
-PClBr	0.2	0.0	0.6	0.7	1.6
$-P(NEt_2)_2$	0.1	0.2	0.4	0.4	1.1
	0.8	-0.4	1.6	1.2	0.6
	0.4	-0.4	1.3	-	0.3
$-PPh_2$	0.1	-0.3	1.0	0.7	1.92
			Phosphorus Anti		
$-PBr_2$	0.3	0.2	0.9	0.5	1.5
$-PCl_2$	0.1	0.1	0.9	0.5	0.8
-PClBr	0.1	0.3	0.0	0.4	1.0
$-P(NEt_2)_2$	0.1	0.3	0.2	0.0	0.7
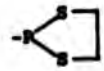	0.2	0.0	0.9	0.6	0.3
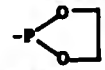	0.3	-0.4	0.8	0.6	-0.1
$-PPh_2$	0.2	-0.1	0.1	0.6	0.9

- not reported

a Substituent chemical shifts in ppm, relative to norborn-2-ene; a minus sign denotes a shift to low frequency on substitution

γ-effect on the Hydrogens of C_1/C_4

The hydrogens on the C_1 and the C_4 carbons are orientated away from the C_7 position and a less pronounced γ-interaction occurs in these systems than say for a γ-interaction in the 2-norbornyl ring. However for all 7-substituted phosphorus derivatives, a slight shift to higher frequency is obtained for the C_1/C_4 hydrogen with respect to norborn-2-one. The presented data also suggests, if one can actually accept that the small shift differences as significant, that as one increases the electronegativity of the phosphorus substituent, a greater γ-effect arises. This is shown in the data for the $-P(NEt_2)_2$, $-PCl_2$, $-PBr_2$ derivatives. The corresponding C_1 hydrogen chemical shift rises from 2.86 to 2.96 and then to 3.12 ppm. When comparing the syn and anti isomer pair for a set of derivatives, the resonances for the syn isomer in most cases occur to higher frequency. This suggests that when the phosphorus substituent is orientated on the olefin side of the ring greater freedom of movement for the substituent is allowed and a greater γ-interaction on the C_1/C_4 hydrogen occurs.

δ-effects on the Hydrogens on C_2/C_3 and C_5/C_6

δ-effects are usually unimportant in most compounds. The substituent which causes the effect, in this case the phosphorus substituent, is usually so far removed with respect to the δ-positioned recipient that effects of little chemical importance can be expected. However, in this bicyclic system the geometry is such that quite substantial interactions can occur (see Structure 15) and indeed significant effects are found.

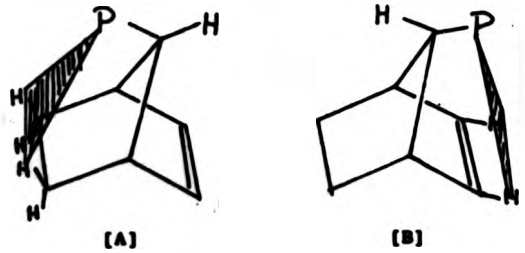

[A] [B]

Structure 15

Two very different environments occur for the δ-effect in this ring system. The sp^2 hybridised C_2/C_3 carbons one have hydrogen each and the sp^3 hybridised C_5/C_6 carbons have two hydrogens each. This δ-effect acts to shift the hydrogen resonance to lower frequency. Therefore by monitoring the side of the ring which shows the δ-effect distinction can be made between the syn and anti isomers. This is illustrated nicely by the $-PPh_2$ derivative. When the phosphorus substituent is syn, a shift to lower frequency occurs for the syn C_2/C_3 hydrogen whereas the C_5/C_6 hydrogens remain largely unaffected. On the other hand when the phosphorus substituent is in the anti position the C_2/C_3 hydrogens are unaffected and the extent of the C_5/C_6 hydrogens shift markedly decreases. Comparing δ-effects for a range of different derivatives shows this effect to be a general one, but detailed comparison of the size of the effect for different substituents was not fruitful. Only when the phosphorus is carrying electronegative substituents and is orientated anti, do the hydrogen chemical shifts (on C_5/C_6) respond and show a slight shift to high frequency. The reason as to why hydrogen chemical shifts are not as sensitive to a change in phosphorus substitution as would be expected may be that these effects are very local and small. Also slight changes in the torsion angles in the ring, arising from changes in the attached substituent, may compensate or mask these effects and thus the small trends may be lost.

Fig. 2. 3-3 A ^{13}C / ^{1}H 2D Shift Correlated Stack Plot of syn, anti 7-norbornenyl 1, 3- dithiolphospholanes

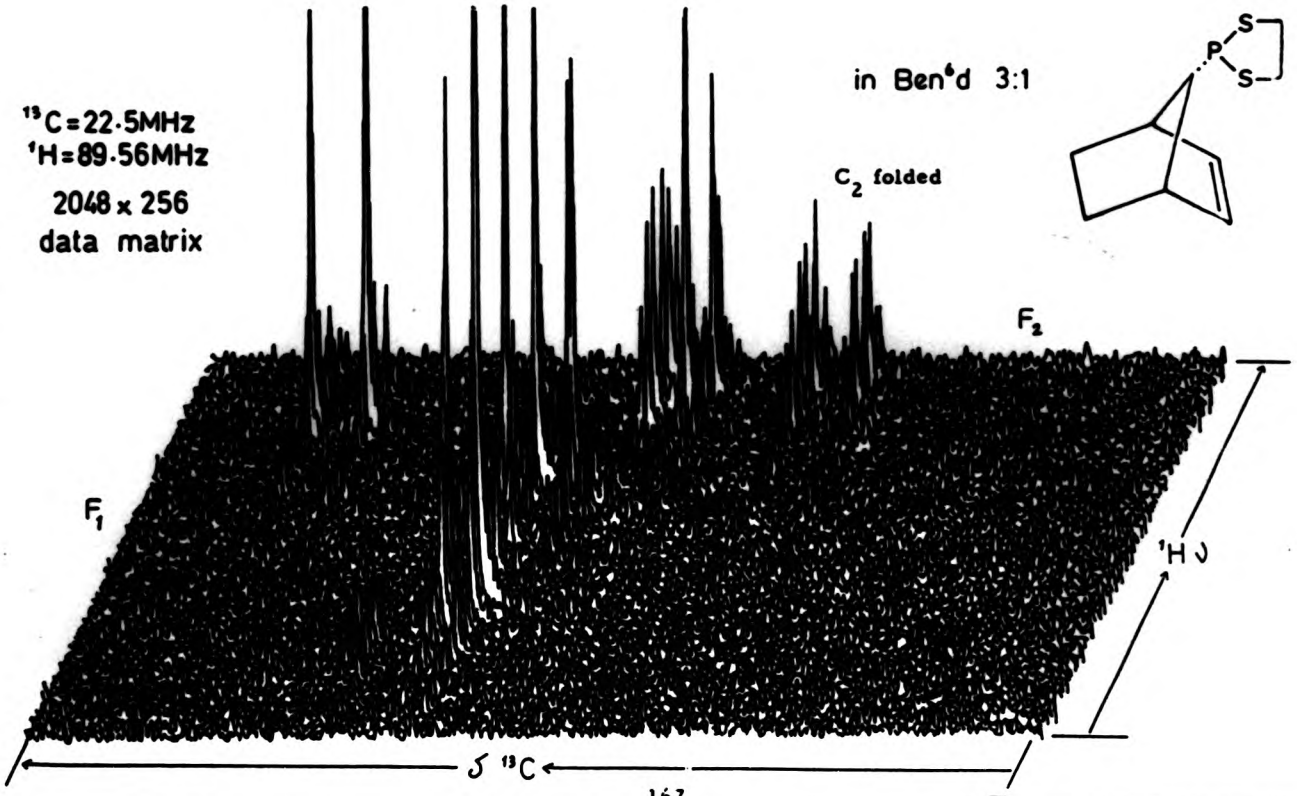

2.3.2.3 Comparison of coupling constants in 7-norbornenyl phosphorus derivatives

Spin-spin coupling constants, as also in the 2-norbornyl system (Structure 2, Section 2.3.1), were used as a basis to determine configurational dependence and to complement data obtained from chemical shift calculations for ^{31}P, ^{13}C and ^{1}H NMR data. In particular values of $^{n}J(P,C)$ and $^{n}J(P,H)$ were used to determine the influence of the different substituents to the 7-norbornenyl ring. This data is given in Tables [B] of 2.3-3 to 2.3-10.

$^{1}J(P,C)$ One-bond Spin-spin Couplings

Here again, as in the 2-norbornyl phosphorus derivatives large one-bond couplings are observed in the 7-norbornenyl phosphorus derivatives. The size of the couplings are usually associated with the ability of the substituent group to concentrate s-character in the electron pair to produce this σ-effect. From the data, it can be seen that electronegative groups produce large one-bond couplings (ca. 40-50 Hz). As the substituent on the phosphorus atom becomes more electropositive and/or bulky, smaller couplings are found. For example, the $-P(NEt_2)_2$ derivative has a value of $^{1}J(P,C)$ ca. 15 Hz. The data also suggests that the anti isomers in the series have a greater ability to hold s-character as the anti isomers have slightly larger couplings than the syn.

$^{2}J(P,X)$ Geminal Coupling Constants

$^{2}J(P,C)$

Geminal coupling data for the C_1/C_4 carbons show that as one decreases electronegativity in the phosphorus substituents smaller couplings arise. Here also the anti orientation of the phosphorus substituent produces a larger value of $^{2}J(P,C)$ than when in the syn orientation. This suggests that smaller bond angles (and hence larger couplings) are available to the phosphorus when in this anti orientation.

Thus steric control seems to play an important role in these two-bond interactions.

$^2J(P,H)$

In the 7-norbornenyl system only one geminal coupling arising from the H_7 is possible. For this H_7 the sensitivity to different substituents is minimal and its coupling extent varies from substituent to substituent. However the magnitudes for the electronegative derivatives do seem to be 1-2 Hz larger than for the other substituents presented. Also when the phosphorus position is anti, the coupling is slightly larger than when the phosphorus is in the syn position. This may be due to the fact that when the phosphorus substituent is in the anti position (this being the more congested side) a greater steric interaction between the lone pair of the phosphorus and the H_7 proton will occur from a smaller bond angle. This will result in a larger β-effect (i.e. a larger coupling).

$^3J(P,X)$ Vicinal Coupling Constants

$^3J(P,C)$

In rigid bicyclic systems similar to the 7-norbornenyl structure it is sometimes possible to relate $^3J(P,X)$ couplings with dihedral angles by a Karplus-like relationship. In such a relation, for the 7-norbornenyl structure the value of $^3J(P,C)$ to the C_5/C_6 carbons should be large as the dihedral angle is large (164°, see Section 3.3). Conversely the coupling for the C_2/C_3 the phosphorus $^3J(P,C)$ should be smaller as the angle is smaller (57°, see Section 3.2). For the P(III) derivatives shown, the resemblance of a Karplus relation seems to exist. The data shown reveals that large couplings are seen for the C_5/C_6 carbons and smaller couplings are shown for the C_2/C_3 carbons for all derivatives. This is agreement with other similar data demonstrated by Quin[29]. This

Karplus relationship is discussed in more depth in Section 3.2.

$^{3}J_{(P,H)}$

For these three-bond couplings, the extent of a dihedral angle contribution is unclear. The hydrogens, unlike the carbon are not held in a rigid structure and seem to respond more importantly to the electronic effect of the particular substituent on the phosphorus atom. See Section 3.3.

$^{n}J_{(P,H)}$ Long range Couplings

Long range couplings were determined between the hydrogens on C_2/C_3 and C_5/C_6 and are listed in Tables [B] of 2.3-3 to 2.3-10. The values are small and do not on their own contribute much chemical information. However it is possible to confirm assignments as to whether the phosphorus substituent is <u>syn</u> or <u>anti</u> when these couplings are considered with the other couplings. This is most striking when the phosphorus substituent is in the <u>anti</u> orientation on the ring. Here the couplings from phosphorus to the C_5/C_6 <u>exo</u> hydrogens are much larger than when the phosphorus is in the <u>syn</u> position. An explanation might be that when the phosphorus is <u>anti</u> there is a direct interaction between the highest occupied, relatively high-lying π-orbitals of the C_5-C_6 carbon bond and the electron pair of phosphorus. This interaction could thus influence the attached hydrogens on these C_5/C_6 carbons.

[ii] Tricyclic Structures - Adamantanes

General: In order to extend the ability to use chemical shifts and coupling constants to predict stereochemistry and conformation in some of the more complicated tricyclic aliphatic systems, a series of 1- and 2-adamantyl phosphorus derivatives were prepared. This was thought useful as it is necessary to obtain data from a great variety of compounds in order to support the theoretical considerations aiming to separate certain contributions to the substituent effects in ^{13}C and ^{1}H nuclear shieldings and in the values of $^{n}J(P,C)$ and $^{n}J(P,H)$. Investigations of relatively rigid molecules are welcome because of the well-defined geometrical situation in these cases and the less likelihood of ring distortion to occur when substituted[50,51]. For example, in adamantane itself the strain energy is low[52,53] due to the tetrahedral angles at carbon, and the ring structure is considered to be rigid as encountered in other cages of this class (e.g. norbornane and norborn-2-ene). Ring flattening, as in cyclohexane derivatives does not occur[54]. Also it is found that distortion does not occur in 2,4-diaxially di-substituted adamantanes[54] or in the case where the molecule is substituted at a bridgehead with groups other than fluorine[55].

Due to the plane of symmetry in the structures of both the 1- and 2-adamantyl substituent derivatives, only one isomer is possible in each case. See Structures 18 in Section 2.4 and 22 in Section 2.5 respectively. However it has been proposed that preparations via a Grignard reagent with subsequent phosphorus addition (as shown in Fig. 1.2-1, Section 1.2), seem to proceed through an adamantene intermediate which may result in a mixture of both 1- and 2-adamantyl substituted derivatives being formed. This seems to be the case when using 1-bromo adamantane or 2-bromo adamantane as starting materials in the preparation of the P(III) derivatives as both structures may be formed from either

reagent. Separation of these 1-adamantyl and 2-adamantyl derivatives was not often worthwhile because yields were usually small and 2D-NMR analysis required maximum quantities of material.

It has also been proposed that dimerized or disubstituted products occur. These may be of the form shown in Structures 16[A] and [B].

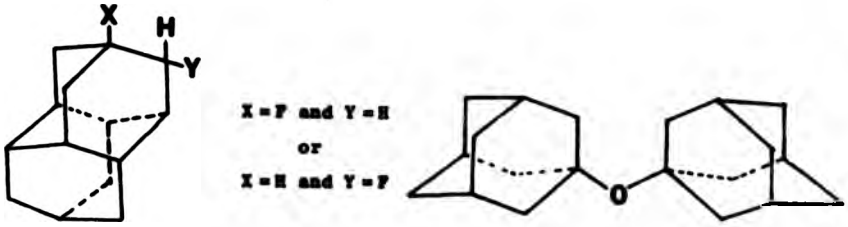

[A] [B]

Structure 16

Structure 16[A] has been thought to occur in the preparation of fluorinated derivatives from 1-hydroxy and 2-hydroxy adamantanes[86]; whereas structure 16[B] was formed when adamantan-1-ol was treated with phosphorus oxychloride[87]. For the P(V) derivative no observable dimeric or di-substituted products were formed, however in some of the reactions using P(III) derivatives, disubstituted products were formed, and seem to have the structures shown in Structure 17. In the case where these side

Structure 17

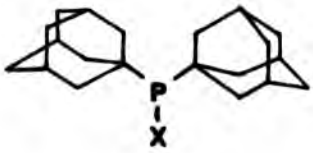

products were formed, they usually made up less than 5% of the raw product mixture, and elemental analyses could not be made on them as attempts at extraction proved unsuccessful. Hence only by way of ^{31}P NMR analysis could one ascertain the amount and type of product formed. However, removal of these disubstituted derivatives was possible from the mono-substituted products. The proportions of products for a few of the

reactions are shown in Table 2.4-1 for the different starting bromo adamantane materials. Fig. 2.4-1 shows a typical ^{31}P NMR spectrum before removal of the disubstituted products (DP).

TABLE 2.4-1 Reaction Ratios of Major Products from Grignard/Phosphorus Addition Reactions for P(III) Derivatives

Final Product Substituent	Approximate % from ^{31}P NMR analysis		
	1-substituted	2-substituted	disubstituted mixture
(From 1-bromo adamantane)			
$-PBr_2$	65	(25-30)	(10-5)
$-PCl_2$	(75)	(20)	~5
-PClBr	80	(15)	(5)
$-P(NEt_2)_2$	75	(20)	(5)
-PPhBr	100	(0)	(0)
-PPhCl	100	(0)	(0)
$-PPh_2$	60	34	6
(From 2-bromo adamantane)			
$-PBr_2$	(15)	(80)	~5
$-PCl_2$	10	85	<5
-PClBr	(0)	95	<5
-PPhBr	(0)	100	(0)
-PPhCl	(0)	100	(0)
$-PPh_2$	40	60	(0)

( ) = estimated

FIG. 2.4-1 ^{31}P NMR Spectrum of Crude Products from a 1-adamantyl dibromo phosphine Preparation from 1-bromo adamantane

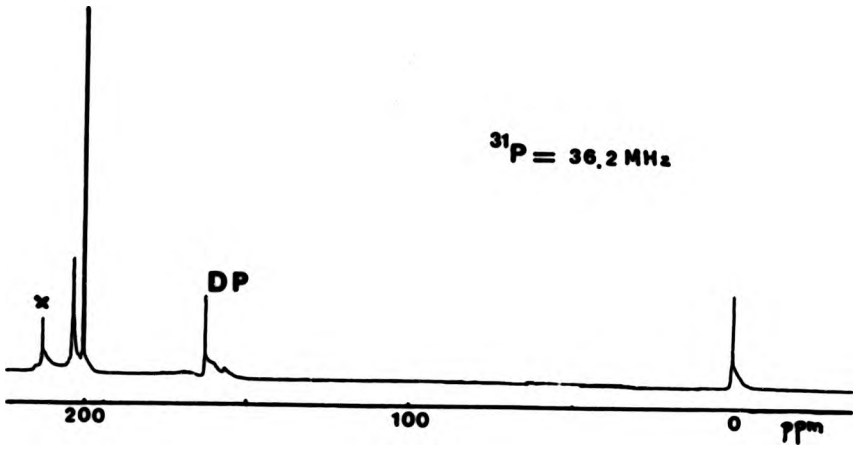

2.4 1-adamantyl Phosphorus Derivatives

General: The 1-adamantyl phosphorus derivatives were prepared usually from 1-bromo adamantane via the Grignard reagent and subsequent addition of PX_3. These are detailed in preparations [37] to [45] in the Experimental chapter. Only one isomer is possible in each case and the molecule is numbered as shown in Structure 18.

For the cases where both the 1-substituted and the 2-substituted phosphorus derivatives were produced, as mentioned above, carbon resonances from the two structures in the ^{13}C NMR spectrum could be differentiated by use of a selective phosphorus decoupling experiment (as described in Section 2.3.1). For the 1-adamantyl phosphorus derivatives only four ^{13}C resonances occur from the cage, whereas seven

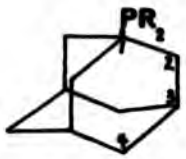

PR_2 = the different phosphorus substituents

Structure 18

resonances are expected for the 2-adamantyl phosphorus derivatives (see Section 2.5). Also in the 2-substituted adamantyl phosphorus derivatives the H_2 resonance lies to high frequency of all other proton resonances in the cage and shows a large value for $^2J(P,H)$. This could be obtained directly from the ^1H spectrum and relative estimates of the 1-adamantyl:2-adamantyl proportions in the mixture could thus be made.

2.4.1 ^{31}P NMR Data of the 1-adamantyl Phosphorus Derivatives

Table 2.4-2 shows the ^{31}P NMR chemical shifts of the 1-adamantyl phosphorus derivatives. Generally this ^{31}P NMR data seems to reflect the normal overall trends expected for P(III) and P(V) chemical shifts in terms of the effects of different substituents. For example in the series $-PBr_2$, -PPhCl, $-P(NEt_2)_2$, and $-PPh_2$ the chemical shift moves to lower frequency as expected. In the 1-adamantyl phosphorus derivatives the carbon carrying the phosphorus substituent (C_1) is not chiral. For derivatives with phosphorus substituents such as -PPhCl, -PPhBr and -PBrCl, the phosphorus atom itself may be chiral, regarding the electron pair as the fourth substituent. However only mirror image isomers will result from this, and these would have identical NMR parameters. Interestingly however, in the preparation of the -PPhCl derivative from the 1-bromo adamantane and phenyl dichloro phosphine, two signals occur in the ^{31}P NMR spectrum. It is proposed that both -PPhCl and -PPhBr

TABLE 2.4-2 ^{31}P NMR Chemical Shifts of Some Prepared 1-adamantyl Phosphorus Compounds

Substituent n =	1-adamantyl-n [a]	Preparation Number
P(III)		
$-PBr_2$	199.2	[37]
-PBrCl	195.9	[38]
$-PCl_2$	192.4	[39]
-PPhCl	162.1	[40]
-PPhBr	158.2	[40]
$-P(NEt_2)_2$	94.6	[41]
	46.9	[42]
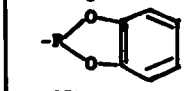	3.3	[43]
$-PPh_2$	-4.9	[44]
P(V)		
$-P(S)Me_2$	93.6	[45]

a in ppm, a minus sign denotes values to low frequency of 85% H_3PO_4 = 0.0 ppm

derivatives were formed. This premise was based on their ^{31}P chemical shift values (given in Table 2.4-2) and from the products likely to form in the reaction. It was not possible however to separate these compounds. The -PPhCl adduct was assigned to lie to higher frequency in the ^{31}P NMR spectrum. This is similar to the patterns shown for other mono halide P(III) derivatives given in Table 2.4-3.

TABLE 2.4-3 Comparison of ^{31}P Chemical Shifts for some Mono-chloride and Mono-bromide P(III) Derivatives

Compound	^{31}P δ/ppm*
$P(CH_3)_2Cl$ [a]	+96.5
$P(CH_3)_2Br$ [a]	+92.0
$P(C_6H_5)_2Cl$ [a]	+81.5
$P(C_6H_5)_2Br$ [b]	+70.8
$P(C_2H_5)_2Cl$ [a]	+119.0
$P(C_2H_5)_2Br$ [b]	+116.2
$C_6H_5(C_6F_5)PCl$ [b]	+87.1
$C_6H_5(C_6F_5)PBr$ [b]	+39.3
$(C_6F_5)PCl$ [b]	+12-37
$(C_6F_5)PBr$ [b]	+13.0

* positive is to high frequency from 85% H_3PO_4 = 0.0 ppm

a taken from ref. 8

b taken from ref. 58

2.4.2 ^{13}C and ^{1}H NMR Data

The ^{13}C and ^{1}H chemical shifts and the values of $^{n}J(P,C)$ and $^{n}J(P,H)$ are presented in Tables 2.4-6 and 2.4-7 and were prepared from 1D and 2D NMR analyses similar to those given for the 2-norbornyl (Section 2.2) and the 7-norbornenyl (Section 2.3) derivatives. The resonances of the carbons in the cage were assigned by the following methods. C_1 could be easily assigned as the phosphorus substituent caused this carbon to be shifted well to high frequency of the other carbon resonances in the

cage. Also the C_1 chemical shift was associated with a large $^1J(P,C)$. Use of a GASPE sequence allowed distinction to be made between the CH_2 and CH carbons in the cage and thus C_3 could be readily assigned. These assignments were also checked by comparing the ^{13}C chemical shifts of these phosphorus derivatives with those of a selection of 1-substituted adamantanes as shown in Table 2.4-4.

TABLE 2.4-4 Some ^{13}C Chemical Shifts of other 1-substituted Adamantanes

Carbon Position	δ/ppm				
	Adamantane a	1-bromo Adamantane b	1-chloro Adamantane b	Adaman-tan-1-ol b	1-Fluoro Adamantane b
C_1	28.5	66.20	67.25	67.90	92.40 (184.0)
C_2	37.7	49.30	48.19	45.3	42.70 (17.8)
C_3	28.5	32.80	32.02	30.8	31.40 (10.6)
C_4	37.7	35.80	36.22	36.1	35.90 (1.5)

a taken from ref. 9 b taken from ref. 40
( ) = $^2J(C,F)$ in Hertz

The comparison was good for carbons C_1 and C_3. However the compounds in this table show that normally C_2 lies to high frequency of C_4 This does not seem to be the case in the 1-adamantyl phosphorus derivatives. In fact differentiation between the two kinds of methylene carbons, C_2 and C_4 was difficult if the chemical shifts only were taken into account as they resonated close together in the phosphorus derivatives. However if one considers the difference in magnitudes between the $^2J(P,C)$ associated in these two carbon sites, a ready distinction can be made. For example, if one compares $^2J(P,C)$ with $^4J(P,C)$, it will be seen as a general phenomenon that the $^2J(P,C)$ is usually the larger. This is

exemplified by the compound 1-fluoro adamantane, where C_2 has a much larger F-C coupling than C_4 (see Table 2.4-4). This is expected because the carbon position at C_2 is much closer to the fluorine substituent on C_1 than the carbon at C_4. This is also true in phosphorus chemistry and C_2 can be expected to have a larger coupling to a phosphorus substituent at C_1 than C_4. This can be seen in a host of phosphorus compounds, some of which are given in Table 2.4-5.

TABLE 2.4-5 Comparison of the values of $^2J(P,C)$ and $^4J(P,C)$ in some Phosphorus Compounds

Structure	$^nJ(P,C)$ / Hz
$P(C_6H_5)_3$ [a]	$^2J(P,C) = 19.65$ $^4J(P,C) = 0.33$
$+P(C_6H_5)_4$ [a]	$^2J(P,C) = 10.9$ $^4J(P,C) = 2.9$
$(C_6H_5)_2P-CH_2-CH_2-CH_2-CH_4$ [b]	$^2J(P,C) = 16.1$ $^4J(P,C) = \sim 0.0$ $^2J(P,C_{ortho}) = +18.1$ $^4J(P,C_{para}) = \sim 0.0$
a taken from ref. 50 b taken from ref. 8	

From observed values of $^2J(P,C)$ and $^4J(P,C)$ for the 2-norbornyl and the 7-norbornenyl-phosphorus derivatives, which the carbons are also contained in a rigid cage structure and the cage is of the same class as the adamantyl phosphorus derivatives, it seemed that deviations from this coupling trend would be unlikely for the adamantyl derivatives. Thus the $^2J(P,C)$ would also be expected to be larger than $^4J(P,C)$ in the

1-adamantyl phosphorus derivatives. On this basis therefore, the assignments given in Tables 2.4-6 and 2.4-7 show that the C_4 chemical shift associated with a small value of $^4J(P,C)$ is to high frequency of the C_2 (associated with the larger $^2J(P,C)$). Since it was now possible to assign the $^{13}C\{^1H\}$ spectrum, determination and assignment of the corresponding ^1H chemical shifts and the values of $^nJ(P,H)$ could be achieved by the use of a 2D $^{13}C/^1H$ shift correlated experiment (as outlined in Section 2.1.3)

2.4.2.1 ^{13}C Chemical Shifts

For the 1-adamantyl phosphorus derivatives the carbon chemical shifts of adamantane itself (CH = 28.7 ppm; CH_2 = 38.2 ppm) can be used as a reference point for discussion of different substitutent effects arising from the different phosphorus groups at C_1 (see Structure 18).

These effects can be described for a particular carbon in terms of the number of bonds separating it from the phosphorus substituent (PR_2) at C_1 (shown in Table 2.4-8). In the adamantyl cage the carbons are held in a strain-free framework and the 6-membered ring sub-units adopt nearly a chair conformation where all C-C-C bond angles are virtually tetrahedral[59]. The rigidity of the structure plays an important part in the final ^{13}C chemical shift values and any chemical shift changes from that of adamantane should be due to the electronic effects of substitution on the cage and not from bond angle distortions.

α and β effects

In Table 2.4-8 it is seen that replacement of a hydrogen at C_1 by a phosphorus substituent causes a shift to high frequency of C_1 (13.3 ppm for the dichloro phosphine derivative). Chemical shifts to higher frequency are expected for these bicyclic cages as a result of α-

TABLE 2.4-6 ^{13}C and ^{1}H NMR Chemical Shifts of Some 1-adamantyl Phosphorus Derivatives

[A] ^{13}C/ppm [a]

Substituent	Carbon number				Other
	C_1 α	C_2 β	C_3 γ	C_4 δ	
$-PBr_2$	42.06	35.63	28.53	36.85	
$-PCl_2$	41.96	35.40	28.50	37.08	
-PClBr	41.15	35.96	28.60	36.98	
-PPhBr	41.16	36.02	28.68	37.02	)
-PPhCl	43.20	37.12	28.70	37.03	) Aromatics: 129-143
$-P(NEt_2)_2$	44.82	-	28.61	39.85	CH_2 = 43.1 CH_3 = 14.8
	49.96	41.49	28.52	42.51	CH_2 = 66.1
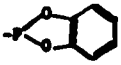	42.56	37.56	28.67	36.08	Aromatics: 116.2, 122.5,142.7
$-PPh_2$	49.50	38.72	28.76	36.51	Aromatics: 129-140
$-P(S)Me_2$					

[B] ^{1}H δ/ppm [a]

Substituent	Hydrogen number			Other
	C_2H γ	C_3H δ	C_4H * ε	
$-PBr_2$	1.80	2.09	1.73	
$-PCl_2$	1.75	2.05	1.69	
-PClBr	1.77	2.05	1.70	
-PPhBr	1.69	2.32	1.21	)
-PPhCl	1.72	2.35	1.20	) Aromatics: cluster between 7.3 - 7.8
$-P(NEt_2)_2$	-	1.92	-	CH_2: — CH_3: —
	1.68	1.96	1.13	CH_2 = —
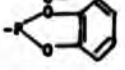	1.63	-	1.09	Aromatics: 7.4
$-PPh_2$	2.05	1.86	0.97	Aromatics: 6.9 - 7.3
$-P(S)Me_2$	1.84	1.22	1.60	CH_3 = 1.7

a in ppm, relative to TMS = 0.0 ppm in $CDCl_3$

- Not reported

* Hydrogens on C_4 are chemically inequivalent, however no chemical shift differences could be detected.

TABLE 2.4-7 NMR (^{31}P-X) Coupling Constants of Some 1-adamantyl Phosphorus Derivatives

[A] $^{n}J(^{31}P,^{13}C)$/Hz

Substituent	Carbon number				Other
	C_1 α	C_2 β	C_3 γ	C_4 δ	
$-PBr_2$	46.1	16.5	8.7	1.6	
$-PCl_2$	48.8	15.5	9.1	1.6	
-PClBr	45.8	16.2	8.8	1.7	
-PPhBr	45.8	16.2	8.7	1.0	
-PPhCl	45.7	16.2	8.8	1.1	
$-P(NEt_2)_2$	25.2	-	6.3	1.4	
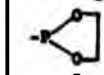	23.7	7.8	4.8	1.8	
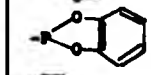	31.4	8.1	2.9	3.2	
$-PPh_2$	34.5	2.4	-	1.0	
$-P(S)Me_2$	-	8.2	3.5	1.5	$(P-CH_2)$ = 73.83

[B] $^{n}J(^{31}P,^{1}H)$/Hz

Substituent	Hydrogen number			Other
	C_2H γ	C_3H δ	C_4H ε	
$-PBr_2$	5.7	2.2	2.1	
$-PCl_2$	4.9	2.1	2.1	
-PClBr	5.6	2.1	1.9	
-PPhBr	3.1	2.8	0.7	
-PPhCl	3.2	2.8	-	
$-P(NEt_2)_2$	-	2.2	-	
	3.3	2.7	0.9	$^{4}J(\underline{P}\text{-}O\text{-}C\text{-}\underline{H})$ = 6.6
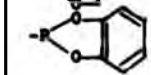	2.9	2.6	1.0	
$-PPh_2$	3.1	2.5	0.8	
$-P(S)Me_2$	7.8	1.6	2.9	

- not reported

a hydrogens on C_4 are chemically inequivalent, however no coupling differences could be detected

TABLE 2.4-8 ^{13}C Substituent Chemical Shifts for 1-substituted Adamantanes[a]

P(III) Substituent	Carbon Position on Cage			
	C_1 α	C_2 β	C_3 γ	C_4 δ
$-PBr_2$	13.4	-2.6	-0.2	-1.4
$-PCl_2$	13.3	-2.8	-0.1	-1.1
-PClBr	12.6	-2.2	0.0	-1.2
-PPhBr	12.5	-2.0	0.0	-1.2
-PPhCl	14.5	-10.8	0.0	-1.2
$-P(NEt_2)_2$	16.1	-	-0.1	1.7
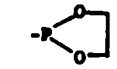	21.3	3.3	-0.2	4.3
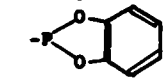	13.9	-0.6	-0.1	-0.1
$-PPh_2$	20.8	0.5	0.0	-1.7

- Not reported

a Substituent chemical shifts in ppm, relative to adamantane, a minus sign denotes a shift to low frequency on substitution.

Structure 18

substituent effects if they are compared with other 1-substituted adamantanes given in Table 2.4-4. Such α effects have been related to the change in electron density at the carbon responding to an electronic effect of the phosphorus atom. However it is not clear from this data how, in terms of overall trends, this effect is responding.

With regard to C_2, which is β relative to the phosphorus-containing group, an overall chemical shift to lower frequency occurs for most of the series. This is in contrast to the general trend for most phosphorus compounds, as the β-effect is usually thought of as a deshielding one causing a shift to high frequency. However it has been noted by Buchanan and Benezra[9] in their study of 2-dimethyl-2-hydroxy adamantane and other cage phosphonates that the β-carbons may also be shifted to low frequency through γ(gauche) interactions. This seems to occur for the 1-adamantyl phosphorus derivatives where the γ(gauche) interactions between the phosphorus electron pair and the C_2 carbons play a dominant part and offsets the expected β-deshielding effect by this γ(gauche) effect. (The usual γ effect is to low frequency.) This may be possible as both β and γ interactions are electronic effects and thus the electron pair of the phosphorus atom may be able to create a change of electron density at the β carbon. The extent of the γ-interaction through the gauche electron pair of the phosphorus will vary depending upon the other substituents on the phosphorus atom. From Table 2.4-8, though the data is somewhat scattered, there seems to be a less dominant γ-effect as one decreases the electronegativity, and the chemical shift of C_2 increases to respond the greater β-effect.

It does not seem likely that the P-C_1 bond is compressed as $^1J(P,C_1)$ behaves in the normal fashion and produces expected trends for a normal bond. See the discussion of $^nJ(P,C)$ below.

Normal γ effects

As stated previously the 6-membered sub-units of the cage are held in a chair conformation (given in Structure 19) and thus there is an anti periplanar pathway (chosen on average) connecting PR_2 and the γ-carbon.

Structure 19

For a phosphorus substituent (PR_2) whose electronegativity is similar to that of a carbon substituent, the γ effect where the phosphorus substituent is predominately anti (γ anti effect) would be small. Even so, small shifts to low frequency would be expected for more electronegative substituents on the phosphorus atom[23]. Table 2.4-8 shows that the C_3 chemical shift is indeed shifted slightly to low frequency for a range of phosphorus substituents. Also those substituents on the phosphorus, which are more electronegative produce a greater shift to lower frequency. Such shifts over anti-periplanar pathways are well known in NMR spectroscopy and occur for many phosphorus and non-phosphorus compounds and are attributed to the favourable arrangement for σ-delocalisation. For example, in ^{19}F NMR anti-periplanar X-C-C-F shifts are observed with increased electronegativity of X[60].

δ effects

The ^{13}C chemical shift data for C_4 shows no particular trends for the effects of different phosphorus groups. However the overall interaction produces a shift to low frequency for most phosphorus substituents. This is unusual as δ-effects seem to be, as in the 2-norbornyl and in the 7-norbornenyl cases, deshielding ones causing a shift to high frequency.

Obviously other factors here contribute to the overall interaction.

2.4.2.2 $^{n}J(P,C)$

For the 1-adamantyl phosphorus derivatives, one-bond P-C couplings are moderate (45.8 Hz for the -PBrCl derivative) and the trends seem to be in keeping with the one-bond couplings in other phosphorus compounds. This suggests that the $P-C_1$ bond in the adamantyl derivatives can be considered normal. As expected, the magnitude seems to be largest when the phosphorus has electronegative substituents. Also as one decreases the electronegativity, the size of the $P-C_1$ coupling also decreases. This similar trend occurs in many phosphorus compounds. For example, as one moves from CH_3PCl_2 to $(CH_3)_2PCl$ to $P(CH_3)_3$, $^{1}J(P,C)$ decreases from 4.80 to -13.5 Hz respectively. This effect also seems to be true for the geminal $P-C_2$ couplings and gives the expected decrease in size as one decreases the electronegativity of the phosphorus substituents. For vicinal $P-C_3$ couplings, the magnitudes of ^{3}J are reasonably large. This result combined with the chemical shift data, as mentioned previously, would suggest that the γ-anti arrangement clearly has a distinct pathway in this chair arrangement (shown in Structure 19). However, changes in electron density alone cannot explain all couplings and hence it also seems reasonable to suggest a probable relationship with the dihedral angles. In this chair unit of the cage the P-C-C-C dihedral angles are ca. 180° and couplings of a large magnitude are to be expected. See Section 3.4 for further discussion.

δ-interaction with C_4 produces small couplings. This is probably due to the great distance away from the phosphorus position at C_1. The only coupling to note is that for the $-PPh_2$ derivative where the interaction produces a larger coupling for $^{4}J(P-C_4)$ than for $^{3}J(P-C_3)$. In this derivative the phenyl rings are not very bulky and would probably be able to freely rotate and may allow the electron pair of the phosphorus

atom to be positioned in such a way as to maximize this coupling.

2.4.2.3 ^{1}H Chemical Shifts

To analyse the hydrogen chemical shifts of the 1-adamantyl phosphorus derivatives, the hydrogen chemical shifts of adamantane itself may be used as a standard (CH = 1.87 ppm; CH_2 = 1.75 ppm). The terminology used is illustrated in Structure 20. Table 2.4-9 shows the effect of substitution on ^{1}H chemical shifts in the cage 1-adamantyl derivatives.

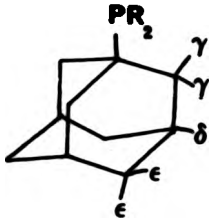

Structure 20

TABLE 2.4-9 ^{1}H Substituent Chemical Shifts for 1-substituted Adamantanes[a]

P(III) Substituent	Hydrogen Position on Cage		
	H_2 γ	H_3 δ	H_4* ε
$-PBr_2$	0.05	0.22	-0.02
$-PCl_2$	0.00	0.18	-0.06
-PClBr	0.02	0.18	-0.05
-PPhBr	-0.06	0.45	-0.54
-PPhCl	-0.03	0.48	-0.55
$-P(NEt_2)_2$	-	0.05	-
	-0.07	0.09	-0.62
	-0.12	-	-0.66
$-PPh_2$	0.30	-0.01	-0.78

- not reported

* Hydrogens on C_4 are inequivalent however no chemical shift differences are seen.

a Substituent chemical shifts in ppm, relative to adamantane. A minus sign denotes a shift to low frequency on substitution.

γ-effects

The hydrogens on C_2 are γ with respect to the phosphorus substituent on C_1 and can therefore be expected to experience a shift to lower frequency. With electronegative groups on phosphorus however, this is not so and in fact a slight shift to high frequency occurs (0.1 ppm for the $-PBr_2$ derivative). However as one decreases the electronegativity of the phosphorus substituents a shift to lower frequency does result.

δ-effects

In these rigid structures, though the data is somewhat scattered, the distant δ-positioned hydrogens on C_3 respond to the effects of substitution on C_1. The data reflects that for the C_3 hydrogens a shift to high frequency occurs for all the derivatives with respect to the CH of adamantane. This seems to suggest that a shift to high frequency occurs for a δ substituent in these bicyclic systems. This has been seen before in the 2-norbornyl phosphorus derivatives for the endo hydrogen on C_6 and the syn hydrogen on C_7 when the phosphorus is orientated in a particular direction. See Section 2.2 and 2.3 respectively. In both of these cases a special geometry has allowed this large interaction. In the 1-adamantyl phosphorus derivatives a large interaction through four bonds may result from the planar W geometry found in the bicyclic ring (shown in Structure 21 and see Section 1.4). This interaction pathway seems most effective for electronegative groups on phosphorus as greater shifts to high frequency occur for these substituents.

Structure 21.

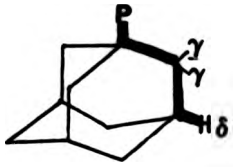

ε-effects

Little is known about five-bond interactions in which hydrogens (for example on C_4) are ε-positioned away from a phosphorus substituent. Usually these interactions are negligible or weak and the overall contribution can not be easily determined. This on the whole, applies to the 1-adamantyl derivatives although a slight overall shift to lower frequency does seem to occur for all derivatives. Also it can be seen that as the substituents on the phosphorus become less electronegative a greater shift to lower frequency occurs. These may be valid trends as in this case 1) the two best bond-interaction pathways are equivalent and 2) the cage is rigid and thereby allows effective through bond transference to these distant positions. It should be noted that although the two hydrogens on C_4 are chemically inequivalent, virtually identical chemical shifts are found for both, and it is not clear just what overall mechanism produces this average chemical shift for the two hydrogens.

2.4.2.4 $^{n}J(P,H)$

In the 1-adamantyl phosphorus derivatives the hydrogens on C_2 are γ-situated from the phosphorus group at C_1 and the interaction is through a three-bond coupling. $^{3}J(P,H)$ has been well documented for pathways in which various intermediate elements were present. In the P-C-C-H system, it appears that this coupling may be dihedral angle dependent. Here the phosphorus is related to the C_2 hydrogen through a dihedral angle ca. 60°. As can be seen in Table 2.4-7[B], the couplings are in the order of 3-6 Hertz for the P(III) derivatives. These would be expected for a Karplus dependence with a minimum at ca. 90° (see Section 3.4). It can also be seen that a decrease in the size of the coupling is associated with a decrease in the electronegativity of the substituents on the phosphorus atom. This is expected as the phosphorus hybridisation is becoming closer to p^3 and thus more s-character is concentrated in the

electron pair. It also suggests that in the 1-adamantyl derivatives, the behaviour is like that of most other phosphorus compounds.

For the hydrogen on C_3, the values of $^4J(P,H)$ although scattered, show a slight increase as one increases the bulkiness of the substituent. For example as one moves from $-PCl_2$ to $-PBr_2$ to -PPhBr the coupling increases by 0.7 Hz. As stated previously a planar geometry occurs for this interaction path, however the coupling is unexceptional.

For the hydrogens on C_4, values of $^5J(P,H)$ are small which can be attributed to the long distances between the interacting sites. However when the substituents on the phosphorus are electronegative, couplings of the same magnitude as to the C_3 hydrogen are seen. In these cases the phosphorus electron pair may be orientated to optimise the angle at 0° or 180° with respect to the C_4 hydrogen. In this case the coupling may become substantially larger.

2.5 2-adamantyl Phosphorus Derivatives

Continuing our attack on the adamantane system, the only other substituent position available on the tricyclic cage is that located on the methylene CH_2. This is shown in Structure 22[A] where the carbons are numbered correspondingly.

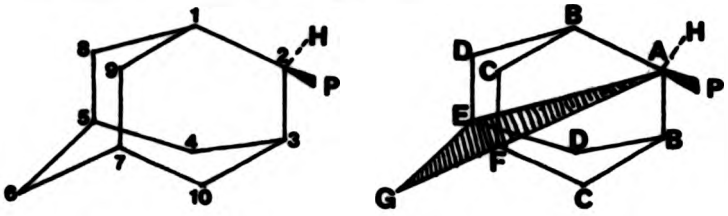

[A] [B]

Structure 22

When a hydrogen on C_2 is replaced by a substituent such as a phosphorus group, the structure still retains one plane of symmetry. This is shown in Structure 22[B]. The carbons above the plane are equivalent to the corresponding ones below the plane. The exceptions are C_2, C_5, C_6 and C_7 which lie in the plane. In Structure 23, the symmetry plane containing C_1-C_2-C_3-C_6 in adamantane itself is destroyed because the phosphorus is attached to C_2. Hence carbons C_4 and C_{10}, for example, which are both two bonds away from the phosphorus substituent will be chemically different and give different ^{13}C chemical shifts. In this thesis the phosphorus group is defined as being orientated to the side denoted by C_{10}-C_7-C_9. This therefore implies that there are two different $\underline{\gamma}$ and $\underline{\sigma}$ carbons - those carbons that are on the same side as the phosphorus are denoted as syn, namely C_{10} (γ_{syn}) and C_7 (δ_{syn}); and those which are away from the phosphorus group are denoted as anti, namely C_4 (γ_{anti}) and C_5 (δ_{anti}). Hence there are only seven different types of carbons, C_2 to C_7 and C_{10} (Structure 22[B]).

Structure 23

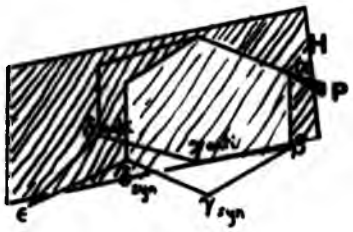

As stated previously in Section 2.4, attempted preparation of 2-adamantyl phosphorus derivatives resulted in some cases of both the 1- and the 2-adamantyl phosphorus derivatives being formed. However, when starting from 2-bromo adamantane, this problem was less serious and the ^{31}P and the ^{13}C intensities showed that the 2-adamantyl derivative predominated. This allowed straightforward distinction between the two compounds. This could be easily verified if a $^{13}C\{^{31}P,^{1}H\}$ experiment was performed and then compared with the normal $^{13}C\{^{1}H\}$ spectrum as up to seven pairs of resonances would be decoupled for the 2-adamantyl derivative.

2.5.1 ^{31}P NMR Data of the 2-adamantyl Phosphorus Derivatives

The phosphorus chemical shifts for the series are shown in Table 2.5-1. It can be seen from this table that expected chemical shifts are obtained for the different substituents and are in line with those for the 1-adamantyl phosphorus derivatives and other similar phosphorus compounds. For example, derivatives with electronegative substituents occur to high frequency (ca. 195 ppm for the -PBrCl derivative) and bulky and/or more electropositive substituents lead to resonances at lower frequency (ca. -10 ppm for the $-PPh_2$ derivative). For derivatives where the phosphorus atom is chiral (i.e. -PPhCl and the -PBrCl derivatives)

TABLE 2.5-1 ^{31}P NMR Chemical Shifts of Some 2-adamantyl Phosphorus Compounds

Substituent n =	2-adamantyl-n [a]	Preparation Number
P(III)		
$-PBr_2$	208.9	[46]
$-PCl_2$	194.6	[47]
-PBrCl	192.2	[48]
$-OPCl_2$	173.5	[49]
-PPhCl	156.8	[50]
-PPhBr	150-7	[50]
	49.7	[51]
$-PPh_2$	-9.9	[52]
P(V)		
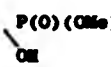	33.1	[53]
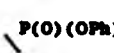	11.7	[54]

a in ppm, a minus sign denotes values to low frequency of 85% H_3PO_4 = 0.0 ppm

the carbons on adamantane which are the same bond distance away, for example C_1 and C_3, will be chemically inequivalent. This can be shown by a Newman projection for the C_1 and C_3 carbons on the 2-adamantyl substituent for a -PPhCl derivative where the axis is through the P-C_2 bond. (Given in Structure 24.) Here the environments of C_1 and C_3 will be different as the substituents on the phosphorus rotate, i.e. as ϕ_1 decreases. Hence a different ^{13}C chemical shift will be seen for C_1 and C_3. In the 2-adamantyl phosphorus derivatives the differences are

Structure 24

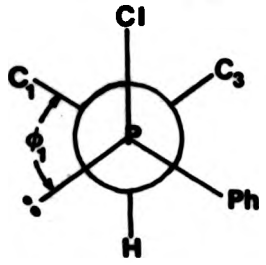

small between these two carbon resonances and are reported as a cluster in the data for C_1 and C_3. The other carbons in the cage to which this might also apply (i.e. C_8 and C_4; C_9 and C_{10}), are too distant from the phosphorus group to feel the slight differences in their local environment to cause a change in chemical shift greater than the observed digital resolution (0.8 Hz).

2.5.2 ^{13}C and ^{1}H NMR Data

The assignments for the different ^{13}C resonances in the P(III) derivatives were achieved by the following methods. The C_2 carbon (carrying the phosphorus atom) could be easily distinguished in the normal $^{13}C\{^{1}H\}$ spectrum as this carbon was associated with a large value of $^{1}J(P,C)$ and lies to high frequency of all other carbon resonances.

A 1D ^{13}C GASPE experiment was used to differentiate between the CH and the CH_2 carbons in the cage. For the CH resonances, C_3 could be distinguished from C_5 and C_7 as it is associated with both a large $^{2}J(P,C)$ and a chemical shift to higher frequency. Tentative assignments have been made for carbons C_5 and C_7 but these may need to be interchanged. C_7, which is defined above as lying syn to the phosphorus substituent, should have a slighly larger P-C coupling and a chemical shift of higher frequency than the C_5 (anti). However values of $^{4}J(P,C)$ are small and it was not often clear which P-C couplings were larger. However comparison of all data for all derivatives seems to suggest the assignment given. For the CH_2 resonances, C_{10} which lies syn to the phosphorus

substituent may be distinguished from C_4, which lies anti, by their large differences in $^2J(P,C)$ and chemical shift. Here C_{10} is associated with the larger $^2J(P,C)$ and a chemical shift of higher frequency. C_6 was distinguished clearly by the use of a 2D $^{13}C/^1H$ shift correlated experiment. The hydrogens associated with the C_6 carbon are inequivalent, being syn and anti positioned to the phosphorus substituent on C_2. This produced a typical AB quartet pattern for the ^1H slices corresponding to the CP_α and CP_β resonances in the ^{13}C spectrum. A normal 1D ^1H spectrum could not be used as the region of interest was too crowded to observe these H_6 resonances.

For the P(V) compounds, the ^{13}C chemical shifts and P-C couplings could be checked by comparison with a similar compound, 2-dimethylphosphono-2 hydroxy adamantane, assigned by Benezra et al[9]. The chemical shifts and P-C couplings are listed in Table 2.5-2. This compound was prepared again and as can be seen no major discrepancies were found.

TABLE 2.5-2 ^{13}C Chemical Shifts and P-C Couplings for 2-dimethylphosphono-2 hydroxy adamantane*

Carbon Number	δ/ppm	δ/ppm*	J(P,C) / Hz	J(P,C) / Hz*
C_2	77.2	77.3	158.4	158.4
C_3	34.2	34.0	4.4	4.4
C_4	32.0	32.2	0.8	0.7
C_5	(27.1)	(27.2)	0.2	-
C_6	38.1	38.2	1.0	-
C_7	(25.6)	(26.7)	1.3	1.5
C_{10}	34.0	33.8	11.9	11.8
OMe	53.5	53.6	-7.2	-7.2+

* Taken from ref. 9 - Not reported

\+ Taken from ref. 61 ( ) Assignment of C_5 and C_7 may be reversed

TABLE 2.5-3 ^{13}C and ^{1}H NMR Chemical Shifts of Some 2-adamantyl Phosphorus Derivatives

[A] ^{13}C/ppm [a]

Substituent	Carbon Number							
	C_2 α	C_3 β	C_4 γ	C_5 δ	C_6 ε	C_7 ϕ	C_{10} γ	Others
$-PBr_2$	58.91	31.09	39.89	28.40	38.08	29.18	33.81	
$-PCl_2$	59.45	30.86	39.49	28.06	37.96	28.76	33.64	
-PClBr	58.67	30.86	39.62	28.12	38.00	28.80	33.60	
-PClPh	47.32	31.27	41.80	27.96	36.69	28.79	33.22	Aromatics: 129-141
-PPhBr	47.86	31.18	41.82	-	36.60	29.05	33.22	
	48.31	32.67	40.35	28.26	38.89	30.20	33.46	
$-PPh_2$	45.23	30.60	38.62	22.60	32.46	29.67	30.2	Aromatics: 129-140
$P(O)(OH)(OMe)_2$	77.2	34.2	32.0	27.1	38.1	25.6	34.0	OCH_3 = 53.5
$P(O)(OH)(OPh)_2$	78.2	35.3	33.3	26.9	37.8	25.7	32.0	Aromatics: 124-129 151 ipso

[B] ^{1}H δ/ppm [a]

Substituent	Hydrogen Number							
	HC_2 β	HC_3 γ	HC_4 δ	HC_5 ε	HC_6* ϕ	HC_7 ε	HC_{10} δ	Other
$-PBr_2$	2.79	2.38	1.39	1.75	1.89	1.74	1.64	
$-PCl_2$	2.7	2.07	1.33	1.76	-	1.73	1.42	
-PClBr	2.7	2.09	1.31	1.77	-	1.74	1.38	
-PClPh	2.42	2.12	1.21	1.90	1.70	1.81	0.98	
-PPhBr	2.16	2.06	1.23	1.90	1.73	1.91	0.99	
	2.53	2.11	0.89	1.63	1.52	1.09	1.21	
$-PPh_2$	1.78	1.67	1.01	1.52	1.61	1.90	1.62	

- Not reported

* Hydrogens on C_6 are inequivalent, however no chemical shift differences are detected

a in ppm, relative to TMS < 0.0 ppm in $CDCl_3$

TABLE 2.5-4 NMR (^{31}P-E) Coupling Constants of Some 2-adamantyl Phosphorus Derivatives

[A] $^{n}J(^{31}P,^{13}C)$/Hz

Substituent	Carbon Number							
	C_2	C_3	C_4	C_5	C_6	C_7	C_{10}	Other
$-PBr_2$	54.3	11.7	4.0	0.9	4.2	1.1	10.8	
$-PCl_2$	48.1	11.9	3.4	0.8	4.0	1.3	10.8	
-PClBr	54.6	11.7	3.9	0.8	4.3	1.1	10.8	
-PClPh	43.2	15.3	3.7	-	5.3	0.8	9.8	
-PPhBr	43.3	15.2	3.6	-	5.4	0.8	9.8	
	31.3	11.6	2.7	-	1.8	0.9	9.6	$^{3}J(PSC) = 9.8$
$-PPh_2$	32.5	6.4	2.1	0.1	1.5	0.2	6.3	
	158.4	4.4	0.8	0.2	1.0	1.3	11.9	$^{2}J(POC) = -7.2$
	148.8	4.4	0.7	-	1.3	1.7	12.2	

[B] $^{n}J(^{31}P,^{1}H)$/Hz

Substituent	Hydrogen Number							
	HC_2	HC_3	HC_4	HC_5	HC_6*	HC_7	HC_{10}	Other
$-PBr_2$	5.0	3.5	0.6	1.8	0.2	0.6	2.3	
$-PCl_2$	5.8	4.6	0.4	1.0	-	-	2.2	
-PClBr	9.6	4.3	0.4	1.2	-	-	2.3	
-PClPh	4.3	4.3	0.2	-	0.2	0.8	-	
-PPhBr	4.3	4.2	0.2	-	0.2	-	-	
	6.8	4.5	0.3	0.9	0.2	0.0	2.8	
$-PPh_2$	4.2	3.2	0.3	0.8	0.0	0.0	2.6	

- Not reported

* Hydrogens on C_6 are inequivalent, however no differences are detected.

The ^{13}C and ^{1}H chemical shifts and the values of $^{n}J(P,C)$ and $^{n}J(P,H)$ are given in Tables 2.5-3 and 2.5-4. NMR analysis of both 1D and 2D techniques were employed (as previously outlined for the other data in Section 2.2) to prepare the data tables. For comparison of the effect of a phosphorus substituent on the particular carbon or hydrogen of interest, the chemical shifts in adamantane will be used again as a standard.

2.5.2.1 ^{13}C Chemical Shifts

The carbon positions may be designated with respect to the phosphorus substituent at C_2 by term effects (previously described in Section 1.4.1.2). These are shown in Structure 25 (shown in Table 2.5-5).

α-effects

P(III) Derivatives

For the 2-adamantyl phosphorus derivatives, the C_2 carbon in all cases is shifted to higher frequency with respect to the carbon of adamantane. As one increases the electronegativity of the substituents on the phosphorus atom a greater shift to high frequency occurs for this C_2 carbon. For example for the $-P\langle^{S}_{S}]$ derivative an α-carbon shift of 10.6 ppm from adamantane results and for a $-PBr_2$ derivative a shift of 21.2 ppm from adamantane occurs. In the 1-adamantyl derivatives however, such large α-carbon chemical shift differences do not occur. For example for the 1-adamantyl dibromo phosphine, the chemical shift difference from adamantane is 13.4 ppm for the α-positioned carbon. Thus this large increase (ca. 7 ppm) for the 2-adamantyl derivatives may be partially due to the remaining hydrogen on C_2 as it would be expected to be very acidic. This in turn would also increase the chemical shift

TABLE 2.8-8 ^{13}C Substituted Chemical Shifts for 2-substituted Adamantanes[a]

P(III) Substituents	Carbon Position on Cage						
	C_2 α	C_3 β	C_4 γ	C_5 δ	C_6 ε	C_7 δ	C_{10} γ
$-PBr_2$	21.21	2.59	2.19	-0.10	0.38	0.68	-3.89
$-PCl_2$	21.75	2.36	1.79	-0.44	0.28	0.26	-4.06
-PClBr	20.96	2.36	1.92	-0.38	0.30	0.30	-4.10
-PClPh	9.62	2.77	4.10	-0.52	-1.01	0.55	-4.48
	10.61	3.57	2.65	-0.24	1.19	1.70	-4.24
$-PPh_2$	7.53	2.10	0.92	-5.90	-5.24	1.17	-7.50

- Not reported

a Substituent chemical shifts in ppm, relative to adamantane. A minus sign denotes a shift to low frequency on substitution.

of this carbon. Large shifts of similar magnitude can be seen for the phosphorus derivatives of the 7-norbornenyl adduct where an acidic proton occurs. (i.e. a 27.4 ppm difference is reported for the C_7 α-carbon with $-PBr_2$ as the substituent.)

β-effects

For the β-positioned C_3 carbons a chemical shift increase of 2-3 ppm is seen for most of the derivatives. Here however the data seems to fluctuate and no trends are observed.

γ-effects

Both C_4 and C_{10} are positioned γ with respect to the phosphorus substituent at C_2. However very different chemical shift patterns are seen. For carbon C_4 no difference or only a small increase in chemical shift is observed from the similar carbon resonances of adamantane.

Whereas for the C_{10}, in all derivatives a shift to lower frequency occurs for this γ-positioned carbon. This suggests that the phosphorus substituent has a greater interaction with one side of the ring than the other and a dihedral angular dependence occurs. See Section 3.3.

Long range effects

Carbons C_5, C_7 and C_6, because of their great distance away from the phosphorus substituent at C_2, show in the most part only slight variations from the chemical shift of adamantane. Of these C_5 shows the greatest overall trend which is to give a slight decrease in chemical shift from that of adamantane. This seems to be found for all of the different substituents.

P(V) Derivatives

From the limited amount of data available no overall trends can be postulated. However it is possible to observe the differences in the two γ-position substituents. Benezra[8] has proposed that this effect is due to a dihedral angular dependence whereby the C_4 has an angle ca. 60° and the C_{10} carbon has an angle of 180° with respect to the lone pair of the phosphorus atom. This large 180° angle causes a shift to low frequency of ca. 6 ppm with respect to adamantane for the C_{10} carbon. This has been noted for the compounds where the carbon is gauche to the C_2-OH function. In each of the present derivatives this similar effect is found. For C_6 little chemical shift difference from that of adamantane is observed.

2.5.2.2 $^n J(P,C)$

P(III) Derivatives

Similar to the 1-adamantyl derivatives, large one-bond couplings are observed for the 2-adamantyl phosphorus substituents. In the cases

where the substituents on the phosphorus are electronegative the largest couplings occur, (i.e. for $-PCl_2$, -PClBr, and PCl_2 they are about 82.0 Hz). As the substituents on the phosphorus atom decrease in electronegativity, smaller values of $^1J(P,C)$ are observed. However some variance is noticed within these one bond coupling data and this may be due to particular effects of the substituent in question.

For the γ-positioned carbon C_3, geminal couplings range from 6-15 Hz for the different derivatives. However it is not possible to see any underlying trends as to the mechanism for these $^2J(P,C)$ in the available data.

The values of $^3J(P,C)$ are discussed in greater detail in Section 3.2 for the two different sites C_4 and C_{10}. However it is interesting to note that, as shown in the ^{13}C chemical shift data for these derivatives, larger interactions are observed for the P-C_{10}(syn) coupling than the P-C_4 (anti) coupling, (by a factor of ca.2). This again suggests that phosphorus interaction is greater on one side of the cage than the other and the differences in dihedral angle are important. Here the dihedral angle between P and C_{10} is ca. 180° and the angle between P and C_4 is ca. 60°. For both C_4 and C_{10} the magnitudes of the P-C couplings decrease as the electronegativity of the substituent on the phosphorus atom decreases in a fairly consistent way.

$^4J(PC)$ is associated with C_5 and C_7. In the case of C_5, the values of $^4J(P,C)$ are almost negligible for all substituent groups. This is not surprising as the distance away from the phosphorus group at C_2 is large. However C_7 which lies syn to the phosphorus shows couplings to be slightly larger than for the C_5. As C_7 is on the same side as C_{10} it is reasonable to assume that the larger couplings should be both on the same side of the cage. On this basis, assignments were made between the two carbons.

The value of $^5J(P,C)$ associated with C_6 is unusually large and has amost the same magnitude as the three-bond coupling noted for C_4. Also this large coupling magnitude for the P-C coupling at C_6 is observed only for P(III) derivatives. This therefore seems to rule out any special path geometry arguments and suggests that perhaps the electron pair of the phosphorus may make an important contribution. This may be likened to long range $^nJ(H,H)$ where groups which are orientated at 0° or 180° produce larger couplings.

P(V) Derivatives

$^1J(P,C)$ in the hydroxy phosphonates is considerably larger than for the simpler phosphates. This is verified in Table 2.5-2 from Benezra's data[9] and also noted by Gray[62]. The two-bond coupling for the P(V) derivatives also seem to fall in place with that of Benezra. This is given in Table 2.5-2 for exo-2-dimethyl phosphono norbornane and for 2-dimethulphosphono-2-hydroxy adamantane. For the P-O-Me coupling McFarlane[61] has determined the sign to be negative in similar $PhP(O)(OMe)_2$ compounds. $^3J(P,C)$ of the P(V) derivatives show large dihedral dependence and this is discussed in Section 3.4.

2.5.2.3 ^1H Chemical Shifts

Here again, as in the 1-adamantyl derivatives, the ^1H chemical shifts of adamantane are used as a reference to interpret the effects of phosphorus substituents at C_2 for the different positioned hydrogens in the cage. The chemical shifts of adamantane and the different hydrogen positions of the 2-substituted adamantane phosphorus derivates are shown in Structure 25.

Structure 25

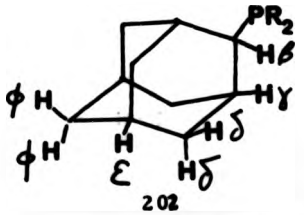

Table 2.8-6 shows the ^1H substituent chemical shifts for 2-substituted adamantyl derivatives.

TABLE 2.8-6 Substitutent ^1H Chemical Shifts for 2-substituted Adamantyl Derivatives

P(III) Substituents	Hydrogen Position on Cage						
	HC_2 β	HC_3 γ	HC_4 δ	HC_5 ε	HC_6* φ	HC_7 ε	HC_{10} δ
$-PBr_2$	1.04	0.51	-0.36	-0.12	-0.16	-0.13	-0.11
$-PCl_2$	0.95	0.20	-0.42	-0.11	-	-0.14	-0.33
-PClBr	0.95	0.22	-0.44	-0.10	-	-0.13	-0.37
-PClPh	0.67	0.25	-0.54	0.03	-0.05	-0.06	-0.77
-PPhBr	0.41	0.19	-0.52	0.03	-0.02	0.04	-0.76
	0.78	0.24	-0.86	-0.24	-0.23	-0.78	-0.84
$-PPh_2$	0.03	-0.20	-0.74	-0.35	-0.14	0.03	-0.13

- Not reported
* Hydrogens on C_6 are inequivalent, however no chemical shift differences are detected.
a Substituent chemical shifts in ppm, relative to adamantane. A minis sign denotes a shift to low frequency on substitution.

β-effects

When one of the hydrogens at C_2 is replaced by a phosphorus substituent, the other β-positioned hydrogen, as shown in Table 2.8-3, shifts to high frequency. This β-effect is seen for all of the phosphorus derivatives and can result in an increase as large as ca. 1.0 ppm for the derivatives with electronegative substituents. A slight decrease in the magnitude of the difference is observed as the substituents on the phosphorus atom decrease in electronegativity though slight variations occur throughout the data for the particular substituents.

γ-effects

For the γ-hydrogen at C_3, an increase in frequency in the chemical shift occurs. This is especially true for the electronegative substituents. As one decreases the electronegativity of the substituents a smaller increase occurs.

Long range effects

C_4 and C_{10} hydrogens are both shifted slightly to lower frequency with respect to adamantane. This suggests that the δ effect acts as a shielding one where the C_{10} hydrogen is less affected than the C_4 hydrogen. Hydrogens on C_8, C_7 and C_6, being very distant from the phosphorus substituent, show little change in the chemical shifts relative to that in adamantane and thus little information with respect to conformation purposes may be had from these particular hydrogens.

2.5.2.4 $^nJ(P,H)$

P-H coupling for the 2-adamantyl phosphorus derivatives show on the whole no observable trends with respect to the substituents of different phosphorus groups. The size of the coupling for a particular hydrogen seems to depend more on the substituent group involved. However, it does seem possible to verify assignment by the differences in magnitude for the compound concerned. For example, C_4 hydrogens show small $^4J(P,H)$ (0.2 to 0.6 Hz) for each of the structures whereas the C_{10} hydrogens, which are also δ-positioned, show much larger values of $^4J(P,H)$ (2.0 to 3.0 Hz). This suggests that interaction with the phosphorus substituent is greater on the C_{10} side of the ring. This is in agreement with the assignments formed by arguments from the ^{13}C analyses. For the C_3 hydrogens, again the $^3J(P,H)$ shows no particular trends but rather varies in size depending on the slight differences for a substituent group. However large couplings (3.0 to 4.5 Hz) are

found which may result from the effects of a dihedral angle. This is discussed in Section 3.3.

References - Chapter 2

1. D.W. White, J.G. Verkade J. Magn. Reson. 3, 111 (1970).
2. G.W. Buchanan, J.H. Bowen Can. J. Chem. 55, 604 (1977).
3. C. Benezra J. Amer. Chem. Soc. 95, 6890 (1973).
4. a) T. Ishihara, T. Ando, T. Muranaka, K. Saito J. Org. Chem. 42, 666 (1977).
   b) S. Winstein, J. Sonnenberg J. Amer. Chem. Soc. 83, 3235 (1961).
5. C.J. Turner Prog. in NMR Specros. 16, 311 (1984).
6. A. Bax Two-Dimensional Nuclear Magnetic Resonance in Liquids Delft University Press, Delft Holland, 50-65 (1982).
7. A. Bax J. Magn. Reson. 53, 149 (1983).
8. a) P.T. Narasimhan, M.T. Rogers J. Chem. Phys. 34, 1049 (1961).
   b) D.G. Gorenstein Prog. in NMR Spectros 16, 1 (1983).
9. G.W. Buchanan, C. Benezra Can J. Chem. 54, 231 (1976).
10. L.D. Quin, M.J. Gallagher, G.T. Cunkle, D.B. Chesnut J. Amer. Chem. Soc. 102, 3136 (1980).
11. C. Benezra Tetrahedron Letters 51, 4471 (1969).
12. J. Thiem, B. Meyer Org. Magn. Reson 11, 50 (1978).
13. H.J. Callot, C. Benezra Can. J. Chem. 50, 1078 (1972).
14. L.D. Quin, M.D. Gordon, S.O. Lee Org. Magn. Reson. 6, 503 (1974).
15. M.G. Newton, N.S. Pantaleo, S. Kirbawy, N.L. Allinger J. Amer. Chem. Soc. 100, 2176 (1978).
16. P. Haake, J.P. McNeal, E.J. Goldsmith ibid. 90, 715 (1968).
17. E. Lippmaa, T. Pehk Kem. Teollisuus 24, 1001 (1967).
18. E. Lippmaa, T. Pehk Eesti NSV Tead. Akad. Toim Kem. Geol. 17, 210 (1968).
19. W.J. Horsley, H. Sternlicht, J. Cohen J. Amer. Chem. Soc. 92, 680 (1970).

20. B.V. Cheney, D.M. Grant ibid. 89, 5319 (1967).

21. D.K. Dalling, D.M. Grant ibid. 89, 6612 (1967).

22. D.E. Dorman, S.J. Angyal, J.D. Roberts ibid. 92, 1351 (1970).

23. J.B. Grutzner, M. Jautelat, J.B. Dence, R.A. Smith, J.D. Roberts ibid. 92, 7107 (1970).

24. a) K.D. Summerhays, G.E. Maciel ibid. 94, 8368 (1972).

b) M. Christl Chem. Ber. 108, 2781 (1975).

25. M. Cohen, C. Beneerra Org. Magn. Reson. 5, 205 (1973).

26. A.A. Bothner-By, R.M. Cox J. Phys. Chem. 73, 1830 (1969).

27. M. Barfield J. Amer. Chem. Soc. 102, 1 (1980).

28. L.D. Quin, L.B. Littlefield J. Org. Chem. 43, 3508 (1978).

29. L.D. Quin, L.B. Littlefield Org. Magn. Reson. 12, 199 (1979).

30. G.S. Poindexter, P.J. Kropp J. Org. Chem. 41, 1215 (1976).

31. E. Lippmaa, T. Pehk, J. Paasivirta, N. Belikova, A. Plate Org. Magn. Reson. 2, 581 (1970).

32. T.D. Alger, D.M. Grant, E.G. Paul J. Amer. Chem. Soc. 88, 5397 (1966).

33. D.M. Grant, B.V. Cheney ibid. 89, 5315 (1967).

34. B.V. Cheney, D.M. Grant ibid. 89, 5319 (1967).

35. D.K. Dalling, D.M. Grant ibid. 89, 6612 (1967).

36. B.V. Cheney ibid. 90, 5386 (1968).

37. T.P. Forrest, J.G. Webb Org. Magn. Reson. 12, 371 (1979).

38. H-J. Schneider, W. Gschwinder, E.F. Weigand J. Amer. Chem. Soc. 101, 7196 (1979).

39. J.B. Stothers, C.T. Tan, K.C. Teo Can. J. Chem. 51, 2893 (1973).

40. P. Brun, J. Casanova, J. Hatem, Org. Magn. Reson. 12, 537 (1979).

41. K. Tori, T. Tsushima Org. Magn. Reson. 6, 334 (1974).

42. D.G. Gorenstein J. Amer. Chem. Soc. 99, 2264 (1977).

43. E.L. Eliel, W.F. Bailey, L.D. Kopp, R.L. Willer, D.M. Grant, R. Bertrand, K.A. Christensen, D.K. Dalling, M.W. Duch, E. Wenkert, F.M. Schell, D.W. Cochran ibid. 97, 3322 (1975).

44. W. Kitching, M. Marriott, W. Adcock, D. Doddrell J. Org. Chem. 41, 1671 (1976).

45. W.A. Ayer, L.M. Browne, S. Fung, J.B. Stothers Can. J. Chem. 54, 3272 (1976).

46. G.C. Levy Ed. Topics in Carbon-13 NMR Spectros. 3, Chapter 3 (1979).

47. R.R. Fraser Can. J. Chem. 40, 78 (1962).

48. J. Paasivirta Suom Kem. 38B, 130 (1965).

49. K. Tori, Y. Hata, R. Muneyuki, Y. Tamkano, T. Tsuji, H. Tanida Can. J. Chem. 42, 926 (1964).

50. G.H. Wahl Jr., R.L. Greene, J. Bordner J. Chem. Soc. Chem. Commun. 927 (1973).

51. D. Chadwick, A.C. Legon, D.J. Millen J. Chem. Soc. Faraday Trans. 2, 2064 (1972).

52. N.L. Allinger, M.T. Tribble, M.A. Miller, D.H. Wahtz J. Amer. Chem. Soc. 93, 1637 (1972).

53. E.M. Engler, J.D. Andose, P.v.R. Schleyer ibid. 95, 8005 (1973).

54. M. Duddeck, M.R. Isalm Org. Magn. Recon. 16, 32 (1981).

55. J-M. Griffiths, M.L. Owen, J. Sheridan J. Chem. Soc. Faraday Trans. 2, 1359 (1972).

56. a) G.A. Olah, J.G. Shih, V.V. Krishnamurthy, B.P. Singh J. Amer. Chem. Soc. 106, 4492 (1984).

b) G.A. Olah, B.P. Singh, B.G.B. Gupta Synthesis, 713 (1983).

57. R.J. Cheolyn, R.M. Ellan, N. Akhtar Phosphorus and Sulphur 7, 257 (1979).

58. G. Mavel Annal. Reports on NMR Spectros. 5B, 1 (1973).

59. R.C. Fort Jr. Adamantane Marcel Dekker, New York, 27, (1976).

60. L. Phillips, V. Wrag J. Chem. Soc. Perkin Trans. 2, 223 (1972).

61. W. McFarlane Proc. R. Soc. London Ser A, 306, 185 (1968).

62. G.A. Gray J. Amer. Chem. Soc. 93, 2132 (1971).

CHAPTER 3

[1] THE EFFECT OF DIHEDRAL ANGLES ON COUPLING CONSTANTS

3.1 Introduction

Vicinal proton-proton couplings $^3J(H,H)$ have been extensively utilised in conformational analysis. However, the calculation of $^3J(H,H)$ is much more complicated than of one-bond or geminal coupling constants since four atoms, three distances, two internal angles, and a dihedral angle are required to describe the saturated system. Vicinal proton-proton coupling constants in saturated systems range between -0.3 Hz to +14 Hz and may depend on all of the above parameters. Obviously there is difficulty in separating the effects of the individual components in order to understand these trends in the coupling variations even on a qualitative basis. However, one of the more fruitful theoretical contributions to the interpretation of coupling constants has been the valence bond treatment by Karplus[1,2] of $^3J(H,H)$ in ethane-like fragments $H_\alpha - C_\alpha - C_\beta - H_\beta$. The most useful conclusion to come out of this study is that this coupling depends dramatically on the dihedral angle ϕ between the $H_\alpha - C_\alpha$ and the $C_\beta - H_\beta$ bonds. The results[3] give a relationship of the form:

$$^3J(H,H) = A + B\cos\phi + C\cos^2\phi \qquad [3.1]$$

ϕ is defined in the Newman projection in Fig. 3.1-1 and typical values of the constants were proposed to be A = 4, B = -0.5 and C = 4.5 Hz.

Fig. 3.1-1

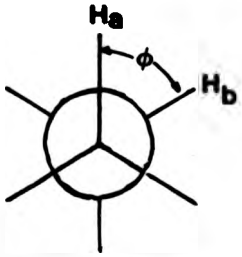

From empirical studies of Bothner-By[4] and others[5], a better set of parameters[4] (A = 7, B = -1 and C = 5 Hz) were obtained. A typical plot of $^3J(H,H)$ against dihedral angle is shown in Fig. 3.1-2.

Fig. 3.1-2 $^3J(H,H)$ Coupling Constants as a Function of Dihedral Angle

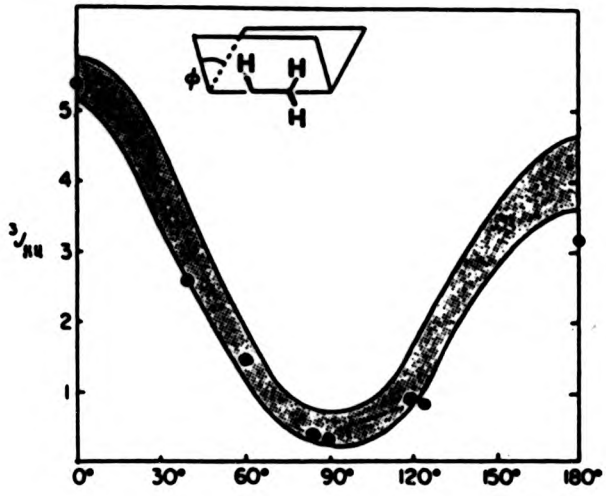

From Fig. 3.1-2 we can see that large values of J are predicted for the cis (0°) and trans (180°) conformations, but small values for the gauche conformation around 60° - 120°. Abraham et al[6] and others have indicated that vicinal coupling constants between a hydrogen and an element of the first or second row, e.g. $^3J(H,C)$, $^3J(H,H)$, $^3J(H,F)$ depend on the H_α-C -C-X_β dihedral angle in a similar relationship to that proposed by Karplus for $^3J(H,H)$. This has been further extended to encompass other $^3J(H,X)$, $^3J(C,C)$ and $^3J(X,Y)$ coupling constants (where X,Y = ^{31}P, ^{199}Hg, ^{119}Sn) - the interest being to explore the factors affecting the magnitude of ^3J.[7-10] However in many cases the correlations have been derived from considerations of rather few

different values of the dihedral angle. Empirical modifications of the Karplus curve to take substituent effects into account by modifying the constants A, B and C have been undertaken and have met with some success with an error margin of a few degrees for a null of 90°[11]. This means of course, one has to be cautious in applying Karplus-like curves to classes of compounds where relationships have not been established.

3.2 Methods of Calculation

Several methods to locate the points corresponding to the (coupling constant/angle) Karplus-like curve may be employed: (1) the rotamer populations corresponding to the observed points may be measured by an independent method such as in a dipole-moment measurement; (2) the populations may also be measured by theoretical treatments of the solvent or temperature dependence of the coupling constants and finally (3) knowledge of values of $^{3}J(X,Y)$ derived from the large number of recorded observations on analogous internally rotating or rigid systems may be used to choose appropriate values of $^{3}J(X,Y)'$, $^{3}J(X,Y)''$, $^{3}J(X,Y)'''$, etc ... to fix the points directly. In this thesis an Apple computer graphics program (Chemdata)[12] was used to estimate the bond and torsion angles from known imputed parent crystal structure data where the X-ray analysis included unit cell coordinates (see Table 3.2-1). These were optimized for the various phosphorus derivatives so that reasonable dihedral angles could be determined in these new structures. Only approximate values may be obtained, even from crystal structure data, as conformation in solution could be different. The $^{3}J(P,X)$ coupling constants from many prepared similar derivatives (2-norbornyl, 7-norbornyl, 1- and 2-adamantyl) as in method (3), were plotted *via* a computer

fit program through the Karplus relation given in Equation [3.1]. A three-parameter iteration was performed on the phosphorus data to give a best fit to the Karplus equation and allowing estimates of constants A, B and C and the standard deviation limit (which measures the closeness of fit of the data to the Karplus model). In addition, one may extract the values of at extreme values ($\phi = 0°$ and $\phi = 180°$) predicted from the fitting program and in the minimal region, the point ϕ_{min} . ϕ_{min} is given as:

$$\cos \phi_{min} = \frac{-B}{4C} \qquad [3.2]$$

Table 3.2-1 X-ray Structures used for First Estimations for Determining Dihedral Angles

Derivative	Parent Structure X-ray Analysis	Reference
2-norbornyl	exo-N-(2norbornyl)benzamide	13
7-norbornenyl	anti 7-norbornenyl p-bromobenzoate	14
1-adamantyl	1-cyanoadamantane	15
2-adamantyl	2-ethynyl-2-adamantanol	16

3.3 The Influence of Conformational and Substituent Effects on $^3J(P,X)$

General: Because of their well-defined molecular geometry, rigid bicyclic systems (e.g. norbornanes) have been extensively utilized for demonstrating the occurrence (or not) of dihedral angular dependences of vicinal couplings. In this section, we will consider briefly some of the conformational (geometric) and substituent (electronic and steric) effects of $^3J(P,C)$ and $^3J(P,H)$ values that have been studied specifically in these systems.

3.3.1 $^{3}J(P,C)$

$^{3}J(P,C)$ couplings have been measured in a range of bicyclic species including phosphines[17], phosphates[8], phosphine oxides[18], phosphine sulfides[17,19] and phosphonium salts[17]. Again some evidence has suggested possible conformational dependence of $^{3}J(P,C)$ which may also be related to the hybridization state of the phosphorus atom. Quin et al[17] has established a dihedral angle dependence for $^{3}J(P,C)$ in syn and anti 7-norbornenyl phosphine sulfides and phosphonium salts. Thiem and Meyer[20] applied a Karplus-like relationship to vicinal couplings. $^{3}J(P,C,C,C)$ in phosphonates which gave the usual minimum at $\phi = 90°$ ($J \approx 0$ Hz) and maximum for J at $\phi = 0°, 180°$ (Structure 26).

Structure 26

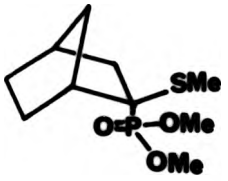

A fitting calculation gave the equation $^{3}J(P,C) = 7.35 - 1.76\cos\phi + 7.86\cos^{2}\phi$.

In the case of P(III) compounds Karplus-like curves either failed[17] to show this type of relationship or had a curve with a minimum quite different from the usual 90° position. PCl_2 and PMe_2 derivatives of norbornane are reported as appearing not to have such a minimum. This may result possibly from the fact that $^{3}J(P,C)$ can have negative values[21]. Other stereochemical effects such as orientations of the electron pair[22] and proximity of the electron pair[23] (whether the electron pair is in an eclipsed or staggered arrangement with respect to the nearest carbon) seem to play an important role and this in turn affects the estimate of the dihedral angles and the coupling ^{3}J. Lack of data in the case of P(III) compounds has not allowed crystallization of thought in this area.

3.3.1.1 Interpretation of $^{3}J(P,C)$ data in terms of dependence on Dihedral angles

As previously stated (Section 3.2, Table 3.2-1) dihedral angle estimations were determined from known crystal structure data for the various P(III) compounds. The various dihedral angles obtained and used with the experimentally calculated $^{3}J(P,C)$ from $^{13}C\{^{1}H\}$ NMR data are summarised in Table 3.3-1. The different values for the dihedral angles were obtained in the following way. The relevant dihedral angles in the 2-norbornyl structure are: $^{3}J(P,C_{7})$/ 81.3°; $^{3}J(P,C_{4})$/ 116.8°; $^{3}J(P,C_{6})$/172° for the exo derivatives and $^{3}J(P,C_{6})$/44.2°; $^{3}J(P,C_{4})$/116° and $^{3}J(P,C_{7})$/150.6° for the endo derivatives. The relevant dihedral angles in the 7-norbornenyl structure are $^{3}J(P,C_{2})$/57° and $^{3}J(P,C_{5})$/164°. The 1-adamantyl structure gave the associated dihedral angle $^{3}J(P,C_{3})$/178.2° and the 2-adamantyl structure determination gave the associated dihedral angles $^{3}J(P,C_{10})$/57.1°, and $^{3}J(P,C_{4})$/177.2°.

Table 3.3-1 $^{3}J(P,C)$ couplings with associated dihedral angles for some P(III) derivatives

Angle (ϕ^0)	Derivatives (Hz)										
	PBr_2	PCl_2	PClBr	PPhCl	$P(NEt_2)_2$	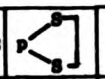	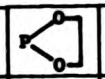	PPh_2	$P(OMe)_2$	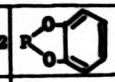	PMe_2
44.2	27.34	27.16	27.09	-	27.93	25.06	24.13	23.44	24.10	27.06	22.7
57.0	12.63	10.02	12.81	-	8.63	9.02	8.96	8.05	-	-	10.0
57.1	10.80	10.80	10.82	9.82	-	9.61	-	6.3	-	-	-
81.3	2.93	4.73	8.79	-	3.67	18.32	19.23	1.02	4.76	16.00	1.83
116.0	4.29	3.33	3.94	-	1.95	6.60	6.40	0.85	(1.5)	6.28	-
116.5	2.74	1.36	3.75	-	1.56	4.76	4.62	1.18	(2.5)	3.98	4.4
150.6	1.56	3.12	4.64	-	2.54	20.89	20.80	1.43	5.50	20.32	3.61
164.0	6.84	6.68	6.93	-	4.46	6.68	6.64	6.04	-	-	7.03
172.1	9.03	7.71	7.30	-	7.82	7.69	8.05	2.63	7.40	8.26	6.64
177.2	4.01	3.40	3.93	3.65	-	2.73	-	2.1	-	-	-
178.2	8.70	8.13	8.83	8.75	6.32	-	4.83	-	-	2.93	-

( ) estimated ___ data points not used in $^{3}J_{PC}$ plots.

Table 3.3-2 Comparison of the Parameters (Hz) for the Karplus equation: $^{3}J(P,C) = A + B\cos\theta + C\cos^{2}\theta$ when $^{3}J_{PC}$ for 116.0° and 116.5° is positive and then negative in sign.

P(III) derivative	ϕ_{min} (deg)	A		B		C	
		Hz	St.Dev.[a]	Hz	St.Dev.[a]	Hz	Std.Dev.[a]
 [A]	119°	10.9	2.10	9.4	3.70	4.9	3.83
 [B]	107°	8.9	1.41	16.2	2.49	13.9	2.58

a = Standard deviation value ($X10^{-2}$)
[A] = ^{3}J is assumed positive for all values
[B] = ^{3}J is assumed negative for 116.0° and 116.5° and positive for rest.

Quin et al[17] has alluded to the possibility of some $^{3}J(P,C)$ couplings being negative in the 2-norbornyl cages. In particular the couplings in Tables 3.3-1 linked with the 116.0° dihedral angle (which is associated with the coupling P_{endo} to C_4) and the 116.5° dihedral angle (which is associated with the coupling, P_{exo} to C_4) seem to lend themselves to a better Karplus fit curve if their couplings are considered to be negative. Unfortunately proper sign determination could not be performed on the prepared derivatives. However a typical comparison can be seen (in Fig. 3.3-1) by examining the different plots and the values in Table 3.3-2 for the dithiol phospholane derivatives. In Fig. 3.3-1[A] the values of ^{3}J are all plotted as positive and in [B] the values corresponding to 116.0° and 116.5° are plotted negative and the rest of ^{3}J are plotted as positive. Clearly a better fit is demonstrated in [B] which includes the two negative ^{3}J values.

Also the ϕ_{min} value is much closer to 90° which should be expected for a dihedral angle control of $^{3}J(P,C)$. Though very few negative

Fig. 3. 3-1 $^{3}J_{P,C}$ Plots of the dithiolphospholane derivatives (Hz) as a function of the dihedral angle ϕ (deg) where:

[A] all values of J are plotted as positive
[B] all values of J are plotted as positive with J values with ca. 116° angles plotted negative

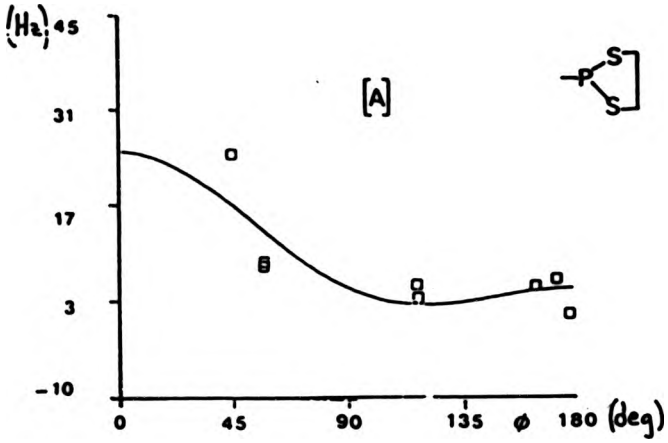

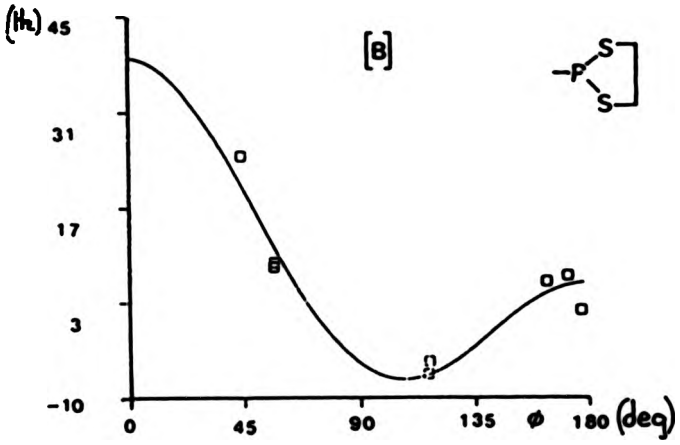

$^3J_{(P,C)}$ couplings have been cited in the literature, the negative values for the $^3J(P,C_4)$ in the 2-norbornyl derivatives seem to be a consistent trend for all of the relationships studied here. Hence the rest of the $^3J_{\underline{PC}}$ plots for the other P(III) derivatives are consistent with the angles 116° and 116.5° being associated with negative values of this coupling. (See Fig. 3.3-2[A] to [I]).

Table 3.3-3 Values of Best Iterations for the Parameters (Hz) in the Karplus Equation $^3J = A + B\cos\theta + C\cos^2\theta$ for evaluation of $^3J(P,C)$.

P(III)	A		B		C		ϕ_{min}
derivative	Hz	Std.dev.[a]	Hz	Std.dev.[a]	Hz	Std.Dev.[a]	(deg)
PBr_2	11.0	1.04	16.6	1.92	12.9	1.78	109
PBrCl	11.6	1.29	15.8	2.39	11.4	2.21	110
PCl_2	10.9	1.31	14.4	2.41	10.6	2.24	110
$P(OMe)_2$	12.6	0.59	15.9	0.94	11.5	0.81	110
$P(NEt_2)_2$	11.3	1.56	16.0	2.69	11.6	2.39	110
	8.9	1.41	16.2	2.49	13.9	2.58	107
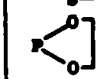	9.4	1.38	16.1	2.20	14.0	2.21	107
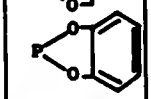	15.2	3.93	18.9	3.42	8.3	5.09	124
PPh_2	7.7	1.48	13.9	2.55	10.5	2.43	109
PMe_2	10.0	0.92	14.8	1.67	12.5	1.64	107
Mean average:	10.9		15.8		11.7		

a Standard deviation value is $(X10^{-2})$

In Table 3.3-3 parameters for A, B and C in the Karplus equation: $^3J_{(P,C)} = A + B\cos\theta + C\cos^2\phi$ are tabulated for each of the plots. Also

the ϕ_{min} value for each plot is included. It can be seen that for $^3J(P,C)$, deviations in comparing the values of A, B and C for all derivatives are moderate and the values of ϕ_{min} are constant. This may be expected as the carbons are held in a rigid structure and hence little distortion in the parameters or ϕ_{min} should be seen. As shown in Table 3.3-4 a minimum dihedral angle algebraic value of ca.110° is found for the P(III) class of compounds which is a new result. In this case when the ϕ_{min} value is larger than 90° (if B/4C is negative and of an absolute value less than one) then the Karplus function predicts that J(0°) > J(180°). This is shown for all plots. This implies that groups orientated cis with respect to the phosphorus will give larger coupling magnitudes than those which align themselves in a trans position (i.e. $^3J(P,C)_{cis} > {}^3J(P,C)_{trans}$ in the 2-norbornyl phosphorus derivatives.

The data underlined in red in Table 3.3-1 have not been used in the calculation of the $^3J_{PC}$ plots as they were so out of line with the rest. This implies that other additional factors including stereochemical effects (as discussed in Chapter 2) are present. Quin[17] and others[24] have shown that dihedral relationships may be different within the phosphorus class and depend greatly upon the coordination of the phosphorus atom. For P(III) derivatives electron pair orientation (see Chapter 2) is also important. Hence the chemical picture is a non-trivial one. Clearly more work is needed to clarify these initial findings.

Fig. 3. 3-2 [A] to [I] Karplus Plots for various P(III) groups as a function of the dihedral angle (deg)--- $^{3}J_{P,C}$

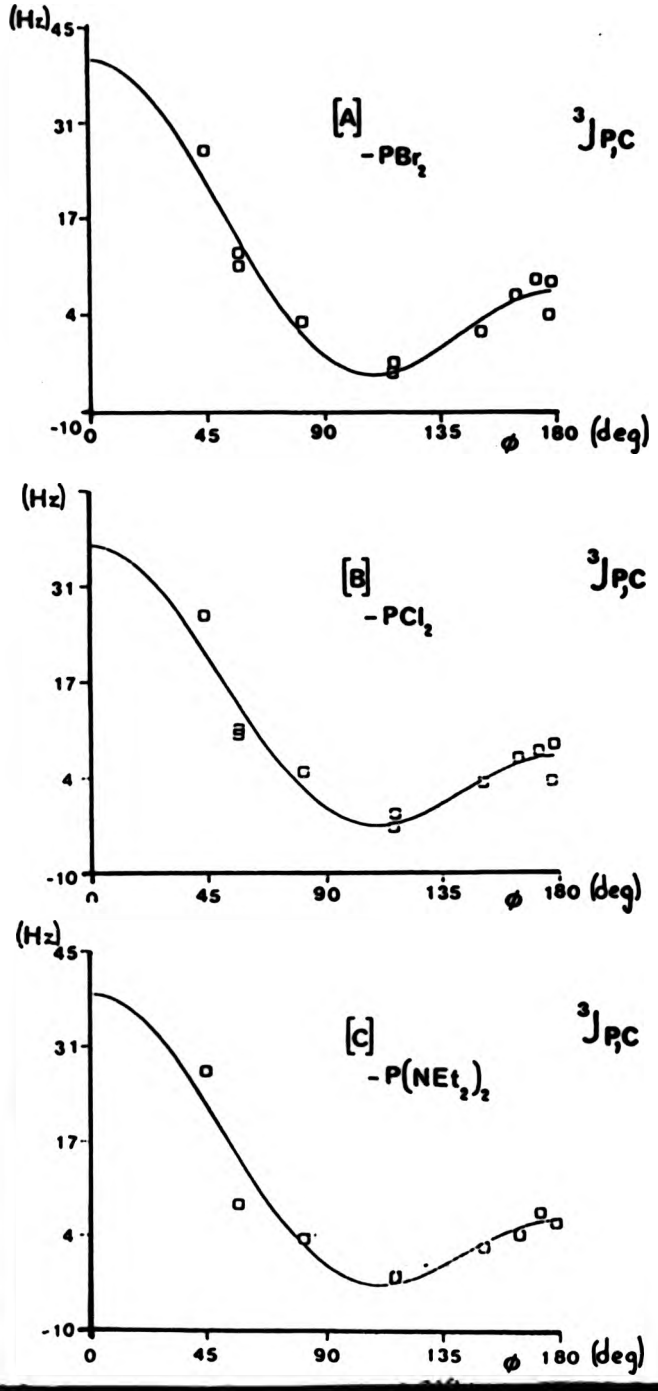

Fig. 3.2-2 cont'd.

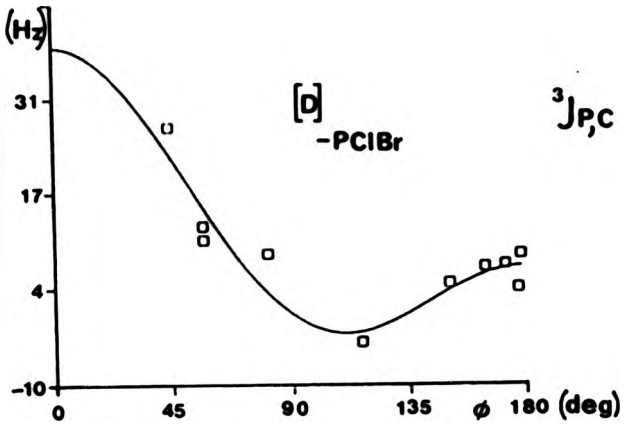

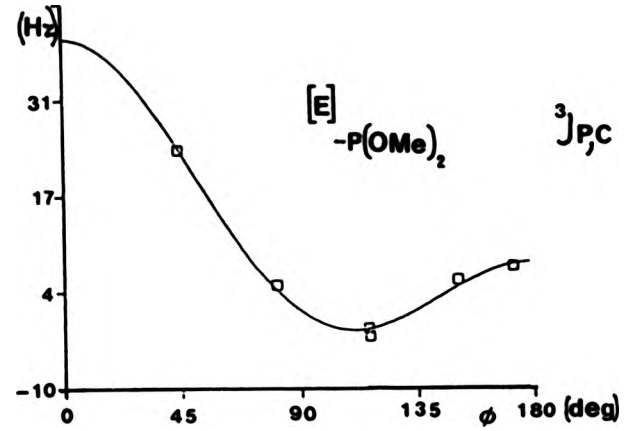

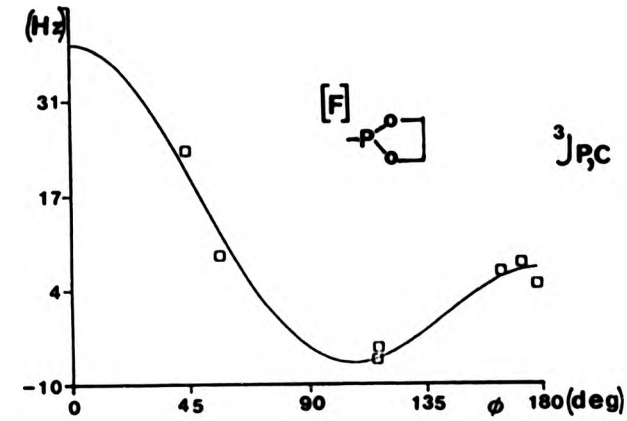

Fig. 3.2-2 cont'd.

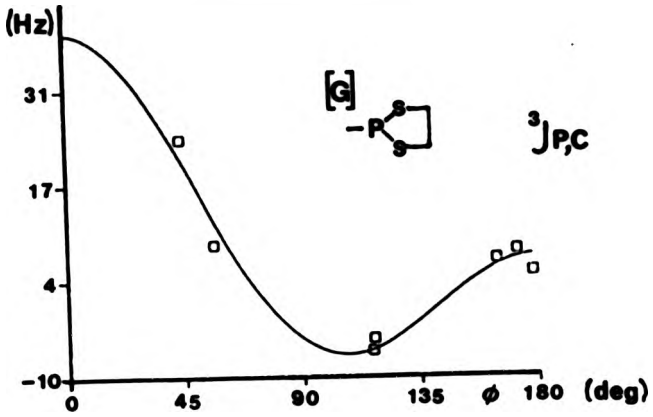

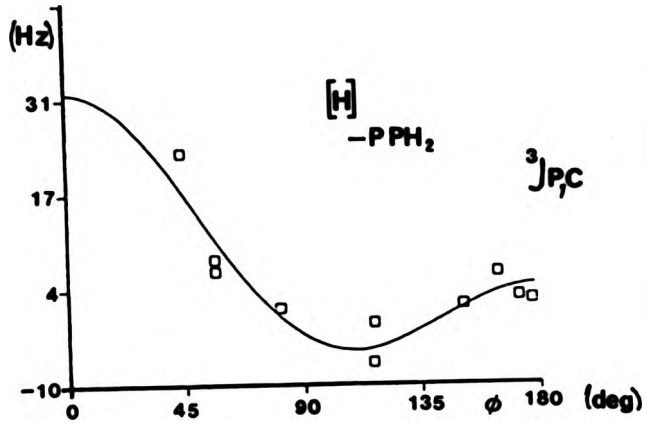

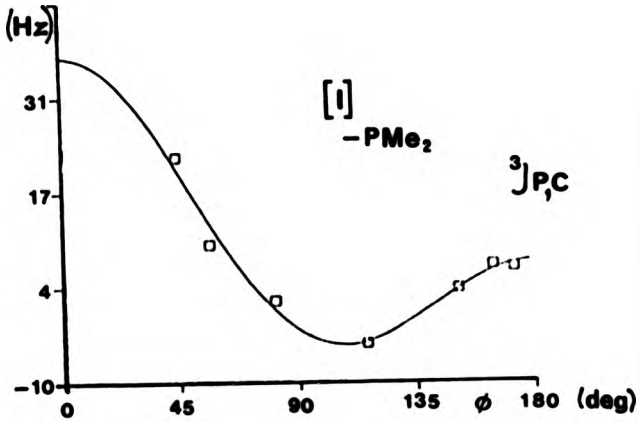

Table 3.3-4 Maximum and Minimum Values for Some P(III) Derivatives for $^3J_{PC}$ plots[a]

P(III) Derivatives	ϕ_{min} deg	Hz	$\phi = 0°$ (Hz)	$\phi = 180°$ (Hz)
PBr_2	109°	-4.66	40.4	6.4
PCl_2	110	-3.10	37.1	6.7
PClBr	110	-2.59	38.8	5.8
$P(OMe)_2$	110	-1.72	39.9	7.7
$P(NEt_2)_2$	110	-3.10	38.8	6.8
	107	-7.07	39.0	6.8
	107	-6.90	39.4	7.2
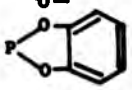	124	-5.52	46.0	5.0
PPh_2	109	-3.45	32.3	3.7
PMe_2	107	-4.48	37.1	8.6

a Values calculated from a three parameter fit iteration

3.3.2 $^2J(P,C)$

For P(III) derivatives dihedral angles may affect not only three bond couplings but also two bond couplings. It is known from several studies of both heterocyclic[25,26] and acyclic[27,28] phosphines the $^2J(P,C)$ is controlled by the dihedral angle relating the lone-pair orbital on the phosphorus atom to the β-carbons, where a small angle is associated with large coupling. Here the unbound electron pair of the phosphorus atom defines another bond direction. This is shown in Structure 27 where the dihedral angle is shown in red.

Structure 27

For cases such as these, this γ-contribution will be greater than the expected β-effect and as well as coupling constants being affected the chemical shifts of C_2 may well be shifted to lower frequency. The analysis of the chemical shift and coupling constant data for the derivatives of endo 2-norbornyl derivatives (Section 2.3) and for the 1-adamantyl derivatives (Section 2.4) seems to suggest that there is dihedral control over $^2J(P,C)$. The torsion angles for these compounds are shown in Structure 28.

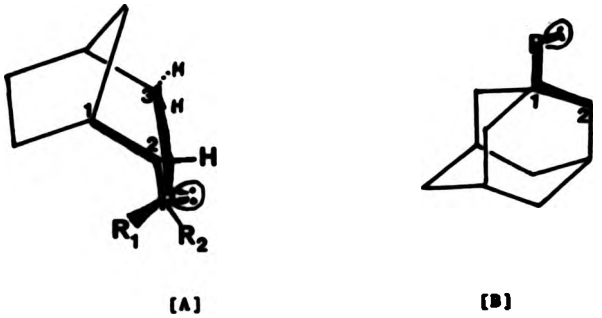

[A] [B]

Structure 28

The 2-norbornyl derivatives

When phosphorus is in the endo position on C_2, steric crowding may cause the preferred orientation to be as shown in Structure 28 with the phosphorus substituents projected away from the norbornyl cage. In this orientation the phosphorus lone pair would be orientated closer to C_3H (2.023 Å) than C_1H (2.874 Å). Hence expected coupling data should show $^2J(P,C_3) > {}^2J(P,C_1)$ and this is reflected for the endo 2-norbornyl data in Table 3.3-5.

Table 3.3-5 Comparison of $^2J(P,C)$ for Carbons C_3 : C_1 in 2-norbornyl P(III) Derivatives

P(III) Derivatives	|J| /Hz			
	endo 2-norbornyl		exo 2-norbornyl	
	C_3	C_1	C_3	C_1
PBr_2	16.8	11.4	11.4	18.1
PBrCl	20.0	7.6	14.6	18.0
PCl_2	27.6	12.1	14.5	18.2
$P(OMe)_2$	15.0	4.8	13.6	-
$P(NEt_2)$	14.6	7.6	18.9	9.0
	29.0	12.5	14.3	21.3
	26.7	12.3	12.0	20.2
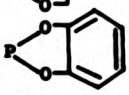	24.6	15.4	13.1	17.4
PPh_2	9.5	0.9	6.5	6.9
PMe_2	11.0	9.2	9.4	15.4

However Table 3.3-5 also reveals that in the exo 2-norbornyl case, the data does not show this steric control. Here when the phosphorus atom is orientated in the exo position on C_2 the phosphorus seems to be less crowded and both values are within the limits of the series.

The 1-adamantyl derivatives

It has been suggested from the data (Section 2.4) that the chemical shifts for β-C_2 in the adamantyl ring (Structure 28) are greatly influenced by γ gauche orientation possibly resulting from the electron pair on the phosphorus atom. However the estimated dihedral angles in these derivatives is about 84°. Hence the control on the coupling

TABLE 3.3-6 $^{3}J(P,H)$ Couplings (Hz) with Associated Dihedral Angles for Some P(III) Derivatives

|ϕ| (deg)	PBr_2	PCl_2	PClBr	PPhCl	$P(NEt_2)_2$		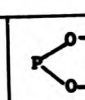	PPh_2	$P(OMe)_2$	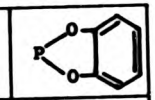
0.0	6.9	1.6	2.0	-	1.4	4.8	2.1	16.5	2.0	2.6
5.8	6.0	1.2	-	-	17.4	2.7	3.5	9.9	1.2	1.2
43.8	3.1	7.3	7.0	-	4.2	0.8	1.0	1.8	-	1.1
59.4	5.7	4.9	5.6	3.1	-	-	3.3	3.1	-	2.9
61.7	3.5	4.6	4.3	4.3	-	4.5	-	3.2	-	-
84.1	6.3	3.0	6.3	-	5.9	1.6	1.6	0.0	6.0	1.6
121.5	10.9	18.0	5.9	-	0.1	0.2	0.2	14.6	1.0	1.6
127.3	3.4	3.5	-	-	13.4	5.7	2.7	7.3	1.2	0.8

magnitude of $^{2}J(P,C)$ by the electron pair would be minimal with this angle and little influence would be seen. Table 2.4-7[A], Section 2.4 reflects this to be the case as normal magnitudes of $^{2}J(P,C)$ are found.

3.3.3 $^{3}J(P,H)$

With respect to $^{3}J(P,H)$ coupling constants, representative dihedral angle relationships have been shown through C, N, O and other hetero-atoms of P(V) compounds[1,29-31]. Results indicate that $^{3}J(P,H)$ couplings may be a function of the state of hybridization of the phosphorus atom. (This may occur when the phosphorus atom coupled to the vicinal hydrogen is P(III) or P(V).) White and Verkade[3] measured vicinal $^{31}\underline{P}\text{-O-C-}^{1}\underline{H}$ couplings in phosphates, phosphites, and thio-phosphates noting that separate correlations were necessary for P(III) and P(V) systems. Also Benezra[31] observed a Karplus-like relationship between $^{31}\underline{P}\text{-C-C-}^{1}\underline{H}$ couplings in a series of P(V) bicyclic- and tricyclic-phosphonates. At present, there is controversy as to the extent that differences in phosphorus coordination actually play an important role in determination of the vicinal $^{31}\underline{P}\text{-C-C-}^{1}\underline{H}$ coupling constants.

Interpretation of $^{3}J(P,H)$ data in terms of dependence on Dihedral Angle

As previously stated (Section 3.2, Table 3.2-1) dihedral angle estimations were determined from known crystal structure data for the various P(III) compounds. The various angles obtained and used with $^{3}J(P,H)$ are summarized in Table 3.3-6. The different dihedral angles were obtained in the following way. Dihedral angles from the 2-norbornyl structure gave the associated dihedral angles:

$^{3}J(P,H_3)_{exo}$/0.0°, $^{3}J(P,H_1)$/43.8°, and $^{3}J(P,H_3)_{endo}$/121.5° for the exo derivatives, and

$^3J(P,H_3)_{endo}$/5.8°, $^3J(P,H_1)$/84.1° and $^3J(P,H_3)_{exo}$/127.3° for the endo derivatives.

The 7-norbornenyl structure gave the associated dihedral angle $^3J(P,H)$ = 60°. The 1-adamantyl structures gave the associated dihedral angle $^3J(P,H_1)$/89.4° and the 2-adamantyl structure gave $^3J(P,H_3)$/61.7°. These vicinal ^{31}P-^1H coupling constants were analysed in terms of the general Karplus relation (equation [3.1]). Again a three parameter computer fit program was performed on the phosphorus data and a best fit calculation was estimated from the standard deviations. The calculated parameters are given in Table 3.3-7 for the various P(III) derivatives. Some of the plots of $^3J_{P,H}$ for the various P(III) groups as a function of the dihedral angle are shown in Fig. 3.3-3[A] to [F] respectively. These show the best of the $^3J_{PH}$ plots. Here all data are plotted as positive. The other derivatives not plotted either failed to show any ϕ_{min} value or their ϕ_{min} value were so far removed from the expected 90° value that they did not seem to conform to any known dihedral relationship. It can be seen that unlike the carbon data, the $^3J(P,H)$ dihedral angle relationship does not seem to play a dominant contribution. This may be the result from poor estimations of the dihedral angles. The hydrogens, unlike the carbons, are not held in a rigid framework and may be able to take up unexpected angles with respect to the phosphorus atom. Also hydrogens are more susceptible to other steric contributions.

In the case of the P(III) derivatives the position of the electron pair may contribute more importantly than the position of the phosphorus atom. This would decrease or increase the angle (depending upon the amount of interaction with respect to the phosphorus atom). Also from Table 3.3-6 it can be seen that for the different derivatives large differences may occur in $^3J(P,H)$ even though the calculated dihedral

$^{3}J_{(P,H_3)_{endo}}$/5.8°, $^{3}J_{(P,H_1)}$/84.1° and $^{3}J_{(P,H_3)_{exo}}$/127.3° for the endo derivatives.

The 7-norbornenyl structure gave the associated dihedral angle $^{3}J_{(P,H)}$ = 60°. The 1-adamantyl structures gave the associated dihedral angle $^{3}J_{(P,H_1)}$/59.4° and the 2-adamantyl structure gave $^{3}J_{(P,H_3)}$/61.7°. These vicinal ^{31}P-^{1}H coupling constants were analysed in terms of the general Karplus relation (equation [3.1]). Again a three parameter computer fit program was performed on the phosphorus data and a best fit calculation was estimated from the standard deviations. The calculated parameters are given in Table 3.3-7 for the various P(III) derivatives. Some of the plots of $^{3}J_{P,H}$ for the various P(III) groups as a function of the dihedral angle are shown in Fig. 3.3-3[A] to [F] respectively. These show the best of the $^{3}J_{PH}$ plots. Here all data are plotted as positive. The other derivatives not plotted either failed to show any ϕ_{min} value or their ϕ_{min} value were so far removed from the expected 90° value that they did not seem to conform to any known dihedral relationship. It can be seen that unlike the carbon data, the $^{3}J_{(P,H)}$ dihedral angle relationship does not seem to play a dominant contribution. This may be the result from poor estimations of the dihedral angles. The hydrogens, unlike the carbons, are not held in a rigid framework and may be able to take up unexpected angles with respect to the phosphorus atom. Also hydrogens are more susceptible to other steric contributions.

In the case of the P(III) derivatives the position of the electron pair may contribute more importantly than the position of the phosphorus atom. This would decrease or increase the angle (depending upon the amount of interaction with respect to the phosphorus atom). Also from Table 3.3-6 it can be seen that for the different derivatives large differences may occur in $^{3}J_{(P,H)}$ even though the calculated dihedral

angles are similar. This suggests the effect of the substituents on the phosphorus atom play an important part in determining the magnitude of the coupling for the dihedral angle (see discussion in Chapter 2). However all of the data are tabulated in Table 3.3-6. The only convincing Karplus curves are those for the PCl_2 and PClBr derivatives. If there is dihedral angle control then it appears as though the ϕ_{min} is at about the expected 90°. From this data it is hard to tell whether the value for large $^3J(P,H)$ favours a cis orientation (0°) or a trans (180°) orientation. For comparison $^3J(H,H)$ usually shows that the magnitude of $^3J(H,H)$ trans > $^3J(H,H)$ cis. This seems to fit in with most of the curves shown in Fig. 3.3-3, however, the PCl_2 derivatives show the opposite effect.

Fig. 3. 3-3 [A] to [F] Karplus Plots for various P(III) groups as a function of the dihedral angle ϕ (deg) -- $^3J_{P,H}$

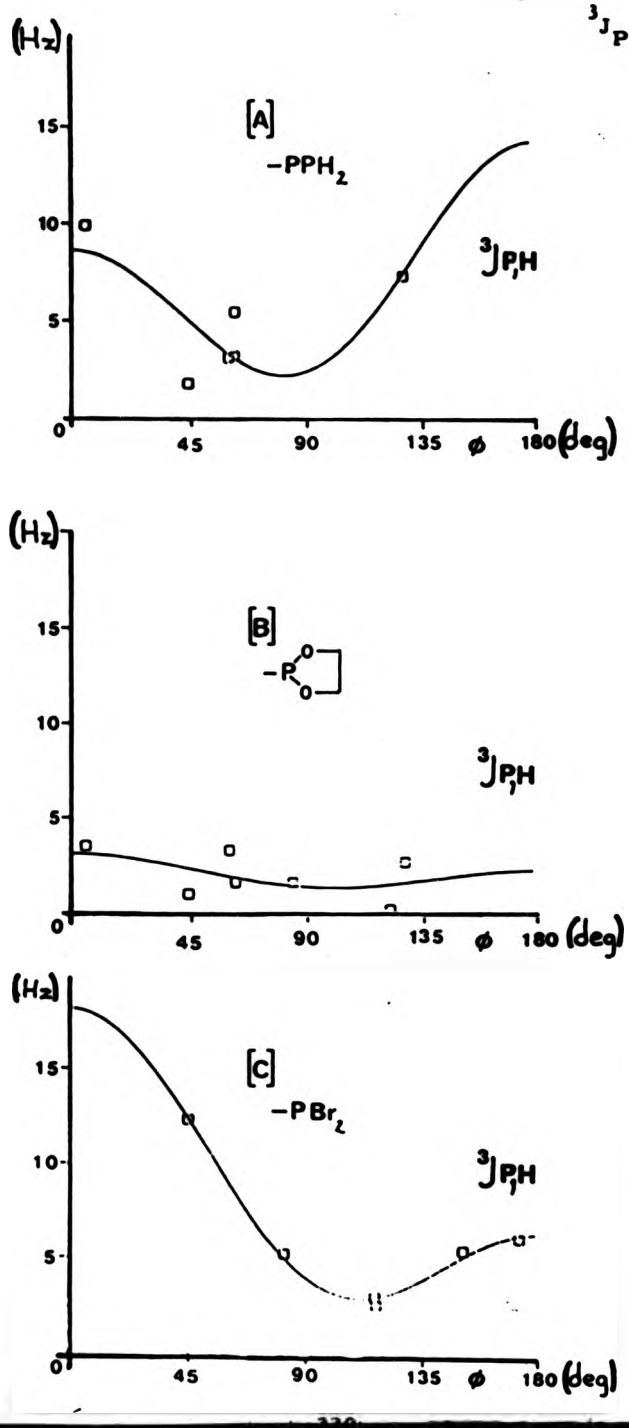

Fig. 3. 3-3 cont'd.

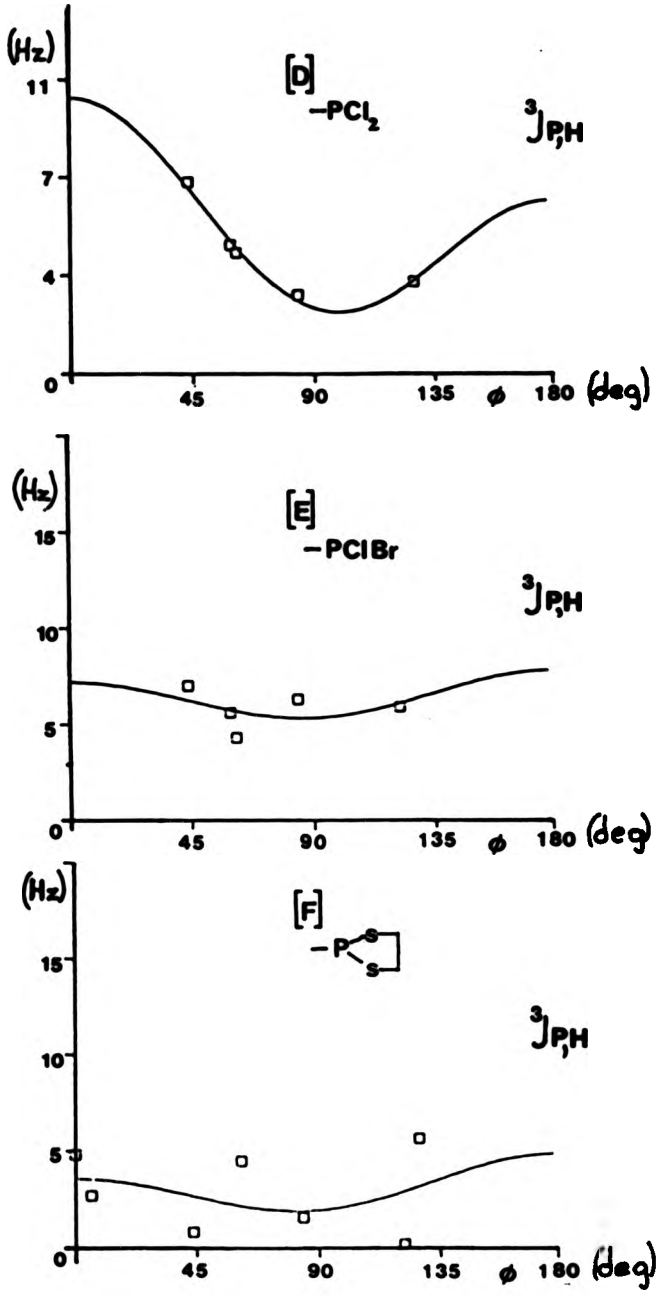

TABLE 3.3.7 Values of Best Iterations for the Parameters (Hz) in the Karplus Equation $^3J = A + B\cos\theta + C\cos^2\theta$ for Evaluation of $^3J(P,H)$.

P(III) derivative	A		B		C		ϕ_{min} (deg)
	Hz	Std.dev[a]	Hz	Std.dev[a]	Hz	Std.dev[a]	
PBr_2	6.4	1.49	1.7	2.50	1.06	2.16	98°
PBrCl	4.8	1.46	0.2	2.29	1.6	1.77	88°
PCl_2	5.8	0.34	1.9	0.40	3.0	0.56	93°
$P(OMe)_2$	1.8	0.81	3.5	1.12	3.7	0.96	b
$P(NEt_2)_2$	9.7	4.89	2.1	9.06	7.5	8.90	b
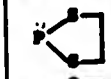	3.1	1.35	0.7	2.41	1.1	2.12	82°
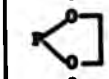	2.0	0.76	0.4	1.19	0.6	1.17	93°
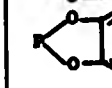	1.3	0.46	0.7	0.76	-0.8	0.76	b
PPh_2	9.16	2.17	5.9	3.31	5.1	3.66	83°
Mean aver.	4.91		1.82		2.28		

a Standard deviation value is ($\times 10^2$)

b No minimum found

3.4 Naphthalene Derivatives

General: When the 2D-NMR pulse sequences were written and first implemented on the Jeol FX90Q spectrometer, various off the shelf samples with known and assigned ^{13}C resonances were made up: 1) to test to see if the 2D modified sequences were giving reasonable and expected results, 2) to check to see whether or where errors or artifacts were occurring and 3) to test the range of complexity one could expect to determine on a low field machine. In some of the more complicated samples used, though the ^{13}C chemical shifts and some of the $^{n}J(C,H)$ assignments were known, their ^{1}H chemical shifts or their values of $^{n}J(H,X)$ were not always accurately determined. In this section we elaborate on those more interesting samples where the use of 2D spectroscopy is justified by the increase in valuable and sometimes otherwise unobtainable information by normal 1D-NMR methods.

A difficulty which has always plagued the spectroscopist is the problem of trying to sort out couplings in tightly bound systems, especially in compounds in which there is a lack of symmetry. Here an attempt has been made to sort out two structures with a single flourine positioned on a naphthalene ring namely: 1-fluoronaphthalene (Structure 29) and 2-fluoronaphthalene (Structure 30).

Substitution of a fluorine on the one or two position destroys the symmetry of the naphthalene ring. Instead of the double AA' BB' hydrogen coupling spin system[32] expected for naphthalene, a highly complex second order, highly overlapped aromatic spin order involving $^{n}J(H,H)$ and $^{n}J(H,F)$ couplings arises. This is because both ^{1}H and ^{19}F have high abundance and are spin = $\frac{1}{2}$ nuclei which gives the possibility of having and seeing both α and β spin systems. A major difficulty with these systems was the existence of many small couplings less than 0.3 Hz. However, many of the sites attached to a carbon-13

nucleus are first order, although still heavily overlapped, and thus a 2D $^{13}C/^{1}H$ shift correlation is possible.

3.4.1 1-Fluoronaphthalene

A $^{13}C\{^{1}H\}$ 22.5 MHz spectrum was obtained (Fig. 3.4-1) and the $^{n}J(C,F)$ and ^{13}C chemical shifts were measured and matched with the original assignments by Ernst[33] and Kitching[34] and shown in Table 3.4-1. The assignments had been based on deuterium labelling and selective decoupling experiments[34] and the selective decoupling experiments were checked by McFarlane *et al*[35]. The assignments could also be related by the size of the associated $^{n}J(C,F)$ couplings especially those of the C_1, C_9 and C_{10} (see Structure 29). As there were no serious discrepancies, the assignments were assumed to be correct. However, the chemical shifts of C_6 and C_7 may need to be interchanged[34].

Structure 29

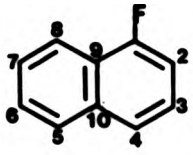

A $^{19}F\{^{1}H\}$ 84.26 MHz NMR spectrum was taken and it showed a single resonance at -110.3 ppm which was typical for an aromatic fluorine. A coupled ^{19}F spectrum revealed a complex overlapped coupling system. Extraction of experimental $^{n}J(F,H)$ couplings from this 1D spectrum gave only crude estimates of their magnitudes. A full 89.56 MHz ^{1}H spectrum was recorded to ensure sample purity and then expanded (2.0 ppm) aromatic region was run (Fig. 3.4-4[A]). Previous attempts at sorting out hydrogen chemical shifts and J(H,F) couplings from this complex system even at 400 MHz *via* a combination of 1D ^{13}C selective and ^{1}H homonuclear decoupling experiments proved unsuccessful[35]. Hence it was decided to perform a 2D $^{13}C/^{1}H$ shift correlation experiment (see Chapter 1,

Table 3.4-1 ^{13}C NMR Chemical Shift Data for 1-Fluoronaphthalene

Carbon Number	^{13}C Chemical Shift			
	Experimental		Literature [b]	
	δ/ppm[a]	Hz	δ/ppm[a]	Hz
C_1	150.6	(256.7)	150.5	(253.6)
C_2	109.8	(21.3)	109.8	(19.8)
C_3	125.8	(7.8)	126.0	(8.0)
C_4	124.4	(5.3)	124.2	(4.6)
C_5	128.1	(2.9)	128.1	(3.0)
C_6	126.7	(0.8)	127.3	(1.0)
C_7	126.6	(1.9)	126.6	(2.0)
C_8	120.9	(5.3)	120.9	(5.0)
C_9	124.6	(16.8)	124.3	(17.2)
C_{10}	135.7	(6.3)	135.7	(5.9)

a Positive signs are to high frequency of TMS = 0 ppm in Acetone-^6D as solvent

b Taken from reference (34)

( ) $^nJ(C,F)$

Section 1.5.2.2) in hopes of sorting out the exact ^1H chemical shifts and assign them to the appropriate assigned and associated ^{13}C resonances. A 256 ^1H (F_1) by 1024 ^{13}C (F_2) data matrix for a 140 Hz (^1H) by 500 Hz (^{13}C) frequency surface was used and decoupling was achieved in both dimensions. A complete 2D Stack Plot is shown in Fig. 3.4-2. 90° cross-sections through the peak maxima were taken parallel to the F_1 axis and cutting the F_2 (^{13}C) axis at a chemical shift frequency for each of the particular ^{13}C resonances (Fig. 3.4-3). The exact ^1H chemical shifts could be calculated (as shown in Chapter 2 Section 2.1.2)

... cont'd on page 239

Fig. 3.4-1 A $^{13}C\{^{1}H\}$ 22.5 MHz 1D NMR Expansion of the aromatic signals of 1-fluoronaphthalene

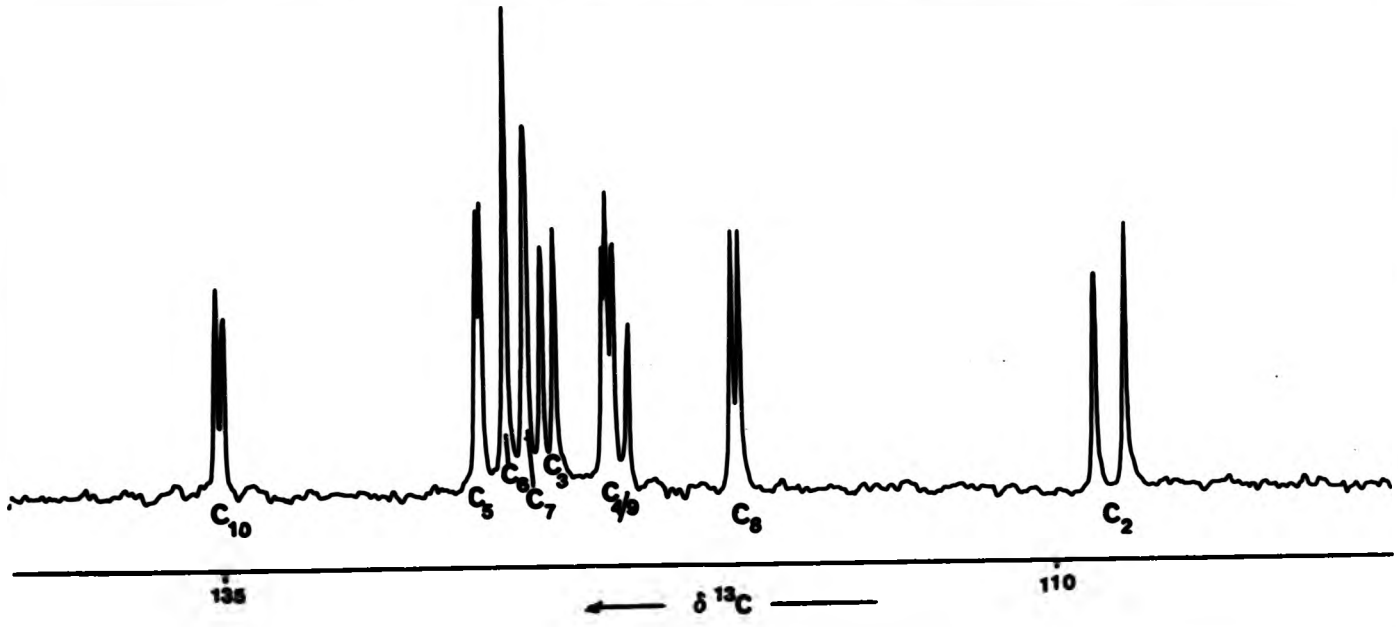

Fig. 3.4-2 A 2D ^{13}C / ^{1}H Shift Correlation Stack Plot of 1-fluoronaphthalene

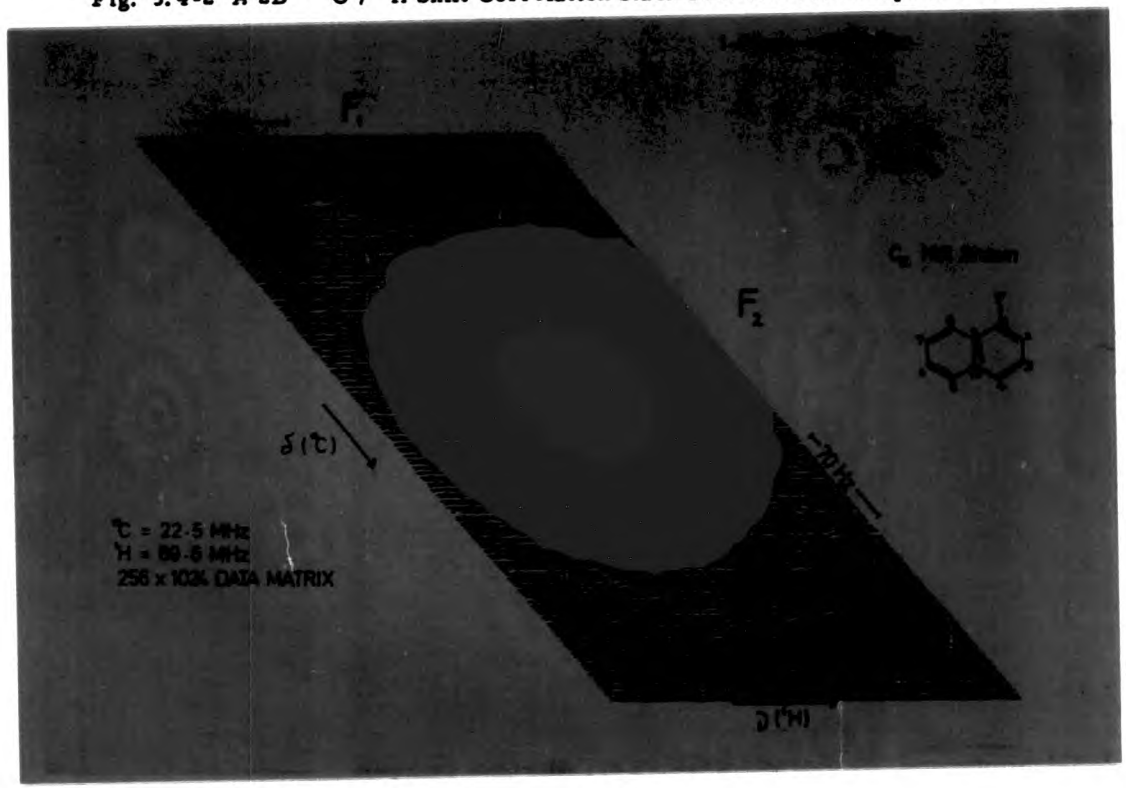

236

Fig. 3.4-3 90° Cross sections through the carbon peak maxima in the F_2 Dimension taken par allel to the F_1 Dimension to show the ^1H resonances

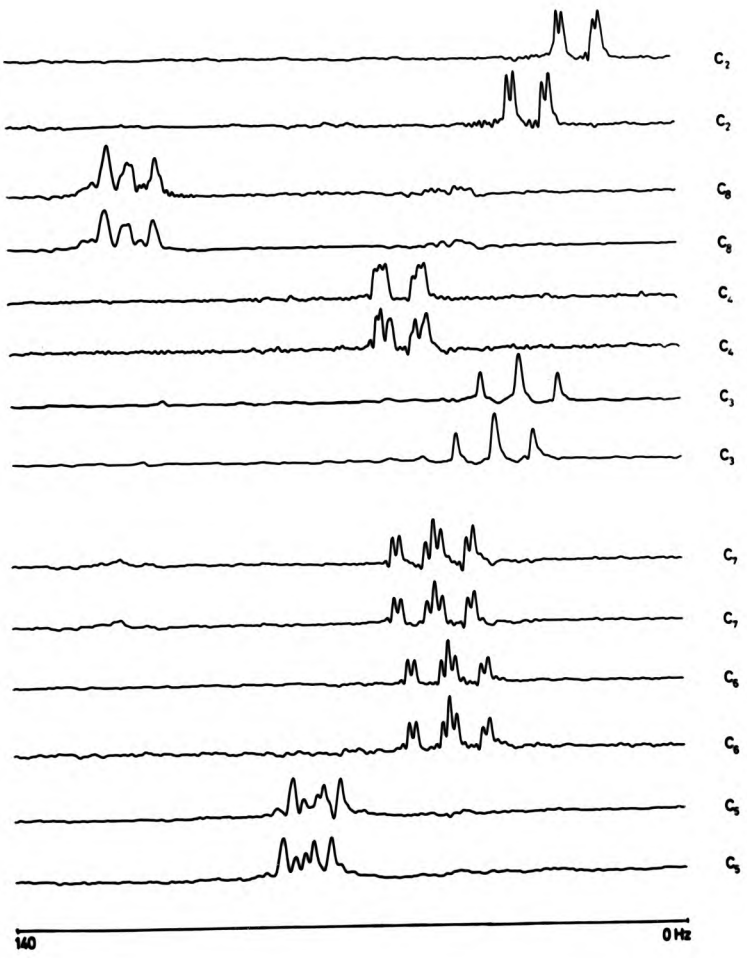

Fig. 3.4-4 [a] An experimental and [b] a calculated ^{1}H 1D NMR spectrum of 1-fluoronaphthalene

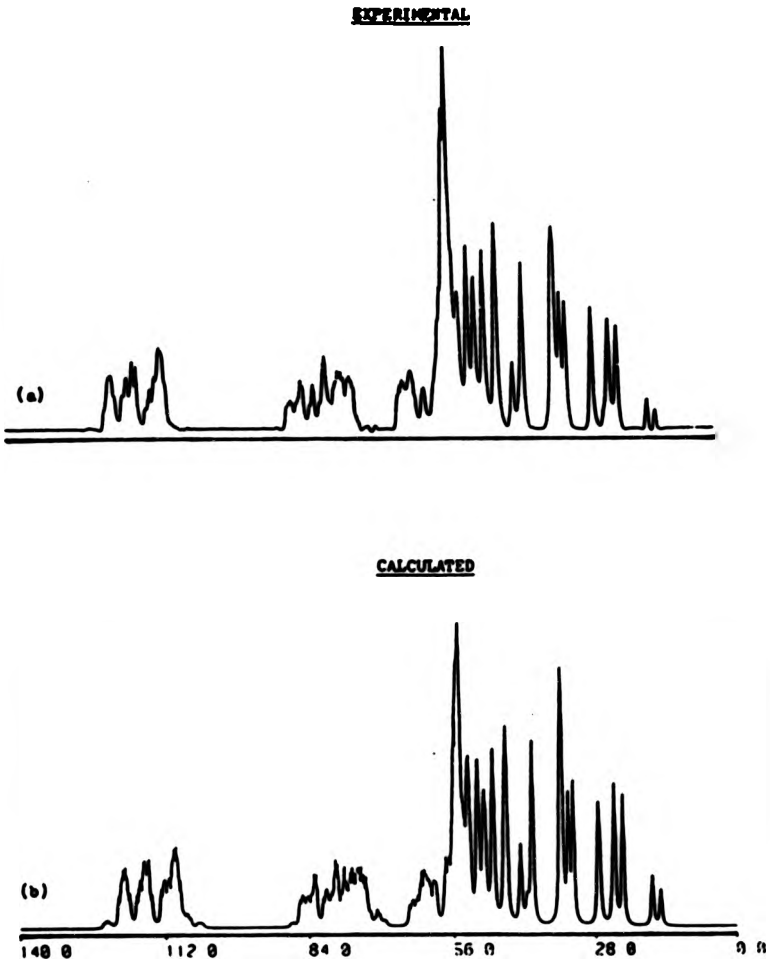

from the two slices arising from the $^{13}CF_{\alpha}$ and $^{13}CF_{\beta}$ resonances for a particular C-H pair. The $^{n}J(H,H)$ couplings are spread out horizontally along the F_1 axis and may be calculated from either of the $^{13}CF_{\alpha}$ or $^{13}CF_{\beta}$ slices. The J(H,F) couplings are given by the difference between the ^{1}H absorptions in these slices.

The experimental ^{1}H data obtained from the 2D spectra were put as raw data into a main frame computer Ueac-6 spin simulation spin program[36]. A least squares fit was applied to the data, and the data was periodically iterated to give a best fit simulated spectrum with that of the experimental 1D one (Fig. 3.4-4). The accurate values of the ^{1}H chemical shifts and strong J(H,F) and J(H,H) couplings were obtained and presented in Table 3.4-2. Small inconsistencies in the long range J(H,H) couplings still exist, however, these will contribute little chemically to the system as a whole. As this is such a tightly coupled system, standard methods of Double Resonance cannot be applied to sort out the absolute sign of the coupling constants since it is impossible to isolate any one coupling in the system. However, if we can make estimates from benzene aromatic rings where all J(H,H) are positive[37], then perhaps the absolute signs are relatively unimportant to the 1-fluoronaphthalene coupling system.

3.4.2 2-Fluoronaphthalene

The same procedure as for 1-Fluoronaphthalene has been carried out for 2-fluoronaphthalene. However, for 2-fluoronaphthalene, the chemical shift range in the proton spectrum is much smaller (80 Hz vs 120 Hz, see Fig. 3.4-5[A]) and this extra overlap gives smaller couplings making the problem more difficult. A full $^{13}C\{^{1}H\}$ 22.5 MHz spectrum (4000 Hz) and an expanded aromatic spectrum was run to check purity and obvious ^{13}C assignments. The carbon assignments according to Kitching[34]

Table 3.4-2 [A] ^{1}H NMR Chemical Shifts and ^{n}J(H,F) Coupling Data for 1-Fluoronaphthalene

Hydrogen Number	δ/ppm	^{n}J(H,F)/Hz
2	7.28	10.8
3	7.41	5.2
4	7.61	1.4
5	7.86	1.8
6	7.55	0.2
7	7.58	0.4
8	8.25	0.5

[B] ^{n}J(H,H)/Hz Couplings for 1-Fluoronaphthalene

Hydrogen Number	2	3	4	5	6	7	8
2	-	7.9	1.1	(0)	0.2	0.2	(0)
3	7.9	-	8.1	(0)	0.2	0.2	(0)
4	1.1	8.1	-	0.5	(0)	(0)	0.8
5	(0)	(0)	0.5	-	8.2	1.3	0.9
6	0.2	0.2	(0)	8.2	-	6.7	1.4
7	0.2	0.2	(0)	1.3	6.7	-	8.4
8	(0)	(0)	0.8	0.9	1.4	8.4	-

( ) Estimated

(listed in Table 3.4-3) were assumed to be correct and were used as a basis for the hydrogen assignments. The numbering is according to Structure 30.

Structure 30

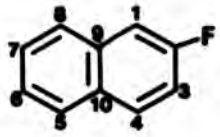

Table 3.4-3 ^{13}C NMR Chemical Shift Data for 2-Fluoronaphthalene

Carbon Number	^{13}C Chemical Shift			
	Experimental		Literature [b]	
	δ/ppm [a]	Hz	δ/ppm	Hz
C_1	111.89	(20.5)	110.9	(21.0)
C_2	161.79	(244.7)	161.0	(248.8)
C_3	117.10	(26.4)	116.2	(25.9)
C_4	131.2	(10.2)	130.5	(10.1)
C_5	128.6	(0.2)	128.1	(~0)
C_6	125.3	(2.9)	125.2	(2.8)
C_7	126.8	(1.3)	127.0	(1.2)
C_8	127.7	(5.1)	127.5	(5.1)
C_9	135.42	(8.8)	134.7	(9.9)
C_{10}	131.1	(0.3)	130.8	(~0)

a Positive signs are to high frequency of TMS = 0 ppm in Acetone-^6D as solvent

b Taken from reference (34)

( ) $^nJ(C,F)$

A $^{19}F\{^1H\}$ spectrum showed a single resonance at -109.93 ppm [Lit.[34] -109.93 ppm] which is typical for an aromatic fluorine. A coupled ^{19}F expanded spectrum showed a spin system in which its

Fig. 3.4-5 [A] An expansion of the aromatic signals of the ^{1}H spectrum
[B] and [C] A fluorine spectrum

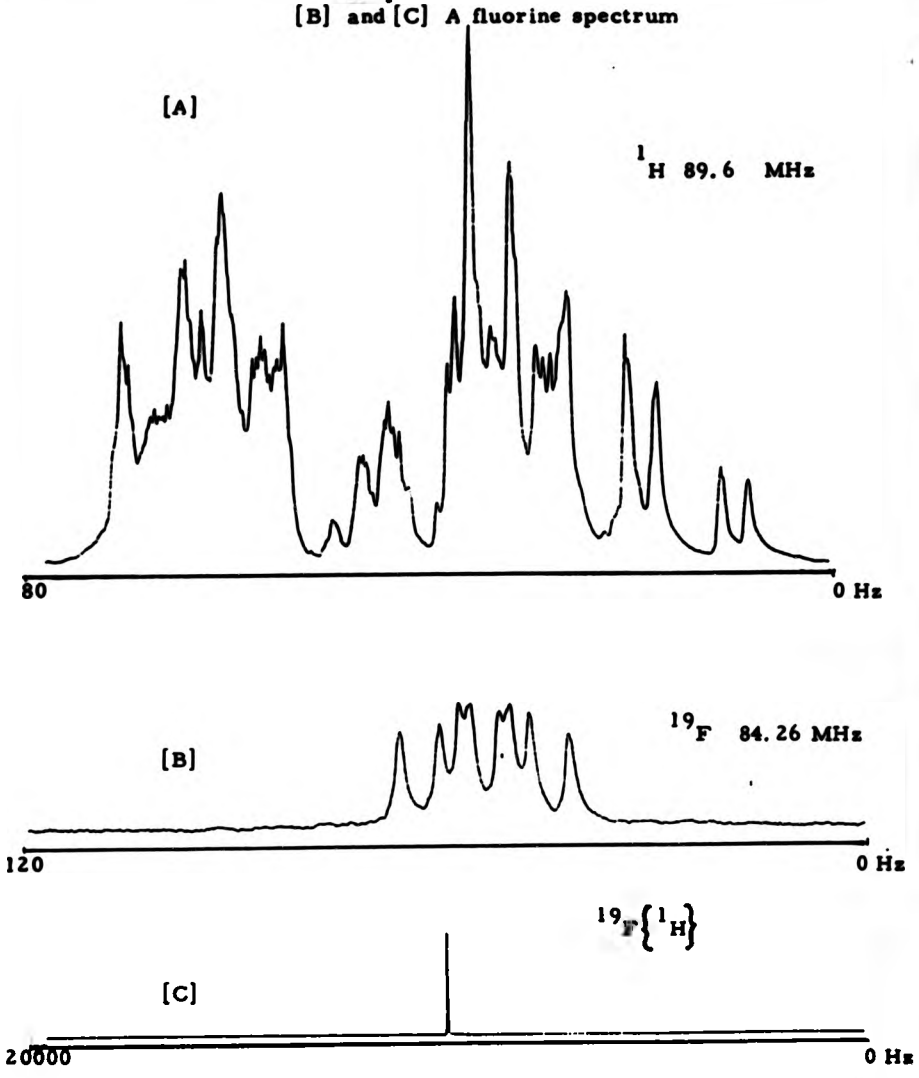

complexity made it impossible to pick out directly any accurate J(H,F) couplings (Fig. 3.4-5[B] and [C]). A 10 ppm ^{1}H spectrum was run to check purity and then an expanded (ppm) aromatic region was run and plotted in Fig. 3.4-5[A]. A 2D $^{13}C/^{1}H$ shift correlated sequence was applied to enable determination of exact ^{1}H chemical shifts (see Chapter 1, Section 1.8.3.2). In this sequence decoupling is applied in both dimensions where the F_2 dimension contains the $^{13}C(^{1}H)$ spectrum and the F_1 dimension will contain homonuclear decoupled ^{1}H spectrum. The full Stack Plot is shown in Fig. 3.4-6. For more accurate estimations of the ^{1}H chemical shifts and assignments, individual cross sections may be taken parallel to the F_1 axis and through the particular ^{13}C peak maxima (shown in Fig. 3.4-7). From these, exact chemical shifts may be calculated, and J(H,F) couplings may be determined as explained in Chapter 2, Section 2.1.2 and are tabulated in Table 3.4-4[A]. A 2D $^{13}C/^{1}H$ heteronuclear shift correlation sequence was used to try to resolve the J(H,H) couplings. In this sequence (Chapter 1, Section 1.8.2.2) the ^{1}H (F_1) dimension was not homonuclear decoupled so that direct couplings can be seen. Again for accurate determinations of J(H,H) coupling constants, data slices may be taken and their couplings calculated to simulate the experimental ^{1}H NMR spectrum. The resulting iterations yielded the J(H,H) couplings in Table 3.4-4[B].

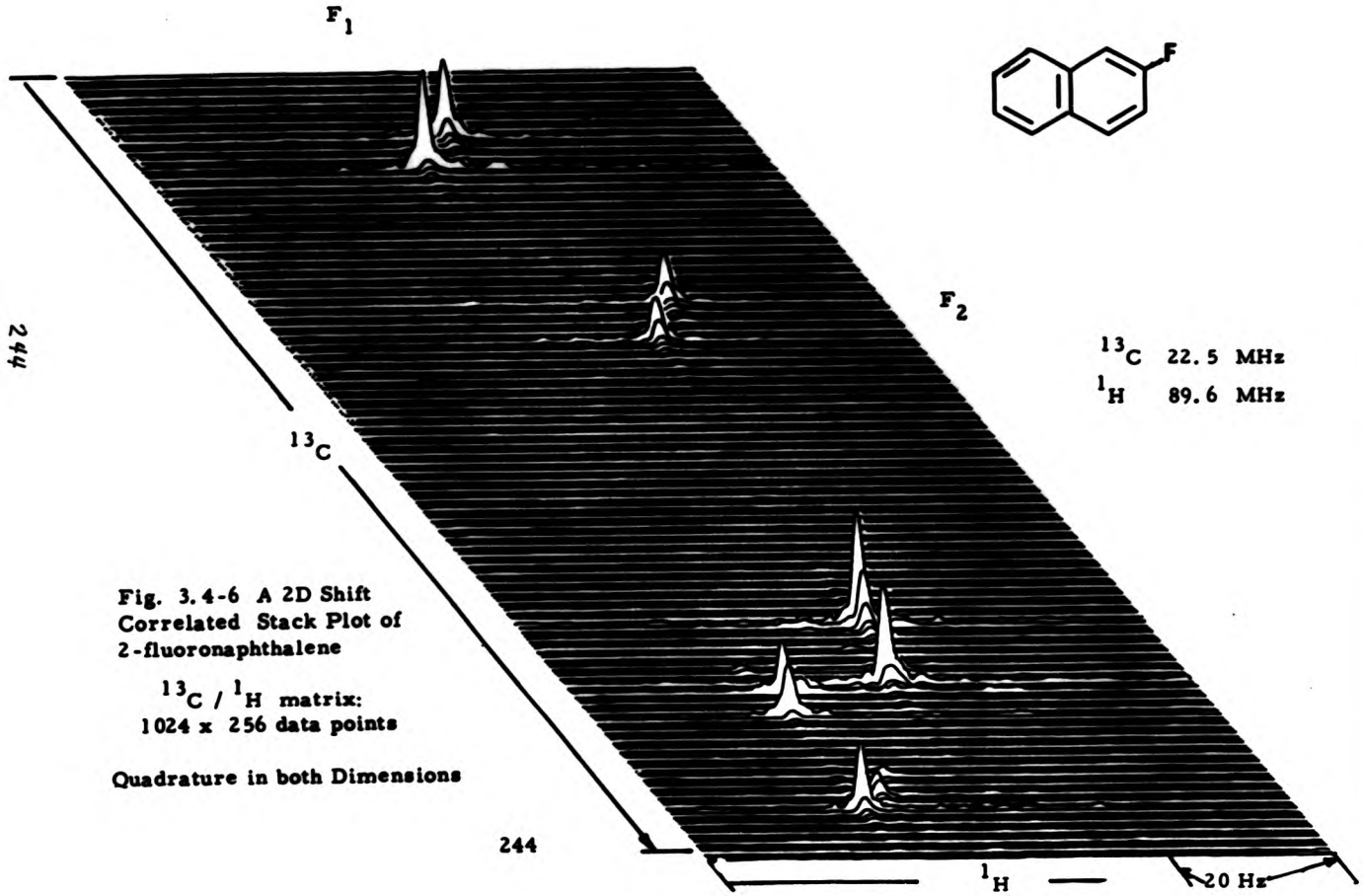

Fig. 3.4-6 A 2D Shift Correlated Stack Plot of 2-fluoronaphthalene

^{13}C / ^{1}H matrix: 1024 x 256 data points

Quadrature in both Dimensions

Fig. 3.4-7 90° Cross sections taken from the 2D Stack Plot through the carbon maximum

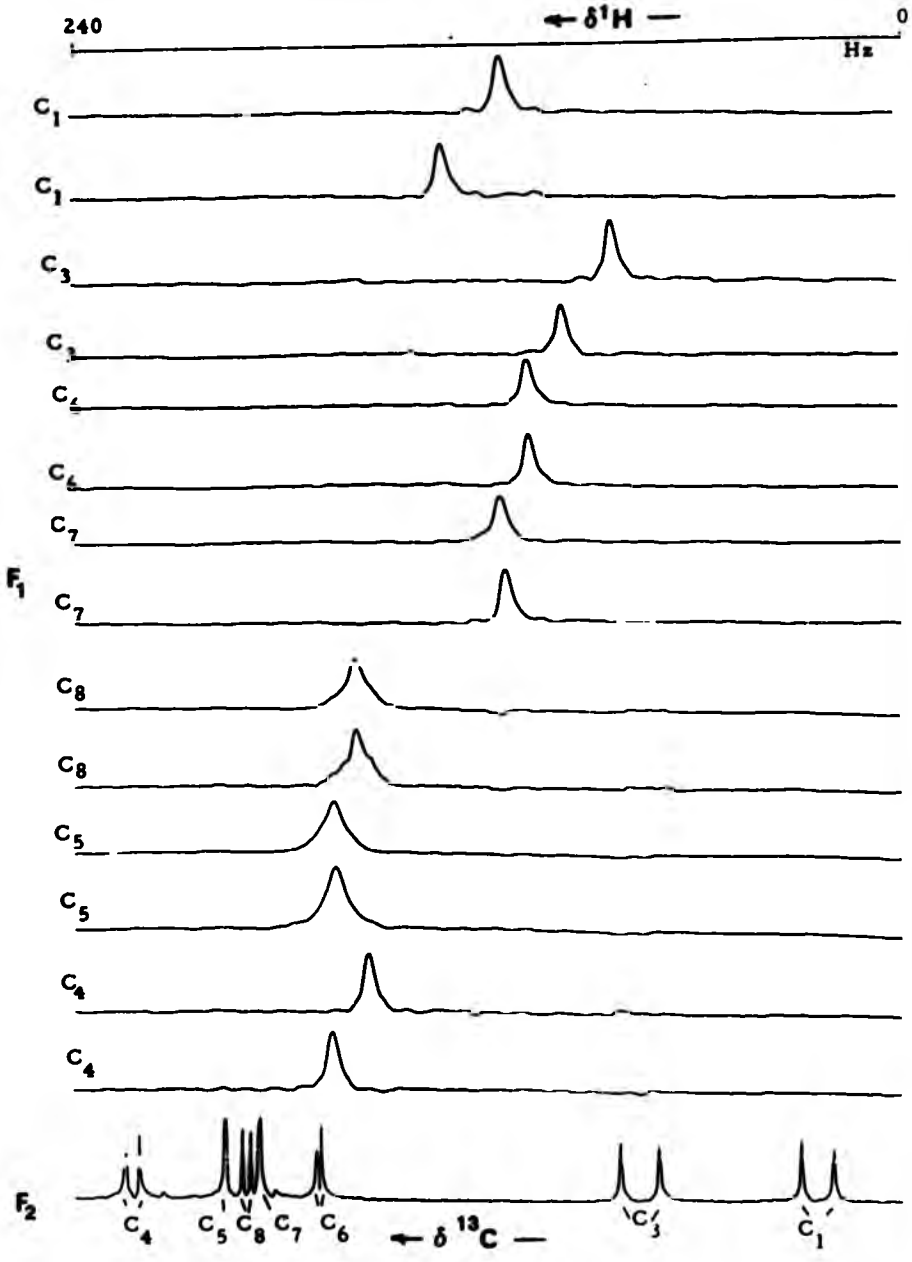

Fig. 3.4-8 A ^{13}C Spectrum and expansion of the aromatic carbons for a sample of 2-fluoronaphthalene in Acetone-^{6}D.

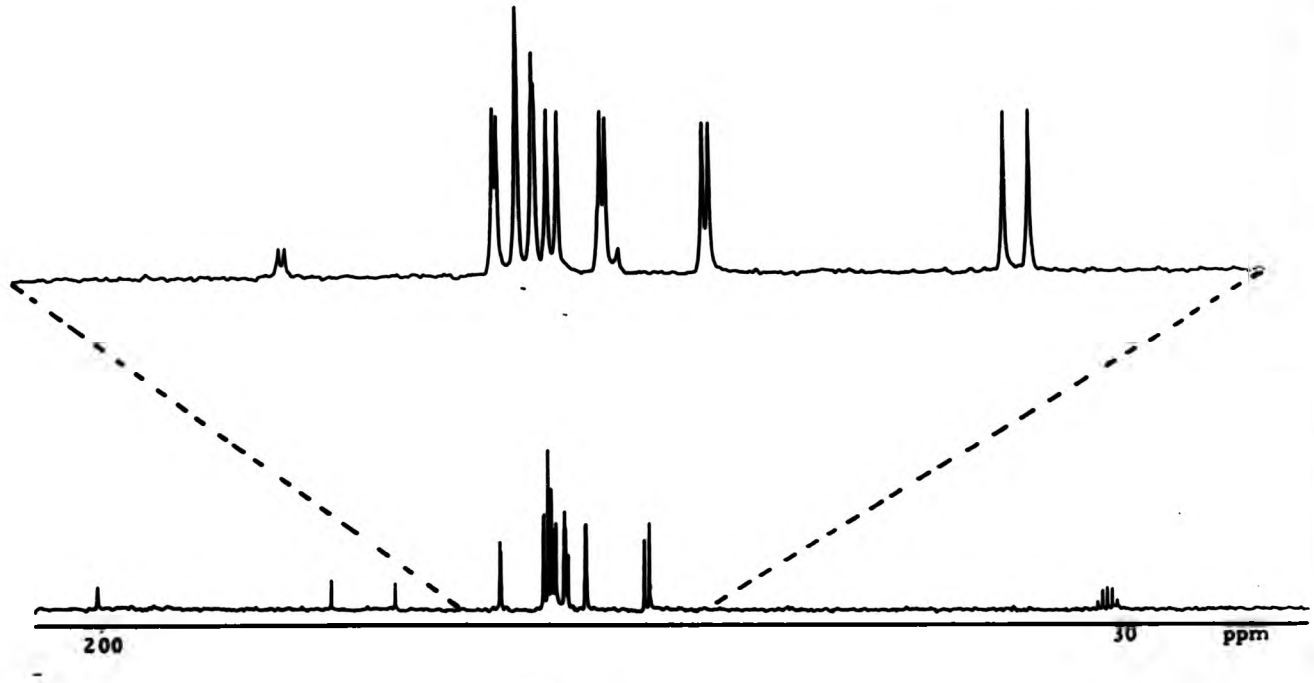

TABLE 3.4-4 [A] ^{1}H NMR Chemical Shifts and $^{n}J(H,F)$ Coupling Data for 2-Fluoronaphthalene

Hydrogen Number	δ/ppm	$^{n}J(H,F)$/Hz
1	7.47	9.9
3	7.26	8.8
4	7.70	5.4
5	7.73	0.15
6	7.37	0.4
7	7.43	1.5
8	7.69	1.8

[B] $^{n}J(H,H)$/Hz Couplings for 2-Fluoronaphthalene

Hydrogen Number	1	3	4	5	6	7	8
1	-	2.6	0.7	1.4	0.7	0.8	1.0
3	2.6	-	9.1	(0)	(o.2)	(0.2)	0.3
4	0.7	9.1	-	1.5	0.3	0.4	1.4
5	1.5	(0)	1.5	-	7.5	1.4	0.8
6	0.7	(0.2)	0.3	7.5	-	7.4	1.6
7	0.8	(0.2)	0.4	1.4	7.4	-	7.5
8	1.0	0.3	1.4	0.8	1.6	7.6	-

( ) Estimated

References - Chapter 3

1. M. Karplus J. Chem. Phys. 30, 11 (1959).

2. M. Karplus J. Amer. Chem. Soc. 85, 2870 (1963).

3. D.W. White, J.G. Verkade J. Magn. Reson. 5, 205 (1973).

4. A.A. Bothner-By, R.E. Glick J. Chem. Phys. 25, 362 (1956).

5. H.J. Bernstein, J.A. Pople, W.G. Schneider Can. J. Chem. 35, 65 (1957).

6. a) R.J. Abraham Proc. 11th Colloq. Ampere, 589 (1963).

   b) A.A. Bothner-By Adv. in Magn. Reson. 1, 195 (1965).

7. K. Kirao, H. Matatsuji, H. Kato, J. Amer. Chem. Soc. 95, 31 (1973).

8. G.W. Buchanan, C. Bensara Can. J. Chem. 54, 231 (1976).

9. P.F. Barron, D. Doddrell, W. Kitching J. Organometal. Chem. 351, 132 (1977).

10. D. Doddrell, I. Barfitt, W. Kitching, M. Bullpitt, C-H. Lee, R.J. Mynott, J. Considine, H.G. Kuivila, R.H. Sarma J. Amer. Chem. Soc. 96, 1640 (1974).

11. D.G. Gorenstein Prog. in NMR Spectros. 16.1, 1 (1983).

12. Molecular Graphics System for Apple II Computers, Chemdata Ltd.(1985).

13. M.G. Newton, N.S. Pantaleo, S. Kirbawry J. Amer. Chem. Soc. 100, 2176 (1978).

14. A.C. MacDonald, J. Trotter Acta. Crystallogr. 19, 456 (1965).

15. J.P. Amoureux, M. Bee Acta. Cryst. B35, 2957 (1979).

16. S.Y. Lin, M. Ionov, Y. Okaya, D.M. Chiov, W.J. Noble Acta. Cryst. B38, 1666 (1982).

17. L.D. Quin, L.B. Littlefield J. Org. Chem. 43, 3606 (1978).

18. R.B. Wetzel, G.L. Kenyon Chem. Commun. 287 (1973).

19. M. Lauer, O. Samuel, H.B. Kagan, J. Organometal. Chem. 309, 177 (1979).

20. J. Thiem, B. Meyer Org. Magn. Reson. 11, 51 (1978).

21. L.D. Quin, M.J. Gallagher, G.T. Cunkle, D.B. Chesnut J. Amer. Chem. Soc. 102, 3136 (1980).

22. S. Sørenson, H.J. Jakobson Org. Magn. Reson 9, 101 (1977).

23. R. Wasylishen, T. Schaefer Can. J. Chem. 50, 2989 (1972).

24. G.A. Grey, S.E. Cremer J. Chem. Soc. Chem. Commun. 367 (1972).

25. S.I. Featherman, L.D. Quin Tetrahedron Lett. 1955, (1973).

26. J.B. Robert, J.D. Roberts J. Amer. Chem. Soc. 94, 4902 (1972).

27. J.P. Datasta, J.B. Robert J. Chem. Soc. Chem. Commun. 747, (1975).

28. G.W. Buchman, F.G. Morin Can. J. Chem. 55, 2885 (1977).

29. G.W. Buchman, J.H. Bowen Can. J. Chem. 55, 604 (1977).

30. L. Ernst Org. Magn. Reson. 9, 35 (1977).

31. C.J. Benezra J. Amer. Chem. Soc. 95, 6890 (1973).

32. J.A. Pople, W.G. Schneider, H.J. Bernstein Can. J. Chem. 35, 1060 (1957).

33. a) L. Ernst Chem. Ber. 108, 2030 (1975).

b) L. Ernst J. Magn. Reson. 22, 279 (1976).

34. W. Kitching, W. Adcock, D. Doddrell et al J. Org. Chem. 42, 2411 (1977).

35. W. McFarlane, I.J. Colquhoun, S.M. Cabral de Menezes unpublished results.

36. R.K. Harris, A.A. Bothner-By UEAC-8 Computer Package, University of East Anglia.

37. E. Lustig , D. Lincoln, V. Wray J. Magn. Reson. 21, 509 (1976).

CHAPTER 4

EXPERIMENTAL

4.1 Instrumentation

The One-Dimensional (1D) NMR spectra for ^{1}H, ^{19}F, ^{31}P, and ^{31}C were recorded on a Jeol FX90Q Spectrometer using internal D lock under the conditions shown in Table 4.1-1.

TABLE 4.1-1 Nuclear Parameters for Field Strength of 2.1 Tesla

Nucleus	Frequency Standard (Reference)	90° Pulse Length	Observation Frequency (Hz)
^{1}H	TMS in Acetone	27 μs	89604330
^{19}F	$CFCl_3$ in $CDCl_3$	35 μs	84293091
^{31}P	85% aq. H_3PO_4	22 μs	36283715
^{13}C	TMS in Acetone	18 μs	22536120

The chemical shift equation (δ) is given by:

$$\delta(x) = \frac{\nu - \nu(\text{reference})}{\nu \text{ reference}} \cdot 10^{6}$$

such that the ^{1}H, ^{19}F, ^{31}P and ^{13}C chemical shifts (δ) are expressed in ppm; positive being to high frequency from their corresponding reference. (See Table 4.1-1)

Medium and high field 1D NMR spectra were obtained on:

(i) Nicolet 1180 200 at Royal Holloway/Bedford New College, University of London; ^{1}H at 200 MHz; ^{13}C at 50.3 MHz.

(ii) Brucker WM-250 at King's College, University of London; ^{1}H at 250.13 MHz; ^{13}C at 62.9 MHz.

(iii) Brucker WH-400 at Queen Mary College, University of London; ^{1}H at 400.14 MHz; ^{13}C at 100.0 MHz.

$^{13}C/^{1}H$ 2D NMR spectra were recorded on the Jeol FX90Q NMR Spectrometer at City of London Polytechnic, with quadrature detection, a Jeol JEC-880B computer and a dual Hard Disc System. The pulse sequences were constructed using the manufacturer's software and all timing and phase changes were under software control. The proton 90° pulse length using the decoupling coils was determined to be 44 μs. A General Radio frequency synthesizer was used to generate a second radio frequency field for the hetero-nuclear-multiple resonance experiments, and was transmitted to the sample via a matched amplifier which was connected to the doubly-tuned decoupler coil within the spectrometer probe. A 10 MHz output from the spectrometer controlled the synthesizer clock so that there were no relative frequency drifts. All samples were examined as solutions in a deuterated solvent which also gave a signal required for internal lock purposes. Spinning 5 mm or 10 mm o.d. precision tubes were used, and measurements were undertaken at ambient temperature (23°C) unless otherwise stated. Where necessary solutions were degassed and sealed with an oxygen/natural-gas flame in the NMR tube. The procedure was carried out by using a series of freeze-pump-thaw cycles. Fig. 4.1-1 shows the apparatus used for the degassing process. Other samples which required only oxygen-free atmospheres were prepared by bubbling nitrogen into the sample and the tops were paraffin-wax sealed. NMR simulations were carried out on a DEC (VAX/VMS) 750 computer at City of London Polytechnic using a UEAC-8 spin NMR simulation package program[1]. The program is based on a LAOCOON package[2] in that it uses a least squares fitting routine to generate a plot. Infrared spectra were recorded on a Perkin-Elmer 197 Spectrophotometer at Royal Holloway/

Bedford New College, University of London and on a Perkin-Elmer 298 Spectrophotometer at City of London Polytechnic, using nujol mulls or KBr discs. Mass Spectra were recorded at Royal Holloway/Bedford New College, University of London on a VG Micromass 12B unit and at City of London Polytechnic on their Jeol JMS-DX300 unit. Elemental analyses were performed either at Royal Holloway /Bedford New College or at The City of London Polytechnic.

For the most part, standard experimental techniques were used in the preparations; however, owing to the viscous, waxy, oily nature of the norbornane and adamantane derivatives, several pieces of specially built distillation apparatus (Figs. 4.1-2 and 4.1-3) were used in their preparations. A Schlenk reflux system was used to react some of the temperature-sensitive phosphorus derivatives (designated in the particular preparation). Boiling points (uncorrected) were taken *in situ* and the pressure was measured on the vacuum line by a McLeod Gauge. Melting points (corrected) were taken in a Mel-Temp apparatus. Most starting materials were checked by NMR prior to use, and were dried when appropriate. All organic solvents were dried by the appropriate method and were distilled. All reactions and manipulations of phosphorus compounds were conducted under an atmosphere of dry nitrogen.

Fig. 4.1-2 and Fig. 4.1-3 Special Microdistillation Apparatus

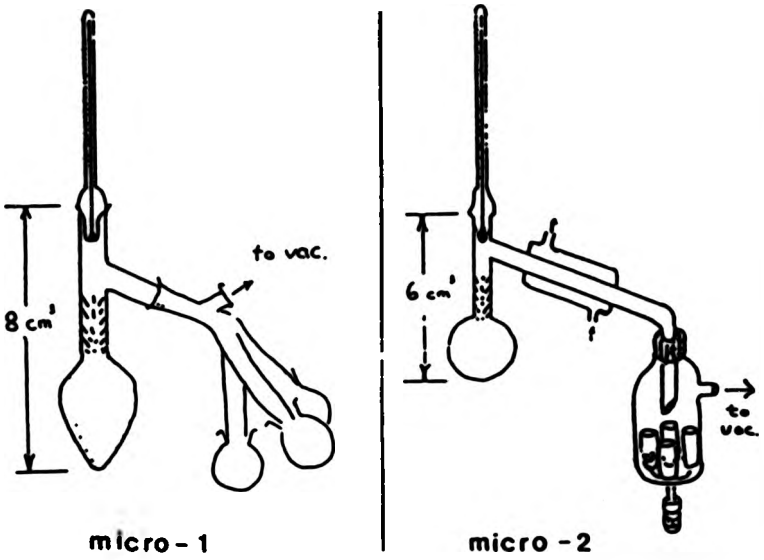

Fig. 4.1-1 NMR Tube Degassing System

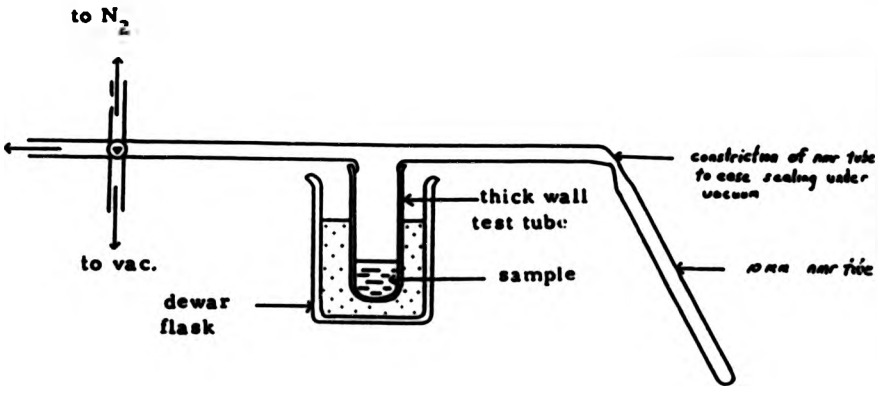

4.2 Preparations

4.2.1 Non-phosphorus Derivatives

[1] 2-phenyl thio-1-chloro acenaphthene

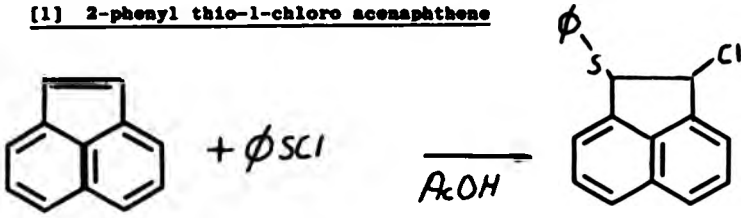

Phenylsulphenyl chloride (0.53 mole) was reacted with acenaphthylene (0.53 mole) in glacial acetic acid at ambient temperature by the method of Kharasch[3]. The product was collected and was washed with water. Drying *in vacuo* gave a 96% yield. The pure compound was obtained by recrystallisation from petroleum ether. M.p. 65-67°C [lit.[3] m.p. 68°C]. ^{1}H NMR (δ/ppm) 5.44 (s, ^{1}H), 5.82 (s, ^{1}H), 7.3-8.0 (m, ^{11}H).

[2] Cis-1,2-bis(phenylthio)acenaphthene

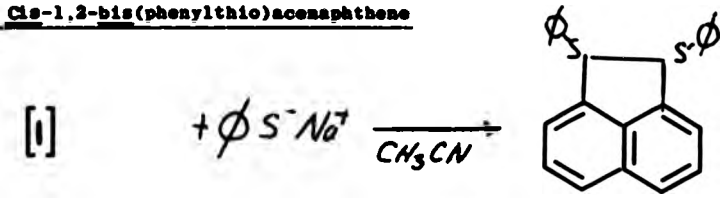

Sodium phenylthiolate (0.011 mole) [prepared[3] by reacting sodium with excess thiophenol in refluxing toluene] was added as a fine powder to [1] (0.01 mole) in 75 cm^3 of acetonitrile at ambient temperature. The reaction mixture was then poured into 100 cm^3 chloroform, washed with 100 cm^3 of water, and then with 200 cm^3 of 0.1 M sodium carbonate. The organic layer was dried (Na_2SO_4) and the solvent was removed *in vacuo* to give an orange solid. This was triturated with petroleum ether (70 cm^3) to give the light yellow solid product. Recrystallisation from chloroform/petroleum ether gave a pure sample in 70% yield. M.p. 144-145°C. Rf = 0.62 10% ether/petroleum ether, silica gel.

M/e for M+ = 370. ^{1}H NMR (δ/ppm) 5.48 (s,2H), 7.3 - 7.9 (m,16H).
Found C = 77.77%, H = 5.04%, $C_{24}H_{28}S_2$ requires C = 77.79%, H = 4.90%.

[3] Exo 2-chloro norbornane

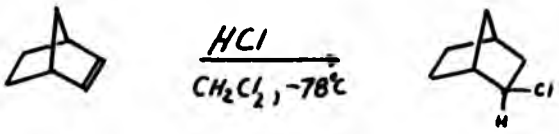

The procedure used was that of Cristal et al.[4] for 2-chloro 3-deutero norbornane. Norborylene (45.8 gm, 0.48 mole) in 800 cm^3 of CH_2Cl_2 was stirred at -78°C (ethyl acetate-N_2(liq.) slush). HCl (gas) (2.6 mole) [generated[5] from conc. H_2SO_4 dropped onto NaCl/HCl paste and dried by passage through conc. H_2SO_4] was then passed into the solution for a period of 6 hours. The solution was stirred and allowed to react for a further 12 hours at -78°C. The reaction mixture was then warmed to 25°C and stirred for 24 hours. The solvent was evaporated. Distillation (40 cm Vigreaux column) gave a colourless liquid (57.31 gm, 90% yield). B.p. 40-41°C (22 mm), [lit.[6,7] b.p. 40°C (22 mm)]. M/e = 150.

[4] 2,7 norbornyl-diol

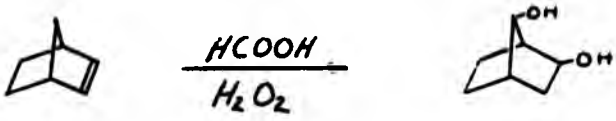

The procedure used was that of Walborsky et al.[8] Norborylene (23.5 gm, 0.25 mole) was reacted with 35 cm^3 of 30% hydrogen peroxide and 150 cm^3 of 58% formic acid at 40°C. The mixture was then extracted with anhydrous ethyl acetate and dried (Na_2SO_4). Removal of the ethyl acetate left a residue which was sublimed at 180°C (8 mm) to give a

white solid (20 gm, 70% yield). M.p. 174-176°C [lit.[8] m.p. 176°C]

[5] exo 7-bromo norcarene

Excess of a solution of potassium t-butoxide [prepared by adding 5grams of potassium to 100 cm^3 of refluxing t-butyl alcohol] was added [by a method[9] adapted from that used for 1,1 dibromo cyclopropane] to 1,3 cyclohexadiene (28 cm^3, 0.29 mole) in 400 cm^3 of t-butyl alcohol at 10°C. The mixture was stirred for 6 hours and then warmed to 25°C. The ether layer was extracted with pentane and dried. Distillation (10 cm Vigreaux column) gave a clear liquid (2.9 gm, 12% yield). B.p. 83°C (4 mm). Found C = 48.4%, H = 5.38%. C_7H_9Br requires C = 48.6%, H = 5.24%.

[6] 7,7-dimethoxy norborn-2-ene

The preparation of 7,7 dimethoxy norborn-2-ene is given by Gassman et al.[10] and was repeated on the same scale (0.93 mole). All melting points and yields of intermediates were in agreement with the literature values. The product was a clear liquid obtained in 41% yield. B.p. 60-66°C (17 mm), n_D^{25} = 1.4590 [lit.[10] b.p. 58-68°C (17 mm), n_D^{25} = 1.4598].

[7] norborn-2-ene-7-one

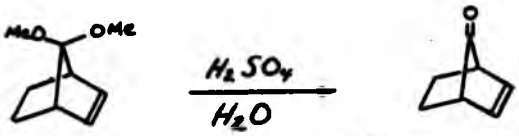

The preparation is given by Gassman et al.[11] and was repeated on half their scale (0.15 mole). B.p. 92-96°C (110 mm), n_D^{25} = 1.4784 [Lit.[11] b.p. 96-100°C (115 mm), n_D^{25} = 1.4706] ^{13}C NMR analysis verified the purity of the compound. The material was stored in solid-CO_2 until used, owing to its instability.

[8] 2,7 dibromo norbornane

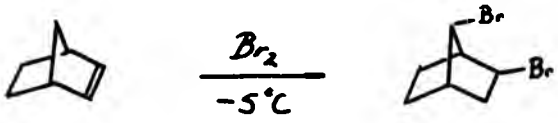

Bromine (0.92 mole) in CCl_4 (100 cm^3) was added [by method of Kwart et al.[12]] to norborylene (1.04 mole) in CCl_4 (200 cm^3) at -5°C (aniline/solid CO_2 slush). The reaction mixture was stirred for a further 2 hours at -5°C, and then at 12 hours at 25°C. Distillation (20 cm Vigreaux column) gave the product (80 gm, 50% yield). B.p. 130-132°C (19 mm) [Lit.[12] b.p. 128-125°C (19 mm)].

[9] syn 7-bromo norborn-2-ene

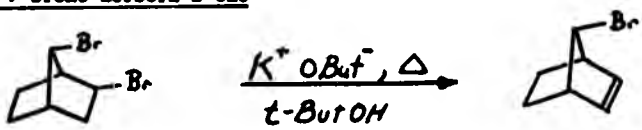

This was prepared by the method of Kwart et al.[12] on a scale using 0.023 mole of [8]. The clear product was obtained in 40% yield. B.p. 56-60°C (10 mm), n_D^{25} = 1.5248 [Lit.[12] b.p. 68-70°C (13 mm), n_D^{25} = 1.5260].

[10] 7-bromo norbornane

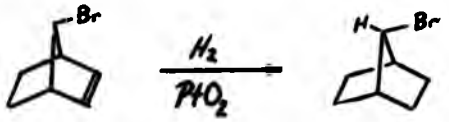

[9] (0.07 mole) in ethyl acetate (150 cm^3) was hydrogenated [by the method of Quin et al.[13]] using a PtO_2 catalyst at 50 p.s.i. over a 24 hour period. The catalyst was filtered off and the solvent was removed. The resulting oil was distilled to give the clear oil in 74% yield. B.p. 60°C (10 mm), n_D^{25} = 1.5189 [Lit.[14] b.p. 70-72.5°C (15-16 mm), n_D^{25} = 1.5169].

3.2.2 2-Norbornyl - Phosphorus Derivatives

[11] mixture of exo and endo 2-norbornyl dibromo phosphines

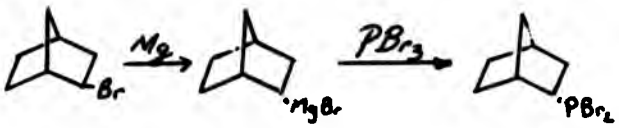

The preparative method[15] was adapted from that of exo and endo 2-norbornyl dichloro phosphine. Exo 2-bromonorbornane (35 gm, 0.4 mole) in 100 cm^3 of ether was added to magnesium (9.8 gm, 0.4 mole) [activated by heating with iodine] in 60 cm^3 of ether. This Grignard solution was then added to a solution of phosphorus tribromide (22.3 cm^3, 0.4 mole) in 150 cm^3 of ether at -40°C (propan-2-ol/solid CO_2 slush). The mixture was stirred for 1 hour at -40°C, and then at 25°C and filtered to remove the $MgBr_2$. Distillation (10 cm Vigreaux column) gave the clear liquid (8.1 gm, 70% yield) for the two isomers in a exo:endo ratio of 4:1 [^{31}P NMR]. B.p. 150°C (22 mm). Great sensitivity to air and light prevented elemental analysis of this material.

[12] mixture of exo and endo 2-norbornyl bromo chloro phosphines

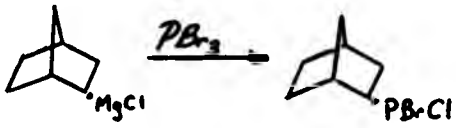

The preparative method used was described in [11] starting instead with [3] (26.7 gm, 0.22 mole). The product was a clear liquid (22 gm, 30% yield) of two isomers in a exo:endo ratio of 5:1 [^{31}P NMR]. B.p. 130-134°C (10 mm), m/e = 239.95 [Lit.[15] b.p. 145-147°C (14 mm), m/e 239.9471].

[13] mixture of exo and endo 2-norbornyl dichloro phosphines

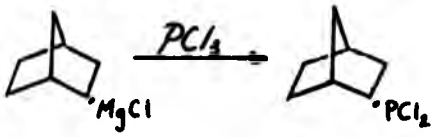

The preparative method is given by Quin et al.[15] and is described in the synthesis of [11] starting instead with [3] (10.7 gm, 0.4 mole) to form the Grignard, and then reacting with phosphorus trichloride (38.4 cm^3, 0.4 mole). Distillation gave a clear liquid (34.3 gm, 60% yield) of two isomers in a exo:endo ratio of 4:1 [^{31}P NMR]. B.p. 96-101°C (20 mm) [Lit.[15] b.p. 118-120°C (22mm)].

[14] mixture of exo and endo 2-norbornyl diphenyl phosphines

[3] (15.0 gm, 0.12 mole) was reacted with magnesium (2.8 gm, 0.12 mole) to form the Grignard. This was added over 1 hour to a solution of chlorodiphenylphosphine (20.5 cm^3, 0.12 mole) in 120 cm^3 of ether at -60°C (chloroform/solid CO_2 slush). The mixture was stirred for 2 hours

at -40°C and then for 4 hours at 25°C, and filtered to remove the $MgCl_2$. Distillation then gave a 50% yield of a mixture of the two isomers in a exo:endo ratio of 1:1 [^{31}P NMR]. B.p. 58-62°C (14 mm). Found C = 81.6%; H = 6.98%, $C_{19}H_{21}P$ requires C = 81.40%; H = 7.55%

[15] mixture of exo and endo 2-norbornyl bis(diethylamino) phosphines

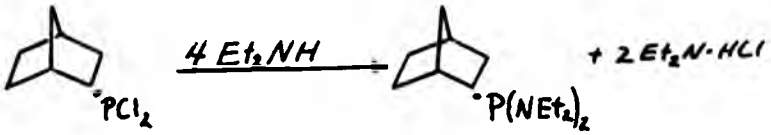

The isomeric mixture [13] (5.6 gm, 0.03 mole) in 30 cm^3 of ether was added over 1 hour to diethylamine (8.3 gm, 0.12 mole) in 200 cm^3 of ether at -60°C. The mixture was stirred for 2 hours at -60°C and for 4 hours at 25°C. It was then filtered to remove the hydrochloride salt. Distillation (20 cm Vigreaux column) gave a clear oil (3.7 gm, 49% yield) of two isomers in an exo:endo ratio of 70%:30% [^{31}P NMR]. B.p. 136-143°C (22 mm). Found C = 62.18%, H = 10.6%, $C_{11}H_{21}N_2P$ requires C = 62.24%, H = 9.97%.

[16] mixture of exo and endo 2-norbornyl dimethyl phosphines

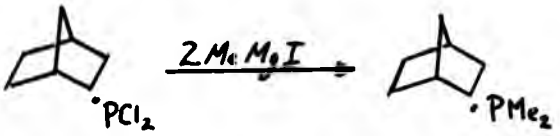

Methyl magnesium iodide (0.94 mole) [freshly prepared by reacting 6 cm^3 of methyl iodide with 2.3 gm of magnesium] in ether (25 cm^3) was added (syringe) over 1 hour to a solution of [13] (9.1 gm, 0.05 mole) in 50 cm^3 of ether at 0°C. The mixture was stirred for 2 hours at 0°C, and then 3 hours at 25°C, after which it was quenched with a saturated NH_4Cl solution and extracted with ether. The organic extracts were dried,

(molecular sieve 5A) and then evaporated to give the crude product (3 gm, 40% yield). ^{31}P NMR analysis revealed two signals -47.0 (endo) and -43.6 (exo) ppm [Lit.[15] -47.4 (endo) and -43.2 (exo) ppm] in a exo:endo ratio of 2:1. The great sensitivity to air of this compound prevented its further purification.

[17] mixture of exo and endo dimethyl 2-norbornyl phosphites

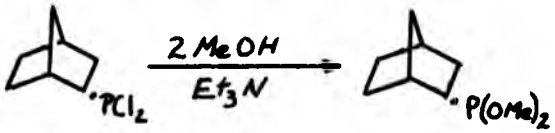

Trimethylamine (20.8 gm, 0.21 mole) and methanol (8 gm, 0.21 mole) in 200 cm^3 of ether were added to a solution of [13] (20 gm, 0.1 mole) in 100 cm^3 of ether at 0°C. The mixture was stirred for 2 hours at 0°C, and then for 4 hours at 25°C and filtered to remove the amine salt. Distillation (10 cm Vigreaux column) gave the clear oil (9 gm, 48% yield) of the two isomers in a exo:endo ratio of 4:1 [^{31}P NMR]. B.p. 66-70°C (1.0 mm) [Lit.[15] b.p. 62-64°C (0.6-0.8 mm)].

[18] mixture of exo and endo 2-norbornyl chloro phenyl phosphines

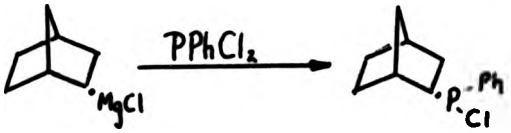

The freshly prepared Grignard from 2-chloro norbornane (0.17 mole) was added to a solution of dichlorophenylphosphine (36 gm, 0.17 mole) in 80 cm^3 of ether at -60°C by the method given in [14]. Distillation (20 cm Vigreaux column) gave a clear oil (4.5 gm, 30% yield) of the four [exo r and s; and endo r and s] isomers in a ca. 2:2:1:1 ratio [^{31}P NMR]. B.p. 128-132°C (12 mm). Found C = 65.31%, H = 6.83%, $C_{13}H_{16}ClP$ requires C = 65.4%, H = 6.76%.

[19] mixture of exo and endo 2-norbornyl 1,3-dioxaphospholanes

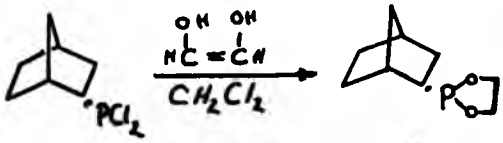

Ethylene glyc[illegible] 1 gm, 5.5 mmole) in 10 cm^3 of CH_2Cl_2 was added (syringe) over [illegible]hour to a Schlenk reflux apparatus containing [13] (1.1 gm, 5.5 mmole) in 10 cm^3 of $CDCl_3$ at reflux. After addition, the solution was refluxed for 24 hours, then cooled to 25°C. Distillation (micro-2 apparatus Fig. 4.1-2) gave the white solid (1.0 gm) of the two isomers in an exo:endo ratio of 2:1 [^{31}P NMR]. B.p. 80-84°C (5 mm). M.p. 50°C. Found C = 57.96%, H = 8.23%; $C_9H_{15}O_2P$ requires C = 58.06%, H = 8.12%.

[20] Mixture of exo and endo 2-norbornyl dioxa o-phenylene phospholes

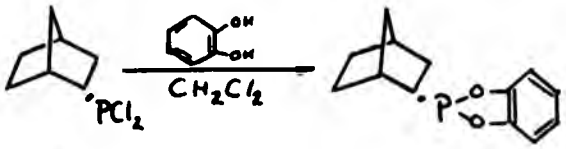

Catechol (0.6 gm, 5.5 mmole) in 10 cm^3 of CH_2Cl_2 was added (syringe) over 1 hour to a Schlenk apparatus which contained [13] (1.1 gm, 5.5 mmole) in 10 cm^3 of CH_2Cl_2 at reflux. This solution was refluxed for a further 24 hours and then cooled to 25°C. Distillation under vacuum gave the two isomers in a ratio of exo:endo of 2:1 [^{31}P NMR] as a waxy solid (0.7 gm, 56% yield).

B.p. 192-196°C (12 mm), m.p. 226°C (decomposed. Found C = 66.56%; H = 6.44% $C_{13}H_{15}O_2P$ required C = 66.66%; H = 6.46%.

[21] Mixture of exo and endo 2-norbornyl 1,3-dithiolphospholanes

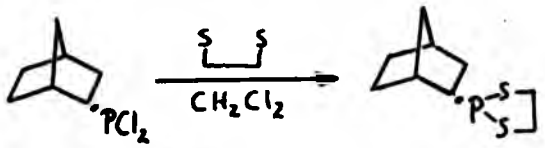

1,2-Ethanedithiol (0.52 gm, 5.5 mmole) in 10 cm³ of CH_2Cl_2 was added (syringe) over 1 hour to a Schlenk apparatus which contained [13] (1.1 gm, 4.2 mmole) in 10 cm³ of CH_2Cl_2 at reflux. The mixture was refluxed for a further 24 hours, then cooled to 25°C. Distillation via a micro-2 apparatus (Fig. 4-2) gave the two isomers in exo:endo ratio of 3:1 [^{31}P NMR] as a clear liquid (1.0 gm, 70% yield).
B.p. 72°C (6 mm). Found C = 49.48%; H = 6.83% $C_9H_{15}S_2P$ requires C = 49.52%; H = 6.92%.

[22] Mixture of endo and exo dimethyl 2-norbornyl phosphates

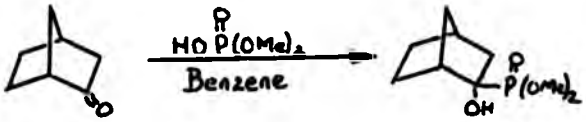

Norcamphor (1.09 gm, 9.9 mmole) in 10 cm³ of benzene was added to dimethyl phosphite (1.2 gm, 10.9 mmole). Distillation via a micro-2 apparatus (Fig. 4-3) gave the two isomers in an exo:endo ratio of 2:3 [^{31}P NMR] as a waxy solid (1.2 gm, 52% yield).
B.p. 125-127°C (10 mm) [Lit. [16] b.p. 127-132°C (10 mm)].

[23] Mixture of exo and endo diphenyl 2-norbornyl phosphates

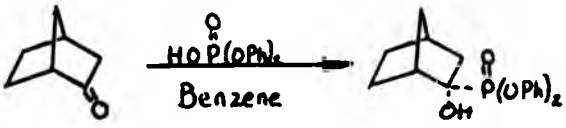

Diphenyl phosphite (2.3 gm, 10.9 mmole) followed by 15 drops of a freshly prepared saturated solution of potassium methoxide in methanol was added [by the method[16] adapted from that for dimethyl 2-norbornyl phosphite] to norcamphor (1 gm, 9.9 mmole) in 10 cm³ of benzene. After the addition the mixture was concentrated and refluxed in a Schlenk apparatus and stirred for 24 hours, and then cooled to 25°C. The solvent was evaporated off. Distillation (10 cm Vigreaux column) gave the two isomers in an exo:endo ratio of 2:3 [^{31}P NMR] as a waxy solid (3.2 gm, 90% yield).

B.p. 64°C (15 mm) [Lit.[17] b.p. 62-65°C (15 mm)].

[24] Exo 2-norbornyl phosphonic dichloride

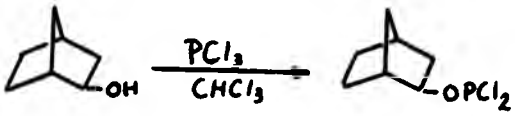

Phosphorus trichloride (1.6 cm³, 18 mmole) was added (syringe) to a solution of exo norborn-2-ol (2 gm, 19 mmole) in 19 cm³ of $CHCl_3$ in a Schlenk tube. The mixture was shaken for 30 minutes at 0°C, then for 30 minutes at 25°C, after which the solvent was evaporated. Distillation gave a clear liquid (3.8 gm, 90% yield).

B.p. 185°C (6 mm), m.p. 152°C.

Found C = 39.46%; H = 4.84% $C_7H_{11}Cl_2OP$ requires C = 39.46%; H = 5.22%.

[25] Mixture of exo and endo 2-norbornyl dimethyl phosphonodithioate

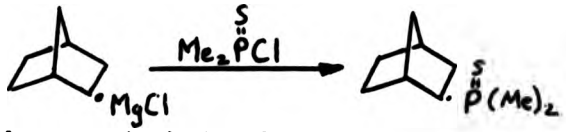

A freshly prepared solution of the Grignard of [3] (0.17 mole) was added to a solution of chlorodimethylphosphine sulphide (17 cm³, 0.168 mole) in 120 cm³ of ether. Distillation in a micro-2 apparatus

(Fig. 4-3) gave the two isomers in an exo:endo ratio of 2:1 [^{31}P NMR] as a solid.

B.p. 110°C (16 mm). Recrystallisation from ethanol gave a white solid with a m.p. 150-155°C (exo isomer). [Lit.[18] m.p. 149-151°C for the exo isomer.] Found C = 57.68%; H = 9.0%; $C_9H_{17}SP$ requires C = 57.45%; H = 9.04%.

4.2.3 7-norbornenyl Phosphorus Derivatives

(7-norb = 7-norbornenyl)

[26] Mixture of syn and anti 7-norbornenyl dibromo phosphines

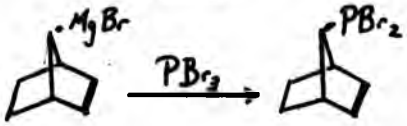

[9]

A freshly prepared solution of the Grignard of [9] (0.17 mole) was added to a solution of phosphorus tribromide (11 cm³, 0.115 mole) in 120 cm³ of ether at -60°C. The mixture was stirred for 2 hours at -60°C, and then for 4 hours at 25°C, and filtered to remove the $MgBr_2$. Distillation gave the two isomers in a syn:anti ratio of 1:5 [^{31}P NMR] as a clear liquid (1.3 gm, 40% yield).

B.p. 136°C (20 mm). The great sensitivity to air of this compound prevented its further purification.

[27] Mixture of syn and anti 7-norbornenyl bromo chloro phosphines
and
[28] syn and anti 7-norbornenyl dichloro phosphines

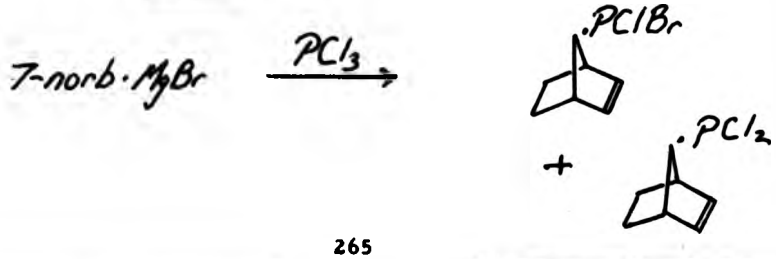

The method was adapted from that of Quin[18] and is described in the preparation of [26]. The Grignard of [9] (0.115 mole) was reacted with phosphorus trichloride (10.5 cm³, 0.119 mole). Distillation gave the two products. The derivative [28] gave two isomers in a syn:anti ratio of 1:4 [^{31}P NMR] as a clear liquid (4.0 gm).

B.p. 54°C (1 mm) [lit.[18] b.p. 80-83°C (3 mm)]. The derivative [28] consisted of two isomers in a syn:anti ratio of 4:1 [^{31}P NMR] as a clear liquid (1.5 gm).

B.p. 46°C (1 mm) [Lit.[18] b.p. 75-78°C (3 mm)].

[29] Mixture of syn and anti 7-norbornenyl chloro phenyl phosphines

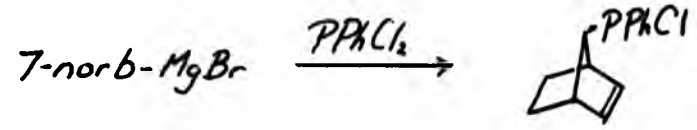

The method was described for [18] starting here with [9] (5.0 gm, 0.029 mole). Distillation gave the four isomers in a syn R and S and an anti R and S ratio of 1:1:1:2 respectively [^{31}P NMR] as a clear liquid (3.2 gm, 48% yield.

B.p. 92°C (4 mm). Attempted separation proved unsuccessful.

[30] Mixture of syn and anti 7-norbornenyl bis(diethylamino) phosphines

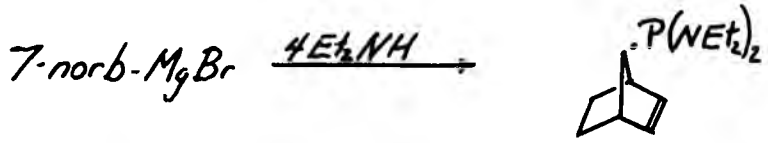

The preparation was adapted from that of [15] starting in this case from [28] (5.5 gm, 0.03 mole). Distillation gave the two isomers in a syn:anti ratio of 1:2 [^{31}P NMR] as a clear liquid.

B.p. 80°C (10 mm). Found C = 62.63%; H = 9.09% $C_{11}H_{19}N_2P$ requires C = 62.84%; H = 9.10%.

[31] Mixture of syn and anti 7-norbornenyl 1,3-dithiolphospholanes

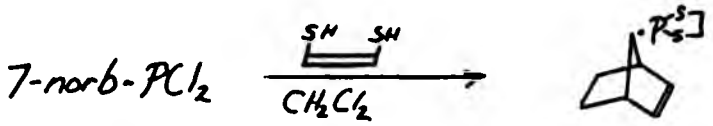

The method was as described previously for [21] and was repeated here starting in this case from [28] (1.1 gm, 5.5 mmole). Distillation gave the two isomers in a syn:anti ratio of 1:3 [^{31}P NMR] as a clear liquid (0.7 gm, 60% yield).

B.p. 68°C. Found C = 49.84%; H = 6.91% $C_9H_{15}S_2P$ requires C = 49.52%; H = 6.93%.

[32] Mixture of syn and anti 7-norbornenyl 1,3-dioxa phospholanes

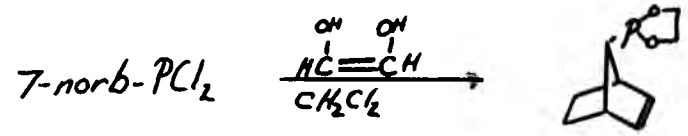

The method was described for [19] starting in this case from [28] (1.1 gm, 5.5 mmole). Distillation gave the two isomers in a syn:anti ratio of 1:2 [^{31}P NMR] as a clear liquid (0.8 gm, 80% yield).

B.p. 73°C (5 mm). Found C = 58.69%; H = 7.24% $C_9H_{13}O_2P$ requires C = 58.7%; H = 7.12%.

[33] Mixture of syn and anti 7-norbornenyl diphenyl phosphines

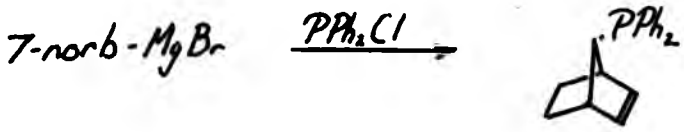

The Grignard of [9] (0.03 mole) was added as in the preparation of [26] to diphenylchlorophosphine (4.7 gm, 0.03 mole). Distillation (10 cm Vigreaux column) gave the two isomers in a syn:anti ratio of 3:1 [^{31}P NMR] as a solid (1.5 gm, 18% yield).

B.p. 178-182°C (10 mm). Found C = 81.97%; H = 6.87% $C_{19}H_{19}P$ requires C = 81.99%; H = 6.88%.

[34] Mixture of syn and anti 7-norbornenyl dimethyl phosphines

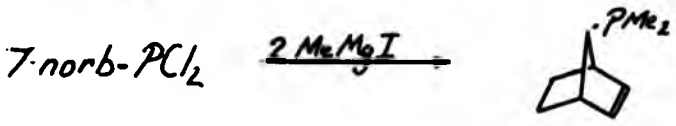

The preparative method was described previously for [16] starting here from [28] (19.5 gm, 0.1 mole). Distillation gave the two isomers in a syn:anti ratio of 2:1 [^{31}P NMR] as a clear liquid (2.2 gm, 80% yield). B.p. 76°C (4 mm). [Lit.[18] b.p. 48-52°C (2.5 mm)].

[35] Mixture of syn and anti dimethyl 7-norbornenyl phosphates

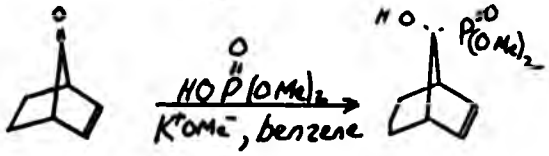

The method was as described previously for [22] and was repeated starting in this case from [7] (1.1 gm, 9.9 mmole). Distillation gave the two

isomers in a syn:anti ratio of 1:2 [^{31}P NMR] as a waxy solid (0.25 gm, 12% yield). B.p. 83°C (10 mm) [Lit.[19] b.p. 85°C (10 mm)].

[36] Mixture of syn and anti diphenyl 7-norbornenyl phosphates

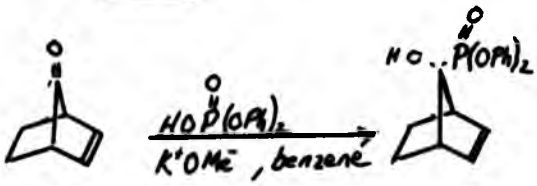

The method was as described previously for [22] and was repeated starting in this case from [7] (1.1 gm, 9.9 mmole). Distillation gave the two isomers in a syn:anti ratio of 1:2 [^{31}P NMR] as a waxy solid (0.9 gm, 22% yield). B.p. 64°C (15 mm) [Lit.[19] b.p. 65°C (15 mm)].

4.2.4 1-adamantyl Phosphorus Derivatives

(1-ada = 1-adamantyl)

[37] 1-adamantyl dibromo phosphine

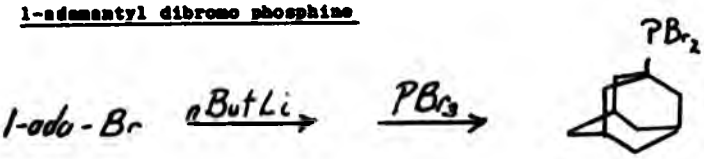

Commercial n-butyl lithium in hexane (80.0 cm³, 0.19 mole) was added (syringe) to 1-bromoadamantane (40.0 gm, 0.19 mole) in 150 cm³ of ether. The mixture was stirred for 2 hours at 25°C and then cooled to -60°C (chloroform/solid CO_2 slush). Phosphorus tribromide (17.8 cm³, 0.19 mole) in 70 cm³ of ether was added and the mixture was stirred for 2 hours at -60°C, and then for 2 hours at 25°C, after which it was filtered and the solvent evaporated. The solid residue was recrystallised from ethyl acetate to leave a mixed product of 1-bromoadamantane and the phosphine [^{13}C NMR]. The great sensitivity to air and light of this compound prevented its further purification.

[38] 1-adamantyl bromo chloro phosphine

and

[39] 1-adamantyl dichloro phosphine

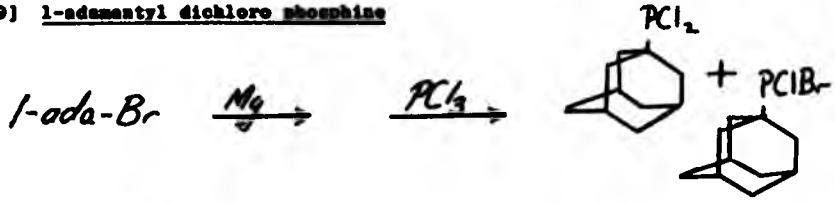

The method was as previously described for [36] and was repeated starting in this case from 1-bromoadamantane (20.0 gm, 0.093 mole). Distillation gave a mixture of the two compounds. B.p. 128-132°C (5 mm). The great sensitivity to air and light of the mixture prevented its separation and further purification.

[40] 1-adamantyl chloro phenyl phosphine

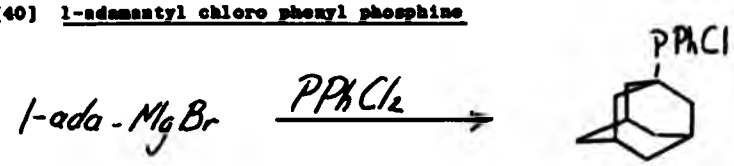

A fresh solution of the Grignard reagent (ca. 33 mmol.) as prepared previously in [11] was added over 2 hours to dichlorophenyl phosphine (4.2 cm³, 33 mmol.) in 100 cm³ of ether at -60°C. The mixture was stirred at -60°C for 3 hours, and then at 25°C for 4 hours. After filtration and evaporation of the solvent, distillation gave a clear liquid (1.3 gm, 14% yield). This solidified at room temperature and was composed of a 2:1 ratio of the chloro phenyl and the bromo phenyl phosphine adducts [^{31}P NMR]. B.p. 135°C (10 mm). Great sensitivity to air prevented separation and elemental analysis.

[41] 1-adamantyl bis(diethylamino) phosphine

[38] (6.0 gm, 0.02 mole) in 30 cm³ of ether was added to diethylamine (5.4 gm, 0.074 mole) in 100 cm³ of ether at -60°C. The mixture was stirred for 2 hours at -60°C, and then for 2 hours at 25°C. It was then filtered to remove the hydrochloride. Distillation (10 cm Vigreaux column) gave an amber liquid (2.2 gm, 40% yield). B.p. 176°C (6 mm). Found C = 69.79%; H = 9.30%; P = 9.90% $C_{18}H_{35}N_2P$ requires C = 69.81%; H = 9.27%; P = 9.92%.

[42] 1'-adamantyl 1,3-dioxaphospholane

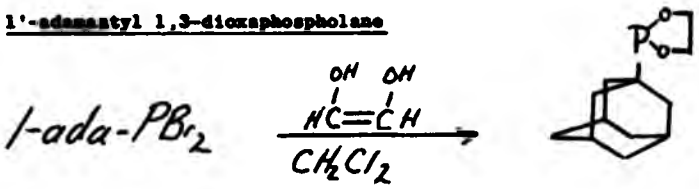

Ethylene glycol (0.4 gm, 65 mmol.) in 10 cm³ of CH_2Cl_2 was added (syringe) to [39] (2.1 gm, 65 mmol.) in 10 cm³ of CH_2Cl_2 in a Schlenk reflux apparatus. The mixture was then concentrated and refluxed for 24 hours. The resulting oil was micro distilled to give a white solid (1.2 gm, 8% yield). B.p. 176°C (22 mm). Found C = 63.72%; H = 8.45%; P = 13.69% $C_{12}H_{19}O_2P$ requires C = 63.70%; H = 8.46%; P = 13.68%.

[43] 1-adamantyl dioxa o-phenylene phospholane

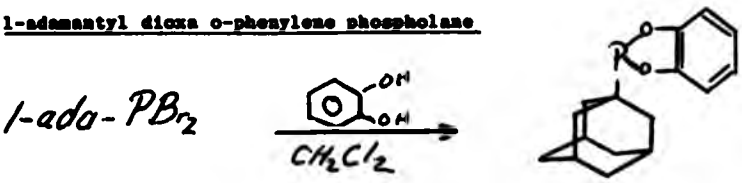

Catechol (0.7 gm, 65 mmol.) in 10 cm³ of CH_2Cl_2 was added (syringe) to [39] (2.1 gm, 65 mmol.) in 10 cm³ of CH_2Cl_2 in a Schlenk reflux apparatus. The mixture was concentrated and refluxed for 24 hours. The solvent was evaporated and the solid was recrystallised with methanol to yield 1 gram of a waxy solid which was composed of the product 70% and 2-bromo 1,3-dioxa o-phenylene phospholane 30% [^{31}P NMR]. Great sensitivity to air and light required its immediate use and prevented further purification.

[44] 1-adamantyl diphenyl phosphine

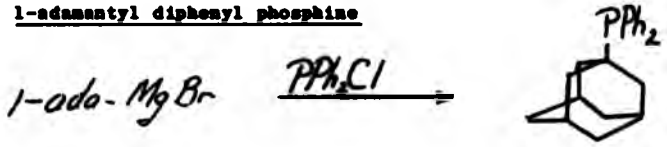

The method was as described previously for [33] and was repeated starting in this case from 1-bromoadamantane (7.0 gm, 32.5 mmole). The Grignard reagent was then reacted with diphenylchloro phosphine (5.8 cm³, 32.5 mmole). Distillation gave a clear liquid (7.0 gm, 67% yield) which solidified at room temperature. B.p. 116°C (65 mm), m.p. 256°C (with decomposition). Found C = 82.36%; H = 7.88% $C_{22}H_{25}P$ requires C = 82.47%; H = 7.86%.

[45] 1-adamantyl dimethyl phosphonodithioate

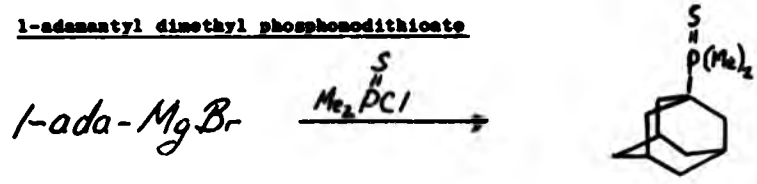

A freshly prepared solution of the Grignard (34 mmol) as prepared previously [25] was added to a solution of thionophosphinyl chloride

(3.5 gm, 34 mmol) in 100 cm^3 of ether at -60°C. The mixture was stirred for 4 hours at -60°C and then for 6 hours at 25°C. The mixture was filtered and then concentrated. Recrystallisation from methanol gave the pure compound. M.p. 196°C (decomposed). Found C = 63.15%; H = 9.30%; P = 13.56% $C_{12}H_{21}BP$ requires C = 63.12%; H = 9.26%; P = 13.56%.

4.2.5 2-adamantyl Phosphorus Derivatives

(2-ada = 2-adamantyl)

[46] 2-adamantyl dibromo phosphine

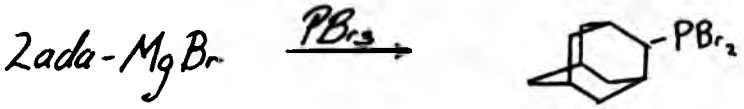

This compound was prepared by the method outlined for [37] on a 0.12 mole scale and starting in this case from 2-bromoadamantane. Distillation gave the liquid compound. B.p. 174°C (1 mm). The great sensitivity to air of this compound prevented its elemental analysis but its identity was confirmed by ^{31}P NMR.

[47] 2-adamantyl bromo chloro phosphine

and

[48] 2-adamantyl dichloro phosphine

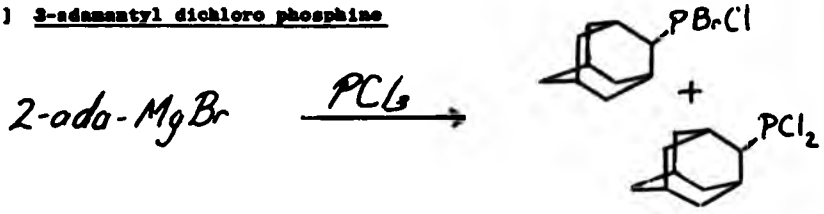

The compounds were prepared by the method outlined for [38] and [39] on a 0.92 mole scale and starting in this case from the 2-bromoadamantane. Distillation gave the two compounds in a ratio of 1:2 [^{31}P NMR]. B.p. 108-112°C (1 mm). Great sensitivity to air prevented further separation.

[49] 2-adamantyl phosphonic dichloride

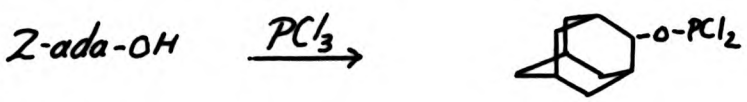

Adamantan-2-ol (3.45 gm, 22.7 mmol) was stirred with phosphorus trichloride (2.0 cm³, 22.7 mmol) in 10 cm³ of benzene for 1 hour in a Schlenk tube to give the dichloridite after solvent evaporation. Recrystallisation from methanol gave the solid product (2.3 gm, 40% yield). M.p. 184-186°C [Lit.[20] m.p. 185-188°C].

[50] 2-adamantyl chloro phenyl phosphine

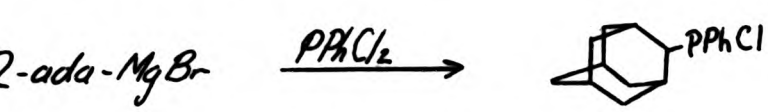

The compound was prepared by the method outlined for [40] on a 23.2 mmol scale starting in this case from 2-bromoadamantane. Distillation gave two compounds with a b.p. 185-187°C. It was assumed from ^{31}P and ^{13}C NMR analysis that both the bromo and the chloro derivative had formed. Great sensitivity to air prevented further separation of these compounds.

[51] 2-adamantyl 1,3-dithiolphospholane

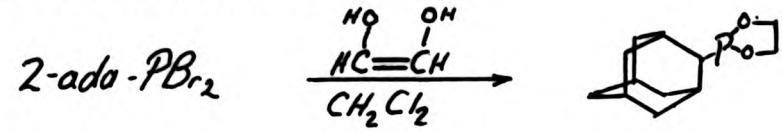

The compound was prepared by the method outlined for [21] on a 4.2 mmol

scale starting with [46]. Distillation gave the liquid product (0.7 gm, 64% yield). B.p. 79°C (6 mm). Found C = 86.77%; H = 7.41%; P = 11.98% C $_{12}H_{19}P_2$ requires C = 86.78%; H = 7.411%; P = 11.98%.

[52] 2-adamantyl diphenyl phosphine

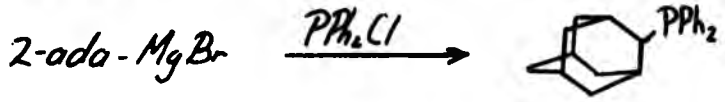

The compound was as prepared by the method outlined for [44] on a 0.03 mole scale and starting in this case from 2-bromoadamantane. Micro-distillation gave the compound (6 gm, 64% yield). B.p. 198°C (0.1 mm). Found C = 82.46%; H = 7.83% $C_{22}H_{25}P$ requires C = 82.47%; H = 7.86%.

[53] 2-adamantyl dimethyl phosphate

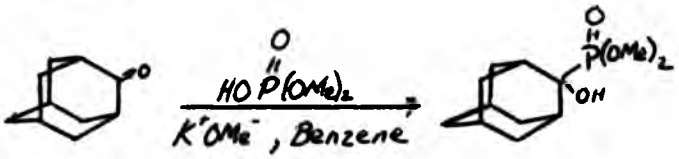

The compound was prepared by the method[19] outlined for [22] on a 9.0 mmol scale starting in this case from 2-adamantone. Recrystallisation with ethyl acetate gave the solid product (1.0 gm, 50% yield). M.p. 162°C. Found C = 55.87%; H = 8.23%; P = 11.82% $C_{12}H_{21}O_4P$ requires C = 55.38%; H = 8.13%; P = 11.90%.

[54] 2-adamantyl diphenyl phosphate

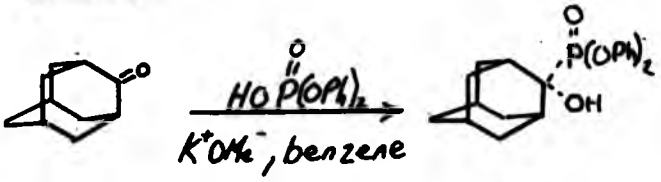

The compound was prepared by the method[20] outlined for [23] on a 9.9 mmol scale starting in this case from 2-adamantone. Recrystallisation with methanol gave the solid product (1.5 gm, 50% yield). M.p. 188°C [Lit.[19]. m.p. 189°C].

4.2.6 Other P(III) Derivatives

[55] 2-chloro 1,3-dioxa o-phenylene phospholane

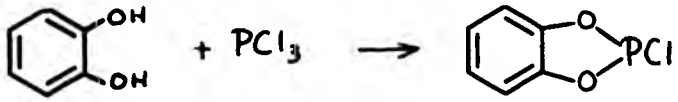

Phosphorus trichloride (94 gm, 0.68 mole) was added to catechol (50 gm, 0.45 mole). After 1 hour further phosphorus trichloride (79 gm, 0.58 mole) was added. The mixture was then heated and stirred at reflux for 3 hours. Distillation gave the solid product (74 gm, 94% yield). B.p. 91°C, m.p. 29°C ([Lit.[21] b.p. 91°C, m.p. 30°C]

[56] 2-chloro 1,3-dioxaphospholane

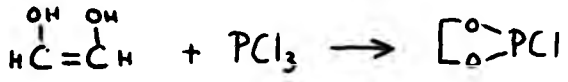

Ethylene glycol (140 cm³, 2.5 mole) in 100 cm³ of CH_2Cl_2 was added to a refluxing solution of phosphorus trichloride (220 cm³, 2.5 mole) in 300 cm³ of CH_2Cl_2. The mixture was further refluxed for 3 hours, then cooled to 25°C. Distillation gave the liquid product (170 gm, 75% yield). B.p. 40°C (12 mm), [Lit.[22] b.p. 45.5-47.0°C (155 mm)].

References

1. R.K. Harris, A.A. Bothner-By University of East Anglia LAOCOON NMR computer simulation package.

2. S. Castellano, A.A. Bothner-By J. Chem. Phys. 41, 3863 (1964).

3. N. Kharash, C.M. Baess J. Amer. Chem. Soc. 71, 2724 (1949).

4. S.J. Cristal, R. Cope J. Org. Chem. 31, 2741 (1966).

5. H. Gillman, A.H. Blatt Ed. Organic Synthesis 1, 534-note 2 (1941).

6. L.D. Quin, M.D. Gordon, S.O. Lee Org. Magn. Reson. 6, 505 (1974).

7. L.D. Quin, M.J. Gallagher, G.T. Cunkle, D.B. Chesnut J. Amer. Chem. Soc. 102, 3136 (1980).

8. H.M. Walborsky, D.F. Loncrini J. Org. Chem. 22, 1117 (1957).

9. P.S. Skell, A.Y. Gorner J. Amer. Chem. Soc. 78, 5430 (1956).

10. P.G. Gassman, J.L. Marshall Organic Synthesis V, 424 Wiley & Sons (1973).

11. P.G. Gassman, J.L. Marshall ibid V, 91 Wiley & Sons (1973).

12. H. Kwart, L. Kaplan J. Amer. Chem. Soc. 76, 4072 (1954).

13. L.D. Quin, L.B. Littlefield J. Org. Chem. 43, 3508 (1978).

14. A.P. Marchand, W.R. Weimar Jr. Chem. and Industry Feb. 15, 200 (1969).

15. L.D. Quin, M.J. Gallagher, G.T. Cunkle, D.B. Chesnut J. Amer. Chem. Soc. 102, 3136 (1980).

16. C. Benezra Can. J. Chem. 48, 3382 (1970).

17. H.J. Callot, C. Benezra Can. J. Chem. 48, 3387 (1970).

18. L.D. Quin, L.B. Littlefield J. Org. Chem. 43, 3508 (1978).

19. G.W. Buchanan, C. Benezra Can. J. Chem. 54, 231 (1976).

20. R.J. Cremlyn, R.N. Ellam, N. Akhtar Phosphorus and Sulphur 7, 257 (1979).

21. P.C. Crofts, J.H.H. Markes, H.N. Rydon J. Chem. Soc. 4250 (1958).

22. H.J. Lucas, F.W. Mitchell, C.N. Scally J. Amer. Chem. Soc. 72, 5491 (1950).

APPENDIX 1

As previously mentioned in Section 1.7.3 either nucleus of the pair in a heteronuclear shift correlation experiment may be detected. Theoretically this is true for the $^{13}C/^{1}H$ pair. However, usually the ^{13}C nucleus is the detected one. The reasons for this, even though one might expect a gain in sensitivity from the fact that the final signal amplitude is dependent upon population difference, magnetogyric ratio and on frequency of the transitions, are essentially practical ones. These are listed below.

(1) Complete broad-band unified decoupling of the large ^{13}C frequency range during acquisition is now technically impossible due to the large power requirements needed and the accompanying stress on the coil.

(2) Suppression of protons which are not coupled to ^{13}C (i.e. solvents, or OH groups) would have to be achieved, which may cause dynamic range problems throughout the spectrum.

(3) Since ^{13}C has a much larger chemical shift range, a larger number of t_1 intervals would be needed to achieve similar digital resolution in the t_1 axis. Hence longer duration to acquire the 2D montage and longer processing time is needed.

(4) The delay between transients is dependent upon the relaxation time of the detected nucleus. As ^{13}C relaxation times are usually larger the ^{1}H relaxation times the repetition rate would be slower.

(5) The decay rate of the proton resonances broadened by unresolved proton-proton coupling is usually larger than those of $^{13}C(^{1}H)$ resonances. Thus a further loss in sensitivity would occur.

For these reasons ^{13}C detection during acquisition is preferred over ^{1}H detection.

In another vein, suggestions using ^{12}C isotopomers instead of ^{13}C and detecting the ^{1}H nucleus have been proposed. Though this would

give a tremendous sensitivity enhancement over ^{13}C and thus make it much more viable, no practical techniques have yet been put forth.

TITLE STUDIES OF ORGANOPHOSPHORUS COMPOUNDS BY NUCLEAR MAGNETIC RESONANCE SPECTROSCOPY WITH TWO FREQUENCY DIMENSIONS.

AUTHOR DON-ROGER PARKINSON.